DOD/ONR/N00014-97-1-0806

# University Research Initiative Program for Combat Readiness

## Annual Report

for the period

June 1, 1997 — June 30, 1998

Jerome D. Odom

University of South Carolina
Columbia, SC 29208

May 1998





Prepared for

THE U.S. DEPARTMENT OF DEFENSE
OFFICE OF NAVAL RESEARCH
GRANT NUMBER N00014-97-1-0806

# EXECUTIVE SUMMARY


## ABSTRACT

The *University Research Initiative for Combat Readiness* includes nineteen (19) research and development projects relevant to combat readiness. Projects being supported by this initiative address six major DoD mission areas including: chemical and biological warfare, target acquisition and identification, anti-submarine warfare, combat medicine, biodeterioration, and command, control, and communications. These projects were selected for support based on an existing research capability that could be accelerated to create cost savings to the ONR by bringing results to the field earlier. For the present report period directors of the individual projects report sixty-three (63) publications in progress, in press, or submitted for publication.


## FORWARD

The total amount of this grant is $9,304,000 for the period of 01 Jun 97 through 29 Jun 00. The award carries a $27,912,001 non-federal matching commitment. The University of South Carolina provides management costs for the project, and indirect costs are being returned to the project in the form of equipment. For the present report period the project supported seventy-three (73) faculty/post doctoral associates and fifty-eight (58) graduate/undergraduate students. Twenty (20) inventions are reported and emanate from the *Technology Development for Chemical Detection, Survivable, and Re-configurable Optical/Wireless Tactical Networks* component projects. For sixteen (16) of these inventions US Patent Office filings are reported. Significant progress is also reported for the wavelet based automatic target detection, recognition, and image processing components. The most significant achievement of the combat medicine portion of the program is the development of a biomimetic bone cement that can attain a compressive strength of over seventy-six (76) megapascals (Mpa) in just twelve hours.

## DESCRIPTION OF ATTACHMENTS

Attached to this Executive Summary are individual Performance (Technical) Reports for the nineteen (19) component projects and their individual SF-298 Report Documentation Pages.

## REPORT

The University Research Initiative Program for Combat Readiness was prepared in response to BAA 97-006. The purpose of this project is to support on-going research activities in six areas related to combat readiness: chemical and biological warfare, target acquisition and identification, anti-submarine warfare, combat medicine, biodeterioration, and command, control, and communications. Simultaneously the project is to identify new projects, which offer potential advancement and improvement in combat readiness while offering specific savings in research and other federal expenditures by the accelerated research covered in the initiative.

**Management** *($0, 4 faculty)*

Effective March 16, 1997, the designated Principal Investigator, Jerome D. Odom, became Executive Vice President for Academic Affairs and Provost for the University of South Carolina. Responsibilities for this new position placed increasing demands on the time that Dr. Odom had initially devoted to the implementation of the *University Research Initiative Program for Combat Readiness*. As such, Dr. Odom designed a management structure for the program and

notified the Office of Naval Research Regional Office-Atlanta on October 17, 1997 that Roger H. Sawyer, Interim Dean of the College of Science and Mathematics at the University of South Carolina, was to serve as Co-PI. Drs. Frank T. Avignone, III and T. S. Little were appointed as Program Director and Manager, respectively.

This management structure, shown on the following page, allows for the effective and efficient management of the program. Dr. Sawyer participated in the development of the research described in the award. As an interim academic dean, Dr. Sawyer has sufficient administrative position to help insure the implementation of the award. Further, Dr. Sawyer has the administrative staff necessary to monitor and maintain fiscal control over the award. Dr. Avignone, familiar with ONR general grant terms and conditions, has sufficient contacts within the DoD to identify outside reviewers and evaluators for the program and to serve as principal programmatic leader. Dr. Little has served, for the past four years, as Program Manager for the South Carolina Department of Defense EPSCoR Program (DEPSCoR) and is proficient in the day to day management of large, complex, multi-task awards.

For each component project, within each major DoD mission area, a single project leader has been identified. The project titles, these leaders and the total amount of funding for the total project period (3-years) are provided below:

| Title | Project Leader | Budget |
|---|---|---|
| The Design and Synthesis of Quantum Dot Based Lasers | Richard D. Adams | $330,000 |
| Line-of-Sight Standoff Identification of Explosive Chemicals and Chemical Warfare Agents | S. Michael Angel | $399,901 |
| Small Molecule Transport Through Polymers: Effects of Polymer Inhomogeneity and Dynamics on the Nanometer Length Scale | Mark A. Berg | $370,000 |
| Wavelet Based Image Processing For Military Applications | Ronald A. DeVore | $440,001 |
| Insure Access to Allogenic Bone Marrow Transplantation for Correction of Marrow Failure and Hematologic Malignancies | Jean Henslee-Downey | $524,001 |
| Accelerated Research in Biofouling Control | Madilyn M. Fletcher | $383,251 |
| Real-Time Biodetection Using PCR-MS | Karen Fox | $450,001 |
| Tissue-Engineered Cartilage and Advanced Bioadhesives for the Rapid Healing of Combat and Training Injuries to Bone | Brian Genge | $900,000 |
| Development of a Field-Portable LIBS System for the Identification of Alloys | Scott R. Goode | $434,700 |
| Wavelet-Based Automatic Detection and Recognition | Terrence L. Huntsberger | $510,000 |
| Wavelet-Based Algorithms for Acoustic/Non-Acoustic Antisubmarine Warfare | Bjorn Jawerth | $525,000 |
| Rapid Biodetection of Bacterial Cells by Laser Pyrolysis/Mass Spectrometry | Stephen L. Morgan | $434,748 |
| Technology Development for Chemical Detection | M.L. Myrick | $1,299,999 |
| Real-Time UV Fluorescence for Dissolved Hydrocarbon Tracking | M.L. Myrick | $290,000 |
| Massively Parallel Optical Image Compression Using Optical Rank Annihilation | M.L. Myrick | $400,000 |
| Dynamic Decision Support for Command, Control, and Communication in the Context of Tactical Defense | J.R. Rose | $410,399 |
| Survivable and Reconfigurable Optical/Wireless Tactical Networks | S. Singh | $409,000 |
| Molecular Scale Electronic Arrays for the Design of Ultra-Fast Computational Systems | James M. Tour | $293,000 |
| Laboratory for Genetic Diagnosis and Control of Mosquitoes | Richard G. Vogt | $500,000 |

# UNIVERSITY RESEARCH INITIATIVE PROGRAM FOR COMBAT READINESS
# UNIVERSITY OF SOUTH CAROLINA

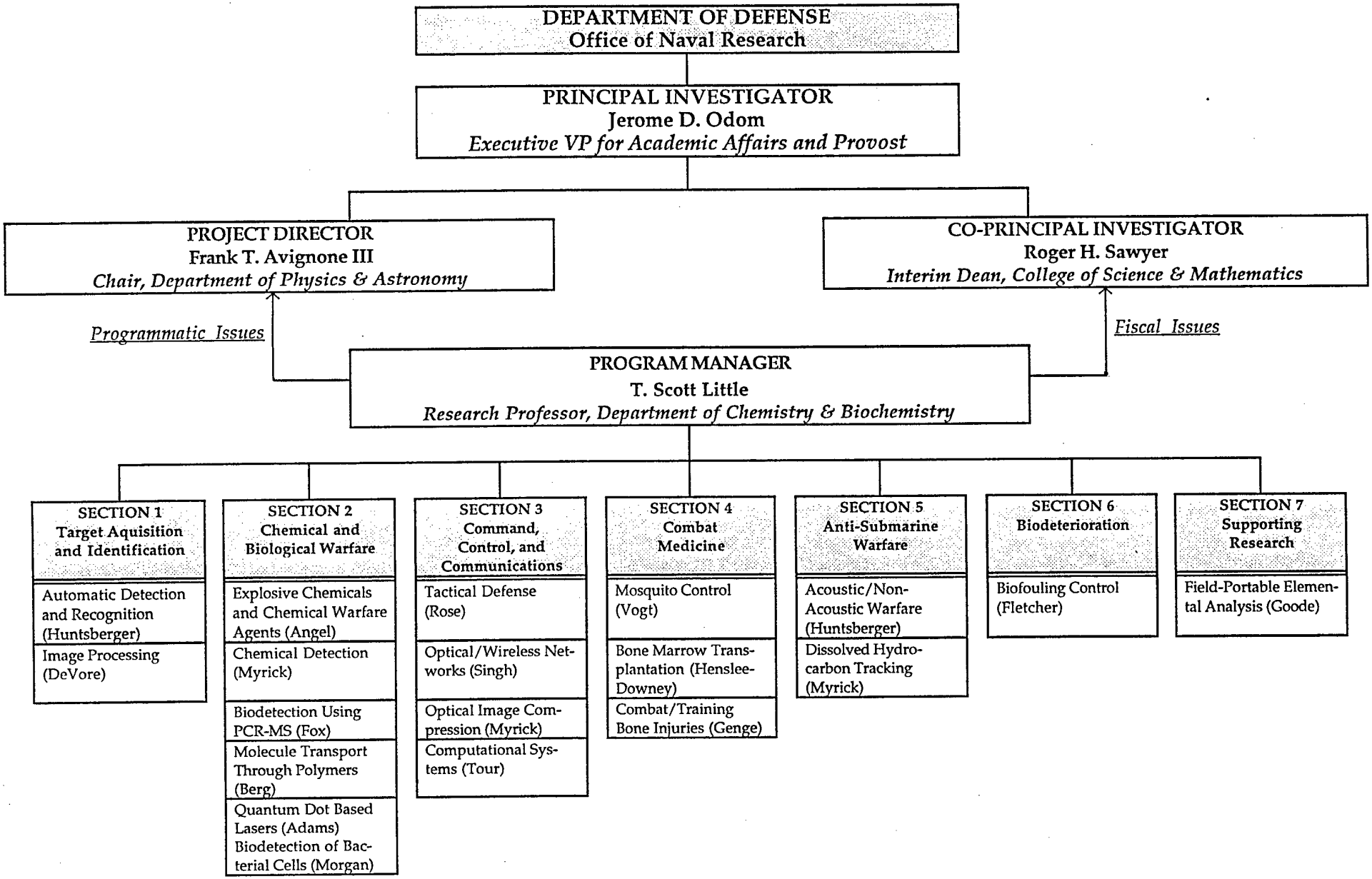

This distribution of program resources is shown graphically below:

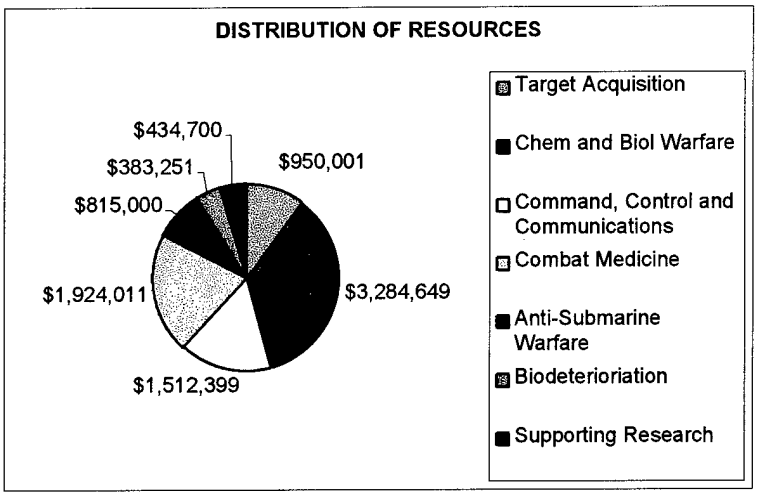


Management activities for the first year have included the distribution of resources and monitoring of expenditures for the individual nineteen project accounts, the organization and implementation of a management structure for the overall program and the development of reporting guidelines for the individual component projects.

**Section 1: Target Acquisition and Identification** *($950,000, 2 component projects, 11 faculty/postdoc, 6 graduate/undergraduate students)*
Investigators report the development of a wavelet-based fractal signature measure that generates an n-dimensional surface, used for classification. Other progress includes the development of two algorithms for combining both color and texture features to assist boundary detection processes and new parametric methods for target detection. Investigators studying image processing for military applications report the development of highly non-linear approximation theoretic techniques, which form the foundation of an "end to end" image processing environment for Automatic Target Detection (ATD).

**Section 2: Chemical and Biological Warfare** *($3,284,649, 6 component projects, 20 faculty/postdoc, 20 graduate/undergraduate students)*
Progress on the development of chemical sensors for nerve agents is reported by the synthesis and electrochemical characterization of several imides. To effectively allow chemical agent analytes to be detected it is necessary to react them with sensing chemistries or indicators. A recently acquired (April 1998) x-ray diffraction system is expected to significantly impact the progress in this program over the next couple of months. Sixteen (16) inventions are reported as having been disclosed to the University of South Carolina from technology developments for chemical detection associated with the project. Primary accomplishments reported for the study of small molecule transport through polymers include the identification of a probe molecule, which can be used to measure viscosity over a nanometer-sized volume. Other progress includes demonstration, for the first time, of the Kerr Effect with Resonant Detection (KERD) which provides significant information on the nanoelasticity of polymers.

**Section 3: Command, Control, and Communications** *($1,512,399, 4 component projects, 17 faculty/postdoc, 11 graduate/undergraduate students)*
Progress in the dynamic decision support for command, control, and communication in the context of tactical defense is reported. Investigators have collected test scenarios and have abstracted salient features that must be considered in the development of the dynamic decision support system. Investigators also report the development or adaptation of algorithms for evaluating reliability of information and accessing the value of missing information. These studies have led to the report of a hybrid algorithm invented to compute marginal and joint beliefs in Bayesian networks. Computer Science faculty studying the problem of developing network management and data transport protocols for multihop wireless networks operating in hostile environments report the development of new UNIX based protocols suited for these environments. These protocols will facilitate high-speed, real-time access and reliable dissemination of intelligence and reconnaissance. Faculty having expertise in basis function optimization using Wavelet theory, optical computation, design and fabrication have collaborated to achieve significant progress in the development of a new optical architecture capable of "instantaneous" image compression. Material scientists striving to develop molecular-sized architectures to push the limits of densely packed computational systems report the synthesis and theoretical testing of several molecular devices. These tests include those to measure the performance of the molecular devices as digital logical gates, the basic units of a molecular central-processor-unit (CPU).

**Section 4: Combat Medicine** *($1,924,001, 3 component projects, 11 faculty/postdoc, 2 graduate/undergraduate students)*
Biology faculty working in collaboration with Walter Reed Army Institute of Research report progress on the international collection of several species of mosquitoes, which are human relevant vectors of the malaria parasite. Progress is also reported on the development of DNA-based diagnostic assays. These studies are expected to contribute to the prevention and control of mosquito born diseases prevalent in areas where US military are stationed. Physicians participating in another combat medicine component project report significant progress in the development of hematopoietic cell transplant protocols. These protocols will be required for transplants needed after exposure to radioactive, chemical, or biological weapons, which result in hematological apalasia or cancer. The high incidence of musculoskeletal injuries reported for Marines, and their related high costs in terms of morbidity, lost training time, and attrition, precipitated a component project to study advanced bio-adhesives for the rapid healing of combat and training injuries to bone. For the present report period investigators involved in these studies report the successful formulation of a self-hardening biocompatible bone paste. The formulation has been characterized using scanning electron microscopy (SEM), infrared spectroscopy and x-ray diffraction. Results of compression tests of the new material are reported, as are preliminary results of the material to support living osteoprogenitor cells.

**Section 5: Anti-Submarine Warfare** *($815,000, 2 component projects, 7 faculty/postdoc, 6 graduate/undergraduate students)*
A cooperative project between computer scientists and mathematicians to study Wavelet based algorithms for acoustic/non-acoustic anti-submarine warfare has yielded impressive results for the detection of submarine wake in Wavelet coefficient space of range-time-intensity plots.

These results combined with algorithm development for automatic target detection and novel methods for surface integration have provided new information for improving the two main detection methods used in tactical anti-submarine warfare, acoustic and non-acoustic. Chemists developing rapid detection techniques to recognize the presence of antrhopogenic hydrocarbons associated with submarine activity report having hired a uniquely qualified postdoc to advance these studies.

**Section 6: Biodeterioration** *($383,251, 1 component project, 5 faculty/postdoc, 11 graduate/undergraduate students)*
Marine scientists report the generation of a range of organic polymer surfaces, the measurement of bacterial attachment to these surfaces and the characterization of microbial communities responsible the formation of biofouling communities. The formation of biofouling communities on deployment devices and sensors and on ship and submarine hulls represents a significant limitation to the efficient operation of instrumentation and vessels.

**Section 7: Supporting Research** *($434,700, 1 component project, 2 faculty/postdoc, 2 graduate/undergraduate students)*
The goal of this research is to define and characterize the factors that influence the speed, accuracy, and precision of the measurement of lead in paint and carbon in steel by a field-portable nondestructive test system. Investigators report that the first task, fabricating a Laser-Induced Breakdown Spectroscopy (LIBS) instrument, is essentially complete. Results are presented from initial studies of reference materials.

# REPORT DOCUMENTATION PAGE

Form Approved
OMB No. 0704-0188



| 1. AGENCY USE ONLY *(Leave blank)* | 2. REPORT DATE | 3. REPORT TYPE AND DATES COVERED |
|---|---|---|
| | **1 June 1998** | **Annual** |

| 4. TITLE AND SUBTITLE | 5. FUNDING NUMBERS |
|---|---|
| **University Research Initiative Program for Combat Readiness** | **Grant: N00014-97-1-0806**<br>**PR: 97PR06312-00** |
| 6. AUTHOR(S)<br>**Jerome D. Odom** | |
| 7. PERFORMING ORGANIZATION NAME(S) AND ADDRESS(ES)<br>**University of South Carolina** | 8. PERFORMING ORGANIZATION REPORT NUMBER<br>**N00014-97-1-0806-1** |
| 9. SPONSORING / MONITORING AGENCY NAME(S) AND ADDRESS(ES)<br>**ONR** | 10. SPONSORING / MONITORING AGENCY REPORT NUMBER<br>**ONR** |
| 11. SUPPLEMENTARY NOTES | |
| 12a. DISTRIBUTION / AVAILABILITY STATEMENT<br>**Approved for public release** | 12b. DISTRIBUTION CODE |

13. ABSTRACT *(Maximum 200 words)*

**The *University Research Initiative for Combat Readiness* includes nineteen (19) research and development projects relevant to combat readiness. Projects being supported by this initiative address six major DoD mission areas including: chemical and biological warfare, target acquisition and identification, anti-submarine warfare, combat medicine, biodeterioration, and command, control, and communications. These projects were selected for support based on an existing research capability that could be accelerated to create cost savings to the ONR by bringing results to the field earlier. For the present report period directors of the individual projects report sixty-three (63) publications in progress, in press, or submitted for publication.**

| 14. SUBJECT TERMS | 15. NUMBER OF PAGES |
|---|---|
| **Target Acquisition and Identification**<br>**Chemical and Biological Defense**<br>**Command, Control, and Communications**<br>**Combat Medicine**<br>**Anti-Submarine Warfare**<br>**Biodeterioration**<br>**Supporting Research** | **223**<br>16. PRICE CODE |

| 17. SECURITY CLASSIFICATION OF REPORT | 18. SECURITY CLASSIFICATION OF THIS PAGE | 19. SECURITY CLASSIFICATION OF ABSTRACT | 20. LIMITATION OF ABSTRACT |
|---|---|---|---|
| **Unclassified** | **Unclassified** | **Unclassified** | **200 Words** |

# LIST OF TECHNICAL PROJECTS

# SECTION 1: TARGET ACQUISITION AND IDENTIFICATION

Office of Naval Research: N00014-97-1-0806
University Research Initiative Program for Combat Readiness

# Wavelet-Based Automatic Target Detection and Recognition

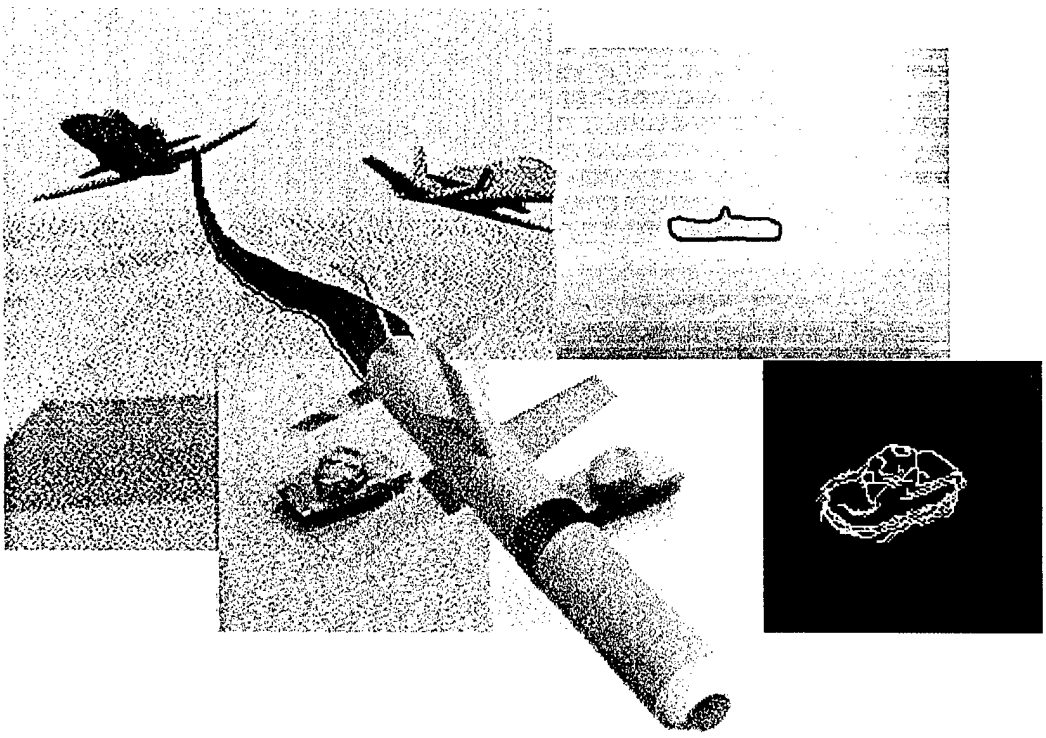

**PI: Terry Huntsberger, PhD**
**Intelligent Systems Laboratory**
**Department of Computer Science**
**University of South Carolina**
**Columbia, SC 29208**
**Ph: (803) 777-2404**
**FAX: (803) 777-3767**
**terry@cs.sc.edu**

**co-PI: Björn Jawerth, PhD**
**Industrial Mathematics Initiative**
**Department of Mathematics**
**University of South Carolina**
**Columbia, SC 29208**
**Ph: (803) 777-6218**
**FAX: (803) 777-3783**
**bj@math.sc.edu**

## Section 1-1: Wavelet-Based Automatic Target Detection and Recognition

Terry Huntsberger, Björn Jawerth

## 1. ABSTRACT

The current down-sizing of DoD manpower has led to the increased reliance on "smart" weapons for effective world-wide tactical response. These systems are based on autonomous and semi-autonomous (man-in-the-loop) techniques for acquisition, identification, targeting, tracking, and damage assessment. During the current contract period we have concentrated on the development of energy minimization methods, FIR/IIR filters, wavelet-based texture features, noise removal, and efficient methods for thermal signature simulation for automatic target detection and recognition.

## 2. FORWARD

This project was funded for $510, 000 for the period June 1, 1997 to May 30, 2000. We have decided to use the SKY Computer system with 4 PowerPCs/36 SHARC DSP chips for the implementation of the algorithms. This decision was made after consideration of Navy needs and examination of the algorithms. The system has been ordered and is to be shipped May 1, 1998. The original Year 1 Milestone was the port of our algorithms to the Intel Paragon system, which was postponed due to system downtime. Accomplishments for this past year, as described in the body of the report, include:

- Demonstrated the utility of the wavelet-based fractal signature for target/clutter discrimination.
- Developed efficient energy minimization methods using the Lattice Boltzmann method for scene segmentation.
- Developed a hardware architecture for scaleable implementation of a wide class of computer vision algorithms.
- Compared wavelet based FIR and IIR filters for compression performance.
- Developed a wavelet-based algorithm that automatically incorporates texture into the compression process.
- Developed efficient wavelet-based algorithms for simulation of infrared target signatures.

## 3. DESCRIPTION of ATTACHMENTS and APPENDICES

None

## 4. BODY

### 4a. Statement of Problem

The problem of decoupling target signatures from background clutter effects lies at the heart of robust ATD/R. Texture measures offer a means of detecting targets in background clutter despite similar spectral characteristics. The "fractal signature" (a feature set based on the fractal surface area function) has previously been shown to be very accurate and robust in multiband texture classification. Extension of this work into a wavelet-based algorithm was recently completed under DARPA funding In addition, operations such as image enhancement can be performed very efficiently in the wavelet coefficient space.

## 4b. Summary of Results

### Wavelet-Based Fractal Signature Analysis for Automatic Target Recognition

We have developed a wavelet-based fractal signature measure that generates an n-dimensional surface, which is used for classification. Besov spaces offer one way to classify functions by their mathematical smoothness, which is very close to our notion of visual smoothness. We build a feature vector using the texture measure returns from the different levels of resolution and orientations in the wavelet detail coefficients for the image subregion for which we are trying to compute a fractal dimension. The low dimensionality of the feature vectors extracted allows for the training of classifiers in relatively short time and with good accuracy.

Our studies with texture mosaics revealed the link between the wavelet-based fractal signature and the smoothness of a texture. Man-made objects such as targets tend to be characterized by linear/angular features which show up well in the wavelet detail channels, thus leading to relatively high values for the signature at every scale. Some examples of the use of the signature for automatic target recognition in two classes of targets with low signal to clutter ratios (SCR) are shown in Figures 1 and 2.

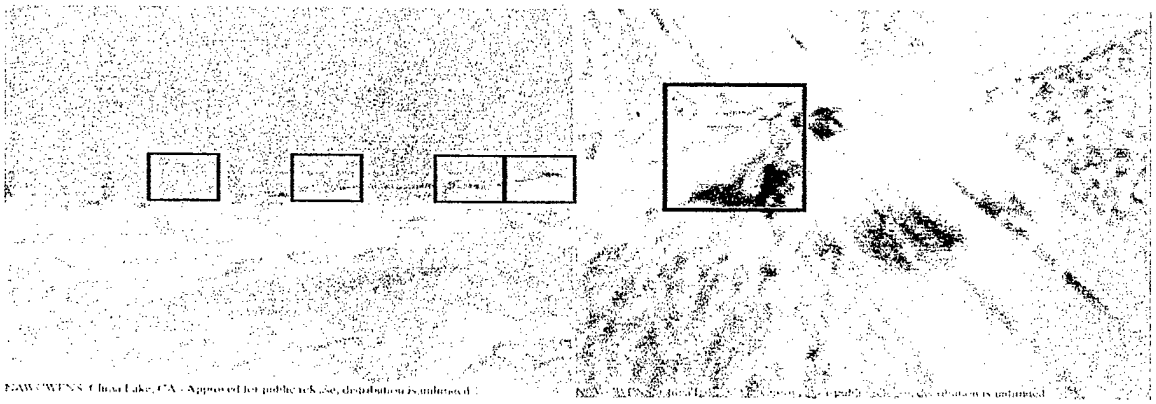

**Figure 1:** ATD for vehicles in thermal images with low SCR (target vehicles are boxed).

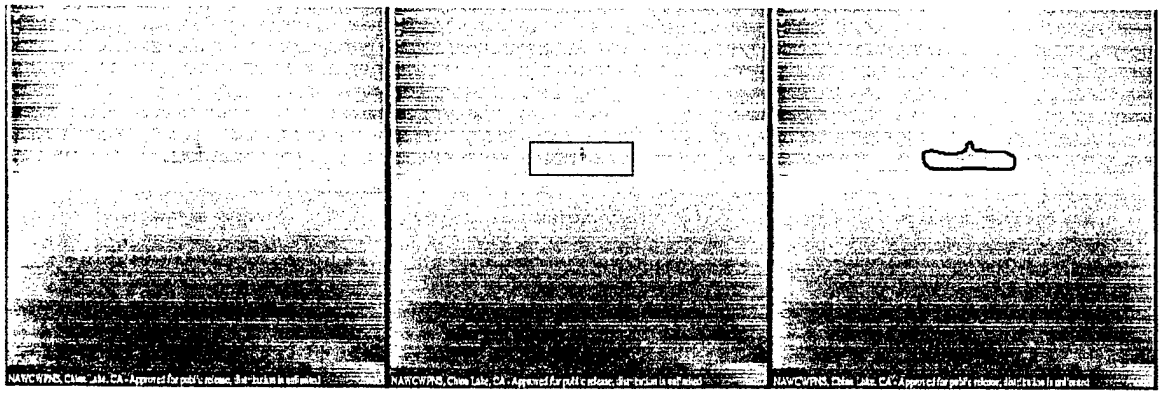

**Figure 2:** ATD/R for ship hidden in "hot horizon" (left image courtesy of China Lake).

### Adaptive Pattern Recognition System for Scene Segmentation

Robust pattern recognition within the Bayesian framework for scene segmentation and boundary detection is oftentimes hampered by the presence of textures within natural images. In

order to improve segmentation/boundary detection on natural images, it is necessary to combine multiple features effectively.

Modeling the image formation process through a discretized system of partial differential equations (PDEs) is one way to address the segmentation and boundary detection problems (JAIN77, JAIN78). We have developed two algorithms for combining both color and texture features to assist boundary detection processes. One combines features through the surface processes and the other through the line processes. The algorithms can be generalized for combining any number of featuresets and can be applied for sensor fusion where each sensor output corresponds to a feature. The region and line detection results from application of this method to the image of a tank in heavily textured background clutter is shown in Figure 3.

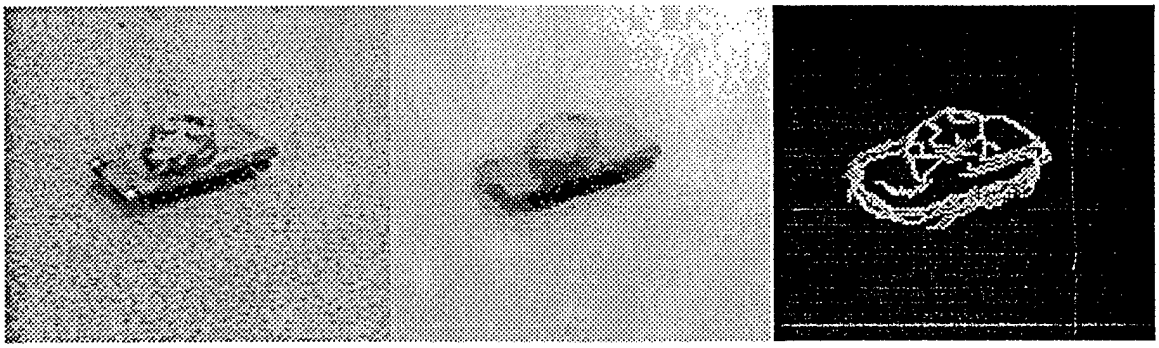

**Figure 3:** Region and line detection results from energy minimization analysis. Left: original; Middle: region; Right: Line.

## An Efficient Line Processing System

Optimization of energy-functionals provides a clear cut and very attractive framework for image segmentation. Based on Mumford and Shah model (MUMF89) for image segmentation, a set of minimizing functionals which incorporate an auxiliary function to determine edges was proposed. By minimizing the functionals, the line processing model can be rewritten as coupled reaction-diffusion equations. The principal advantage of this system, which makes it especially attractive, is that the evolution equations proceed to their stationary limit without the need for a difficult and time-consuming global search to stop the system.

We are using the Lattice Boltzmann model to simulate the improved line processing model based on the Lattice Boltzmann computation of the reaction-diffusion systems. Since the Lattice Boltzmann model is fully parallelizable, we expect a very fast line processing system. We have worked out an algorithm, which still needs to be further refined. This algorithm will be implemented on the SKY Computer SHARC array.

## A Vision System with Real-Time Feature Extractor and Relaxation Network

There are at least two application areas that fast vision systems are important. The first one is for real-time applications. Such systems have to operate at a certain required rate to be useful. Applications include automatic target recognition/tracking, factory inspection, face recognition for security check, and robotics. Each application has different timing requirements. The other area is for algorithm development. Many vision algorithms are computationally intensive and time consuming to run on a sequential computer. As a matter of fact, the amount of computation for new algorithms tends to grow as more powerful microprocessors become available to the research community. Thus, we often find ourselves in the situation where we have to wait for hours to collect the results each time we change the value of one parameter. The research community can benefit greatly from a fast inexpensive general purpose vision system.

Many vision algorithms and vision tasks can be divided into two stages in terms of the characteristics of the computations involved. They are the feature extraction stage and the localized iterative interaction (relaxation) stage. We have developed a system which has a simple pipeline structure suitable for VLSI implementation, and has very small latency and memory requirements compared to an FFT based system. The architecture is general enough so that any types of spatial filters can be implemented on the system. They include Gabor filters, Gaussian filters, difference of Gaussian filters, Canny's edge detector (CANN86), Laws' texture filters (LAWS80), various classes of wavelets (RIOU91), Freeman-Adelson's steerable filters (FREE91), Simoncelli {\it et al} shiftable filters (SIMO92), Watson's cortex transform (WATS87), Marr-Hildreth filters (MARR82), Burt pyramid (BURT89), Young Gaussian derivatives (YOUN87), and Perona deformable kernels (PERO90).

## Autoregressive Texture Segmentation/Synthesis for Wavelet Image Compression

Wavelet based compression is particularly efficient in the compression of smoothly varying regions of image data. It is the discontinuities located between the regions, along with high contrast textured regions, which cause large transform coefficients and erroneous artifacts, such as blurring or starring, at high compression ratios. Region-based techniques potentially facilitate image compression since a homogeneous region of pixels can theoretically be described with a more compact representation than a non-homogeneous one.

We have developed a unique region-based wavelet image compression scheme which synthetically replaces texture data attenuated as a result of the compression process. We perform texture segmentation on an estimated residual image which approximates the information that would be lost at the requested compression ratio. The segmentation process utilizes an estimation-minimization (EM) multi-resolution algorithm which is a modified version of the method proposed in (BOUM91). It identifies image regions which are expected to suffer a significant amount of texture loss and additionally computes the parameters for an autoregressive model for each region of distinct texture. Region-based wavelet compression is performed on the original image using the partitions which result from the segmentation process. We have compared the performance of several texture models, in terms of coding efficiency and texture quality, to the use of standard wavelet compression methods.

## IIR Approximation by FIR Filters

Finite impulse response (FIR) filters have a wide area of applications in image and audio processing. The class of FIR filters is rather narrow (e.g. the inverse of an FIR filter is generally an infinite impulse response filter (IIR)). Although the FIR filters are more versatile, the IIR filters offer generally a greater flexibility in their design (rational vs. polynomial approximation of the transfer function).It would be beneficial to combine the versatility of the FIR filters with the flexibility in the design of the IIR filters by approximating of the later by the former.

Following an approach of Beylkin (BEYL95), we implemented an approximation algorithm that is proposed in the former paper. We are now about to compare the compression performance of the wavelets associated with the FIR filters with the ones associated to the IIR filters.

## Parametric methods for target detection

The problem of finding the targets' types and their locations can be approached using a Jump-Diffusion method based on a Bayesian approach. We have developed a new method by creating the "clever" target generator in the jump process. In the current jump process, a new target and its type are simulated randomly (and depending on the previous target distribution information). In our method, the remainder image is obtained after each diffusion process is performed.

There are two processes involved in the Jump-Diffusion method. First we have the diffusion process in which the number of targets and target types can not be changed; the positions of targets are found using Lanevian stochastic differential equations. Second, we have a jump process in which the number of targets and target types will be changed. We can estimate a new target and its position on purpose by using other image properties, such as moment and curvature features.

## Heat Transfer Simulation Using Overlapping Wavelets

The heat transfer equation can be solved using finite element methods. Use of wavelets in the finite element setting has helped in making the algorithm linear in the number of polygons at the finest level. For complex scenes wavelet based algorithms are still slow, taking up huge amounts of computer memory. Using them for real time application such as tactical simulations requires real time synthesis of images of complex scenes made up of millions of polygons with varying lighting conditions. Towards this goal, we have developed a novel and fast wavelet method for solving the heat transfer equation.

A major advantage of using wavelets is in their property of capturing smooth functions with a minimal number of coefficients. We have found in our ongoing work that most of the kernel coefficients for smooth functions have value zero or near zero for spline wavelet bases. Multiresolution analysis (MRA) of global heat transfer helps in computing only those kernel coefficients that are significant in reproducing the final image. We use biorthogonal spline wavelets as a basis for our MRA framework. Initially each surface is projected with the basis at the coarsest level. The given function is then refined to a finer level if the heat variation over the spatial domain or directional domain is greater than a given threshold. We follow Schröder's method of refinement by sampling basis function at two different sample points at the sender. Christensen's method of coarse integration of the kernel as a check for refinement is used at the receiver. This helps to avoid computation of any additional kernel coefficients which have near zero values. We use standard basis with standard decomposition for our MRA as it is better suited for adaptive subdivision of both spatial and directional components.

## Invariant Face Recognition using Fuzzy Self-Organizing Feature Map

Recognition of objects from a database of objects under varying conditions of such as lighting and orientation is an important problem in computer vision. The specific class of images used in this research was a large database of human faces acquired under varying conditions. Invariance to orientation is achieved using a preprocessing registration phase to normalize input using wavelet coefficients as features. Another important issue in such systems is the learning and recognition overhead. Such characteristics of recognition systems are important in real-time systems. The system being developed uses a combination of wavelet based feature extraction and dimensionality reduction and fast self-organizing feature maps to achieve high speed learning and recall.

The energy compaction properties of the wavelet transform are used in this system to reduce the size of input images to a few pixels. The wavelet coefficients are used as multi-resolution feature detectors in regions of discontinuities. Our systems uses a separate registration phase during both the training and recall processes to normalize the input data so that there in minimal variance in the input to the feature map. The high valued wavelet coefficients at different levels are used to locate key features such as eyes and ears which then form the basis of registration. The reduction in dimensionality afforded by the wavelet transform and the fact that we use a very small subset of the scaling and wavelet coefficients in the recognition process enables us to perform complicated preprocessing and overhead computations. Thus we can remove the effects of affine transformations such as rotations and scales to augment the global translational

invariance that is seen in the DC channel. A certain degree of resilience to noise is supported by the FSOFM.

## 4c. Publications

1. T. Kubota and T. L. Huntsberger, "Edge dipole and edge field for boundary detection," in *Proc. SPIE Conf. Hybrid Image and Signal Processing VI*, Vol. 3389, Orlando, FL, Apr 1998.
2. F. Espinal and R. Chandran, "Wavelet-based fractal signature for texture classification," in *Proc. SPIE Conf. on Wavelet Applications V*, Vol. 3391, Orlando, FL, Apr 1998.
3. T. Kubota and T. L. Huntsberger, "Adaptive pattern recognition system for scene segmentation," *Optical Engineering, Special Section on Advances in Pattern Recognition*, Vol. 37, No. 3, pp. 829-835, 1998.
4. F. Espinal, T. L. Huntsberger, B. Jawerth, and T. Kubota, "Wavelet-based fractal signature analysis for automatic target recognition," *Optical Engineering, Special Section on Advances in Pattern Recognition*, Vol. 37, No. 1, pp. 166-174, 1998.
5. G. Fernandez and T. L. Huntsberger, "Wavelet-based system for recognition and labeling of polyhedral junctions," *Optical Engineering, Special Section on Advances in Pattern Recognition*, Vol. 37, No. 1, pp. 158-165, 1998.
6. T. Kubota, T. L. Huntsberger and C. O. Alford, "A vision system with real-time feature extractor and relaxation network," to appear in *Int. Journal Pattern Recognition and Artificial Intelligence*, May 1998.
7. T. L. Huntsberger and J. Rose, "Computer Simulation of Bimodal Neurons and Networks: Integrating Infrared and Visual Stimuli," chapter in Computer Simulation of Complex Biological Systems, (Ed. I. S. Iyengar), CRC Press, 1998.
8. T. L. Huntsberger, "Autonomous multirover system for complex planetary retrieval operations," in *Proc. SPIE Symposium on Sensor Fusion and Decentralized Control in Autonomous Robotic Agents*, Vol. 2905, Pittsburgh, PA, Oct 1997, pp. 11-17.
9. B.D. Jawerth, P. Lin, and E.D. Sinzinger, "Lattice Boltzmann methods for anisotropic diffusion of images", *Mathematical Imaging*, in review.
10. K. Debure and T. Kubota, "Autoregressive Texture Segmentation and Synthesis for Wavelet Image On Compression", 10th Image and Multidimensional Digital Signal Processing Workshop, July 1998, Austria.
11. S. Godavarthy and T. L. Huntsberger, "Global illumination using Overlapping Wavelets", Proc. 8th International Conference on Engineering Computer Graphics and Descriptive Geometry (ICECGDG), Aug 1998, Austin, TX.

## 4d. Personnel

| | |
|---|---|
| PI: | Dr. Terry Huntsberger |
| co-PI: | Dr. Björn Jawerth |
| Research Associates: | Dr. Toshiro Kubota |
| | Dr. Weimin Zheng |
| | Dr. Peng Lin |
| | Fausto Espinal |
| | Srinadh Godavarthy |
| | Rajesh Chandran |
| | Ognian Voynikov |
| | Henrik Storm |
| | Goran Kronquist |

## 5. LIST of INVENTIONS

None

## 6. BIBLIOGRAPHY

[BEYL95] G. Beylkin "On factored FIR approximation of IIR filters", *Applied and Computational Harmonic Analysis*, Vol. 2,pp 293-298, 1995

[BOUM91] C. Bouman and B. Liu, "Multiple resolution segmentation of textured images", *IEEE Trans. Pattern Recog. and Machine Intel.*, Vol. 13, pp. 259-302, 1991.

[BURT89] P. J. Burt, "Multiresolution techniques for image representation analysis, and 'smart' transmission", *Proc. SPIE Conf. on Visual Communication and Image Processing,* pp. 2-15, 1989.

[CANN86] J. F. Canny, "A computational approach to edge-detection", *IEEE Trans. on Pattern Analysis and Machine Intelligence*, Vol. 8, pp. 679-700, 1986.

[FREE91] W. T. Freeman and E. H. Adelson, "The design and use of steerable filters", *IEEE Trans. Pattern Analysis and Machine Intel.*, Vol. 13, pp. 401-412, 1991.

[JAIN77] A. K. Jain, "Partial differential equations and finite difference methods in image processing-Part I: Image representation", *J. Optimiz. Theory and Applications*, Vol. 23, pp. 65-91, 1977.

[JAIN78] A. K. Jain and J. R. Jain, "Partial differential equations and finite difference methods in image processing-Part II: Image restoration", *IEEE Trans. on Automatic Control*, Vol. 23, pp. 596-613, 1978.

[LAWS80] K. I. Laws, "Rapid texture identification", *Proceedings of SPIE*, Vol. 238, pp. 376-380, 1980.

[MARR82] D. Marr, Vision, W. H. Freeman and Company, San Francisco, CA. 1982.

[MUMF89] D. Mumford and J. Shah, "Optimal approximation by piecewise smooth functions and associated variational problems", *Communications on Pure and Applied Mathematics*, pp. 577-685, 1989.

[PERO90] P. Perona and J. Malik, "Scale-space and edge detection using anisotropic diffusion", *IEEE Trans. Pattern Analysis and Machine Intel.*, Vol. 12, pp. 629-639, 1990.

[RIOU91] O. Rioul and M. Vetterli, "Wavelets and signal processing", *IEEE Signal Processing Magazine*, pp. 14-38, Oct 1991.

[SAIT96] N. Saito and R. R. Coifman, "Improved Local Discriminant Bases using empirical probability density estimation, in *Proc. Conf. on Statistical Computing*, American Statistical Assoc., 1996.

[SIMO92] E. P. Simoncelli, W. T. Freeman, E. H. Adelson and D. J. Heeger, "Shiftable multiscale transforms", *IEEE Trans. on Information Theory*, Vol. 38, pp. 587-607, 1992.

[WATS87] A. B. Watson, "The cortex transforms: rapid computation of simulated neural images", *Computer Vision, Graphics, and Image Processing*, Vol. 39, pp. 311-327,1987.

[YOUN87] R. A. Young, "The gaussian derivative model for spatial vision: I. Retinal mechanism", *Spatial Vision*, Vol. 2, pp. 273-293, 1987.

| REPORT DOCUMENTATION PAGE | Form Approved OMB No. 0704-0188 |
|---|---|



| 1. AGENCY USE ONLY *(Leave blank)* | 2. REPORT DATE | 3. REPORT TYPE AND DATES COVERED |
|---|---|---|
| | 1 June 1998 | Annual |

| 4. TITLE AND SUBTITLE | 5. FUNDING NUMBERS |
|---|---|
| Wavelet-Based Automatic Target Detection and Recognition | Grant: N00014-97-1-0806<br>PR: 97PR06312-00 |
| 6. AUTHOR(S)<br>PI: Terry Huntsberger, co-PI: Björn Jawerth | |
| 7. PERFORMING ORGANIZATION NAME(S) AND ADDRESS(ES)<br>University of South Carolina | 8. PERFORMING ORGANIZATION REPORT NUMBER<br>N00014-97-1-0806-1 |
| 9. SPONSORING / MONITORING AGENCY NAME(S) AND ADDRESS(ES)<br>ONR | 10. SPONSORING / MONITORING AGENCY REPORT NUMBER<br>ONR |

11. SUPPLEMENTARY NOTES
Prepared in coordination with University Research Initiative Program for Combat Readiness

| 12a. DISTRIBUTION / AVAILABILITY STATEMENT | 12b. DISTRIBUTION CODE |
|---|---|
| APPROVED FOR PUBLIC RELEASE | |

13. ABSTRACT *(Maximum 200 words)*

The current down-sizing of DoD manpower has led to the increased reliance on "smart" weapons for effective world-wide tactical response. These systems are based on autonomous and semi-autonomous (man-in-the-loop) techniques for acquisition, identification, targeting, tracking, and damage assessment. During the current contract period we have concentrated on the development of energy minimization methods, FIR/IIR filters, wavelet-based texture features, noise removal, and efficient methods for thermal signature simulation for automatic target detection and recognition.

| 14. SUBJECT TERMS | 15. NUMBER OF PAGES |
|---|---|
| Automatic Target Recognition, Wavelets | 8 |
| | 16. PRICE CODE |

| 17. SECURITY CLASSIFICATION OF REPORT | 18. SECURITY CLASSIFICATION OF THIS PAGE | 19. SECURITY CLASSIFICATION OF ABSTRACT | 20. LIMITATION OF ABSTRACT |
|---|---|---|---|
| UNCLASSIFIED | UNCLASSIFIED | UNCLASSIFIED | 200 words |

# Wavelet Based Image Processing for Military Applications

Ronald A. DeVore, PI

Department of Mathematics
University of South Carolina
Columbia, SC 29208

Tel: 803-777-2632
Fax: 803-777-6527
Email: devore@math.sc.edu

## Section 1-2: Wavelet based Image Processing for Military Applications

Ronald A. DeVore

### ABSTRACT

The Principal Investigator, Ronald A. DeVore, and other researchers at USC's Department of Mathematics, are developing wavelet based image processing for automated target recognition and related military applications including autonomous landing of aircraft, registration of images from a database, and identification of cracks in skin of aircraft.

The goal of this research is to substantially reduce imaging times for signal, image, and graphical databases which will enable the real-time processing of images for the purposes of image registration and feature extraction. An "end-to-end" image processing environment for these applications is being created by developing fast wavelet based algorithms for the generic problems of image compression, denoising, feature extraction and pattern recognition, image registration and correlation, path tracking, and motion detection.

The research takes advantage of recent developments in wavelet research including local time-frequency decompositions based on adaptive basis selection and greedy algorithms; nonlinear algorithms for compression and noise removal derived from functional analytic extremal problems; customized encoders; and the integration of neural networks into the wavelet framework.

Wavelet based multiscale methods were emphasized since they provide a uniform platform for the various tasks. Nonlinear and highly nonlinear methods have been developed for these tasks using recent advances of the researchers at USC in the areas of nonlinear wavelet approximation. This includes greedy algorithms, adaptive basis selection, and adaptive pursuit. Emphasis was placed on fast algorithms which can be implemented in real time scenarios.

### FORWARD

The first year project was supported from July 1, 1997 through June 30, 1998 at a level of $146,000, with a total three year budget of $440,001. Basic research on Automatic Target Detection was performed with significant advances made on noise removal and feature extraction. This includes:

- developing wavelet based methods to solve extremal problems for noise reduction
- development of highly nonlinear methods (greedy algorithms) for feature extraction.

## REPORT

### *Statement of Problem Studied*

The goal of this research is to develop an "end-to-end" image processing environment to handle in real time the generic tasks encountered in Automated Target Detection (ATD) and related military applications. The research undertaken includes the derivation of complementary theory and algorithms for automated target detection, rapid retargeting, the registration of digitized images, rapid data querry, and data navigation.

### *Summary of Most Important Results*

Major advances were made during Year 1 of this grant through the development of highly nonlinear approximation theoretic techniques which form the foundation of an "end to end" image processing environment for Automatic Target Detection (ATD). These advances provide direct applications to advanced data compression algorithms, noise removal, feature extraction/registration, greedy algorithms, adaptive pursuit, and neural networks, brief descriptions of which are provided below. This project collaborated with the Naval Air Warfare Center (NAWC) through a workshop at Patuxent River on wavelet based methods for automated target detection and by a return visit of research assistants for more intense collaboration.

### Image Processing

Entropy encoding and compression. Compression is a vital component of Automatic Target Recognition (ATR), providing real time communication of images and serving as a preprocessor to other image processing tasks. We have used nonlinear wavelet approximation in our past work to design compression algorithms for images and signals. More recently, we have collaborated with Cohen (Paris VI), Daubechies (Princeton), and Dahmen (RWTH Aachen) [CDDD] to design tree based encoders which have optimal compression properties. The advantage of the tree based algorithm is that more structure results in the encoded file which allows not only high compression but provides a platform for progressive transmission of the image. In other words, a coarse resolution of the image is followed by finer and finer detail. This platform also allows for local refinement ("burning in" to find finer detail in selected localized regions of the image).

Image processing using statistical characteristics. Several optimization problems occur in noise removal. One such extremal problem consists of finding minimizers for the $K$-functional for $L_2$ and BV (functions of bounded variation). Techniques for finding minimizers for this functional based on variational calculus and nonlinear partial differential equations have been put forward by several authors (most notably [DMS], [LOR], [MS], [CL]). The main disadvantage of these approaches is that they are numerically intensive. In [CDPX], we prove the surprising result that wavelet thresholding is a minimizer for the K-functional. The proof is deep and depends on a new adaptive algorithm for nonlinear piecewise constant approximation. Our analysis of this extremal problem exposes many interesting properties of Haar decompositions in the space BV. We are now numerically implementing these ideas.

Feature extraction and registration. In [DLY], we previously developed wavelet based methods for extracting microcalcification clusters in mammograms. These techniques utilize image

enhancement, very high compression for noise suppression, and pixel enhancement. Using similar ideas, we have developed in [D et al.] wavelet methods for image registration. The method identifies a few hot pixels in the image and registers two images by hot pixels matching. The software implementation currently applies only to images, which are affine transformations of one another, but other transformations are being investigated.

**Nonlinear Approximation**

In our previous work, ideas from nonlinear approximation have provided fundamental insight and advances to several different areas, including image processing, nonlinear PDE's, function spaces, and statistics. Our current interest is focused on highly nonlinear approximation, which includes approximation from libraries (families) of bases and dictionaries (redundant systems).

Greedy algorithms and adaptive pursuit. Adaptive pursuit from a dictionary of functions is used frequently in feature extraction. We analyze the theoretical advantages and disadvantages of these highly nonlinear methods. Our main goal is to construct simple and efficient algorithms which provide near best $m$-term approximation. DeVore and Temlyakov [DT], [DT1], [T], [T1], [T3], [T4], have analyzed the problem in various different settings. Temlyakov [T] proves that greedy type algorithms realize near best $m$-term approximation in $L_p$, $1 < p < \infty$ , from the multivariate Haar system and other systems equivalent to the Haar system. In [T3], it is shown, however, that this is not valid for the trigonometric system, nevertheless, the greedy algorithm realizes the best $m$-term approximation for wide variety of function spaces. In fact, DeVore and Temlyakov [DT] have established a universal estimate for the accuracy of the greedy algorithm. In [T1] a sufficient condition on dictionaries is provided, which guarantees that the greedy algorithm gives the order of the best approximation.

Restricted nonlinear approximation. We have recently considered restricted nonlinear wavelet approximation since it appears naturally in image processing, and in particular noise reduction. Cohen, DeVore, and Hochmuth [CDH] characterize the approximation spaces for restricted nonlinear $n$-term wavelet approximation. The results provide the basis to establish theorems about interpolation of Besov spaces, which required the development of new techniques for nonlinear wavelet approximation.

Kolmogorov' widths. Temlyakov [T3] investigates a generalization of Kolomogorov's width that is suitable for estimating best $m$-term approximation. He generalizes Carl's inequality, which gives a lower bound estimate for Kolmogorov's widths in terms of the entropy numbers. Some relations between best $m$-term approximation and the entropy numbers are also given in [DT].

**Neural Networks**

Neural networks are frequently used in statistical decision theory, classification, and feature extraction. Our main goal in this research is to understand their advantages over more traditional numerical methods. In [DOP], DeVore, Oskolkov, and Petrushev proved the first tight theorems on linear approximation by neural networks. An interesting fact was discovered that the feed-forward neural network with one hidden layer of computational nodes given by the unit impulse

function has efficiency of approximation $O(n^{-3/2})$ in two dimensions. Petrushev [P] generalized this result to arbitrary space dimension. New areas and techniques were developed and uitilized. These include (a) the Radon transform, (b) orthogonal decomposition of a general function into ridge polynomials, (c) quadrature formulas on the sphere exact for spherical polynomials of degree $n$.

Oskolkov [O], [O1] elaborates Radon-Fourier analysis with special emphasis on comparison of free (nonlinear) and equispaced ridge approximation. He established exact duality relations of the problem of ridge approximation and optimization of quadrature formulas. This interpretation enabled him [O], in particular, to obtain lower estimates of free ridge approximation via equispaced one for radial functions. A new and unexpected result was recently proved by Oskolkov [O1] in this direction for harmonic functions. It turns out that freedom in the choice of the wave vectors in unconstrained ridge approximation brings a quite essential gain in the orders of approximation. For each fixed harmonic function, free ridge approximations are "square times" more efficient than equispaced ones, with the same admissible number of wave vectors along a parallel path, a new effect of collapsed nodes in optimization of quadrature formulas was discovered. The highest harmonic in a bound limited signal (trigonometric polynomial) can be recovered with high accuracy even in conditions of an essential deficiency of point values of the signal.

The results of DeVore and Temlyakov [DT1] on greedy algorithms also have strong implications for nonlinear neural networks.

***Publications and Technical Reports***

**Papers in Print**

[DSPKLC] R. DeVore, W. Shao, J. F. Pierce, E. Kaymaz, B. Lerner, and W. J. Campbell, *Using nonlinear wavelet compression to enhance image registration*, SPIE, Vol. 3078, Orlando, FL (1997).

[DOP] R. DeVore, K. Oskolkov, and P. Petrushev, *Approximation by feed-forward neural networks*, Ann. Numer. Math. **14** (1997), 261-287.

[DT] R. DeVore and V. Temlyakov, *Nonlinear approximation in finite-dimensional spaces*, J. Complexity **13** (1997), 489-508.

[O] K. Oskolkov, *Ridge approximation, Chebyshev-Fourier analysis and optimal quadrature formulas*, Proc. Steklov Inst. Math. **219** (1997), 269-285.

**Papers in Press**

[P] P. Petrushev, *Approximation by Ridge Functions and Neural Networks*, SIAM J. Math. Anal., to appear.

[T] V. Temlyakov, *The best m-term approximation and greedy algorithm*, Advances in Comp. Math., to appear.

[T1] V. Temlyakov, *Nonlinear m-term approximation with regard to the multivariate Haar system*, East J. on Approximations, to appear.

[T2] V. Temlyakov, *Nonlinear Kolmogorov's widths*, Math. Notes, to appear.

[T3] V. Temlyakov, *Greedy algorithm and m-term trigonometric approximation*, Constructive Approximation, to appear.

**Papers Submitted**

[CDH] A. Cohen, R. DeVore, and R. Hochmuth, *Restricted nonlinear approximation*, preprint.

[CDPX] A. Cohen, R. DeVore, P. Petrushev, and H. Hu, *Nonlinear approximation and the space* BV($R^2$), preprint.

[CDDD] A. Cohen, W. Dahmen, I. Daubechies, and R. DeVore, *Tree approximation with applications to encoding and Kolmogorov entropy*, preprint.

[O1] K. Oskolkov, *Non-linear versus linearity in ridge approximation*, preprint.

[T4] V. Temlyakov, *Greedy algorithms and m-term approximation with regard to redundant dictionaries*, preprint.

## BIBLIOGRAPHY

[B] A. Barron, *Universal approximation bounds for superposition of sigmoidal functions*, IEEE Transactions on Information Theory **39** (1993), 930-945.

[CL] A. Chambolle and P.-L. Lions, *Image recovery via total variation minimization and related problems*, Numerische Mathematik **76** (1997), 167-188.

[DLY] R. DeVore, B. Lucier, and Z. Yang, *Feature extraction in digital mammography*, Wavelets in Biology and Medicine (Akram Aldroubi and Michael Unser, eds.), CRC, Boca Rotan, Florida (1996), 145-161.

[DMS] G. Dal Maso, J.-M. Morel and S. Solimini, *A variational method in image segmentation: existence and approximation results*, Acta Math. **168** (1992), 89-151.

[DT1] R. DeVore and V. Temlyakov, *Some remarks on greedy algoritihms*, Advances in Computational Math. **5** (1996), 173-187.

[LOR] P.-L. Lions, S. Osher, and L. Rudin, *Denoising and deblurring using constrained nonlinear partial differential equations*, SIAM J. Numer. Anal., to appear.

[MS] D. Mumford and J. Shah, *Boundary detection by minimizing functionals*, Proc. of IEEE Conf. on Computer Vision and Pattern Recognition, IEEE, 1985, pp. 22-26.

# REPORT DOCUMENTATION PAGE

Form Approved
OMB No. 0704-0188



| 1. AGENCY USE ONLY *(Leave blank)* | 2. REPORT DATE | 3. REPORT TYPE AND DATES COVERED |
|---|---|---|
| | June 1, 1998 | Annual |

4. TITLE AND SUBTITLE

Wavelet Based Image Processing for Military Applications

5. FUNDING NUMBERS

Grant Number N00014-97-1-0806
PR Number 97PR06312-00
PO Code 353
Disbursing Code N68892
AGO Code N66020
Cage Code 4B489

6. AUTHOR(S)

Ronald A. DeVore

7. PERFORMING ORGANIZATION NAME(S) AND ADDRESS(ES)

University of South Carolina

8. PERFORMING ORGANIZATION REPORT NUMBER

N00014-97-1-0806-1

9. SPONSORING / MONITORING AGENCY NAME(S) AND ADDRESS(ES)

ONR

10. SPONSORING / MONITORING AGENCY REPORT NUMBER

ONR

11. SUPPLEMENTARY NOTES

Prepared in coordination with University Research Initiative Program for Combat Readiness

12a. DISTRIBUTION / AVAILABILITY STATEMENT

APPROVED FOR PUBLIC RELEASE

12b. DISTRIBUTION CODE

13. ABSTRACT *(Maximum 200 words)*

Research was conducted on fundamental problems related to Automated Target Recognition (ATR). Immediate applications include the image processing tasks of compression, noise reduction, feature extraction, image registration, and target identification. Wavelet based multiscale methods were emphasized since they provide a uniform platform for the various tasks. Nonlinear and highly nonlinear methods have been developed for these tasks using recent advances of the researchers at USC in the areas of nonlinear wavelet approximation. This includes greedy algorithms, adaptive basis selection and adaptive pursuit. Emphasis was placed on fast algorithms which can be implemented in real time scenarios.

14. SUBJECT TERMS

Chemical and Biological Warfare, Target Acquisition, Anti-
Submarine, Combat Medicine, Biodeterioration, and Command
Control and Communication

15. NUMBER OF PAGES

8

16. PRICE CODE

| 17. SECURITY CLASSIFICATION OF REPORT | 18. SECURITY CLASSIFICATION OF THIS PAGE | 19. SECURITY CLASSIFICATION OF ABSTRACT | 20. LIMITATION OF ABSTRACT |
|---|---|---|---|
| Unclassified | Unclassified | Unclassified | 200 Words |

# SECTION 2: CHEMICAL AND BIOLOGICAL DEFENSE

# Line-of-Sight Standoff Identification of Explosive Chemicals and Chemical Warfare Agents

S. Michael Angel, M.L. Myrick

Department of Chemistry & Biochemistry
The University of South Carolina
Columbia, SC 29208

Tel: (803) 777-2779
Fax: (803) 777-9521
Email: angel@psc.sc.edu, myrick@psc.sc.edu

# Section 2-1: Line-of-Site Standoff Identification of Explosive Chemicals and Chemical Warfare Agents

S.M. Angel, M.L. Myrick

## ABSTRACT

This work is divided into two main areas: 1) development of the technology for optical detection and identification of chemical agents using absorbance/reflectance spectroscopy in the NIR/MID spectroscopic regions, combined with optical computation pattern recognition. 2) demonstration of a standoff instrument for identification of dangerous chemicals using a small-footprint Raman spectrometer with an LCTF, and demonstrate the use of an LCTF for NIR measurements using star light as a source. Dr. Myrick's research group is performing work in the first area while Dr. Angel's research group is carrying out the latter area. In the first area, selection of chemical agent simulants has been performed; instrumentation for recording the NIR and MIR spectroscopic signatures of simulants has been purchased, as has the software necessary for pattern recognition using linear multivariate methods. Software to design optical elements incorporating these patterns has been obtained, and the hardware necessary for its implementation is presently under contract, with delivery scheduled in June, 1998. In the second area, the LCTF instrument has been purchased and is currently being debugged, and the small footprint Raman system has been tested for standoff operation. Arrangements have been made to do remote Raman and NIR measurements using The University of Hawaii Institute of Geophysics mobile LIDAR system.

## FORWARD

The purpose of the first project area is to develop the technology for optical detection and identification of chemical agents using absorbance/reflectance spectroscopy in the NIR/MID spectroscopic regions combined with optical computation pattern recognition. The purpose of the second project area is to develop and test instruments for standoff identification of explosives and CW agents using laser-induced remote Raman spectroscopy, as well as NIR absorption using star light as a source. The unique aspect of each system is the use of an LCTF for spectral discrimination, and fiber-optically coupling the optics and detection system.

## REPORT

### *Summary of the Most Important Results*

**Area 1** (This work is being performed by Dr. Myrick's research group)

The tasks we expect to face during this project are to (a) hire a post-doctoral assistant for the project, (b) purchase the equipment and software necessary for all the computation

and construction tasks that follow, (c) select chemicals that will serve as simulants of chemical agents and as model interferents, (d) record optical spectra of these agents in the gas phase in the NIR spectral region in the presence of atmospheric gases and particulate matter, (e) correlate these spectra with concentrations of the agents using multivariate modeling methods, (f) extract linear combinations of principal spectroscopic factors (principal components) that correlate with the agent concentrations (i.e., regression vectors), (g) mathematically synthesize a multilayer dielectric structure that models the regression vector, (h) model the behavior of an optical system using the projected dielectric structure, (i) refine the system mathematically if necessary, (j) construct a multilayer dielectric filter according to the synthesized design, (k) evaluate the performance of the filter, and (l) estimate the analytical usefulness of this procedure for passive monitoring.

The first task has been the most troublesome to date: we identified a post-doctoral candidate (Glenn Fried of New Mexico State University), but he accepted a position with a national laboratory. A second post-doc (Dr. Pramod Khulbe) was identified and hired. Part of whose duties were to begin this research project. Dr. Khulbe remained with us for two months, at the end of which he accepted a position at Arizona State University. Consequently we have struggled to obtain the necessary personnel to advance this project at the rate we would like. We presently have another candidate scheduled to arrive and begin work in mid-May, 1998, half of their duties being to serve this project.

The second task has been completed. A NIR/MIR instrument (Mattson Infinity FT-NIR/FT-MIR) with a gas cell, software (TF-Calc from SpectraSoft, Inc. for interference-filter synthesis and Matlab 5.0 for multivariate analysis), and a dielectric deposition system were ordered. The first NIR/MIR was received early in 1998, while the software was received in late 1997. The deposition system is funded by a separate project, and is due for delivery in June, 1998 (approximately 3 months were spent in bidding and selecting the instrument, and delivery was originally scheduled for 120 days from the date of ordering. However, the manufacturer has since postponed the mid-April delivery date until June).

The third task, selection of simulants and obscurants, is complete. We began the task by considering the chemical structures of common nerve agents. A variety of commercially available phosphonate-type molecules were selected for review. After consultation with Dr. Jack Dermigan of Argonne National Laboratory, we have selected diisopropyl methyl phosphonate (DIMP) and dimethyl methyl phosphonate (DMMP) as optical simulants of nerve agents. As obscurants (in addition to normal atmospheric gases) we have selected methanol and isopropanol, the latter of which occurs in binary chemical weapons but which has a relatively weak spectroscopy. The structures of these chemicals are shown below in comparison to Sarin, the most similar of the "top four" nerve agents:

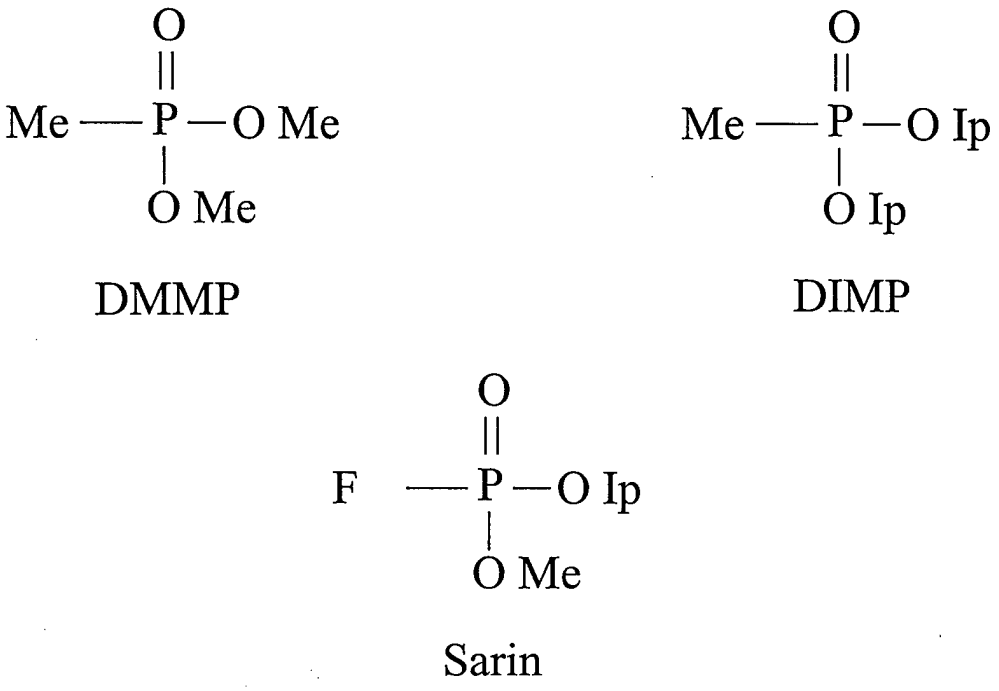


*Figure 1: Structures of DMMP and DIMP (simulants) and the nerve agent Sarin (O-isopropyl methylphosphonofluoridate)*

These simulants have some similar structure (and consequently vibrational spectroscopy) to Sarin and other organophosphonates, but lack the toxicity of the others because they lack the easily removed subunit of the nerve agents. In the case of Sarin, this group is the Fluorine atom, which can be displaced by the active serine residue in the acetylcholinesterase enzyme.

The remaining tasks have yet to be fulfilled, but should be advanced rapidly upon hiring a post-doc for this project. The procedures for the remaining tasks are straightforward in principle. All the remaining steps are outlined in our recent publications "Multivariate Optical Computation for Predictive Spectroscopy" and "Design of Thin Film Filters for the Monitoring of Chemical Reactions".

**Area 2:** (This work is being performed by Dr. Angel's research group)
The tasks we expect to face during this project are to (a) obtain a student or students to work on the project, (b) purchase the equipment and software necessary for integrating the LCTF into Raman spectral acquisition software, (c) build the portable LCTF imaging Raman spectrometer, (d) test the Raman system for measuring spectra remotely using compounds of known Raman cross section for comparison with Raman cross sections of CW agents and explosives, (e) field test the system at a suitable site that will allow long-range tests to be carried out safely, and (g) attach the LCTF to a small telescope and measure NIR spectra using star light, (h) determine the sensitivity of this technique, and (i) estimate the analytical usefulness of both procedures for active and passive monitoring.

Tasks: (a) Two graduate students are currently working part-time on this project. (b) the LCTF has been delivered and is still being debugged. There are still problems with the software that was delivered with the device. However, preliminary experiments show that the resolution of the device is sufficient, ~0.25 nm, to acquire high-quality Raman spectra (see Figure 2). We have obtained and tested a suitable portable Raman spectrometer, Kaiser Holospec f/1.8 with attached fiber-optic probe. In preliminary tests using a collimated beam from the fiber the sensitivity of this instrument looks very good. Figure 3 shows Raman spectra of $TiO_2$ measured at 1 ft and at 60 ft with this system and using about 300 mW of laser power. (e) We have an invitation to perform field tests of our completed systems with Professor Shiv Sharma of the Institute of Geophysics at the University of Hawaii. This group has considerable experience with Raman Lidar and has a mobile spectroscopy laboratory with a large telescope and laser that can be used for our field tests. A short field test is expected some time during the summer. The tests would be completed next Spring.

The remaining tasks have not yet been completed.

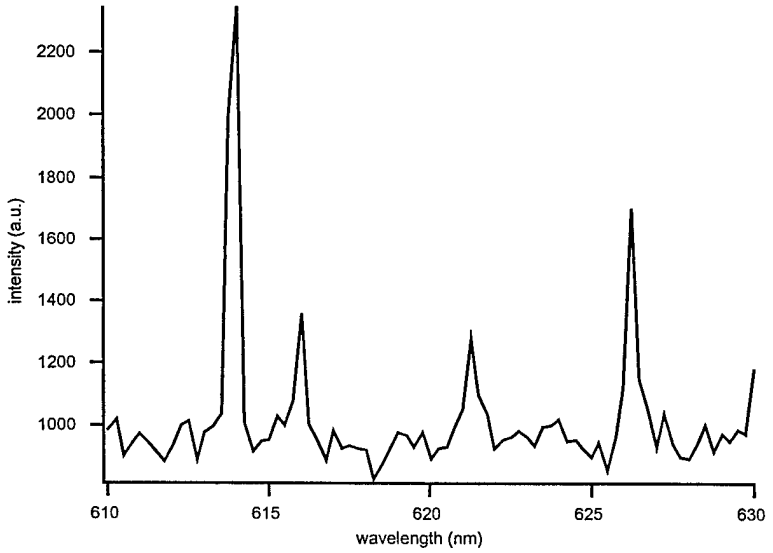


*Figure 2: Low-pressure neon lamp emission spectrum measured by scanning the LCTF in 0.25 nm increments.*

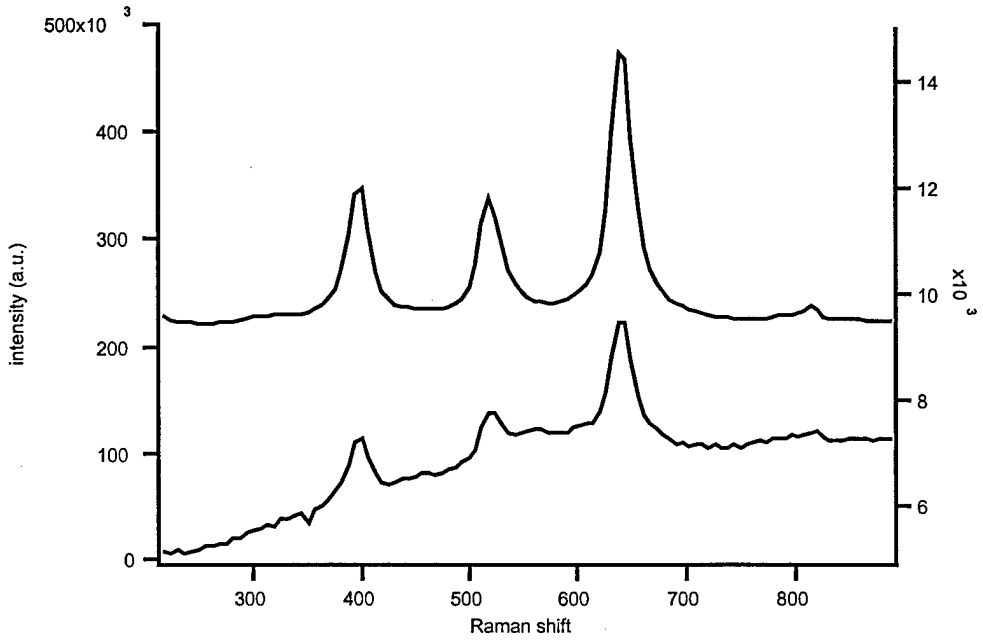


*Figure 3: Raman spectrum of TiO2 measured at 60 ft (bottom) versus 1 ft (top) using the Kaiser f/1.8 Holospec with a ~1-cm diameter collimated laser beam from a fiber-optic probe.*

***Area 1: Publications and Technical Reports***

"Design of Thin Film Filters for the Monitoring of Chemical Reactions". J..A. Dobrowolski, P.G. Verly, J.F. Aust, M.P. Nelson and M.L. Myrick, in Proceedings of the SPIE Annual Meeting on Optical Science and Engineering, San Diego, California, July, 1997 (in press, 1998).

"Single-Shot Multiwavelength Imaging of Laser Plumes". M.P. Nelson, W.C. Bell, M.L. McLester, and M.L. Myrick, *Appl. Spectrosc.* 52(1998), 179.

"Multivariate Optical Computation for Predictive Spectroscopy". M.P. Nelson and M.L. Myrick, *Anal. Chem.* 70(1998), 73.

"Single-Shot Multiwavelength Imaging of Laser Plumes". M.P. Nelson, W.C. Bell, M.L. McLester, and M.L. Myrick, presented at Pittsburgh Conference, New Orleans, LA, Mar 1-6, 1998.

"Multivariate Optical Computation for Predictive Spectroscopy". M.L. Myrick, M.P. Nelson, J.F. Aust, J.A. Dobrowolski, and P.G. Verly, presented at Pittsburgh Conference, New Orleans, LA, Mar 1-6, 1998.

***Area 2: Publications and Technical Reports***

None yet published.

***Area 1: Personnel***

Matthew P. Nelson, graduate assistant (3 months)
Dr. Pramod Khulbe, post-doctoral associate ( 1/2 time, 3 months)

***Area 2: Personnel***

Chance Carter, graduate assistant (half time)
Dimitra Strais (half time)

Area 1: *No inventions or attachments*

Area 2: *No inventions or attachments*

# REPORT DOCUMENTATION PAGE

Form Approved
OMB No. 0704-0188



| 1. AGENCY USE ONLY *(Leave blank)* | 2. REPORT DATE | 3. REPORT TYPE AND DATES COVERED |
|---|---|---|
| | June 1, 1998 | Annual |

**4. TITLE AND SUBTITLE**

Line-of-Sight Standoff Identification of Explosive Chemicals and Chemical Warfare Agents

**5. FUNDING NUMBERS**

Grant Number N00014-97-1-0806
PR Number 97PR06312-00
PO Code 353
Disbursing Code N68892
AGO Code N66020
Cage Code 4B489

**6. AUTHOR(S)**

S. Michael Angel & Michael L. Myrick

**7. PERFORMING ORGANIZATION NAME(S) AND ADDRESS(ES)**

University of South Carolina

**8. PERFORMING ORGANIZATION REPORT NUMBER**

N00014-97-1-0806-1

**9. SPONSORING / MONITORING AGENCY NAME(S) AND ADDRESS(ES)**

ONR

**10. SPONSORING / MONITORING AGENCY REPORT NUMBER**

ONR

**11. SUPPLEMENTARY NOTES**

Prepared in coordination with University Research Initiative Program for Combat Readiness

**12a. DISTRIBUTION / AVAILABILITY STATEMENT**

APPROVED FOR PUBLIC RELEASE

**12b. DISTRIBUTION CODE**

**13. ABSTRACT** *(Maximum 200 words)*

Selection of chemical agent simulants has been performed; instrumentation for recording the NIR and MIR spectroscopic signatures of simulants has been purchased, as has the software necessary for pattern recognition using linear multivariate methods. Software to design optical elements incorporating this patterns has been obtained, and the hardware necessary for its implementation is presently under contract, with delivery scheduled in June, 1998. Instrumentation for spectroscopic imaging of explosives and simulants has been purchased and is currently being debugged. Arrangements have been made to do remote Raman and NIR measurements using The University of Hawaii Institute of Geophysics mobile LIDAR system. A small-footprint rugged Raman spectrometer has been selected and used to measure Raman spectra at a distance of 132 feet using a ~1-cm collimated laser beam from a fiber-optic probe.

| 14. SUBJECT TERMS | 15. NUMBER OF PAGES |
|---|---|
| Chemical and Biological Warfare, Target Acquisition, Anti-Submarine, Combat Medicine, Biodeterioration, and Command Control and Communication | 7 |
| | 16. PRICE CODE |

| 17. SECURITY CLASSIFICATION OF REPORT | 18. SECURITY CLASSIFICATION OF THIS PAGE | 19. SECURITY CLASSIFICATION OF ABSTRACT | 20. LIMITATION OF ABSTRACT |
|---|---|---|---|
| UNCLASSIFIED | UNCLASSIFIED | UNCLASSIFIED | 200 words |

# Technology Development for Chemical Detection

M.L. Myrick

Department of Chemistry and Biochemistry
University of South Carolina
Columbia, SC 29208

Tel: (803) 777-6018
Fax: (803) 777-9521
Email: myrick@psc.sc.edu

## Section 2-2: Technology Development for Chemical Detection

M.L. Myrick

### ABSTRACT

The work by B. Salvatore is focusing on developing transducer molecules for the remote detection of organophosphonate-based nerve gases via both electrochemical and optical changes of signaling groups. We are focusing on the syntheses and studies of sensors (**1**) and (**2**), in which nerve gas simulant molecules are covalently trapped within a molecular cleft as their oxime esters. Changes in the redox potential or fluorescence properties of the reporter groups in the sensor molecules are two possible bases for detection of oxime ester formation with nerve gas simulants [*e.g.*, diethyl cyanophosphonate (DECP)]. Work to date has focused on the synthesis and electrochemical studies along the synthetic route of electrochemical sensor (**1**).

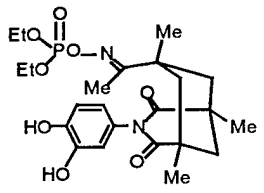


**1**

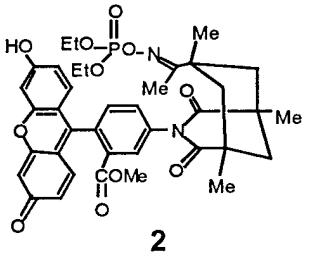


**2**

The zur Loye group is initially concentrating on dispersing cyclohexanone oxime on high surface area supports. Once a suitable support has been identified, samples will be given to Branko Popov for an investigation of the electrochemical response of these materials.

Prior to working with the Salvatore/zur Loye chemistry, the Popov group has studied catalytic oxidation of nerve gases by electrochemically generated iodine cyclic voltammetry, which showed that diethyl cyanophosphonate (DECP, a simulant for the electrochemistry of nerve agents) can not be effectively oxidized or reduced neither on gold, platinum or graphite electrodes. Also, CV's obtained for different concentrations of DECP in the presence of oximes showed a very small increase of current, which indicates that P=O and -CH=N- functional groups are not electrochemically active. However, it was found that DECP compound could be catalytically oxidized in the presence of electrochemically generated iodine. On a second front, the Popov group has been developing a new detection technique based on Double-Potential-Step Chronoamperometry (DPSCA).

The work of the group of T. Bryson is focusing on recognition chemistry for natural toxins, using saxitoxins (STXs) as model compounds. In their approach, an optical transducer is being structurally fitted to the hydrogen bonding (NH or $NH_2$) groups and the rarely encountered gem diol of STXs. They plan to exploit the unusual acid stability and the presence of the gem diol functional group of STX to target such molecules for partially-selective chemical recognition, with the chemically-induced selectivity augmented by the optical selectivity of the methods being developed by the M. Myrick group.

Prior to working with the Bryson chemistry, the Myrick group is refining the theory of optical-computing methods for rapid, sensitive, and selective "optrode" type determinations. A new facility for the fabrication of the optical computing devices is being constructed and installed (June, 1998), and software development methods for computing devices are being refined. Once this facility is on-line, the first chemical evaluation of the system is planned to be the enhancement of selectivity in Fujiwara chemistry. This chemistry is irrelevant to C&BW applications, but serves as a model for the trial and testing of the optical computation method.

## FORWARD

This project was initially funded in June, 1997 at the level of $1.3 M over three years.

## REPORT

### *Statement of the Problem Studied*

The objective of this proposal by the research team of Myrick, Popov, Salvatore, and zur Loye is to develop remote sensors for chemical agents based on optical and electrochemical effects, using methodologies applicable to all classes of CW agents. The specific objective of this proposal is to develop new and novel input transducers that will be responsive to the concentrations of nerve agents using optical or electrochemical signal transduction, with responses that reflect the concentration of the chemical agent used, condition of aeration, temperature of the environment, and relative humidity. All these data are of importance to US military preparedness in determining the avoidance and decontamination strategy in the case of use of chemical agents.

### Background

In the Hague Declaration of 1899, most world powers pledged not to use "projectiles the sole object of which is the diffusion of asphyxiating or deleterious gases." Nevertheless, Germany began using poisoned gas weapons less than two decades later during World War I when the opposing French and British forces were far less sophisticated in chemical operations than the Germans themselves. German use of chemicals in WWI only ceased when the opposition reached a level of skill comparable to themselves.[1]

The Geneva Protocol of 1925 also sought to eliminate the use of poisoned or toxic weaponry in war, yet the Japanese used chemical weapons (CW) in China during the 1930s, and both sides during WWII possessed offensive capabilities for waging war in a chemical environment. The US military alone kept reserves of gas weaponry sufficient to completely bridge the Italian peninsula with a toxic barrier.[2] Why were these weapons not used by either side (including the Japanese) during WWII? German military archives indicate that one major reason is that the Germans and Japanese felt the Allies had a superior defensive and offensive capability to themselves. History seems to bear out that chemical weapons are most likely to be used when the enemy is perceived as relatively vulnerable.[3] General Omar Bradley stated that, had the Germans used even a small amount of poisoned gas on Omaha Beach, the action would have been decisive and would have resulted in the failure of the Invasion of Normandy in June1944.[2]

Thus, sophistication and technical progress in the area of chemical weaponry, including detection capabilities, can have a profound impact on survivability during chemical attack - but perhaps an even greater impact as a deterrent.

A number of government studies have indicated that US military forces are currently vulnerable to chemical attack. The DoD's assessment has been that most US forces would survive an initial chemical attack, with the possible exception of Navy shore establishments. The General Accounting Office, however, notes that the primary means of detecting chemical agents all have serious flaws and reports an Army assertion that the major difficulty in the development of new detection methods is the lack of technological breakthroughs upon which those detection methods would be based.[4]

The problems of achieving an effective detection capability have grown through the years as the number of chemical agents and their modes of operation have increased. Agents that a military unit could encounter today range from persistent (weeks of activity) to non-persistent (minutes to hours of activity). They include acetylcholinesterase inhibitors (nerve gases such as sarin, tabun, soman, and VX), compounds that block oxygen transport (blood agents such as HCN and cyanogen chloride), compounds that cause choking (e.g., phosgene and diphosgene), agents that cause severe blistering (e.g., sulfur mustard, nitrogen mustard, and lewisite), and plant toxins such as the trichothecene family of toxins (e.g., Diacetoxyscirpenol, T-2, verricanol, zearalenone, DON, and nivalenol, all produced by Fusarium, which attack the major organs.

According to the Army, the nuclear, biological, and chemical (NBC) threat has developed into one of the world's most troubling concerns,[5] with as many as 25 nations producing and stockpiling chemical weapons of all types. Current research on new CW agents is being conducted on materials that will be more difficult to detect, decontaminate, and treat, and may penetrate standard charcoal filters in protective equipment such as the Army's M-40 series masks.

The detection technologies for chemical weapons (CW) can be divided into two general categories; point and standoff.[6-8] Point detectors sample the air for presence of CW agents in the immediate vicinity of the detector using techniques such as ion mobility spectrometry, flame photometry, mass spectrometry, photoacoustic, infrared spectroscopy, detection kits, and electrochemistry. Standoff detectors use infrared remote sensing techniques to detect the presence of CW agents in a range of one to five kilometers.

Most of the point CW agent detectors in use by military forces worldwide utilize ion mobility spectrometry (IMS) and reagent-based detection kits and tickets. IMS operates by drawing an air sample directly into a reaction region where all constituents in the air are ionized. The sample is then injected through a shutter and into a drift tube where the ions move under the influence of a weak electric field gradient to a detector plate. As the ions collide with the detector plate, the dependence of the signal (either charge or current) on drift time is registered as is done for a vacuum time-of-flight instrument. The generated graph of current vs. time is the ion mobility spectrum. This method is simple and sensitive, but is affected adversely by environmental factors such as changing humidity, temperature, and the composition of the air sample, all of which may influence the detector response.

Detection kits and tickets use chemical reactions that occur when CW agents interact with the various solutions and substrates. The most common indicator is a color change. This technology is even simpler and more sensitive, but it can not be used for continuous monitoring. Also oxidizing agents such as $Cl_2$, $Br_2$, and $NO_2$ or acidic species $CO_2$, $SO_2$, and $NO_2$ cause a false response.[6]

Other detection technologies are not commonly used because of their practical limitations. Flame photometry and mass spectrometry are only used extensively as laboratory analytical techniques. Flame photometry suffers from interference from other compounds containing the same elements, while mass spectrometry is too complex and expensive. IMS is, in fact, the only version of mass spectrometry (albeit of lower selectivity) that has found any significant usage for *in situ* chemical agent detection.

Photoacoustic IR spectroscopy is a relatively recent CW detection technology. This technique is easily affected by humidity and other environmental factors[6], and is exactly equivalent to standard infrared spectrocopy except that absorbance is detected by the heating of a sample instead of a photoelectric effect. Given the additional factors that complicate this detection scheme, its applicability is probably less than that of standard IR spectroscopy.

Several CW agent detectors operate on the elecrochemical principles. A common type of electrochemical cell for nerve gas detection monitors the hydrolytic activity of cholinesterase by interaction with butylthiocholine followed by an electrochemical determination of the hydrolysis product, thiocholine, using a graphite-working electrode. This type of sensor can utilize a continuous supply of butylthiocholine to provide long-term continuous detection. Electrochemical sensors based on conductivity also can be used for continuous monitoring. However conductivity meters suffer from interference from acidic gases, which dissociate into ions in aqueous solution.

Much of the hoped-for future technology may require revolutionary breakthroughs (e.g., new materials, new chemistries, new detection concepts, and new integrations of technologies) in detection capability, rather than evolutionary progress down the same paths already trod repeatedly.

***Summary of the Most Important Results***

The project can be divided into the following tasks:

Task 1. Design and Synthesize Sensing Chemistries. Changes in the redox potential or absorption/fluorescence of small transducer molecules, or changes in the conductivity of the sensor support media are all viable bases for detection.

Task 2. Design Supports for the Chemistries. To effectively allow the nerve gas analyte to be detected, it will be necessary to react it with the sensing chemistries or indicator. This can best be achieved if the indicator is dispersed on an inert high surface area support. Candidates for such supports range from insulating high surface area silica, alumina, and titania to framework-type materials, such as zeolites, to conducting supports, such as high surface area carbon.

Task 3. Develop Wide-Band Optical Detection Methods. We can capitalize on existing and new optical-detection reagent chemistries (colorimetric, fluorescimetric, etc.) by using the selectivity of multivariate data analytic methods, provided a sensitive and cost-effective means of implementing them can be developed. Our approach to this problem is through multivariate optical computation.

Task 4. Develop Remote Sensors Based on Electrochemical Effects. Potentiometric and microgalvanic transducers and transduction mechanisms are the basis for making small electrochemical sensors. We will develop such microtransducers to serve as efficient and selective ion and molecule detectors using ion-selective membranes and selective redox cycles for dissolved and airborne nerve gas species.

Our progress in each of the task areas is summarized below.

**Task 1**

Synthesis of Chemical Sensors for Nerve Agents

We seek to apply the high reactivity between oximes and organophosphonates toward the development of a new class of nerve gas sensors. We are currently developing sensor molecules which form covalent adducts with organophosphonates. These sensors are based on a molecular cleft scaffold[9], and incorporate both an oxime and either a redox or fluorescent transducer group. Detection is not based on the identification of specific nerve gas hydrolysis by-products (e.g., HF) but rather on the electrochemical or spectroscopic differences between the unbound sensor and the nerve gas-sensor oxime phosphate ester adducts. It is our goal to detect organophosphonate nerve gas mimics [e.g., diethylcyanophosphonate (DECP), Figure II], regardless of the byproducts of the adduct formation reaction. Such an approach is advantageous, since all nerve gases will form similar oxime phosphonate esters. Thus one type of transducing moiety would able to detect any of several different nerve gases (VX, tabun, or sarin, for example).

There is a sound basis for the development of electrochemical sensors possessing cleft-like architectures. Evidence exists that electrostatic interactions between groups juxtaposed in molecular clefts can greatly influence redox potentials. Rottello et al.[10] have used molecular cleft-based receptors to examine the effects of $\pi$-stacking on flavin recognition and redox potentials. These studies have established that aromatic stacking interactions between such receptors and their flavin guests can effectively modulate redox potential over a 91 mV (2.1 kcal/mol) range.[10] Thus, recognition by molecules containing a transducing moiety has been demonstrated. Such a transducing unit (i.e., a catechol) could be subjected to a continuously sweeping alternating electrical potential (e.g. 0 to +/- 0.5 V)[11]. Binding of the phosphonate in the molecular cleft directly adjacent to the catechol/quinone moiety should result in a measurable change in the monitored current and/or oxidation potential (Figure I).

**Figure II**

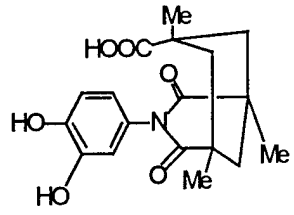


**7**

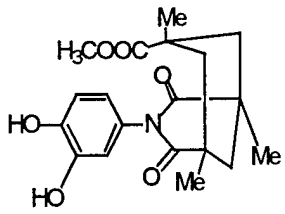


**8**

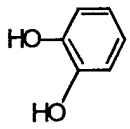


**9**

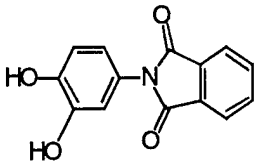


**10**

Two synthetic intermediates (7) and (**8**) have being investigated by cyclic voltametry to characterize the reduction and oxidation peak potentials, as well as the reversibility of the redox process within this molecular cleft system. Both acid (7) and ester (**8**) displayed irreversible electrochemical behavior. Neither one shows the pronounced oxidation/reduction peaks nor the reversibility obtained with 1,2-catechol (**9**). Although the electrochemical behavior witnessed thus far could form a basis for nerve gas sensors, the irreversibility of the observed oxidation process is undesired. Further electrochemical studies are warranted.

Other recent work has focused on the preparation of a model compound, imide (**10**), in which the molecular cleft unit is replaced by a phthalimidyl group. This model compound (**10**) is not sterically hindered and will assist us in determining whether the pronounced differences in the cyclic voltamagrams of both **7** and **8** with respect to 1,2-cataechol (**9**) are due to steric or to the electron withdrawing nature of the imide moiety. The electrochemical studies are currently in progress in the Popov laboratory in the USC Dept. of Chemical Engineering.

To synthesize the Cleft Intermediates (7) and (**8**), Commercial Kemp's triacid (**3**) was suspended in xylene and heated at reflux for about 10 h with a Dean-Stark trap under $N_2$. The resulting mixture was concentrated under vacuum to give the anhydride. Treatment with thionyl chloride under reflux, followed by distillation afforded acid chloride/anhydride (**4**) in 86% yield overall. Condensation of **4** with 4-aminoveratrole (**5**) in hot pyridine containing a catalytic amount of 4-(dimethylamino) pyridine (DMAP), followed by removal of the pyridine by vacuum distillation and flash chromatography of the residue (hexane/EtOAc: 3/2) furnished amide (**6**) in 73% yield.

The two methyl protecting groups on the catechol moiety could be readily removed with 1 *M* boron tribromide in $CH_2Cl_2$. Imide (**6**) was dissolved in $CH_2Cl_2$, and then a solution of boron tribromide (1 M in $CH_2Cl_2$) was added dropwise at -78°C. The resulting mixture was stirred overnight at room temperature and the reaction was terminated by the careful dropwise addition of water. The organic phase was then evaporated to dryness and purified by column chromatography (hexane/EtOAc: 4:1) to provide catechol/acid 7 (yield = 85%). Treatment of 7 with a solution of diazomethane in ether gave the corresponding methyl ester (**8**) in 98% yield.

**Scheme I**

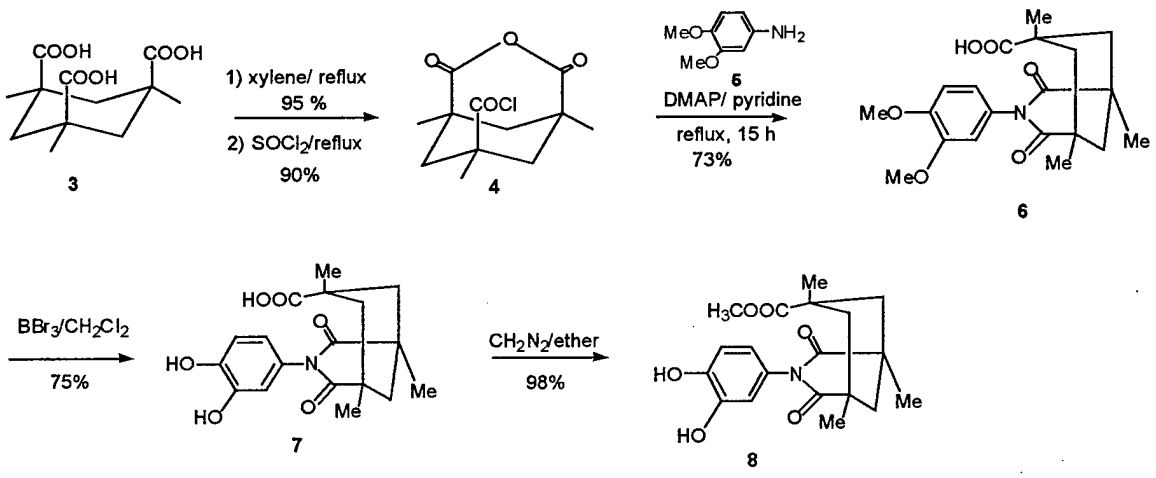


To prepare a model compound (**11**) for electrochemical studies, phthalic anhydride (500 mg, 1.0 eq) and 4-aminoveratrole (500 mg, 1.0 eq) in dimethyl formamide (DMF) were stirred overnight at r.t. Dilution with water and extraction with ethyl acetate provided 1 g of crude product. Flash chromatography (hexane/EtOAc: 1:1) provided 600 mg of pure imide (**11**, yield = 60%). Deprotection of the catechol moiety was then accomplished as before, with $BBr_3/CH_2Cl_2$ (1 *M* solution in dichloromethane) [1] to provide **10** in 65% yield.

Over the course of the next year, our research will be directed toward the completion of the molecular cleft receptor (**13**) and formation of the corresponding phosphate ester adducts (**1**). A strategy for completion is shown in scheme **III**. Reprotection of the catechol moiety in **7** as the diacetate and subsequent acid chloride formation will provide **12**. Cuprate addition into acid chloride followed by oxime formation on the resulting ketone will then give **13**.

**Scheme II**

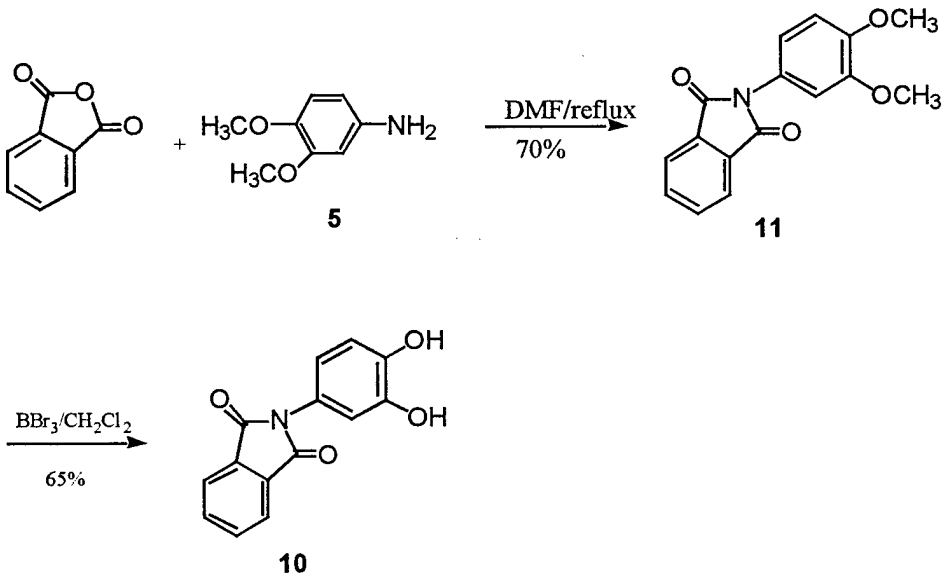

We plan to then establish optimal conditions for oxime phosphate ester (**1**) formation with various nerve gas simulants, both in solution and on inert clay supports. Additionally, we are looking for reversible electrochemical behavior and distinct changes in this behavior (either changes in the current or oxidation potential) upon oxime ester formation. Concurrently, we plan to synthesize the fluorescent-based sensors for future studies.

**Scheme III**

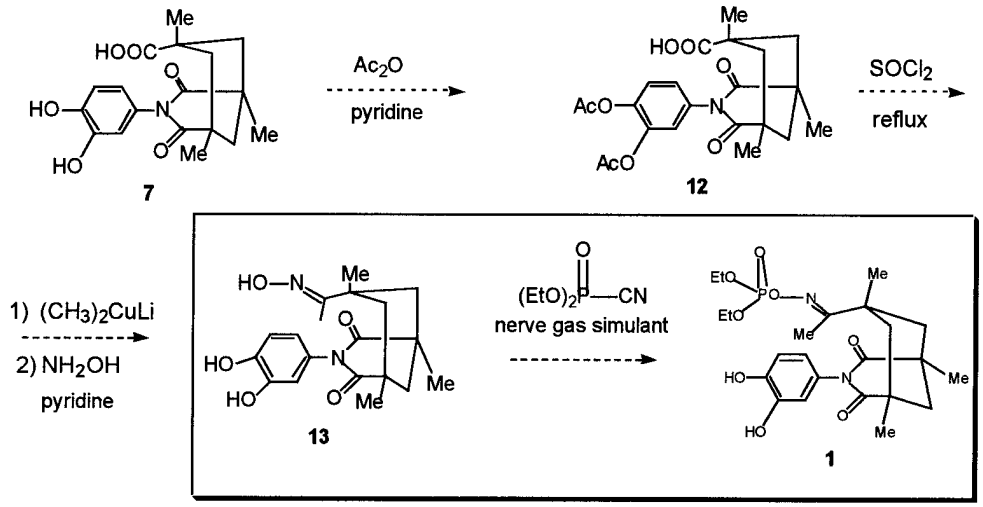


Synthesis for Specific Chemical Recognition of Toxins

Saxitoxins (**STX**) are among many substances that has been banned under the UN International Chemical Warfare Agreement (summer of 1997). Natural toxins are generally only available in quantity from their natural source because they are structurally too complex for large scale preparation. However the lab prep of **STX** requires only reasonable MS lab skills and access to quantities of very common stockroom chemicals.

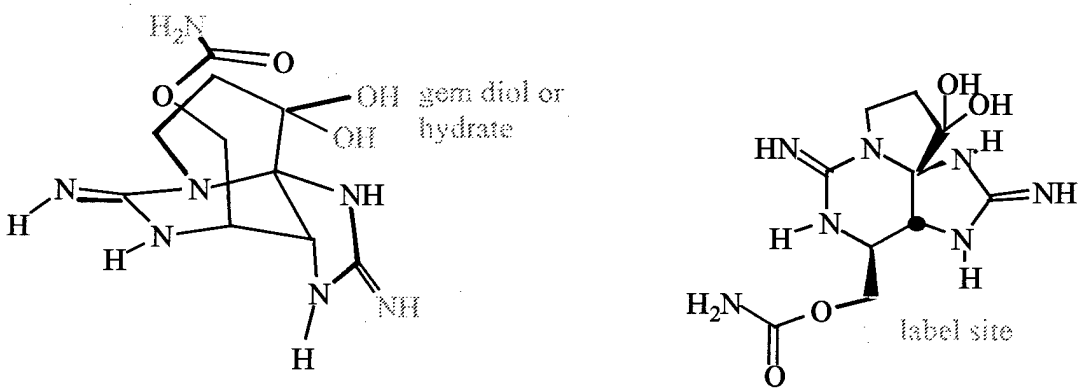


**Saxitoxin (STX or 1)**

Labeled STX will be prepared by degrading natural STX, converting it back to the natural form (**1, above**) containing a deuterium and/or tritium label at a non-exchangeable site in the

molecule. This is an expensive but very time efficient approach to having a labelled form of STX available for biological, medicinal, and detection studies.

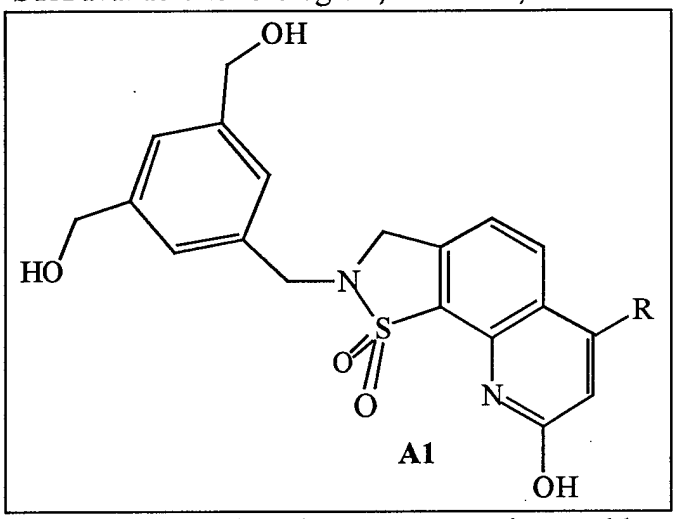


**A1**

Extensive modeling of saxitoxin reveals two strong hydrogen bonding sites (**NH** or **$NH_2$/O** groups) approximately 5.3 Å from the unique **gem diol** functionality in STX. This modeling of saxitoxin suggests initial recognition target compound **A1** shown in the figure to the left. These active sites are illustrated on the 3D depiction of STX, below. On the rare occasion that gem diols are stable, this functional group forms very strong associations with polar (donor) solvents, particularly sulfoxides like DMSO. (DMSO-hexafluoroacetone exist a stable crystalline solid.) The designed agent(s) have a "bite" size, anchored by a very strong **S-O** to **gem diol** association. Relative to this hexafluoroacetone - DMSO interaction there are either of two exploitable hydrogen bonding sites in STX, one site of which is illustrated below using agent **A1** and STX. In structures **A1** the minimized bite size is indicated (in Å). Sulfonamide **A1** has two S-O bonds (two distances given) either of which could associate with STX's gem diol. The flexibility of agent **A1** makes this compound our first target. Studies of STX-**A1** interactions might suggest refinement of the more rigid recognition agents. The R group in **A1** is hydrogen for these proposed studies.

**3D depiction of STX's targeted sites**

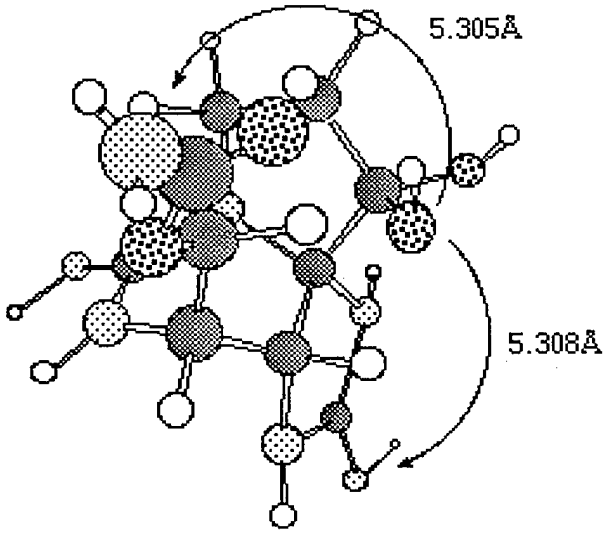


**Hydrate donor complex**

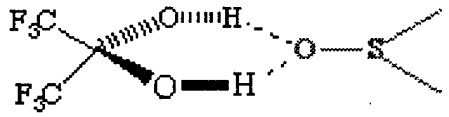

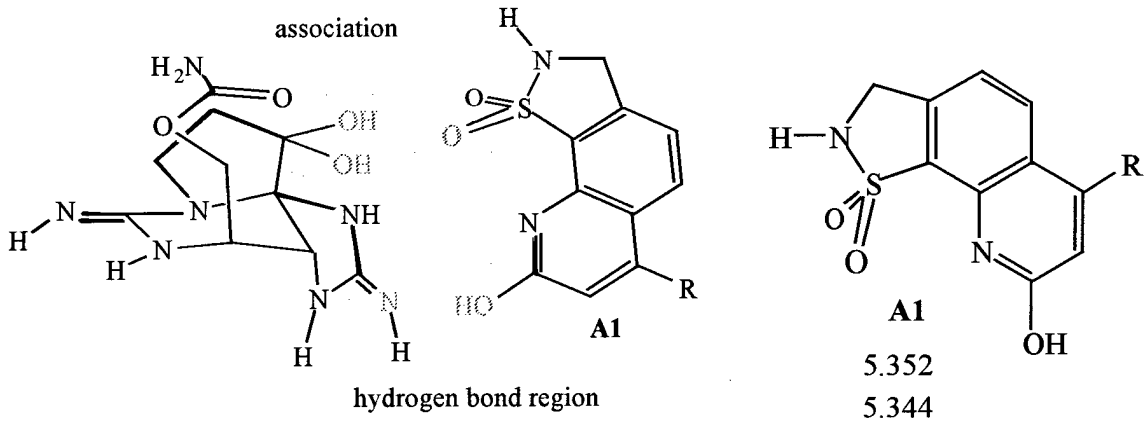


In future investigations, R is envisioned to be a hydrocarbon tether for immobilization on silica gel or glass for a "field detection kit." The spectroscopies of pure **A** (1-4) and **A** (1-4) with **STX** will be investigated for reliable detection bands that verify complexation. The structure of **A** may have to be slightly modified to optimize association and hydrogen bonding (opening or narrowing of the bite size) which we are prepared to do. Dyes **A2-4** can be prepared by oxidation of known sulfides and **A1** should be available from sulfonation of an aminomethyl quinolone.

**Task 2**

Support Development

To effectively allow the chemical agent analyte to be detected, it will be necessary to react it with sensing chemistries or indicators. This can best be achieved if the indicator is dispersed on an inert high surface area support. Candidates for such supports range from insulating high surface area silica, alumina, and titania to framework-type materials such as zeolites, to conducting supports such as high surface area carbon. The surface chemistry of the support must be chemically compatible - that is, there must not be any detrimental interactions - with the indicator as well as the analyte, and in addition, the support must not interfere with the electrochemical characterization of the indicator-analyte complex. Therefore, we will identify a suitable high surface area support. Once one or two suitable supports have been identified, the procedures necessary to disperse the diverse indicators on the support must be established.

The work by B. Salvatore is focusing on the reaction between an oxime and the phosphorous based nerve gases. Therefore we will initially concentrate on dispersing cyclohexanone oxime on high surface area supports. Once a suitable support has been identified, samples will be given to B. Popov for an investigation of the electrochemical response of these materials. B. Popov is working on the development of an amperometric sensor based on direct reduction of the P=O functional groups present in all nerve gases. To ensure that our support and the oxime (to represent the type of molecule that B. Salvatore is developing) do not interfere with the electrochemistry, several tests must be carried out.

The interaction between the oxime and nerve gas simulants and between the Bryson chemical recognition chemistry and STXs will be carried out on the supporting media to determine under

which conditions a suitable signal is produced that can be detected by either electrochemical or optical means. Since we cannot use real nerve gases, structural analogs for these compounds will be used instead. In addition to diethylcyanophosphonate (DICP), being used by B. Popov as a simulant for the chemistry of nerve agents, and diisopropyl methyl phosphonate (DIMP) and dimethyl methyl phosphonate (DMMP), being used by M. Myrick as simulants for the optical properties of nerve agents, two additional potential candidates as simulants for the chemistry of these agents are diisopropyl fluorophosphate (DIFP) and diethyl 4-nitrophenylphosphate (DENP).

Reactions between the oxime and the analogs will lead to the formation of a covalent bond between the oxime oxygen and the phosphorous atom. The leaving groups will be fluoride, p-nitrophenyl, and cyano, respectively, all of which have the potential of being electrochemically detectable.

The powder x-ray diffraction system with hot stage, which is the key piece of equipment for our part of the research project, was delivered during the third week of April, 1998. Set up will begin during the last week of April and should be completed by the second week of May, 1998. This will allow us to start collecting structural data on the high surface area supports we have purchased and to determine the changes they undergo as a function of temperature. The next step will be the addition of an oxime to the support and the determination of the thermal stability of the loaded supports.

Up to now, our progress was limited by the lack of our diffraction system. Since it has now arrived, we can begin our part of the research. Until we are supplied with the functional organic complexes that Salvatore and Bryson are preparing we are, of course, limited to structural analogs, which may or may not interact the same way with the support. Nonetheless, these analogs allow us to proceed and to effectively work with Prof. Popov on the electrochemical characterization of the loaded supports.

To identify a suitable support, numerous candidates will be characterized structurally by powder x-ray diffraction, chemically by determining the acid base properties of the support surface, and compositionally by establishing the degree of hydration of the support. Several high surface area supports will be synthesized and/or purchased and characterized with respect to water content and surface pH. Thermal analysis will be carried out to determine under which condition water can be removed and what the effect of water removal is on surface pH. In collaboration with B. Popov, the support will be evaluated with respect to possible interference with the electrochemical measurements.

**Task 3**

Optical chemical recognition using reagents can be improved in selectivity by the use of multivariate data analyis. Unfortunately, most multivariate measurements are complex and expensive to implement. We developed a method for applying multivariate statistics that relies on the simplest forms of optical computing, i.e., shadowcasting, which requires no lasers or other coherent optical sources. The basis of this method is to generate a "regression vector" for an analyte using standard chemometric methods, but then to design and construct an interference

filter with a spectral transmission profile given by the magnitude of the regression vector. This is not easy but is possible, as shown in the papers listed under our publications for this subgrant.

The interference devices we plan to construct will consist of alternating layers of $Nb_2O_3$ and $SiO_2$. Software and hardware for designing the filter elements has been purchased or ordered, the most important piece of which is a $280,000 reactive magnetron sputtering system with fully automated computer control based on quartz-crystal microbalance and optical reflectance monitoring, capable of manufacturing complex optical coatings for optical computation elements. This system was placed out for bids in early fall of 1997. Bids closed during September/October of 1997, with Corona Vacuum Coaters, Inc. of Vancouver, B.C., being selected as the vendor. At that time, the delivery date was set for mid-April, 1998; since that time, however, delivery has been postponed until 1st June, 1998. Upon delivery and installation, we will have a facility with deposition capabilities found in only two commercial locations on the North American continent (these locations, found after considerable effort, are at Coherent Laser Optics in California and at the National Research Council of Canada in Ontario. Of these, the former has just received their equipment and have not yet used it, while the second is not truly a commercial vendor). Standard oxide interference filters are prepared by electron beam evaporative deposition, which is almost an order of magnitude more rapid and therefore more cost-effective, but which produces films that are porous and rough. These two properties of standard films are deleterious to the final product because the films age (water and other contamination of the pores) and they are rough (reducing the total number of films that can be deposited in series). The magnetron system produces films with nearly bulk properties and with almost atomic smoothness, making complex interference devices practical, as long as the thickness of the total deposition does not exceed approximately 25 micrometers (strain in the film causes delamination near this thickness).

We have searched diligently to locate a post-doctoral associate capable of operating this instrumentation, but the combination of skills necessary for the project is elusive. In addition to chemical spectroscopy, the assistant must have skills in chemometrics and materials preparation by reactive deposition. Optics skills are also useful. This combination of talents has proven impossible to find, so we refined our search to that skill most elusive in our own labs - the materials science of oxide deposition by reactive sputtering. We have placed an offer to Raju Prajesh of Louisiana State University, whose training is in physics rather than chemistry, and whose skills lie with reactive magnetron sputtering. All the remaining skills he will need to conduct this research can be learned directly from personnel already at the University of South Carolina.

While awaiting the deposition system, we have pursued modeling of the optical computation process and developed refinements of the technique that will help us deal with some of the problems to which the computational process is subject. The first of these problems is the that of "lamp drift". A typical colorimetric measurement uses a lamp with some initially-defined spectrum to interrogate a sensor. For any real lamp, however, the spectrum of the lamp changes as a function of voltage applied to the filament, and changes as the lamp ages and the filment develops "thin spots". In this case, the regression vector, defined for a system under illumination with the initial lamp spectrum, is no longer appropriate. How strongly the change

of lamp spectrum affects the regression, and whether there are any corrective measures that can be taken, is the subject of our mathematical analysis.

We begin by analysing the direct product between the regression vector and a spectrum modified by lamp drift. $\vec{L}$ is the regression vector determined for a set lamp profile and for a set of samples as is usually done. $\vec{S}_0$ is the spectrum of the sample that would have been observed if the lamp had been operating properly. $\vec{S}'$ is the observed spectrum after the lamp has changed its spectral output. $\vec{T}$ is the transmission vector for the sample. $\vec{I}'$ is the modified lamp spectrum and $\vec{I}_0$ is the proper lamp profile.

$$\vec{L}\bullet\vec{S} = \vec{L}\bullet\vec{T}\vec{I}' = \sum_i l_i T_i I_i' = \sum_i l_i T_i (I_{i0} + \Delta I_i)$$

$$\vec{L}\bullet\vec{S} = \sum_i l_i T_i I_{i0} + \sum_i l_i T_i \Delta I_i = \vec{L}\bullet\vec{S}_0 + \vec{L}\bullet\Delta\vec{S}$$

where $\vec{\Delta S} = \vec{T}\Delta\vec{I}$.

In this set of equations, the summations are taken over the wavelengths at which the spectrum is measured. This group of equations says that in zeroth order, when the change in intensity of the lamp is small at any wavelength compared to the "correct" intensity, no correction is required and no error in prediction occurs. The fundamental prediction will become identical with the true prediction when the error of the lamp tends toward zero, as expected. When the lamp error tends toward a larger value, the second term introduces a prediction error. What we really need to understand is the nature of this change in prediction. We can expand this second term by relating the transmission vector to the average sample transmission spectrum (this is an average over all samples used in the calibration).

Substitute $\vec{T} = \vec{T}_{avg} + \vec{\Delta T}$

Therefore

$$\vec{L}\bullet\vec{S} = \vec{L}\bullet\left(\vec{T}_{avg} + \vec{\Delta T}\right)\vec{\Delta I} = \vec{L}\bullet\vec{T}_{avg}\,\vec{\Delta I} + \vec{L}\bullet\vec{\Delta T}\,\vec{\Delta I}$$

$$= \gamma + \vec{L}\bullet\vec{\Delta T}\,\vec{\Delta I}$$

and

$$\vec{L}\bullet\vec{S} = \vec{L}\bullet\vec{S}_0 + \gamma + \vec{L}\bullet\Delta\vec{\Delta S}$$

where $\vec{\Delta\Delta S} = \vec{\Delta T}\,\vec{\Delta I}$.

In other words, the change in prediction, to first order, is a change in offset. If the variation of the sample transmission from the average sample transmission is small, and if the change in

intensity at any wavelength for the lamp is small, this is the only correction required. Given that the change in transmission for a sample is never as large as the average transmission in the calibration set, the last term will always be smaller than $\gamma$. For the sample with the average transmission, the last term can be ignored completely - only when the spectra vary towards the ends of the calibration range will this term begin to affect performance significantly. Even then, the effect is not entirely to destroy the calibration. We can resolve $\vec{\Delta\Delta S}$ into components both parallel to and perpendicular to the original spectrum, $\vec{S}_0 = \vec{T}\vec{I}_0$. The component parallel to the original spectrum will affect the sensitivity of the measurement to the analyte, but will not introduce any components of interference. We resolve $\vec{\Delta\Delta S}$ by first finding a unit vector in the direction of $\vec{S}_0$ by dividing $\vec{S}_0$ by its length. The length of $\vec{S}_0$ is:

$$\left|\vec{S}_0\right| = \sqrt{\sum_i T_i^2 I_{0i}^2}$$

so this unit vector is:

$$\vec{s}_0 = \frac{\vec{S}_0}{\sqrt{\sum_i T_i^2 I_{0i}^2}}$$

Then we take the direct product of $\vec{\Delta\Delta S}$ with $\vec{s}_0$:

$$\vec{\Delta\Delta S} \bullet \vec{s}_0 = \frac{\sum_i \Delta T_i \Delta I_i T_i I_{0i}}{\sqrt{\sum_i T_i^2 I_{0i}^2}}$$

Therefore

$$\vec{\Delta\Delta S} = t'\vec{s}_0 + b\vec{s}\perp = t\vec{S}_0 + b\vec{s}\perp$$

where $t = \dfrac{\sum_i \Delta T_i \Delta I_i T_i I_0}{\sum_i T_i^2 I_{0i}^2}$ comes from substituting the original spectrum for the unit vector.

Therefore:

$$\vec{L} \bullet \vec{\Delta\Delta S} = t\vec{L} \bullet \vec{S}_0 + b\vec{L} \bullet \vec{s}\perp$$

This last term is evaluated as:

$$b\vec{L}\vec{s}\perp = \frac{\sum_i 1_i \sum_{j \neq i} T_j I_{0j} \left(\Delta T_i \Delta I_i - \Delta T_j \Delta I_j T_i I_{0i}\right)}{\sum_i T_i^2 I_{0i}^2}$$

and this is where all the introduced interference must appear. We can re-cast our original equation as:

$$\vec{L} \bullet \vec{S} = (1+t)\vec{L} \bullet \vec{S}_0 + \gamma + b\vec{L} \bullet \vec{s}\perp$$

This last term is by no means entirely detracting from the measurement either. Instead, it should be looked at as a factor that partially removes the orthogonality of the regression vector to interferences. The degree to which this can possibly happen depends on the variation of the sample set along the direction of the regression vector, versus its variability in directions orthogonal to the regression vector. Consequently, the "uncorrectable" errors introduced by lamp intensity changes can be viewed as "third-order" effects, that only become significant when the lamp spectrum changes substantially, and then only when dealing with samples at the extreme of the calibration.

To summarize, the zeroth-order effect of a lamp intensity change is none. The first order effect of a lamp intensity change is to introduce an offset. The second order effect of a lamp intensity change is to change the sensitivity (slope) of the prediction line. The third order effect is to introduce sucseptibility to interferences.

A second area of refinement to the original optical regression concepts contained in the proposed work for this subproject has been the development of "data metrics", i.e., methods for determining or cross-checking whether the data from which calculations have been made is appropriate for this treatment. We have made theoretical investigations of two well-known data metrics (i.e., Euclidean and Mahalanobis distances) used with conventional chemometrics and have developed concepts for how these metrics can be implemented in an optical environment. This discussion follows.

Euclidean distance is calculated as:

$$r = \sqrt{(X-m)^T (X-m)},$$

or if we can live with the square of the function,

$$\begin{aligned} r^2 &= (X-m)^T (X-m) = (x_1 - m_1)(x_1 - m_1) + (x_2 - m_2)(x_2 - m_2) + \ldots \\ &= x_1^2 - 2x_1 m_1 + m_1^2 + x_2^2 - 2x_2 m_2 + m_2^2 + \ldots \\ &= \left( \sum_i x_i^2 + \sum_i m_i^2 \right) - 2\sum_i x_i m_i \end{aligned}$$

How can this be done optically? Well, there is one major problem - the calculation of the first term, which requires a square of the light intensity at each wavelength. If the light were spatially coherent, that could potentially be done since intensities are not additive in that case. However, we much prefer the incoherent situation because it is more experimentally feasible. One way to do this would be to electrooptically produce $\left( \sum_i m_i^2 - \sum_i x_i m_i \right)$ under the condition $\sum_i x_i^2 = \sum_i m_i^2$. Can this last be arranged? Again, not exactly, but $\sum |x_i| = \sum |m_i|$ can be arranged - that's just the same as saying the total integrated intensity is the same for the spectrum and the average, and that can be arranged easily. In other words, the experimental set up for this would be to compare the signal intensity to a standard, then use that comparison to set an amplifier gain. When a spectrum with an "average" signal is used, the resulting signal should be

subtracted from a constant to produce zero. Any deviation from that would be evidence for drift from the classified samples.

A second method for accomplishing the same determination would be to take the equation for squared Euclidean distance given above and divide both sides by $\left(\sum_i x_i^2 = \sum_i m_i^2\right)$. Then we get:

$$\frac{r^2}{\left(\sum_i x_i^2 + \sum_i m_i^2\right)} = 1 - \frac{2\sum_i x_i m_i}{\left(\sum_i x_i^2 + \sum_i m_i^2\right)},$$

If X and M are the spectra of the sample and of the average sample, then X and M should be similar to one another. However, you will note that, since r is always a real number, it is not possible for $2\sum_i x_i m_i$ to be larger than $\left(\sum_i x_i^2 = \sum_i m_i^2\right)$. If X=M, then these terms are equal to one another and r is 0.

Now, if we assume that $\left(\sum_i x_i^2 = \sum_i m_i^2\right)$ is approximately $2\sum_i m_i^2$, this equation reduces to the form:

$$\frac{r^2}{2\sum_i m_i^2} \approx 1 - \frac{\sum_i x_i m_i}{\sum_i m_i^2}.$$

We've made one approximation thus far, and that's all that's necessary. Since $2\sum_i m_i^2$ is just a constant, we can rewrite this in the simpler form:

$$\frac{r^2}{2} = G - \sum_i x_i m_i .$$

Hence, if we make a single mask with a transmission profile proportional to the average spectrum M, we quickly monitor a function proportional to the last term in equation 3. Let's call this measurement "A". Then we can rewrite the last equation as:

$$r^2 = 2G - k A = G' - kA$$

The one thing we can be certain of is that if we observe a sample with a spectrum, X, very similar to M, then $r^2$ must be very near zero. This can be obtained by replacing the vector for M with a vector for $M^2$ and viewing the source light (in the case of a NIR measurement). Or we can just view a sample that is actually nearly identical to M. If we take the amplified output of that measurement, negate it, and add an offset to it to obtain a zero result, the result obtained from any other sample will be proportional to the *square of the Euclidean distance* between our

test sample and the original. How that proportionality is calculated depends on the gain of the amplifier following the offset.

The Euclidean distance between samples is interesting, but only important if the space happens to be uniform. In most cases this condition is not met - the space is scaled differently for different dimensions. There is a scale invariant version of the Euclidean distance in which each individual wavelength is scaled by its standard deviation. This calculation is also easily obtained by making a filter mask that is the "normalized" average spectrum and carrying on the same calculation.

The Mahalanobis distance is calculated not just using the standard deviation normalization, but using the covariance of the wavelengths. If we consider the samples not as individual wavelengths but in principal component space, the covariance of the space is lost, and we need only consider the variance of each component at the wavelength of interest. In this case we get:

$$M = Q - k' B,$$

where B is proportional to $\sum_i x_i b_i$, and $b_i$ is $\sum_j \frac{l_{ij}}{e_j c_j}$, where $l_j$ is the loading of PC (j) at the wavelength i, $e_j$ is the relative eigenvalue of PC(j) and $c_j$ is the variance of PC(j). You will note that, if the data has not been mean centered, the first PC is the average spectrum, and so the first term is similar to the term used in the scale-invariant Euclidean metric - but not exactly. This metric is accomplished by calculating the term $\sum_j \frac{l_{ij}}{e_j c_j}$ at each wavelength i and preparing a mask with transmission scaled to that value. This may require two masks, since it is possible that the summation will yield a negative; in a non-centered spectroscopic system like ours, however, this seems unlikely. After that, everything is done just as was described for the Euclidean distance above.

*Task 4*

The objective of this work is to develop potentiometric or microgalvanic transducers which are selective and sensitive to compounds of similar structure to nerve gases. In this study, an attempt was made to use double-potential-step chronoamperometry as a detection method for the analytical detection of nerve gases. Our specific objective during this first year was to develop a novel amperometric sensor based on oxidation of nerve gas (diethyl cyanophosphonate simulate) by electrochemically generated $I_2$.

In this work, diethyl cyanophosphonate (DECP) was used to simulate nerve gas because its chemical structure is similar to those agents. Also the following compounds were used as received: dimethyl methylphosphonate (DMMP, Aldrich, 97%), dimethylphosphinic acid (Aldrich, 97%), trimethyl phosphate (Aldrich, 97%), methyl phosphonic acid (Aldrich, 98%), diethyl chlorophosphate (Aldrich, 97%), 2-pyridinealdoxime methiodide (2-PAMI) (Aldrich, 99%), 2-pyridinealdoxime methochloride (2-PAMC) (Aldrich, 99%), sodium perchloride (Sigma, 90%), sodium iodide (Fisher, >99%), $NaH_2PO_4$, and $Na_2HPO_4$ (Fisher, >99%).

Nerve gases are stable in neutral solutions, but decompose rapidly in alkaline and acidic electrolytes. In order to keep the nerve gas concentration in the electrolyte constant a solution containing 0.05 M $NaClO_4$ and 0.05 M phosphate (pH=6.3) was used as the supporting electrolyte. All experiments were carried out at room temperature and in air atmosphere.

The electrochemical cell employed for the CV and potential-step studies was a conventional three-electrode cell. The reference electrode was a saturated Ag/AgCl electrode, while the auxiliary electrode was made from platinum wire. A gold disc electrode with area of 0.03 cm2 was used as a working electrode. The experiments were conducted using an EG&G electrochemical system Model 342 with an EG&G 273 potentiostat/galvanostat. The working electrode does not need any pretreatment for the long term consecutive experiments.

Cyclic Voltammetry showed that DECP cannot be effectively oxidized or reduced neither on gold, platinum, or graphite electrodes. Also, CVs obtained for different concentrations of DECP in the presence of oxime showed a very small increase of current, which indicates that P=O and -CH=N- functional groups are not electrochemically active. However, it was found that DECP compounds can be catalytically oxidized in the presence of electrochemically generated iodine. In a typical experiment, DECP was studied in 0.05 M $NaClO_4$ + 0.05 M phosphate buffer (pH=6.3) in the presence of 0.4 mM NaI. In these studies, NaI in the absence of DECP gives oxidation and reduction peaks at approximately 0.55 V vs. an Ag/AgCl reference electrode, which is close to the redox potential of the $I_2/I^-$ couple. We observed an increase of the anodic peak current with the introduction of DECP which results from the electrocatalytic oxidation of DECP by the $I_2/I^-$ redox couple through an inner-sphere electron transfer mechanism.

In the absence of DECP, the cyclic voltammogram can be explained by Equation (1) in which iodide is oxidized to iodine during the anodic sweep and the iodine is reduced back to iodide during the cathodic sweep.

$$2I^- - 2e \Rightarrow I_2 \qquad (1)$$

In the presence of DECP a charge-transfer complex is formed and oxidized, which may be written through the following equations:

$$DECP + I^- \Rightarrow [DECP\text{-}I^-] \qquad (2)$$

$$[DECP\text{-}I^-] - e^- \Rightarrow [DECP\text{-}I] \qquad (3)$$

$$[DECP\text{-}I] \Rightarrow\Rightarrow I^- + Products \qquad (4)$$

The peak potential for the CV shifts in the anodic direction with increasing the concentrations of DECP, indicating that the currents may arise from both Eqs. (1) and (3). Since the binding reaction (Eq. (2)) is not so complete, there is no peak separation between these two reactions. The observed increase in the peak height as a function of DECP concentration can be explained by taking into account that chemically formed $I^-$ species (Reaction (4)) can be either further oxidized by reaction (1) or form the intermediate again by reaction (2) and then be oxidized by reaction (3). If the reactions (2) and (3) are faster when compared to reaction (1), the anodic reaction rate is much higher due to the reactions (2), (3), and (4). This results in the formation of less $I_2$ with increasing DECP concentration. This explains the decrease in the peak height during the cathodic sweep because less iodine is available for reduction due to an increase in the

concentration of the intermediate [DECP-$I^-$]. The observed shift of the anodic peak potentials with increasing the concentration of DECP is probably due to the formation of the intermediate complex between iodine and DECP. According to this mechanism, this reaction is selective for DECP. Accordingly, the other similar compounds such as diethyl chlorophosphate, DMMP, methyl phosphonic acid, dimethylphosphinic acid, and trimethyl phosphate cannot be oxidized by $I_2$.

In addition to the work reported above, we have devoted effort to developing a new analytical electrochemical method calld Double-Potential-Step Chronoamperometry (DPSCA).

In DPSCA experiments, The rest potential (E1) is initially chosen so that no net electrochemical reaction occurs. At some time (defined afterward as t=0) a pulse is made to a potential E2, where the oxidation of $I^-$ to $I_2$ is diffusion-controlled. After time $t_1$ at this potential it is stepped back to a value E3, where $I_2$ is re-reduced to $I^-$ again at a diffusion-controlled rate. The ratio of current detected for these pulses is expressible as a simple function of the DECP concentration.

If the current ratios are plotted against the concentrations of DECP, we find that the slopes of the straight lines depend on the concentration of NaI. If an increase of 50% in current ratio is considered to be discriminable, the detection limit of this method for DECP is determined to be $2x10^{-6}$ M. This is comparable with other kinds of detection technologies if coupled with a suitable built-in motor pump and more sensitive than currently available electro-chemical sensors based on conductivity and enzyme reactions. We find DPSCA to be more sensitive than single-potential-step chronoamperometry (SPSCA). This is because, unlike SPSCA, DPSCA measures both the anodic and cathodic currents and then uses their ratio as the measuring parameter. This makes DPSCA relatively insensitive to factors such as evaporation of solvent and adsorption of harmful gases, and thus more reproducible. Research on developing sensors based on immobilization of chemical catalysts and enzymes is now in progress.

In the future, we plan to work on developing sensors based on immobilization of catalysts on electrode surfaces. In previous work, the catalyst, iodide was added to the solution. For single-potential-step chronoamperometry, there is a sgnificant background current because of the continuous diffusion of iodide to the electrode even when nerve gases are absent. However, if a catalyst can be immobilized on the electrode surface, the background current will be very small in the absence of nerve gases and the sensitivity can be greatly improved even with single-potential-step chronoamperometry. The catalysts include iodide, metal oxides, or other oxidizing agents. The immobilization methods are direct adsorption, ion exchange, and carbon paste mixtures.

We also plan to work on sensors based on enzymes. The adopted enzymic-amperometric method is based on the following two reactions:

$$\text{Acetyl-choline} \xrightarrow{\text{acetylcholinesterase}} CH_3COOH + \text{Choline}$$

$$\text{Choline} + 2O_2 + H_2O \xrightarrow{\text{choline oxidase}} \text{betaine} + 2H_2O_2$$

In the absence of nerve gases, the first reaction is catalyzed by acetylcholinesterase and the second reaction is catalyzed by choline oxidase, so that the dissolved oxygen in the solution decreases. In the presence of nerve gases, the acetylcholinesterase covalently binds to the nerve gases and becomes irreversibly inhibited, so that the first reaction is slowed down and more oxygen can be detected.

We also plan to work on flow injection detection for electrochemical sensors. Electrochemical detection in flowing systems is usually performed by controlling the potential of the working electrode at a fixed value and monitoring the current as a function of time. The current response reflects the concentration profiles of these compounds as they pass through the detector. Here, detection for liquid chromatography or a flow injection system results in sharp current peaks. Accordingly, the magnitude of the peak current serves as a measure of the concentration. . The used detector is based on the thin-layer or well-jet configuration, and the detection electrode with the immobilized catalyst. In the absence of analytes or nerve gases, the background current is very small, which is caused by redox reactions of the mobile phase or carrier solutions. Such fixed-potential amperometric measurements have the advantage of being free of double-layer charging and surface-transient effects. As a result, extremely low detection limits on the order of 1-100 pg or about $10^{-14}$ moles of analyte can be achieved.

***Publications and Technical Reports***

"Design of Thin Film Filters for the Monitoring of Chemical Reactions". J.A. Dobrowolski, P.G. Verly, J.F. Aust, M.P. Nelson and M.L. Myrick, in Proceedings of the SPIE Annual Meeting on Optical Science and Engineering, San Diego, California, July, 1997 (in press, 1998).

"Single-Shot Multiwavelength Imaging of Laser Plumes". M.P. Nelson, W.C. Bell, M.L. McLester, and M.L. Myrick *Appl. Spectrosc.* 52(1998), 179.

"Multivariate Optical Computation for Predictive Spectroscopy". M.P. Nelson and M.L. Myrick *Anal. Chem.* 70(1998), 73.

"Single-Shot Multiwavelength Imaging of Laser Plumes". M.P. Nelson, W.C. Bell, M.L. McLester, and M.L. Myrick presented at Pittsburgh Conference, New Orleans, LA, Mar 1-6, 1998.

"Multivariate Optical Computation for Predictive Spectroscopy". M.L. Myrick, M.P. Nelson, J.F. Aust, J.A. Dobrowolski, and P.G. Verly presented at Pittsburgh Conference, New Orleans, LA, Mar 1-6, 1998.

"Molecular Transducers for Detecting Organophosphonate Nerve Gas Simulants". Mehrnaz Kamal and Brian A. Salvatore (to be presented at the 217th American Chemical Society National Meeting (Organic Chemistry Division), August 17-23, 1998, Boston, MA.)

"A Novel Electrochemical Detection Technology for Nerve Gases". Yuanwu Xie, Branko N. Popov and Ralph E. White, Extended Abstract, Annual AIChE meeting, 1998, 11, Miami, Florida.

"A Novel Electrochemical Detection Technology for Nerve Gases". Yuanwu Xie, and Branko N. Popov (in preparation to be submitted in Journal of Electrochem. Soc.)

***Personnel***

In addition to the principal investigators (M. Myrick, B. Salvatore, H. zur Loye, B. Popov and T. Bryson), the following personnel are involved in this research project:

Delia Ciurtin – graduate student with H. zur Loye
John Claridge - postdoctoral associate with H. zur Loye
Chris Dyke - graduate student with T. Bryson
Jeanne Jennings - graduate student with T. Bryson (partial support)
Bill Kemnitzer - graduate student with T. Bryson (partial support)
Wendy Bell - graduate student with M. Myrick (partial support)
Matthew Nelson - graduate student with M. Myrick (partial support)
Dr. Mehrnaz Kamal - postdoctoral associate with B. Salvatore

We anticipate the addition of a post-doctoral associate to the Bryson group in the near term, as the position has been offered to a candidate. The Myrick group will add Raju Prajesh, currently a graduate student in Physics at Louisiana State University with expertise in probe microscopy and oxide film preparation, Baton Rouge, LA, in May, 1998. Mr. Prajesh will work on optical computational devices during summer, 1998 as a research associate, and will finish his Ph.D. during early fall, 1998. After that time he will be converted to a post-doctoral associate.

## LIST OF INVENTIONS

During work on this subproject, the following inventions have been disclosed to the University of South Carolina, related to work done on this subproject.

1. Negative Dispersion Filter to Counteract Dispersion in Optical Fibers.
2. Filter Modifiers and Erbium-Doped Fibers as Superfluorescent Light Source
3. Data Metrics
4. Shaping Filters
5. Spectrometer on a Chip
6. ElectroOptic Filters
7. Color Separation Filters
8. Artificial Neural Network Stages
9. Hybrid Chemical-Orthogonal Methods
10. Designer Fluorophores
11. Autocorrelation Function and Normalization
12. Filter Simplification
13. Temperature Correction For Optical Devices

14. Spectrum-corrected Light Source
15. Gratings
16. IR Up-Conversion Materials

## BIBLIOGRAPHY

1. Hearing before the Committee on Armed Services. United States Senate, Ninety-Ninth Congress, May 1, 1985.Chemical Warfare Review Commission, S. Hrg. 99-255.
2. Brooks E. Kleber and Dale Birdsell, *The Chemical Warfare Service: Chemicals in Combat*. U.S. Government Printing Office, 1966.
3. Other examples include: (a) Vietnam, suspected of chemical operations against Kampuchea but not against the US during the Vietnam War, and (b) Iraq, known to have conducted chemical operations against the Kurdish population of Iraq and against Iran during the Iran-Iraq War, but not against the Allies during Desert Storm.
4. For example: (a) *Chemical Warfare Progress and Problemsin Defensive Capability*. General Accounting Office, PEMD-86-11, July 31, 1986; (b) *Chemical Warfare. Soldiers Inadequately Equipped and Trained to Conduct Chemical Operations*. General Accounting Office, NSIAD-91-197, May 29, 1991.
5. *The 1996 United States Army Modernization Pl*an, Department of the Army, 1996.
6. N. R. Brletich, M .J. Waters, G. W. Bowen and M. F. Tracy, *Worldwide Chemical Detection Equipment Handbook*, Chemical and Biological Defense Information Analysis Center, 1995.
7. J.Emsley, *The Chemistry of Phosphorus*, John Wiley & Sons, N.Y., 1976, p 494.
8. A. J. Bard and H. Lund, Eds, *Encyclopedia of the Electrochemistry of the Elements*, vol.3, Marcel Dekker, N.Y., 19XX.
9. J. Rebek Jr., "Molecular Recognition with Model Systems", Angew. Chem. Int. Ed. Eng., 1990, 29, 245.
10. E.C. Breinlinger, V. M. Rotello, *J. Am. Chem. Soc.*, 1997, 119, 1165-1166.
11. B. Eggins, *Biosensors: An Introduction* Wiley-Teubner, New York, 68-71 and 179-83, 1996.

## APPENDICES

Attached to this document, following Form 298, please find the following appendix:

Appendix I: Patent Descriptions for US Patent Office for inventions listed in section 6.0.

| REPORT DOCUMENTATION PAGE | Form Approved OMB No. 0704-0188 |
|---|---|



| 1. AGENCY USE ONLY *(Leave blank)* | 2. REPORT DATE | 3. REPORT TYPE AND DATES COVERED |
|---|---|---|
| | June 1, 1998 | Annual |

| 4. TITLE AND SUBTITLE | 5. FUNDING NUMBERS |
|---|---|
| Technology Development for Chemical Detection | Grant Number N00014-97-1-0806<br>PR Number 97PR06312-00<br>PO Code 353<br>Disbursing Code N68892<br>AGO Code N66020<br>Cage Code 4B489 |
| 6. AUTHOR(S)<br>M.L. Myrick, B. Salvatore, H. zur Loye, T. Bryson, and B. Popov | |
| 7. PERFORMING ORGANIZATION NAME(S) AND ADDRESS(ES)<br>University of South Carolina | 8. PERFORMING ORGANIZATION REPORT NUMBER<br>N00014-97-0806-1 |
| 9. SPONSORING / MONITORING AGENCY NAME(S) AND ADDRESS(ES)<br>ONR | 10. SPONSORING / MONITORING AGENCY REPORT NUMBER<br>ONR |

11. SUPPLEMENTARY NOTES

Prepared in coordination with University Research Initative Program for Combat Readiness

| 12a. DISTRIBUTION / AVAILABILITY STATEMENT | 12b. DISTRIBUTION CODE |
|---|---|
| APPROVED FOR PUBLIC RELEASE | |

13. ABSTRACT *(Maximum 200 words)*

The work by B. Salvatore is focusing on developing transducer molecules for the remote detection of organophosphonate-based nerve gases via both electrochemical and optical changes of signaling groups. Work to date has focused on the synthesis and electrochemical studies along the synthetic route of an electrochemical sensor. The zur Loye group is initially concentrating on dispersing cyclohexanone oxime on high surface area supports. Once a suitable support has been identified, samples will be given to Branko Popov for an investigation of the electrochemical response of these materials. Prior to working with the Salvatore/zur Loye chemistry, the Popov group has studied catalytic oxidation of nerve gases by electrochemically generated iodine cyclic voltammetry. On a second front, the Popov group has been developing a new detection technique baseed on Double-Potential-Step Chronoamperometry (DPSCA). The work of the group of T. Bryson is focusing on recognition chemistry for natural toxins, using saxitoxins (STXs) as model compounds. In their approach, an optical transducer is being structurally fitted to the hydrogen bonding (NH or $NH_2$) groups and the rarely encountered *gem* diol of STXs. The Myrick group is refining the theory of optical-computing methods for rapid, sensitive and selective "optrode" type determinations. A new facility for the fabrication of the optical computing devices is being constructed and installed (June, 1998), and software development methods for computing devices are being refined.

| 14. SUBJECT TERMS | 15. NUMBER OF PAGES |
|---|---|
| Chemical and Biological Warfare, Target Acquisition, Snti-Submarine, Combat Medicine, Biodeterioration, Command Control and Communication | 13<br>16. PRICE CODE |

| 17. SECURITY CLASSIFICATION OF REPORT | 18. SECURITY CLASSIFICATION OF THIS PAGE | 19. SECURITY CLASSIFICATION OF ABSTRACT | 20. LIMITATION OF ABSTRACT |
|---|---|---|---|
| UNCLASSIFIED | UNCLASSIFIED | UNCLASSIFIED | 200 WDS |

*Appendix I - Descriptions for US Patent Office Filing of Inventions Listed in Section 6.0 (without figures)*

Negative Dispersion Filter to Counteract Dispersion in Optical Fibers.

In certain embodiments disclosed in the USC-4 application, optical filters were used to selectively filter light over a given wavelength range. Primarily, the filters transmitted a predetermined percentage of the light's magnitude at each wavelength, the transmission rate at each wavelength being independent of the transmission rate at any other wavelength. Optical filters may also, however, affect the phase of the light, and may do so differently at different wavelengths. That is, due to the configuration of the materials comprising the filter, the filter may pass light at different wavelengths at different speeds. Accordingly, the filter creates a phase shift that varies with wavelength over the wavelength range of the light passing through the filter.

This did not matter for most of the embodiments of the invention described in the USC-4 application. Those embodiments filtered light magnitude by wavelength so that the light magnitude output by the filter provided certain desired information. Phase shift was irrelevant. The phase shift effect may, however, be useful in other environments in which optical filters may be used to counteract wavelength dependent phase shift effects.

Fiber optic communications systems provide one such environment. Channels used to transmit signals over optical fibers typically have a finite bandwidth within which signals, for example pulses, are transmitted. In conventional systems, it is desirable to simultaneously transmit as many pulses as possible within the bandwidth, and narrow pulses are therefore desired. Although it is possible to use a laser to create a very narrow pulse, laser signals are often unstable, sometimes exhibiting sudden shifts in wavelength. Accordingly, signal pulses are typically produced by modulating a series of light sources, where each light source emits light over a limited wavelength range within the channel's bandwidth. Each resulting pulse includes light over a certain wavelength range that does not overlap the wavelength ranges of simultaneously transmitted pulses.

Unfortunately, light at different wavelengths travels at different speeds through a fiber optic medium. Thus, for example, a square pulse tends to distort and broaden as it travels along the fiber. If a pulse is close to an end of the channel bandwidth, distortion may broaden the pulse beyond the channel. Adjacent pulses may broaden so that they overlap, causing crosstalk. By the time the signal reaches the end of the fiber optic cable, information may be lost.

Although the USC-4 embodiments primarily include filters constructed to scale light magnitude, such systems may also selectively modify phase. Specifically, a system may include one or more filters that have a predetermined phase shift at each wavelength. If the phase shift characteristics of a fiber optic cable are known, a filter may be designed that reverses the phase shift over the cable to reproduce the original

sharp input pulse.

In general, phase shift filters may be constructed using the same techniques used to construct magnitude filters except that a desired phase shift pattern, not necessarily a desired magnitude transmission pattern, is the guiding design criteria. An exemplary optical filter design procedure that accounts for phase shift is discussed at J. A. Dobrowolski and D. Lowe, "Optical Thin film Synthesis Program Based on the Use of Fourier Transforms," Applied Optics, Vol.17, No.19, p.3039 (Oct. 1, 1978).

The construction of any particular filter may depend on the length of cable to which it is to be attached. Thus, filters might be constructed for cables of predetermined lengths, for example, 1 or 10 kilometers. To correct distortion in a particular system, as many filters as needed are intermittently installed over the length of cable. For example, if filters are designed for 10 kilometer lengths of a certain type of fiber optic cable, and the system includes a 95 kilometer length of this cable, nine filters may be installed, each at a 10 kilometer interval. Although the remaining 5 kilometers may cause no significant distortion, a filter may be designed for this length as well.

Filter Modifiers and Erbium-Doped Fibers as Superfluorescent Light Source

In fiber optic communications, erbium doped fibers are often used to amplify signals. Specifically, the fibers are inserted periodically in long fiber optic cables, for example, every 10 kilometers. An adjacent laser stimulates the fiber so that it emits radiation. Normally, a fluorescing erbium fiber emits radiation in a random pattern. However, if it is in line with a fiber optic cable, the erbium fiber emits two photons along the fiber optic path for each single photon received from the cable. In this manner, the erbium-doped fiber acts as a fiber optic amplifier, the gain of which is typically described in dB. Multiple fibers may be disposed in the system to achieve a desired gain.

Although erbium fibers are traditionally used as amplifiers, they may also be used as light sources in conjunction with optical filter systems as disclosed in the pending patent application. In general, erbium fibers may be used to create light signals having a relatively broad, yet limited, wavelength band favorable for the construction of optical filters. In addition, optical filters may be produced to modify the light signal from the fibers to a standard predetermined form, thus allowing the use of standard, easily manufactured optical filters. These "modifying filters" may be used to shape light from other sources, for example, WDM sources.

As noted in the USC-4 application and in the discussion above, one problem with conventional fiber optic communication systems is their limited bandwidths. Since it is desirable to simultaneously transmit as many signals as possible in order to maximize the amount of information transmitted, it is desirable in conventional systems to use signals, such as pulses, having as narrow bandwidths as possible. The pulses must be sufficiently separated in wavelength, however, to avoid crosstalk caused by phase distortion affects of the optical media.

As described in the pending application, one solution to this problem is to use signals comprising orthogonal pulses which overlap in wavelength. Because the signals are orthogonal, downstream optical filters are able to compress the data to retrieve the information carried by the signals.

Given that a system transmits wavelength-overlapping orthogonal functions, the question then becomes how to create these signals. In general, the signals are created by passing light through USC-4 optical filters that output to an optical fiber cable. Each filter shapes the light to a predetermined shape that is orthogonal to the shapes created by the other filters. Pulses are created by pulsing the input light. Because the overlapping signals, or "channels," are orthogonal, each channel's pulses can be detected by a corresponding downstream filter without interference from the other channels.

There are an infinite number of ways to create a set of orthogonal functions. One simple method is to use orthogonal sine waves. Thus, it is possible to create a set of filters that generates a set of orthogonal sine waves and to use these filters as standard filters in any given system. The use of filters as standard, interchangeable filters, however, requires a standard light input, since the shape of the output light depends on the shape of the input light. For example, an optical filter whose transmission pattern defines a sine wave will output a sine wave signal only if the input light has a constant intensity across the wavelength band. Of course, if the intensity is not constant, this may be accommodated by the filter design so that the filter nevertheless produces a sine wave output.

Orthogonal filters may be standardized to individual light sources. For example, it is possible to identify the output spectra of various types of light sources, for example lamps or lasers, and create filter sets for each. Each filter set is configured to produce orthogonal functions for the particular light pattern produced by each particular light source. It is also possible, however, to standardize the orthogonal filters to a standard light source spectrum and to create modifying filters for the various light sources to modify their output to the standard spectrum. One convenient standard light source output is a constant intensity ("flat") signal.

The second approach has certain advantages over the first. Primarily, it permits the use of standard filter sets for all optical communications systems. Light sources can be packaged with an appropriate modifying filter or filters so that these light source "packages" can be used interchangeably in any system. That is, it might be easier to provide light source packages with modifying filters than to provide orthogonal filter sets specific to the light source.

The next issue involves the orthogonal signal bandwidth. The orthogonal signals of either filter approach discussed above have some operative bandwidth. Because some light sources output light over wider, or different, bandwidth ranges than others, the choice of a given set of orthogonal functions over a given bandwidth range may

preclude the use of light sources which do not output light over that range.

One answer would be to simply use a very sharp, square, narrow bandwidth laser pulse. This has the advantage of providing flat input light signals to the orthogonal filter set without the use of modifying filters. Flat input signals allow, for example, the use of orthogonal filters with sine wave transmission patterns to produce sine wave orthogonal signals. Because the construction of Dobrowolski optical filters depends upon the Fourier transform of the orthogonal transmission functions, construction of sine wave filters is relatively simple. Thus, the use of flat pulses permits the use of easily constructed sine wave filters.

Unfortunately, the bandwidths of laser pulses are so narrow, typically a fraction of a nm, that it is impractical to create orthogonal pulses within the Dobrowolski filters, even where Fourier components are used. The size of a Dobrowolski filter is dependent on the signal bandwidth. Thus, even though the use of Fourier components would result in a relatively simple filter design, the filter itself would be very large.

Accordingly, at least when using filters constructed by the Dobrowolski method, it is desirable to use a broad band light source such as a lamp, which emits light covering hundreds of nm. Lamps, however, are inefficient. They require a relatively great deal of power, and, while they also output a great deal of power, it is distributed over the long wavelength range. Thus, there is relatively little power over the operative bandwidth.

On the other hand, an excited erbium-doped fiber emits light over a relatively broad, yet limited, wavelength range (about 10 nm to 20 nm). Thus, the power output over its output bandwidth is greater than the output over a similar range from a lamp, yet the range is broad enough to permit construction of filters of an acceptable size.

Referring to Figure 3, an erbium fiber 2 (or multiple fibers attached end to end) is attached to a fiber optic cable 4 by an optical connector 6. An adjacent laser 8 excites the fiber 2 so that it emits its broader band light into the fiber optic cable. Although the excited erbium fiber emits light in a random pattern, sufficient light will be input to the cable to create an adequate signal. The output of erbium fibers should be understood by those of ordinary skill in the art, and the number of erbium fibers used may be selected according to the requirements of a given system. Furthermore, erbium fiber amplifiers may be used at suitable points to amplify the signal if needed.

The output signal from fiber 2 travels along fiber 4 to a collimating lens 10 which directs the light to a modifying filter 12. The modifying filter is, as described above, designed specifically to modify the erbium fiber's output signal to a predetermined output, for example a flat signal. A lens 14 focuses this signal to a fiber optic cable 16 for output to an electrooptic modulation unit. Erbium fiber 2 and modifying filter 12 may be packaged as a unit disposed in a housing 18, which may be interchanged with other units which may have different light sources but which produce the same

standard output signal.

The electrooptic modulation unit includes a collimating lens 20 that receives and collimates the signal from fiber optic cable 16 and outputs the collimated light to a set of optical filters 22. Each filter 22 filters light received from lens 20 into a light signal that is orthogonal to the signals from every other filter 22. A respective lens 24 focuses the signal from its filter 22 to a fiber optic cable 26 that, in turn, carries its signal to a modulator 28. Each modulator 28 is controlled, for example by a computer or other suitable processing device, to intermittently pass the signal to a respective fiber optic cable 30, thereby creating a series of pulses in such a manner that the number and/or frequency of pulses carries information. If the signal output by unit 18 is a standard shaped signal, the filters 22 may be standard filters generating a set of standard orthogonal functions. A lens 32 receives the orthogonal pulses and focures them to an output fiber optic cable 34.

A series of downstream optical filters (not shown) receives the signal carried by cable 34. One or more downstream filters filter the same function as a corresponding filter 22 in the electrooptic modulation unit. Thus, the downstream filter(s) detects the presence of each pulse emitted by the modulator 28 of the corresponding upstream filter 22. Since the pulses of the signal on line 24 are orthogonal to each other, each downstream filter detects pulses only from its corresponding upstream filter 22.

Although the upstream filter filters the same function as the downstream filter, the upstream and downstream filters need not be identically constructed. For example, the upstream filter may comprise two physically distinct filters that combine to generate a signal that is detected by a single downstream filter having a transmission pattern different from that of either upstream filter.

In another embodiment, modifying filters and orthogonal filters are retrofit into existing WDM systems. The WDM systems may transmit a series of individual pulses spaced apart over a particular wavelength range. Orthogonal filter pairs may be inserted into the WDM system to divide the WDM pulses themselves into orthogonal sub-components. This creates a plurality of orthogonal channels within the existing WDM channels.

Because the WDM pulses are not exactly squared, it may be desirable to include a modifying filter as described above to square each individual WDM pulse. A plurality of off-the-shelf standard orthogonal filters, for example using sine functions, can create orthogonal channels within each WDM channel, which can then be transmitted over a single optical line.

Data Metrics

USC-4 optical filters are used in this embodiment for error detection purposes. In general, an error is detected when a sample spectrum input into the system is significantly different from spectra the system normally processes. Typical error

detection methods utilize euclidian distance and Mahalanobis distance. To determine euclidean distance, an average spectrum is first determined from a predetermined number of samples. The distance between a measured spectrum and the resulting average spectrum is then determined by taking the square root of the squared difference between the average spectrum and the measured spectrum at each wavelength.

One way to detect errors in a USC-4 optical system is to output the intensity of the sample spectrum to a computer which performs a suitable mathematical analysis. It is also possible, however, to estimate the euclidean distance in a manner that can be effected by an optical filter.

Shaping Filters

The use of bandpass filters to assure that only light within the optical filter's operative range is passed to a light detector is disclosed in the pending application. In a specific embodiment, however, each optical filter in the system is disposed on a substrate which includes the bandpass filter. This permits mass production of bandpass blanks upon which optical filters may be deposited.

Spectrometer on a Chip

In this embodiment of the USC-4 application, a detector device includes a linear array of photodiodes to create an optical filter. An IC chip may include an array of potentially thousands of very small (for example approximately 25 micrometers wide) photodiodes. An optical filter having approximately the same width and length is disposed on each photodiode.

Each optical filter is constructed to transmit an orthogonal component of the light to its photodiode. If the principal components of the incoming light are known, for example, each optical filter may be a principal component filter. Thus, each photodiode instantly detects the magnitude of the principal component filtered by its optical filter and outputs this magnitude to a computer which, from this information, reproduces the spectrum. The computer is then able to perform any desired spectral analysis.

Accordingly, the optical filters permit the construction of a spectrometer on an IC chip which can replace conventional spectrometers in existing spectroscopy systems. These IC's enjoy a signal-to-noise advantage over conventional spectrometers, which may lose 70% to 90% of incident light. Losses for the IC are generally less than 50%.

Of course, this embodiment is not limited to principal component analysis. The filters may filter any set of orthogonal functions to compress the light data. Thus, for example, filters might separate light into a set of Fourier components or into very narrow wavelength bands. The computer performs the inverse transform of the components to reconstruct the signal. An IC may therefore be used as a generic filter to compress any incident light, regardless of the source.

ElectroOptic Filters

In this embodiment, an optical filter is constructed to have a changeable response. Referring to Figure 1, optical filter 10 includes an optical filter 12 configured to selectively filter light by wavelength over the filter's wavelength range, for example to effect a regression vector. A layer 14 constructed from a non-linear optical material (for example lithium niobate or poled polymer films) exhibits refractive indices over the wavelength range of filter 12 that vary in the presence of an electric field. Layer 14 is sandwiched between conductive glass plates 16 and 18. A voltage generated by a voltage/signal source 20, which may include a voltage regulator circuit, applied across layer 14 at plates 16 and 18 changes the refractive indices of layer 14 from a first state to a second state. Since both filter 12 and layer 14 contribute to the overall transmission pattern of filter 10, the selective application of voltage 20 across layer 14 changes filter 10 from one transmission pattern to another.

Both filter 12 and layer 14 (which is also an optical filter) may be constructed using the Dobrowolski iterative layering approach referenced in the pending patent application. The process begins with a base material having a particular refractive index. Subsequent layers are added in an iterative procedure to achieve a desired transmission spectrum. This is generally done by a computer program. If phase shift is not a concern, there may be many, if not an infinite number of, ways to construct the layers to achieve a desired transmission pattern for the filter.

Creating filter 10 is similar to solving simultaneous equations. Because there may be various ways to make each of the filters 12 and 14, they are designed so that they cooperate to produce a first desired transmission pattern when voltage 20 is applied across filter 14 and to produce a second desired transmission pattern when the voltage is not applied. In other words, the requirement that filters 12 and 14 must produce the predetermined transmission patterns under the different conditions is a limitation in the layering design for each filter. This process should be relatively straightforward, for example, if filter 10 embodies a Fourier function, since changing the filter's overall refractive index merely shifts from one Fourier function to another.

A filter 10 might be designed to effect a certain regression vector when the voltage across filter 14 is disconnected but the negative of the regression vector of the voltage is applied. Thus, light from an illuminated sample may be passed through filter 10 with voltage 20 disconnected so that the filter dots the incoming light with the regression vector. When voltage 20 is then applied across filter 14, however, filter 10 applies the negative of the regression vector. If measurements of light intensity under these two conditions are subtracted, the result is proportional to the property to which the regression vector corresponds. This is a convenient way to remove any DC component that may otherwise arise from a variety of causes and that may interfere with accurate measurement.

This embodiment of the USC-4 technology also allows construction of a single filter to analyze a sample for multiple properties by selectively applying one or more voltages

to particular filter layers. For example, the filter may include several non-linear optical material layers 14 to produce a single filter 10 that can apply multiple functions. The number of desired functions increases the complexity of filter design.

For layer 14 to exhibit the desired non-linear electrooptic characteristic, molecular elements of the material comprising the layer must be aligned to facilitate application of the electric field. This may be achieved by a number of methods of producing non-linear optical material wafers, for example poling or brushing a polymer layer, as should be understood by those of ordinary skill in the art.

In another method, however, a polymer layer is deposited on plate 18, for example, by a vaporization technique. Light polarized 90% to the desired direction is applied to the polymer layer to remove molecular elements of undesirable polarization. The light quickly excites and burns away those elements aligned with its polarization. Continued application of the light burns away elements increasingly angularly offset from the light's polarization until elements approaching a 90% offset are removed. The light does not excite the elements disposed at the 90% angle, and those elements will remain intact within the layer. The duration of the light's application to the polymer layer determines the degree to which elements not exactly aligned in the desirable direction are retained.

Color Separation Filters

Color videography or photography systems typically use three color channels: red, green, and blue. USC-4 optical filters may be used in a color system to detect characteristics of a sample and to output color signals indicative of these characteristics.

In one exemplary embodiment illustrated in Figure 4, a sample 2 is illuminated by a light source 4 so that light from the illuminated sample is received by a collimator 6. A bandpass filter 8 receives the collimated light and passes light within the operative wavelength range of the downstream optical filters 10 to a beam splitter 12. Beam splitter 12 separates the light into three light beams, each directed to a respective filter 10.

Each filter 10 filters a function; for example, a regression vector that is associated with a particular characteristic of the sample. Thus, the light output from each filter is proportional to the strength of its characteristic in sample 2. Each filter 10 directs its output to a detector 14; for example, a CCD camera that includes a colored light output (red, green, or blue). The intensity of filters 10 determines the intensity of the red, green, or blue light output by detectors 14. Thus, the relative strengths of the regression vector characteristics determine the color output by the system from a lens 16, which combines the light from detectors 14.

The system components downstream from sample 2 may be disposed in a housing 18. The collimator, bandpass filter, beam splitter, detectors, and lens may be relatively

small devices, as should be understood by those of ordinary skill in this art. The filters 10 may be similarly small devices, and the housing 18 may be a hand-held color measurement device. For example, assume sample 2 is the surface of an aircraft and that three regression vectors may be developed that identify characteristics of the surface that contribute to structural weakness. A hand-held (or larger) detector 18 may be passed over the aircraft surface to collect reflected light. The color of the light that the detector outputs indicates both the overall strength of the characteristics and their strength relative to each other. Accordingly, a color scale may be developed to which the sensor output may be quickly compared to identify those surface areas where the characteristics exist in such proportion to indicate a serious weakness.

It should be understood that Figure 4 is provided for illustrative purposes and that the device may be constructed in various suitable manners. For example, the components 6, 8, 12, 10, 14, and 16 may be constructed as a unitary device. Further, beam splitter 12 may be replaced by other suitable devices or arrangements and, for example, omitted where filters 10 are all disposable to receive the output of collimator 8.

Artificial Neural Network Stages

Referring to Figure 2, wavelength bands (I1 - I4) from a spectrograph may be used as inputs to an artificial neural network. Specifically, light from each wavelength band is weighted by a weighting factor at A before passing to a non-linear step B. The weighting factors A are effected by USC-4 optical filters, one per wavelength $I_n$ per non-linear step B.

Hybrid Chemical-Orthogonal Methods

Substances are sometimes contaminated with other substances that are not readily apparent to visual, chemical, or spectroscopic analysis. By addition of a certain reagent, however, a new compound is formed that has a larger spectroscopic signature and that is, therefore, more easily detected. For example, the chemical TCE is an environmental hazard that may be almost undetectable when present in water. In the Fujiwara process, for example, a reagent added to TCE-contaminated water reacts with TCE to color the water so that the presence of the contaminant is apparent.

Unfortunately, the Fujiwara reagent may react with other substances to produce a nearly identical color, making visual identification difficult. However, even where the different reactions produce similar colors and spectroscopic signatures, there are differences. A USC-4 optical filter may embody a regression vector to identify a particular chemical produced only by the reaction with the searched-for contaminant, thereby eliminating the need for visual inspection and the possible resulting uncertainty.

Designer Fluorophores

In prior art DNA systems, fluorescent "tags" are attached to DNA splices by a DNA sequencer, and the DNA is output in a fluid stream through which light is passed to a spectroscope. The resulting spectrum is analyzed to determine which tags are present,

thereby identifying the DNA splices.

There are significant limitations with this approach. Primarily, it is relatively inaccurate, and tags are therefore typically selected from fluorophores having widely differing spectral signatures. That is, the euclidean distance between the spectra of these fluorophores is large. Since each tag must be significantly different from all other tags, the number of available tags is limited.

USC-4 optical filters, however, may apply regression vectors that recognize and distinguish any fluorophore tag, no matter how close it is to any other tag. For example, referring to Figure 5, a DNA sequencer 2 applies fluorophore tags to DNA splices and outputs the splices to a fluid stream through a fluid conduit 4. A laser 8 excites an erbium fiber 6, which outputs a light signal to a fiber optic cable 10 to illuminate the fluid as it passes through the conduit. A collimator 12 receives the light from the illuminated fluid and directs the light to a series of optical filters 14, each of which effects a regression vector to identify a particular fluorophore tag. Although three filters are illustrated, it should be understood that any number may be used, depending on the number of fluorophore tags the system employs. Bandpass filters 16 limit the light to the operative wavelength range of the filters 14. Each detector 18 outputs an electrical signal to, for example, a computer that corresponds to the intensity of the light signal received from a corresponding filter 14. By monitoring the detector outputs, the computer is able to identify specific fluorophore tags.

Autocorrelation Function and Normalization

To normalize a signal's magnitude, the signal magnitude is measured in any suitable and consistent manner (for example at a peak or as integrated over a given wavelength range) to proportionally scale the amplification level of an amplifier. For example, assume a signal is input to an amplifier having a 10 times gain. A signal coming into the amplifier with a peak magnitude of 5 exits with a peak magnitude of 50. A signal entering with a magnitude of 10 exits with a magnitude of 100. To normalize the signal, a detector is placed upstream from a variable amplifier. The detector is configured to measure the signal magnitude and to output a corresponding electrical signal to the amplifier, or to a circuit controlling the amplifier, so that the amplifier gain is divided by the signal magnitude. Thus, if the incoming signal has a magnitude of 5, the amplifier gain of 10 is divided by 5 so that the signal is magnified by a factor of 2. If the incoming signal has a magnitude of 10, the amplifier gain is 1. Thus, within the operating range of the amplifier, the magnitude of the amplified signal is always 10.

A system for normalizing an optical filter signal is illustrated in Fig. 6. A sample 2 is illuminated by a light source 4. A collimator 6 collimates the light and directs it to an optical filter 8, which effects a desired function such as a regression vector. A detector 10 receives the light from the filter and outputs an electrical signal 12 that corresponds to the intensity of the light it detects. An amplifier 14 amplifies this signal, outputting the amplified signal to a computer 16.

Amplifier 14 is a variable amplifier whose gain is controlled by an input signal 18. Amplifier 14 may be any well understood device, and its particular configuration does not form an essential part of the present invention in and of itself. It may be considered to include any associated control circuitry for receiving signal 18 and determining the amplifier's gain responsively thereto. In this embodiment, the amplifier's gain is understood to be divided by the magnitude of signal 18.

In Figure 6, signal 18 is equal to signal 12. Thus, amplifier 14 is scaled by the instantaneous magnitude of the signal output by the detector. It should be understood, however, that other scaling factors may be used. For example, an integrating circuit may be disposed along the path of signal 18 so that the amplifier gain is scaled by the average detector output over a predetermined time period. Further, while computer 16 is illustrated as the output device, this is for exemplary purposes only, and the amplifier output may be directed to any suitable downstream processing device, depending on the function of the particular system.

Normalization may be employed to perform an autocorrelation of the input signal, specifically the dot product of the input signal with the average of the input signal, to indicate the input signal's reliability. If the input signal is equal to the average signal, the dot product is maximized. As the input signal moves away from the average, however, the dot product is reduced.

In spectroscopy systems, the overall intensity of the input signal generally depends upon the intensity of the light source used to illuminate the sample. Information is carried by the spectral shape of the light from the sample. Since light source intensity tends to vary over time, it is desirable to normalize the input signal in performing the dot product. Once the signal is normalized, deviation in the dot product from a maximum value is due to differences between the shapes of instantaneous input signals, not to differences in overall signal strength.

If $S_{IN}$ is equal to the normalized instantaneous input light signal, considered as a vector in wavelength space, and $S_I$ is equal to the unnormalized instantaneous input light signal vector, and $S_A$ is equal to the average input light signal, then
$S_{IN} \cdot S_A = (S_I/\text{n.f.}) \cdot S_A = (S_I \cdot S_A)/\text{n.f.}$,
where n.f. is a normalization factor.

A system for performing this function is illustrated in Figure 7. The instantaneous input signal is output from collimator 6 to a beam splitter 20, which directs the signal to an optical filter 22 and to a detector 10B. Although the beam splitter reduces the overall intensity of the two divided signals from that of the input signal, the ratio of the overall intensities of the divided signals is typically unimportant as long as it remains constant, and the output of detector 10B may be suitably used as a normalization factor. Under this condition, the signal output from the beam splitter 20 to filter 22 may be considered $S_I$ in the above equation.

Filter 22 is an optical filter having a variable transmission spectrum patterned after the shape of the average input signal spectrum $S_A$. This pattern is determined by recording and averaging the spectra of several samples. Thus, the output of filter 22 is equal to the dot product of the unnormalized instantaneous input light signal vector and the average input light signal vector, or $(S_I \cdot S_A)$. To divide by the normalization factor, variable amplifier 14, which amplifies the $(S_I \cdot S_A)$ signal received by detector 10A, is scaled by the output of detector 10B. As discussed above, the normalization factor may be configured to any desired form, for example by an integrator circuit.

Computer 14, or other suitable monitoring device, receives the output from amplifier 14 to determine the difference between it and the maximum dot product value. This difference is an indication of input signal quality.

The system illustrated in Figure 7 may be used within a larger optical filter system. For example, beam splitter 20 may also direct the input signal to a set of optical filters configured to monitor the input signal for one or more characteristics of interest. Thus, computer 16 monitors data quality in real time.

Filter Simplification

Optical filters made by the Dobrowolski method are based on the Fourier transform of the filter function. Accordingly, filter design and construction may be complex where the filter function's Fourier transform contains high-frequency components. Filter design may be simplified, however, if the filter function is separated into segments. An appropriate offset function is added to the segments so that if filters are constructed for each function segment, subtraction of the segment filters' output is equal to the output of a filter effecting the original filter function. Segment filter construction may be simplified where the offset function is chosen to minimize the effect of high frequency Fourier components of the segment functions.

One convenient manner in which to divide the filter function into segments is by positive and negative values. In the pending application, the exemplary filter functions are separated into positive and negative segments. Filters are constructed for each segment, and the output is subtracted to provide the output of a filter that would embody the original function. Referring to Figures 8A, 8B, and 8C, an exemplary filter function A shown in Figure 8A is separated into its positive segment B and its negative segment C in Figures 8B and 8C, respectively. Segment C is inversed so that B - C = A. Thus, if optical filters are constructed to embody B and C, their output may be subtracted to achieve the same output as a filter embodying the function A.

If any arbitrary function D (not shown) is added to both B and C, the result is the same. The new functions may be described as B+D and C+D. Their subtraction, (B+D) - (C+D), is still equal to B-C, which is equal to A as described above.

It is desirable to choose a function D that minimizes the effect of high frequency

components in the segments. Exemplary Fourier transforms of segments B and C are provided in Figures 8D and 8E, respectively. These graphs are for exemplary purposes only and are not intended to represent the actual Fourier transforms of the functions shown in Figures 8B and 8C.

Function D is determined by analyzing the Fourier transforms of B and C. To begin, a frequency E is chosen above which the two transforms will be minimized. Obviously, frequency E may be selected as the lowest frequency in either transform, thereby increasing filter simplification. However, function D is an additive signal in the time domain, and functions B and C represent transmission rate patterns. If the transmission rate at one or more wavelengths in either segment is 100%, there can be no addition to the signal at these wavelengths. Further, the degree to which function D can be added at wavelengths having transmission rates near 100% will be limited. Thus, while the full value of function D is added at most wavelengths, the function may be added only partially, or not at all, at others. This causes a certain distortion and, when the respective outputs of the two segment filters are subtracted, the result may not exactly equal B-C. Because the magnitude function D adds to functions B and C is increased as frequency E decreases, choosing a higher frequency E decreases this possible error. Thus, frequency E is chosen to best optimize the objectives of filter simplification and data quality.

The effect of high frequency Fourier components on filter complexity can be described by the "power" of the combined transforms. For example, at frequency $X_1$, the power of the combined transforms is $(-3)^2 + 1^2 = 10$. The power at frequency $X_2$ is $4^2 + (-2)^2 = 20$. Obviously, the power at each frequency is minimized if the values of both the 8D and 8E graphs at those frequencies are zero. This is impossible, however, because the same function D must be added to both segment B and segment C. A value of 3 must be added to bring the B transform to zero at frequency $X_1$. That value would also be added to the C transform at frequency $X_1$, however, leaving a value of 4 and an overall power of 16.

Power is minimized, however, where the transform values are averaged at each frequency and where the average is subtracted from both transforms. At frequency $X_1$, for example, the average value is $(-3 + 1)/2 = -1$. When this value is subtracted from both the B transform end the C transform, the transforms have a value of -2 and 2, respectively, resulting in a power of 4. Repeating this process at frequency $X_2$ provide a power of 10.

Accordingly, the Fourier transform of function D at each frequency is determined by averaging the value of the B transform with the value of the C transform at that frequency, for all frequencies above E, and taking the inverse of the result. Inverse transforming this frequency domain function produces the wavelength domain function D. If D is added to both the B and C segments, the resulting segment filters are less complex in design and construction than filters designed from segment functions B and C alone, while providing an equal or approximately equal combined response.

Temperature Correction For Optical Devices

Certain of the USC-4 optical filters are constructed by layers of interference films. Materials, for example certain plastics and metals such as copper and brass, used to make these films have a relatively large coefficient of thermal expansion. Specifically, the refractive indices and linear dimensions of the materials may change with temperature change. This may cause the filter's transmission spectrum to shift to longer or shorter wavelengths. For example, a certain filter may be designed to have a 70% transmission rate at 900 nm. A given temperature change, however, may cause a wavelength shift so that the 70% transmission rate shifts to 895 nm, with all other transmission rates experiencing a similar shift.

To combat this effect, the filter may be rotated about an axis perpendicular to the light's direction of travel to change the angle at which the light hits the filter surface. This also causes a wavelength shift, either to longer or shorter wavelengths. The rotation is correlated with the temperature change so that the wavelength shift caused by one counteracts the wavelength shift caused by the other, leaving the filter's resulting transmission spectrum substantially constant.

In one preferred embodiment, the filter is mounted on a frame so that it is rotatable about an axis perpendicular to the incident light. A temperature-sensitive material that expands and contracts with temperature is attached at one end to the filter and at the other end to a support stationary with respect to the filter's frame. Thus, the expansion and contraction of the element with temperature change rotates the filter on the frame about the axis. The material and dimensions of the element, and its place of attachment to the filter relative to the axis, determine how much the element rotates the filter about the axis. These parameters may be determined by trial and error with a given filter construction or may be predicted if the thermal expansion characteristics of the filter material and of the temperature sensitive material are known.

Spectrum-corrected Light Source

In spectroscopy systems, the light intensity from sources such as lamps typically varies with age. Lamp filaments, for example, tend to develop thin spots. As a constant voltage is applied across the filament, current through the filament decreases due to the thin spots' higher electrical resistance. This reduces the lamp's output power. To maintain an average light intensity, conventional systems employed one or more light or heat detectors proximate the lamp and corrected the filament voltage responsively to the detector. Specifically, the output of the detector was directed to a control mechanism which controlled the voltage applied to the filament so that as intensity decreased with the development of thin spots, the voltage was increased to offset the power output loss.

While such an arrangement maintains the overall intensity of light from the source, it changes the light's spectrum. As the system increases filament voltage due to thin spots, the heat generated at the higher-resistance thin spots increases. However, even

with the increased voltage, there is less current passing through the filament than when the filament was new, and the areas of the filament other than the thin spots are cooler than normal. Thus, where the spectrum of a new filament may have a curve that peaks at a central wavelength range and lessens above and below that range, the increased voltage causes the spectrum to decrease in the central wavelength range and increase at the higher and lower levels corresponding to the increase in light contributed to the spectrum at the higher and lower temperatures. The shift toward the blue range is more dramatic since more light is contributed by the hotter thin spots.

Because information is carried by the spectral shape of light from an illuminated sample, a change of the light source's spectrum affects the accuracy of a spectroscopy system. While a lamp's spectrum changes due to filament aging, conventional systems aggravate the problem by maintaining a constant overall intensity. This is particularly unnecessary in view of the present invention which, as described above, minimizes or eliminates the effects of changes in the overall light intensity by signal normalization.

Accordingly, the control system described below adjusts the filament voltage to optimize the light source spectrum shape rather than its intensity. Specifically, sample spectra are measured for several identical new filaments to determine an average spectrum, and an optical filter embodying this function is designed. To design such a filter, the transmission rate at the wavelength of the highest magnitude of the average spectrum is set to 100%, with the transmission rates at all other wavelengths scaled accordingly.

A system as described with respect to Figure 7 employs the average spectrum filter to monitor the light source output. A computer 16 controls the filament voltage responsively to this measurement to maximize the output of amplifier 14, thereby keeping the spectrum of the lamp's light as constant as possible.

Gratings

The optical filters discussed in the pending patent application may also comprise gratings designed to compress an incident light signal into a desired function. Optical gratings may be constructed in various well-understood manners. For example, a top view of a volume holographic grating 2 is provided in Figure 9A. The grating comprises a polymer or gelatin layer whose density varies in a predetermined pattern from higher density regions 4 to lower density regions 6. The density modulation determines the angle at which light at a given frequency is reflected from the grating's surface. Since the reflection angle varies with frequency, reflected light is separated into its spectrum.

Figures 9B and 9C illustrate side views of two types of grooved gratings, which may be constructed of various suitable materials including metals and polymers. The grooves in the grating 2 of Figure 9B define a substantially sinusoidal shape and can be formed from a conventional photographic process. The distance A between the grooves' peaks and valleys is the modulation depth. The distance B between groove peaks may be

used to calculate the groove density (modulation density) C, which is typically within the range of 300 grooves/mm to 4800 grooves/mm.

If the angle of incidence is constant, the angle of reflection depends upon the modulation depth A and modulation density C. Referring to density in terms of distance B, $\sin\alpha + \sin\beta = \frac{\lambda}{B}$, where $\lambda$ is the wavelength of the incident light. Thus, assuming that the incident light is collimated (i.e. that $\alpha$ is constant) and that the grating has a uniform density (i.e., that B is constant), the angle of reflection $\beta$ varies with wavelength $\lambda$, and the reflected light is separated into its spectrum.

The grooves of the grating 2 of Figure 9C define a sawtooth shape which may be formed by a mechanical or laser cutting tool. In this grating, modulation depth and density again affect the reflection angle, but the pitch (or "blaze angle") D is also a factor. If the groove pattern is uniform over the groove, the angle of reflection of polarized light again varies with wavelength, and the grating separates the reflected light into its spectrum.

When a grating is used to separate light into its spectrum, the reflected light is directed to a light detector that detects light intensity regardless of the angle at which the light hits the detector. Thus, if a beam of polarized light is directed to a grating and reflected to such a detector, the light intensity at each wavelength can be measured by measuring the intensity of light at the area of the detector corresponding to that wavelength.

Referring to Figure 9D, however, a target light detector 8 detects light at only one angle of incidence. The detector detects no incoming light at other angles. A grating 2 includes three regions $G_1$, $G_2$, and $G_3$ having grooves separated by different modulation distances $B_1$, $B_2$, and $B_3$, respectively. Detector 8 is disposed with respect to grating 2 so that light 10 reflected from grating 2 at an angle $\beta$ is received by detector 8 at its operative angle of incidence. Thus, the detector measures the intensity of light 10.

Because the modulation density of grating 2 varies among regions $G_1$, $G_2$, and $G_3$, the regions reflect light at angle $\beta$ having different wavelengths $\lambda_1$, $\lambda_2$, and $\lambda_3$, respectively. Accordingly, if polarized light is directed to the entire surface of grating 2, target area $T_1$ of detector 8 receives only light of wavelength$_1$, target area $T_2$ receives only light of wavelength $\lambda_2$, and target area $T_3$ receives light only of wavelength$_3$.

By varying the areas of regions having certain modulation densities, an optical filter 2 as in Figure 9D may be configured to compress light data as do the Dobrowolski filters described in the pending patent application. For example, assume a Dobrowolski filter transmits 50% of light of wavelength $\lambda_1$, 100% of light of wavelength $\lambda_2$ and 25% of light at wavelength $\lambda_3$. A grating 2 as in Figure 9D may effect the same function where area $G_1$ is half of area $G_2$, and area $G_3$ is one-fourth of area $G_2$.

Although modulation density is used as the variable in the embodiment illustrated in Figure 9D, it should be understood that modulation depth and pitch may also be used.

IR Up-Conversion Materials

Direct detection of infrared light is sometimes difficult. There are certain well-known materials that, however, when energized by a laser, receive infrared photons and release photons of visible light. These materials are used in infrared light detectors to receive infrared light. Their output of visible light is proportional to the amount of received infrared light and is directed to a visible light detector. Thus, the output of the visible light detector is proportional to the input infrared light.

This combination of devices may be used as a detector in the optical filter systems disclosed in the pending application to facilitate the use of these systems for IR chemical imaging.

# Real-Time Biodetection Using PCR-MS

Alvin Fox and Karen Fox

Department of Microbiology and Immunology
School of Medicine
University of South Carolina
Columbia, SC 29208

Tel: (803)733-3288
Fax: (803)733-3192
afox@med.sc.edu
kfox@med.sc.edu

# Section 2-3: Real Time Biodetection Using PCR-MS

Alvin Fox and Karen Fox

## ABSTRACT

There is a real need for an approach for the rapid detection/identification of potential biological warfare (BW) agents during an airborne attack. Ideally, such a method should be fast (<~15 min), highly specific, sensitive, and flexible for use against new threats. Conventional microbiological and molecular biology based techniques are far too slow to meet the needs of biodetection. The first technology for real-time detection/identification of pathogenic microbes (based upon the combination of polymerase chain reaction [PCR] and electrospray ionization [ESI] mass spectrometry) was recently developed by the P.I. and his collaborators. The power of the approach is the use of mass spectrometric analysis that provides rapid detection/ identification (<1 min), a speed that greatly exceeds that of conventional electrophoresis approaches. This work involved the use of a state-of-the-art Fourier transform ion cyclotron resonance mass spectrometer (FTICR-MS). We propose to now extend this approach to integrate the various steps of PCR amplification, clean-up and mass spectrometry into one procedure/instrument for field use. Further to evaluate the use of PCR-MS for trace detection of appropriate virulence genes in environmental matrices. ESI-FTICR-MS analysis of PCR products is precise and rapid, but more conventional instrumentation based upon triple quadrupole and/or quadrupole ion trap instrumentation is likely to suffice, and the utility of such instrumentation will be determined. The achievement of such high-speed analysis with high levels of sensitivity and specificity represents a major improvement over existing technologies for biodetection.

## FORWARD

The total award was $309,000 (direct costs) for the period 9/1/98 to 9/2001. The original goals of this project encompassed the following:

1. Develop high speed isolation of DNA from bacterial cells present in a dust matrix collected from aerosols in a form suitable for PCR-MS analysis.

2. Incorporation of an approach for rapid fully automated on-line continuous PCR-MS, incorporating the various steps of capillary based PCR amplification, clean-up, and mass spectrometry into one integrated procedure.

3. Determination of the relative sensitivity/specificity obtainable by ESI-FTICR vs. triple quadrupole and ion trap MS instrumentation for the characterization of PCR products. Although the resolution and accuracy of triple quadrupole and quadrupole ion trap instruments are lower (compared to FTICR), these instruments are less expensive and have already been adapted for field use.

4. Evaluation and extension of PCR-MS to trace analysis of appropriate chemical markers

(including virulence genes and the ribosomal RNA operon) in environmental matrices. Additional development in sample preparation and/or instrumental analysis are anticipated as we extend analysis from PCR of isolated bacterial cells to more complex environmental matrices.

We are currently focusing on goals 2-4. Goal 1 is the first step of a fully developed biodetection technology but can not be implemented without the prior success of goals 2-4. We will detail under Section 4. **Body of the Report** (Results) our current progress.

## REPORT

***Statement of the problem***

There is great interest in an approach for the rapid detection of potential biological warfare (BW) agents during in potential threat. Ideally, such a biodetection method should be fast (<~15 min), highly specific, sensitive and flexible for use against new threats. Fortunately, there are only a limited number of organisms that are likely BW agents and the number one threat is considered by many to be *Bacillus anthracis* ( the causative agent of anthrax). This organism has the following characteristics: high virulence for man, ease of production, infection by the respiratory route and ability to survive under adverse environmental conditions. However, a biodetection approach should be sufficiently flexible to be adaptable to identification of multiple and previously unknown threats.

The use of modern instrumental analytical chemical approaches (including electrospray and/or matrix assisted laser desorption mass spectrometry) is essential. Biodetection is based on detecting chemical markers; structures present in specific target microbes and absent in other related bacterial species. The organisms that are key agents for biodetection (including *Bacillus anthracis*) are not widely studied and chemotaxonomic differentiation schemes have required further development in our laboratory.

***Summary of the most important results***

Progress in Goal 2: The focus of our research has been on improving sample preparation and instrument (source) optimization to improve sensitivity and molecular weight accuracy by improving the quality of MS spectra. The nature of the sample also dramatically affects sensitivity of MS analysis. The requirements for mass spectrometry analysis of PCR products are much more demanding than for electrophoresis. The presence of metal ions, primers, and other components of the PCR reaction mixture suppress ionization and produce broad mass spectral peaks respectively. This lowers sensitivity and decreases the accuracy of molecular weight determinations; preparing clean samples is essential. We have thus focused on improving sample clean-up for MS analysis. However, additionally if mass spectrometry is to compete with electrophoresis technology, this clean-up methodology must be simple, rapid, economical and reproducible.

Over the past few months, we have adapted a procedure based on affinity capture of biotin-labelled PCR products (developed for MALDI) (Ross, Belgrader Analyt Chem. 69: 3966-3972, 1997) for electrospray MS analysis. This procedure involves using a silica column to partially

purify a double stranded PCR products (including removal of primers) followed by binding of the PCR product by one biotin labeled strand to an avidin-labelled magnetic bead. At this stage, remaining metal ions are removed by washing with ammonium acetate. Finally, the non-biotinylated single strand is removed, for MS analysis, by heating at 100°C. In our hands the procedure takes 15-25 min. We agree with Ross that the procedure is rapid and simple but it has not yet been optimized for routine analysis; this is the primary focus of our current work. It is worthy of note that a single stranded PCR product is half the molecular weight and simpler biochemically than its double stranded counterpart. This also should improve the quality of analysis.

Y. Johnson, M. Krahmer, P. Ross, K. and A. Fox. Rapid and simple preparation of single stranded PCR products for ESI quadrupole MS analysis. American Society for Mass Spectrometry (ASMS), Annual Meeting. May, 1998 (to be presented).

Progress in goal 3: Our initial studies were performed with a state-of-the-art mass spectrometer (a Fourier transform ion cyclotron resonance instrument). This instrument can not be setup on a battlefield. It is vital to demonstrate that analysis of PCR products can be achieved using a low resolution (quadrupole) instrument. Our instrument had a megaflow source, which was not configured for high sensitivity analysis. Since funds were not available to buy a commercial source (approximately $50,000) or a new instrument (approximately $200,000 for an MS/MS ion trap) my students converted the megaflow source of our instrument to microflow; although sensitivity was still not optimal this modification was vital in allowing detection of PCR products on the quadrupole instrument. More recently we converted the source for nanospray analysis. The total conversion from megaflow to nanospray was achieved for under $2,000. The nanospray conversion has not yet been evaluated for analysis of PCR products but it has dramatically increased the sensitivity of our quadrupole instrument (as expected) in analysis of standards. This work is still in progress.

Progress in goal 4: We continue to focus on the interspace region in the 16S- 23S RNA operon since it is present universally in all bacterial pathogens. However, since there is limited selection pressure on the interspace region, there is great diversity on the sequence and nucleotide length of this genomic region. However, the genes on either side of the spacer region (16S and 23S rRNA respectively) contain several conserved regions. Accordingly using primers against two conserved regions (in the 16S and 23S rRNA), different lengths/sequences of 16S-23S rRNA interspace region are generated for each characteristic BW agent. Experience gained with one group of BW agents is readily applied to other groups.

The 16S-23S rRNA region of the genome consists of multiple operons. Until recently, 16S ribosomal rRNA (16S rRNA) sequences were accepted to be the gold standard for comparing the degree of genetic relatedness of bacterial species. 16S rRNA sequences are highly conserved and there are only minor sequence differences among the multiple operons within an organism and between closely related species. For example, the 16S rRNA sequence similarity between *B. anthracis* and *B. cereus* is 99.9-100%. In comparison, the more distantly related *B. subtilis* is still 92-94% similar to *B. anthracis /B. cereus*. *B. globigii* (originally referred to *B. subtilis var. niger* and more recently *B. atrophaeus var. niger*) is often used as a BW simulant for *B. anthracis* (a member of the *B. cereus* group)

Strains W23 and 168 represent two distinct genetic clusters within the species *Bacillus subtilis*. *B. atrophaeus* var. *niger* was selected as a member of a group of species closely related to *B. subtilis*. Comparison of the 10 rDNA operons, available from genbank, for *B. subtilis* 168 shows 3 distinct types of interspace (ISR) regions. Two of the ten 16S-23S ISRs contain the sequences for isoleucine and alanine tRNA and are identical in sequence. The reamaining 8 ISRs lack tRNA sequences and have 2 distinct sizes. Variability among non-tRNA operons ranged from 97-100%. Counting the tRNA insert as one change, variability between tRNA and non-tRNA containing sequences ranged from 95.3-97%. The sequences of equivalent 16S-23S ribosomal operon interspace regions (ISRs) are highly conserved between W23 and 168 (99.9-100%). Thus the sequence differences between strains 168 and W23 are less than between multiple operons within 168. However, the sequence of an ISR from *B. atrophaeus var. niger* is quite distinct from any of the ISRs found in *B. subtilis* (range 88.2-91.6%). These observations are consistent with the previous suggestion that *B. atrophaeus* is a separate but closely related species to *B. subtilis*. This is the first study to make sequence comparisons at the level of operon, strain and species for the rRNA interspace region. Considerations of this type will be important in using ISRs to differentiate other closely related bacterial species.

M. Nagpal, K. F. Fox and A. Fox. Utility of 16S-23S rRNA spacer region methodology: How variable are interspace regions within a genome and between strains for closely related organisms? Submitted to *J. Microbiol. Meth.*

M., Nagpal, A. Fox and K. Fox. Discrimination of *Bacillus subtilis* and *Bacillus atrophaeus*: Inter and intra-species comparison of the 16S-23S intrgenic spacer region. Amer. Society for Microbiology. Annual Meeting. May, 1998.

***Publications and Technical Reports***

Y. Johnson, M. Krahmer, P. Ross, K. and A. Fox. Rapid and simple preparation of single stranded PCR products for ESI quadrupole MS analysis. American Society for Mass Spectrometry (ASMS), Annual Meeting. May, 1998 (to be presented).

M. Nagpal, K. F. Fox and A. Fox. Utility of 16S-23S rRNA spacer region methodology: How variable are interspace regions within a genome and between strains for closely related organisms? Submitted to J. Microbiol. Meth.

M., Nagpal, A. Fox and K. Fox. Discrimination of *Bacillus subtilis* and *Bacillus atrophaeus*: Inter and intra-species comparison of the 16S-23S intragenic spacer region. Amer. Society for Microbiology. Annual Meeting. May, 1998

***Participating Personnel***

K. Fox (Research Associate Professor) and A. Fox. (Professor) - Co-P.I.s
M. Nagpal (Research Associate Professor)
Y. Johnson, M. Krahmer and M. Kozar (Graduate students)
P. Steinberg (Technician)
P. Ross (Collaborator, Armed Forces Institute of Pathology)

## BIBLIOGRAPHY

1. Wunschel, D., Fox, K., Black, G. and Fox, A. Discrimination among the *B.cereus* group, in comparison to *B. subtilis*, by structural carbohydrate profiles and ribosomal RNA spacer region PCR. System. Appl. Microbiol. 17: 625-635. 1994
2. Wunschel D., Fox K., Fox A., Bruce J., Muddiman D. and Smith R. Analysis of double stranded polymerase chain amplification products from the *B.cereus* group by electrospray ionization fourier transform ion cyclotron resonance mass spectrometry. Rapid Commun. Mass Spectrom. 10: 29-35. 1996.
3. Muddiman D.C., Wunschel D. , Liu C., Pasa-Tolic L., Fox K., Fox A. and Smith R. Characterization of PCR products from bacilli using electrospray ionization FTICR mass spectrometry. Analyt Chem. 68:3705-3712. 1996.
4. Wunschel D., Fox K., Fox A., Nagpal M., Kim K. and Stewart G. Quantitative analysis of neutral and acidic sugars in whole bacterial cell hydrolysates using high performance anion exchange liquid chromatography electrospray ionization tandem mass spectrometry. J. Chromatogr. 776: 205-219. 1997.
5. Fox K., Wunschel D., Fox A. and Stewart G. Complementarity of GC-MS and LC-MS analyses for determination of carbohydrate profiles of vegetative cells and spores of bacilli. J. Microbiol. Meth. (in press)
6. Wunschel D., Muddiman D., Fox K., Fox A. and Smith R.D. Heterogeneity in *B. cereus* PCR products detected by ESI-FTICR mass spectrometry. Analyt. Chem. 1998 (in press)]

# REPORT DOCUMENTATION PAGE

Form Approved
OMB No. 0704-0188



| 1. AGENCY USE ONLY *(Leave blank)* | 2. REPORT DATE | 3. REPORT TYPE AND DATES COVERED |
|---|---|---|
| | June 1, 1998 | Annual |

4. TITLE AND SUBTITLE

Real-time biodetection using PCR-MS

5. FUNDING NUMBERS

N00014-97-1-0806; 97PR06312-00; PO Code 353; Disbursing Code N68892; AGO N66020; Cage Code 4B489

6. AUTHOR(S)

Alvin Fox, Ph.D. & Karen Fox, Ph.D.

7. PERFORMING ORGANIZATION NAME(S) AND ADDRESS(ES)

University of South Carolina

8. PERFORMING ORGANIZATION REPORT NUMBER

N00014-97-1-0806-1

9. SPONSORING / MONITORING AGENCY NAME(S) AND ADDRESS(ES)

ONR

10. SPONSORING / MONITORING AGENCY REPORT NUMBER

ONR

11. SUPPLEMENTARY NOTES

Prepared in coordination with University Research Initiative Program for Combat Readiness

12a. DISTRIBUTION / AVAILABILITY STATEMENT

APPROVED FOR PUBLIC RELEASE

12b. DISTRIBUTION CODE

13. ABSTRACT *(Maximum 200 words)*

There is a real need for an approach for the rapid detection/identification of potential biological warfare (BW) agents during in airborne attack. Ideally, such a method should be fast (<~15 min), highly specific, sensitive and flexible for use against new threats. Conventional microbiological and molecular biology based techniques are far too slow to meet the needs of biodetection. The first technology for real-time detection/identification of pathogenic microbes (based upon the combination of polymerase chain reaction [PCR] and electrospray ionization [ESI] mass spectrometry) was recently developed by the P.I. and his collaborators. The power of the approach is the use of mass spectrometric analysis that provides rapid detection/ identification (<1 min), a speed that greatly exceeds that of conventional electrophoresis approaches. This work involved the use of a state-of-the-art Fourier transform ion cyclotron resonance mass spectrometer (FTICR-MS). We propose to now extend this approach to integrate the various steps of PCR amplification, clean-up and mass spectrometry into one procedure/instrument for field use. Further to evaluate the use of PCR-MS for trace detection of appropriate virulence genes in environmental matrices. ESI-FTICR-MS analysis of PCR products is precise and rapid, but more conventional instrumentation based upon triple quadrupole and/ quadrupole ion trap instrumentation is likely to suffice, and the utility of such instrumentation will be determined. The achievement of such high-speed analysis with high levels of sensitivity and specificity represents a major improvement over existing technologies for biodetection.

14. SUBJECT TERMS

Chemical and biological Warfare, Target Acquisition, Anti-Submarine, Chemical Medicine, Biodeterioration, and Command Control and Communication

15. NUMBER OF PAGES

7

16. PRICE CODE

| 17. SECURITY CLASSIFICATION OF REPORT | 18. SECURITY CLASSIFICATION OF THIS PAGE | 19. SECURITY CLASSIFICATION OF ABSTRACT | 20. LIMITATION OF ABSTRACT |
|---|---|---|---|
| UNCLASSIFIED | UNCLASSIFIED | UNCLASSIFIED | 200 words |

# Small Molecule Transport Through Polymers: Effects of Polymer Inhomogeneity and Dynamics on the Nanometer Length Scale

Mark A. Berg

Department of Chemistry
University of South Carolina
Columbia, SC 29208

Tel: 803-777-1514
Fax: 803-777-9521
Email: berg@psc.sc.edu

# Section 2-4: Small Molecule Transport Through Polymers: Effects of Polymer Inhomogeneity and Dynamics on the Nanometer Length Scale

M. Berg

## ABSTRACT

This project seeks to elucidate the mechanism of small-molecule diffusion through polymers by examining the polymer dynamics on a nanometer length scale using both new and existing ultrafast spectroscopies. A probe molecule suitable for use as a nanoviscosity sensor has been calibrated in a small-molecule liquid. Hydrodynamic modeling provides an accurate connection between the measured molecular rotation time and the nanoviscosity of the cavity containing the molecule. An interfering hole burning effect has been identified and can be controlled for. The feasibility of a new dichroism technique, the Kerr-Effect with Resonant Detection (KERD), has been demonstrated in both a small-molecule liquid and a polymer melt. This technique enhances the early time components of rotation, thereby allowing characterization of the elastic properties and $\beta$-relaxation components of the cavity containing the probe. These cavity characteristics play a central role in recent theoretical models of small-molecule diffusion in polymers. Preliminary results indicate that the cavity in a polymer is more rigid and has less $\beta$-relaxation than in a small-molecule solvent.

## FORWARD

This project entails total costs of $370,000 over a period of three years. Its goal is to generate a better understanding of penetrant diffusion through polymers by using ultrafast spectroscopy to examine polymer dynamics at the nanometer length scale. The diffusion of small organic penetrants through polymers is important for both chemical warfare defense and for general military and civilian applications of polymers. Control of penetrant diffusion is essential to improving barrier materials for control of chemical agents and for the design of catalytic or selectively permeable polymers for use in sensors for chemical agents. Penetrant diffusion also plays a critical role in other applications of polymers including chemical coating and processing, adhesion, curing behavior, degradation processes, advanced ultrafiltration, and separations processes, and long-term drug delivery.

Both theory and macroscopic experiments suggest that the mechanism of penetrant diffusion in polymers is different than in small-molecule solvents. For example, diffusion in polymers slows below the glass transition, but does not cease, as it does in small-molecule solvents. Computer simulations have suggested that the entanglement of the polymer chains favors the formation of nanometer-sized cavities in the polymer and that the penetrant occupies these cavities.[1,2] In the so-called "Red-Sea" mechanism, transport occurs when a channel opens between these cavities, and the penetrant hops to a new cavity, before the channel closes.[1,2] In transition-state theories of polymer diffusion, it is hypothesized that the channel opening and closing is governed by simple elastic movement of the polymer chains and does not require structural relaxation.[1-3]

These models make clear the difficulty in understanding penetrant diffusion in polymers solely on the basis of macroscopic properties of the polymer. For example, the macroscopic viscosity of a polymer is governed by the dynamics of entanglement and flow on length scales corresponding to the full polymer chain length, whereas small-molecule diffusion is determined by the mechanical properties of the nanometer-sized cavities and channels in the polymer structure. Although pictures such as Red-Sea mechanism are intuitively appealing, there is little experimental data on the structure and dynamics of polymers at short lengths to support or refute the theoretical models.

In this project, ultrafast spectroscopic techniques are being employed to characterize the nanoscale mechanical properties of polymers which govern penetrant diffusion. Measurements of the rotation and electronic solvation of small organic molecules in polymers are being used to determine the mechanical properties of the cavity surrounding a penetrant. Comparisons to better understood small-molecule solvents provide a basis for isolating the aspects of transport which are unique to polymers. Comparison of the mechanical properties of the penetrant nanocavity to the bulk mechanical properties of the polymer provide a basis for understanding the role of the long length-scale introduced to the problem by the polymer chains.

The primary accomplishments of the current period are:

- **Identification and Calibration of a Nanoviscosity Sensor.** A probe molecule has been identified which can be used to measure the viscosity over a nanometer-sized volume. Calibration studies have been successfully completed. This sensor will be used in the next stage to relate the nanometer scale viscosity of polymers to their macroscopic viscosity.
- **Demonstration of a New Multiple Pulse Dichroism Spectroscopy.** Kerr-Effect with Resonant Detection (KERD) has been successfully demonstrated for the first time. This technique greatly enhances the early components of rotational motion and is needed to determine if fast $\beta$-relaxation processes exist in polymers. In addition, recent theoretical work has shown that understanding penetrant diffusion requires information on the nanoelasticity of the polymer in addition to the nanoviscosity emphasized in the original proposal. The KERD experiments will allow us to gather the needed information on the nanoelasticity of polymers.

The primary change in the experimental plan has been the acceleration of the studies based on rotational motion and a corresponding delay in the studies based on solvation dynamics. This change has been forced by equipment problems, but should not endanger the overall completion of the project.

## REPORT

### Nanoviscosity Measurements

A major goal of the project is to relate nanometer scale dynamics to macroscopic transport properties in polymers. In small-molecule solvents, this relationship is relatively well established. The rotational rate of a solute molecule is governed by the macroscopic viscosity through simple hydrodynamic models. These models are successful if the solvent molecules are smaller than the solute molecule, if there is no strong perturbation of the solvent structure by the

solute, and if there is no specific complexation between the solvent and solute. In polymers, where the solvent molecules are much larger than the solute, there is not an *a priori* expectation that the large scale polymer movements measured by the bulk viscosity will be simply related to the small segmental movements which affect small-molecule rotation. Instead, the rotation rate of the molecule defines a nanoscale viscosity of the cavity containing the solute. In turn, this nanoviscosity is expected to be the property relevant in modeling penetrant diffusion. A goal of this project is to make such measurements of the nanoviscosity in polymers and relate them to the macroscopic viscosity, temperature and chain length of the polymer.

Our first task was to identify a suitable probe molecule, confirm that it is an accurate viscosity probe and verify our experimental procedures. Anthracene was chosen as a probe because of its simple and well understood photophysics, its symmetric rotational properties, its solubility in a wide range of polymers and the expectation that it would have benign interactions with most solvents. As a test solvent, benzyl alcohol was chosen. It is significantly smaller than anthracene and should provide a nanoviscosity equal to its bulk viscosity. On the other hand, it has the potential for both hydrogen bonding and $\pi$-stacking interactions, and the effects of complexation should be evident, if anthracene is susceptible to them.

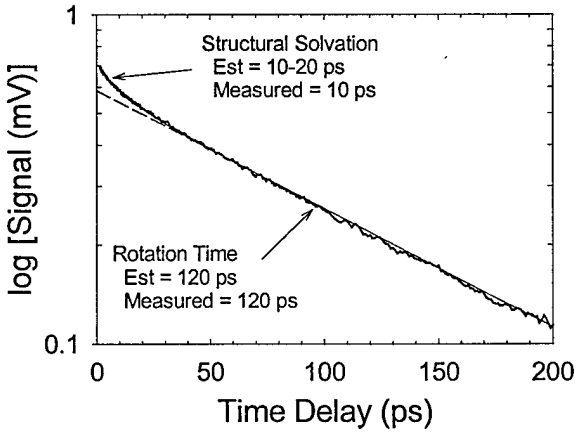


Figure 1. Time-resolved dichroism measurements of anthracene in benzyl alcohol. The long decay component (dashed) measures the molecular rotation time. The early decay component is an interference which has been identified as electronic solvation. This interference can be corrected for, permitting accurate measurement of the anthracene rotation time. A fit to both components (smooth solid curve) is obscured by the data (noisy curve).

Measurements were made by time-resolved heterodyned-detected dichroism with a time resolution of ~150 fs. Typical results are shown in Figure 1. The decay is clearly multiexponential. The longest decay time corresponds well to predictions of the rotation time from hydrodynamic models, but the shorter component is unexpected. We have assigned the short component to an electronic solvation process. A model developed by us [4] correctly predicts the decay time of this interfering process and allows us to remove it from the measurements with confidence.

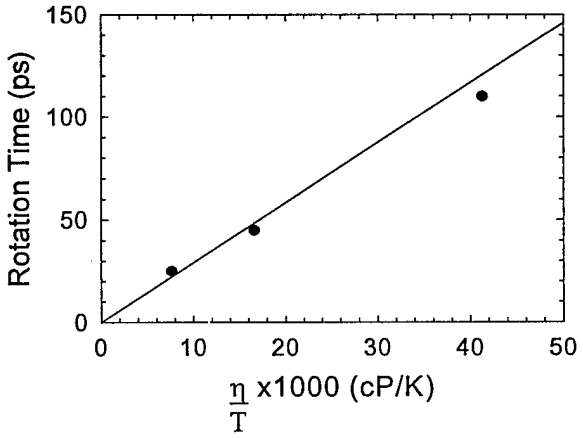


Figure 2. The rotation time of anthracene in benzyl alcohol at various viscosities (temperatures). The line is a prediction of a hydrodynamic model. This calibration will be used to derive accurate measurements of local nanoviscosity in polymers from anthracene rotation times.

Aside from this complication, anthracene is a good probe of viscosity. Corrected measurements of its rotational time at various viscosities (generated by varying the temperature) are shown in Figure 2. The predictions of a hydrodynamic theory are also shown. The anthracene is modeled as an ellipsoid with dimensions taken from computer simulation.[5] The agreement is excellent, confirming that anthracene is a good probe for its local viscosity. In the next stage of this project, the hydrodynamics model and anthracene parameters from this calibration will be used to find the nanoviscosity within solute cavities in polymers.

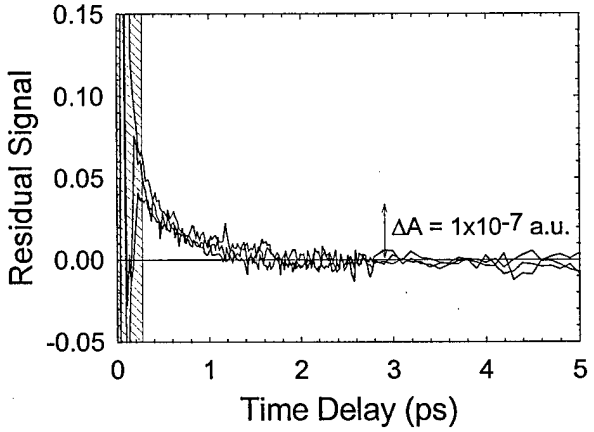


Figure 3. Residuals from the time-resolved dichroism measurements after removing the contributions from rotation and solvation. The same decay time is seen at three different viscosities, suggesting an origin in the local elastic properties of the solvent. The amplitude of these components is small, amounting to a change in absorbance of ~$10^{-7}$ absorbance units.

In addition to the rotational relaxation and solvation processes described above, another small and very fast component has been identified at very short times. Figure 3 shows the residuals when the two known components are subtracted from the measurements. The time scale of this component is subpicosecond and is invariant to the viscosity. We believe that this represents an

elastic, rather than viscous, response of the anthracene's environment. Another approach to obtaining information on elastic responses is discussed in detail below. However, the fast component shown in Fig. 3 may provide supporting or supplementary information. Additional modeling and analysis is required to make a detailed assignment of the origin of this component.

**Nanoelasticity and $\beta$-Relaxation Measurements**

This work relates to three distinct goals, two that were explicit in the proposal and one that has developed from new theoretical work on penetrant diffusion. New theoretical approaches to penetrant diffusion in polymers place great emphasis on the elastic properties of the polymer cavities and channels, because the speed of elastic deformations makes them much more effective than major structural changes in promoting diffusion. Thus it has become clear that as a part of our characterization of the nanostructure in polymers, we need good information on the nanoelasticity as well as the nanoviscosity. In small-molecule solvents, $\beta$-relaxation has been established as another source of rapid relaxation. A goal of the project is to look for evidence of $\beta$-relaxation in the nanostructure of polymers. A third goal of the project is to develop improved multiple pulse dichroism spectroscopies to examine these issues.

Although elastic and $\beta$-relaxation effects can be studied in principle using standard dichroism techniques, in practice the amplitude of these components is small and difficult to measure. We have developed a new dichroism technique, the Kerr-Effect with Resonant Detection (KERD), to address this problem. In standard dichroism measurements, an anisotropy in the orientations of the molecules is created by resonant polarized absorption. The resulting measurement is an orientational correlation function. In KERD, an anisotropy is created in the rotational velocities by the nonresonant Kerr-effect. The resulting measurement is the derivative of the orientational correlation function. The amplitude of rapid components such as elastic responses and $\beta$-relaxation are greatly enhanced in the derivative.

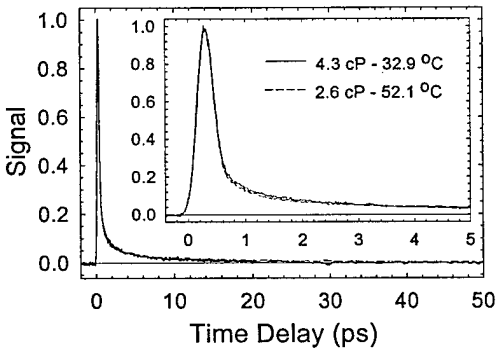


Figure 4. Kerr-Effect with Resonant Detection (KERD) measurements on anthracene in benzyl alcohol. Short-time effects are greatly enhanced relative to regular dichroism measurements. The subpicosecond peak is attributed to the elastic response of the solvent. The picosecond decay is attributed to $\beta$-relaxation.

Despite its usefulness, the KERD experiment had not been previously proposed or performed. Figure 4 contains our first demonstration of the feasibility of the KERD experiment. The measurements are on anthracene in benzyl alcohol. The signal level is large. At the viscosities used, the primary rotational time is >20 ps (see above). The short time components have been greatly enhanced. Moreover, the dynamics have a negligible viscosity dependence, in contrast to the long-time rotational dynamics. This lack of a strong viscosity dependence is typical of an elastic response. The strong, subpicosecond peak is believed to be the elastic response of the local environment of the anthracene. The slow, ps decay is much longer than the expected elastic response, but is also much faster than the primary rotational time. This

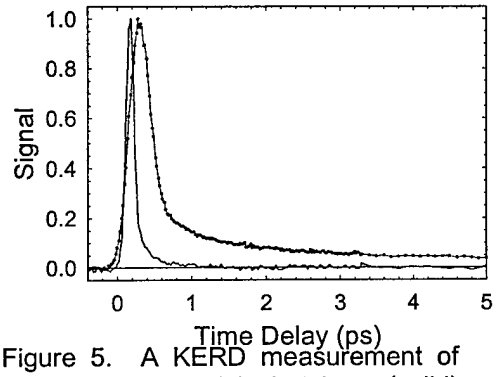


Figure 5. A KERD measurement of anthracene in polyisobutylene (solid) compared to a measurement in benzyl alcohol (dotted). Significant differences in the both the elastic peak and $\beta$-relaxation decay are seen between the polymer and the small-molecule solvent.

component is tentatively assigned to a $\beta$-relaxation process. The long, primary rotational time measured above is suppressed to such an extent that it is not visible in this set of data.

Figure 5 shows KERD results in a polymer liquid, polyisobutylene (PIB), and compares them to results in benzyl alcohol. In the polymer, the elastic peak is faster, implying a stiffer local environment. This result is contrary to expectation for very small solutes (e.g. $O_2$, $CH_4$), which are believed to rotate easily within oversized cavities.[1, 2] Rather it is suggestive of a solute in an undersized cavity, which restricts movement of the solute.

The $\beta$-relaxation relaxation region in PIB is suppressed relative to benzyl alcohol. However, closer examination of the PIB result (Fig. 6) shows that there is a low amplitude relaxation on a longer time scale than the elastic peak. This component may be the polymer analogue to the small-molecule $\beta$-relaxation process sought in this project.

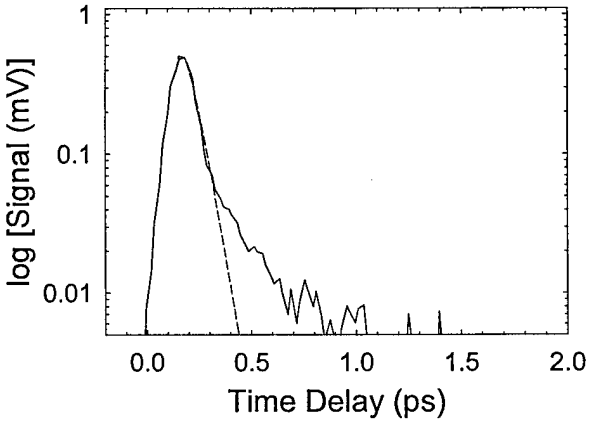


Figure 6. A KERD measurement on anthracene in polyisobutylene on a log scale. The dashed line is a fit to the elastic peak. An additional low amplitude component is attributed to $\beta$-relaxation.

These conclusions are still highly tentative. However, they illustrate the potential for this new technique to discern the differences in nanoscale structure and dynamics of polymers and small-molecule liquids. The next tasks are two-fold. Additional work is needed to create general acceptance of KERD measurements and to permit quantitative modeling in terms of local mechanical moduli. In particular, relationships between early rotational motion measured by KERD and long-time rotation measured by standard dichroism must be established theoretically and confirmed experimentally. Secondly, the measurements will be extended to compare polymers with distinctly different diffusivities. Specifically, measurements in polyisobutylene, a

low diffusivity polymer, will be compared to measurements in polydimethylsiloxane, a high diffusivity polymer.[6, 7]

**Equipment Development**

The fluorescence and phosphorescence experiments in the proposal are contingent on the completion of a home-built, time-correlated, single-photon counting system, which received primary funding from another source. Completion of this equipment has been delayed by delays in final funding, in receipt of essential components and in finding appropriate personnel. These problems are now resolved and construction is proceeding at a good pace. The fluorescence and phosphorescence experiments will be particularly important when our studies reach the stage of extending the measurements to low temperatures and very high viscosity to probe the approach to the glass transition. The equipment should be complete in time to perform these measurements. As a result of these delays on the fluorescence and phosphorescence experiments, work on the dichroism measurements was accelerated.

As a result of funding on another project, construction of an amplifier for the Ti:sapphire laser system used in the dichroism measurement will soon be completed. With increased pulse energy from the amplifier, the dichroism experiments can be performed at lower average power and lower heat load to the sample. Again this capability will be come important as our studies move closer to the glass transition, where the high viscosity of the samples prevents heat dissipation by stirring.

***Participating Scientific Personnel.***

Mark A. Berg (PI)
Xuexin Fang
Yunhan Zhang (PhD in progress)
Xiotian Zhang

## BIBLIOGRAPHY

1. *Diffusion in Polymers*, edited by P. Neogi (Marcel Dekker, New York, 1996).
2. "Dynamics of Small Molecules in Bulk Polymers," A.A. Gusev, F Müller-Plathe, W.F. van Gunsteren and U.W. Suter, Adv. Poly. Sci. **116**, 207 (1994).
3. "Transition-State Theory Model for the Diffusion Coefficients of Small Penetrants in Glassy Polymers," A.A. Gray-Weale, R.H. Henchman, R.G. Gilbert, M.L. Greenfield and D.N. Theodorou, Macromolecules **30**, 7296 (1997).
4. "A Viscoelastic Continuum Model of Nonpolar Solvation. I. Implications for Multiple Time Scales in Liquid Dynamics," M. Berg, J. Phys. Chem. A **102**, 17 (1998).
5. "Influence of Temperature and Viscosity on Anthracene Rotational Diffusion in Organic Solvents: Molecular Dynamics Simulations and Fluorescence Anisotropy Study," G.S. Jas, Y. Wang, S.W. Pauls, C.K. Johnson, and K. Kuczera, J. Chem. Phys. **107**, 8800 (1997).
6. *Polymer Permeability*, edited by J. Comyn (Elsevier Applied Science, London, 1985).
7. *Diffusion in Polymers*, edited by J. Crank and G. S. Park (Academic Press, London, 1969).

PART 53-FORMS 53.301-298

# REPORT DOCUMENTATION PAGE

Form Approved
OMB No. 0704-0188



| 1. AGENCY USE ONLY *(Leave blank)* | 2. REPORT DATE | 3. REPORT TYPE AND DATES COVERED |
|---|---|---|
| | June 1, 1998 | Annual |

| 4. TITLE AND SUBTITLE | 5. FUNDING NUMBERS |
|---|---|
| Small Molecule Transport Through Polymers: Effects of Polymer Inhomogeneity and Dynamics on the Nanometer Length Scale | Grant Number N00014-97-1-0806<br>PR Number 97PR06312-00<br>PO Code 353<br>Disbursing Code N68892<br>AGO Code N66020<br>Cage Code 4B489 |
| 6. AUTHOR(S)<br>Mark A. Berg | |
| 7. PERFORMING ORGANIZATION NAME(S) AND ADDRESS(ES)<br>University of South Carolina | 8. PERFORMING ORGANIZATION REPORT NUMBER<br>N00014-97-1-0806-1 |
| 9. SPONSORING / MONITORING AGENCY NAME(S) AND ADDRESS(ES)<br>ONR | 10. SPONSORING / MONITORING AGENCY REPORT NUMBER<br>ONR |

11. SUPPLEMENTARY NOTES

Prepared in coordination with the University Research Initiative Program for Combat Readiness

| 12a. DISTRIBUTION / AVAILABILITY STATEMENT | 12b. DISTRIBUTION CODE |
|---|---|
| APPROVED FOR PUBLIC RELEASE | |

13. ABSTRACT *(Maximum 200 words)*

This project seeks to elucidate the mechanism of small-molecule diffusion through polymers by examining the polymer dynamics on a nanometer length scale using both new and existing ultrafast spectroscopies. A probe molecule suitable for use as a nanoviscosity sensor has been calibrated in a small-molecule liquid. Hydrodynamic modeling provides an accurate connection between the measured molecular rotation time and the nanoviscosity of the cavity containing the molecule. An interfering hole burning effect has been identified and can be controlled for. The feasibility of a new dichroism technique, the Kerr-Effect with Resonant Detection (KERD), has been demonstrated in both a small-molecule liquid and a polymer melt. This technique enhances the early time components of rotation, thereby allowing characterization of the elastic properties and $\beta$-relaxation components of the cavity containing the probe. These cavity characteristics play a central role in recent theoretical models of small-molecule diffusion in polymers. Preliminary results indicate that the cavity in a polymer is more rigid and has less $\beta$-relaxation than in a small-molecule solvent.

| 14. SUBJECT TERMS | 15. NUMBER OF PAGES |
|---|---|
| Chemical and Biological Warfare, Target Acquisition, Anti-Submarine, Combat Medicine, Biodeterioration, and Command, Control and Communication | 8 |
| | 16. PRICE CODE |

| 17. SECURITY CLASSIFICATION OF REPORT | 18. SECURITY CLASSIFICATION OF THIS PAGE | 19. SECURITY CLASSIFICATION OF ABSTRACT | 20. LIMITATION OF ABSTRACT |
|---|---|---|---|
| UNCLASSIFIED | UNCLASSIFIED | UNCLASSIFIED | 200 words |

# The Design and Synthesis of Quantum Dot Based Lasers

Richard D. Adams, PI

Department of Chemistry and Biochemistry
University of South Carolina
Columbia, SC 29208

Tel: (803)777-7187
Fax: (803)777-6781
Email: adams@psc.sc.edu

# Section 2-5: The Design and Synthesis of Quantum Dot Based Lasers

R. Adams

## ABSTRACT

These studies involve the synthesis and characterization of thiolate containing cadmium sulfide cluster complexes and investigation of their photoemission properties. The first members of a new series of these complexes have been synthesized and characterized by single crystal x-ray diffraction analysis. Their photoemission has been recorded and compared with that of similar complexes that have been reported previously. Our new complexes appear to have longer lifetimes in the excited states and large shifts toward lower emission energies than the previously reported complexes.

## FORWARD

Amount: $330,000. Period: July 1, 1997 - June 30, 2000.
We have prepared and crystallographically characterized the first halide-substituted $Cd_{10}S_4$ thiolate cluster complex and measured is photoluminescence spectra. This complex exhibits longer excited state lifetimes and has significant shifts of its photoemission to lower energy compared to similar complexes reported previously.

## BODY OF THE REPORT

### *Statement of the Problem Studied*

Semiconductor quantum dots are a new class of nanoscale particles that exhibit novel optoelectronic properties.[1] One of these properties of particular interest is known as photoluminescence, a photoemission property that varies with the size of the particle. The photoluminescence arises from the presence of electronic holes or traps (defects) on the particles that affect the return of electrons from excited states to the ground energy state with the formation of a photon.

### *Summary of results*

In our first year of work on this project we have synthesized the first members of a new family of halide substituted cadmium sulfide-thiolate clusters that exhibit photoluminescence. The new compound $(Et_4N)_4[Cd_{10}S_4Br_4(S\text{-totyl})_{12}]$, **1** was obtained from solutions of $Cd(NO_3)_2$, p-thiocresol, triethylamine and tetraethylammonium bromide in methanol at 25°C. The compound was characterized by single crystal x-ray diffraction methods and was found to possess the structural type previously found for the compound $(Et_4N)_4[Zn_{10}S_4(SPh)_{16}]$.[1] The molecule consists of a tetrahedral $Cd_{10}S_4$ cluster core with 12 bridging tolylthiolato ligands. The new feature is the presence of a terminally coordinated bromide ion on each of the four cadmium ions at the vertices of the $Cd_{10}S_4$ tetrahedron. A line structure and an ORTEP diagram of the molecular structure of **1** are shown below.

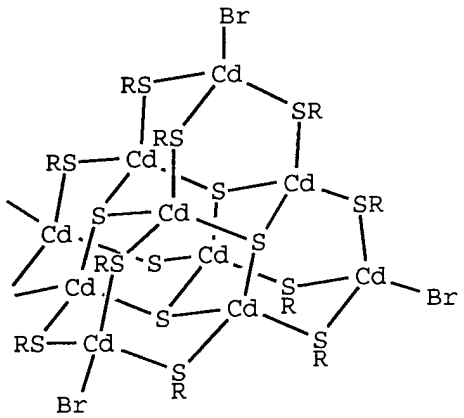


**1** R = p-tolyl

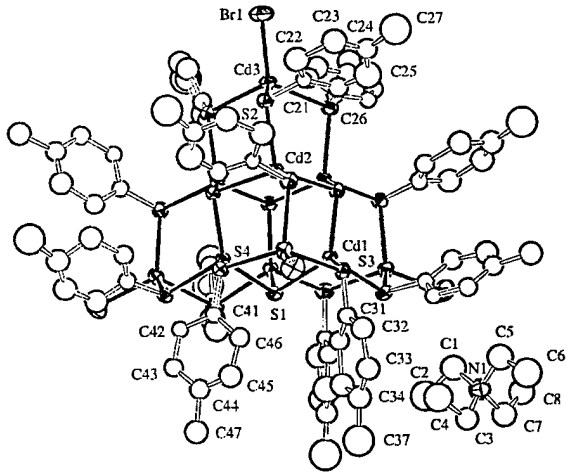


Figure 1 shows a packing diagram of the cluster anions (without the tolyl groups) and the $NEt_4$ cations as they are arranged in the solid state.

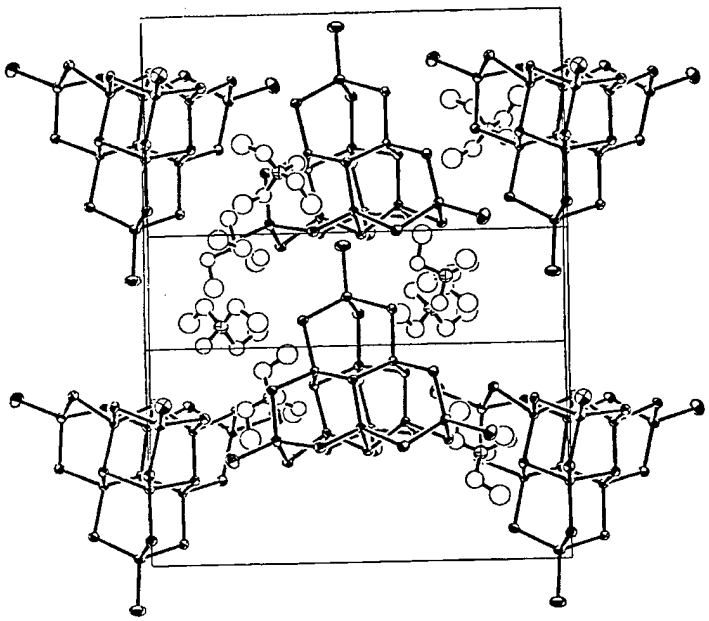

Figure 1

The photoluminescence of **1** and two previously related cadmium sulfide cluster complexes $(Et_4N)_4[Cd_{10}S_4(SPh)_{16}]$ and $(Et_4N)_4$ $[Cd_{10}Se_4(SPh)_{16}]$ were measured and compared. These results are described below.

From Figure 2, it is apparent that the molecular CdS clusters all absorb in the ultraviolet and have no significant absorption in the visible. This is expected for such nanoscale semiconductor materials. The bands have some structure, indicative of the quantum confinement of the electron-hole pair. The slight red shift for the mixed CdSe/CdS cluster is consistent with the smaller bandgap of bulk CdSe compared to bulk CdS.

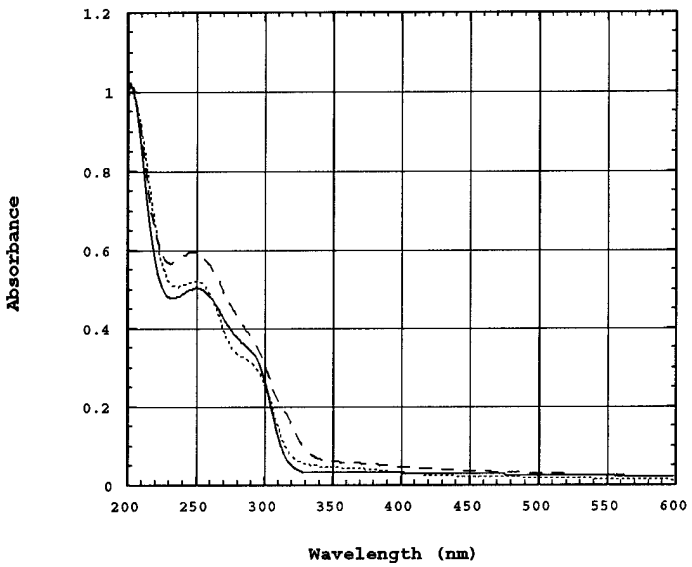


Figure 2. Absorption spectra of clusters. Solid line = $(Et_4N)_4[Cd_{10}S_4(SPh)_{16}]$, dashed line = $(Et_4N)_4$ $[Cd_{10}Se_4(SPh)_{16}]$, and dotted line = compound **1**.

The key feature of these materials is their photoluminescence spectra (Fig. 3). Upon excitation at ~340 nm, all of these molecular clusters emit substantial amounts of blue light (~450 nm) and the emission tails into the green and red (~600 nm). Again, the slight red shift of the mixed CdSe/CdS cluster compared to its CdS analog is expected, due to the smaller CdSe bandgap. Unexpectedly, compound **1**, which has a $Cd_{10}$ core but a mixture of terminal bromides and bridging tolylthiolate ligands, is significantly red-shifted compared to the known clusters. The typical interpretation of such red-shifted emission is that either the presence of defects on the surface has introduced trap states into the bandgap, or a larger cluster with a smaller bandgap has been formed. From the crystal structure analysis of compound **1**, neither of these interpretations is valid: the surface atoms are all completely capped, and the cluster still possesses a $Cd_{10}$ core. Thus, the introduction of substituents on the aromatic thiolates and the presence of halide has introduced a significant change in the electronic structure of this cluster. Preliminary luminescent lifetime evidence (lifetime of parent $Cd_{10}SPh$ cluster is less than ~5 ns, while compound **1** emits with a lifetime of 68 ns) is in agreement with this general conclusion.

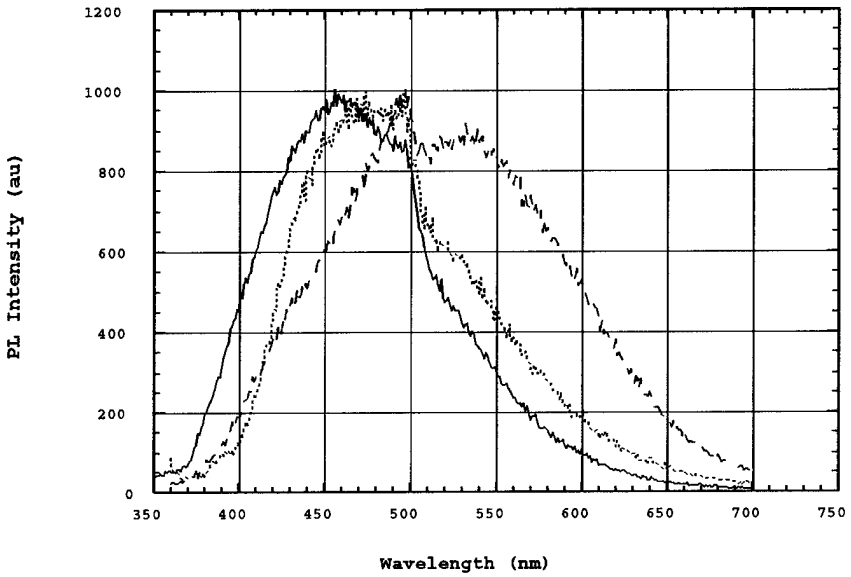


Figure 3. Photoluminescence spectra of clusters. Solid line = $(Et_4N)_4[Cd_{10}S_4(SPh)_{16}]$, dashed line = $(Et_4N)_4$ $[Cd_{10}Se_4(SPh)_{16}]$, and dotted line = compound **1**.

The presence of the easily-exchangeable halide ligand on the cluster is also a key element for the future derivatization and possible linking of these molecular quantum dots into groupings. Future studies will be focused on preparing additional derivatives of **1** by replacing the bromide ligands with chloride and iodide, and by substituting the tolyl groups with phenyl, p-chlorophenyl, p-methoxylphenyl and p-nitrophenyl groups, etc. It may also be possible to abstract the halide ligands and systematically replace them with uncharged ligands such as acetonitrile, pyridine, pyrazine and related bifunctional nitrogen donors. The photoemission properties of these new derivatives will be investigated to ascertain the effect of the changes on the photoemission processes.

***Scientific Personnel***

Richard D. Adams, PI
Catherine J. Murphy, CoPI
Lee Yeung
Bin Zhang

## BIBLIOGRAPHY

1) R. F. Service, *Science* **1996**, *271*, 920.
2) I. G. Dance, A. Choy, M. L. Scudder, *J. Am. Chem. Soc.* **1984**, *106*, 6285.

# REPORT DOCUMENTATION PAGE

Form Approved
OMB No. 0704-0188



| 1. AGENCY USE ONLY *(Leave blank)* | 2. REPORT DATE | 3. REPORT TYPE AND DATES COVERED |
|---|---|---|
| | June 1, 1998 | Annual |

4. TITLE AND SUBTITLE

The Design and Synthesis of Quantum Dot Based Lasers

5. FUNDING NUMBERS

Grant No. N00014-97-1-0806
PR No. 97PR06312-00
PO Code 353, Disbursing Code N68892
AGO Code N66020, Cage Coge 4B489

6. AUTHOR(S)

Richard D. Adams

7. PERFORMING ORGANIZATION NAME(S) AND ADDRESS(ES)

University of South Carolina

8. PERFORMING ORGANIZATION REPORT NUMBER

N00014-97-1-0806

9. SPONSORING / MONITORING AGENCY NAME(S) AND ADDRESS(ES)

ONR

10. SPONSORING / MONITORING AGENCY REPORT NUMBER

ONR

11. SUPPLEMENTARY NOTES

Prepared in coordination with University Research Initiative Program for Combat Readiness

12a. DISTRIBUTION / AVAILABILITY STATEMENT

APPROVED FOR PUBLIC RELEASE

12b. DISTRIBUTION CODE

13. ABSTRACT *(Maximum 200 words)*

These studies involve the synthesis and characterization of thiolate containing cadmium sulfide cluster complexes and investigation of their photoemission properties. The first members of a new series of these complexes have been synthesized and characterized by single crystal x-ray diffraction analysis. Their photoemission has been recorded and compared with that of similar complexes that have been reported previously. Our new complexes appear to have longer lifetimes in the excited states and large shifts toward lower emission energies than the previously reported complexes.

14. SUBJECT TERMS

Chemical and Biological Warfare, Target Acquisition, Anti-Submarine, Combat Medicine, Biodeterioration, and Command Control and Communication

15. NUMBER OF PAGES

7

16. PRICE CODE

| 17. SECURITY CLASSIFICATION OF REPORT | 18. SECURITY CLASSIFICATION OF THIS PAGE | 19. SECURITY CLASSIFICATION OF ABSTRACT | 20. LIMITATION OF ABSTRACT |
|---|---|---|---|
| UNCLASSIFIED | UNCLASSIFIED | UNCLASSIFIED | 200 Words |

# Rapid Biodetection of Bacterial Cells by Laser Pyrolysis/Mass Spectrometry

Stephen L. Morgan

Department of Chemistry & Biochemistry
The University of South Carolina
Columbia, SC 29208

Tel: (803) 777-2461
Fax: (803) 777-6104
Email: slmorgan@sc.edu

# Section 2-6: Rapid Biodetection of Bacterial Cells by Laser Pyrolysis/Mass Spectroscopy

S. Morgan

## ABSTRACT

This research project involves a systematic investigation of novel methods for biodetection of bacterial agents based on a combination of laser ablation/pyrolysis, fast gas chromatography (GC), and time-of-flight mass spectrometry. The new instrument to be developed combines a 266 nm Nd-Yag UV laser for micro sample ablation with time-of-flight mass spectrometry (TOF-MS) for rapid bacterial characterization. Microlaser ablation will be employed to pyrolyze single cells or small populations of cells. Time-of-flight mass spectrometry (TOF-MS) will then be used to identify chemical markers in the mixture of cellular fragments. By rastering the surface of the sample with the laser, mass spectrometric "images" of the sample's chemical content can be produced. Goals include targeting specific cellular structures (cell wall, lipopolysaccharides, cytoplasm, intercellular content, *etc.*), reducing sample size requirements, and achieving high selectivity. Another focus of these studies is to couple extremely fast (< min) gas chromatographic separations to TOF-MS for bacterial characterization. Chemometric data analysis using principal component analysis, multivariate discriminant analysis, and cluster analysis will permit statistical validation of the significance of differences observed between different samples.

## FORWARD

The total amount of the grant award is $434,748.00 for the period from 6/1/97 to 6/29/00. Significant achievements during this first reporting period include:

- Design of the new instrument is progressing. The current instrument design includes a microlaser ablation system coupled to a time-of-flight mass spectrometer.
- We have conducted preliminary investigations of a new rapid gas chromatographic technique (Flash™ GC, Thermedics Detection, Inc.) for extremely rapid (< 2 min) separations. We are currently investigating the potential for interfacing this technology to the laser ablation/pyrolysis TOF-MS system.
- Data from experiments involving qualitative and quantitative analysis of monomeric carbohydrate content in bacterial polysaccharides by Py-GC/MS has been analyzed by a variety of univariate and multivariate approaches. We are currently comparing information available from the use of 3-mode principal component analysis to that produced by 2-D PCA of stacked data matrices.

## REPORT

### *Problem Studied*

Traditional microbial identification is performed after isolation and growth, and taxonomic decisions are often based on morphology. The development of instrumental methods for

characterization of bacteria is of continuing relevance to rapid identification of bacteriological warfare agents. We have selected laser ablation coupled to time-of-flight mass spectrometry as a candidate method for rapid characterization of bacterial samples. We propose to investigate the use of existing commercial as well as some novel approaches to sample introduction to TOF/MS systems. A microlaser ablation/pyrolysis time-of-flight mass spectrometer system is under development for pyrolysis/desorption of material from single cells or small populations of cells. By focusing on single cells with a high resolution optical system, this approach also may be able to target specific cellular structures (cell wall, lipopolysaccharides, cytoplasm, intercellular content, *etc.*), reduce sample size requirements, and offer high selectivity.

***Summary of most important results***

The laser microprobe-TOF/MS system design is progressing. To satisfy the original design goal of using laser ablation to vaporize components of bacterial cells, we have selected the Merchantec LUV266 laser ablation system (Carlsbad, CA). The system uses a computer controlled, frequency quadrupled, Q-switched Nd: YAG UV laser at 266 nm. A variable aperture enables control of the 5 mJ beam in 255 increments and the laser spot size is continuously adjustable from 5 μm to 400 μm. The flat beam profile allows reproducible analysis of thin layer sample surfaces with a 4 ns laser pulse length and repetition rate adjustable from 1-20 Hz.. The targeting of the laser beam can automatically raster in patterns evenly spaced around the crosshair focus with 0.25 μm resolution. The laser ablation cell is a laminar flow cell constructed of Teflon and Viton with a replaceable laser grade window. Gas flow is computer controlled for on-line, bypass, and purge operation. High resolution color imaging from 100X to >1000X is provided on a computer monitor using a CCD camera and Parfocal video microscope. The laser microprobe is operated independently or in conjunction with the host mass spectrometer's data system with full bi-directional exchange of numerical and visual data, status, and control information.

TOF/MS offers high sensitivity for single ionization processes because the entire collection of ions produced can be simultaneously analyzed. TOF/MS is especially attractive because of its high sensitivity and relatively high mass resolution for identification of components from macromolecular sources in microbial cells. The time-of-flight mass spectrometer selected for this project is a Comstock (Oak ridge, TN) Model LTOF-110 with a laser ionization source. The source has two accelerated regions, separated by a double grid assembly which provides second order spatial focusing. The 1 meter flight tube is maintained at high potential to allow the ion source to operate near ground potential. Mounted within the flight tube is a pair of X deflector plates, a pair of Y deflector plates, and a lensing element. The instrument uses dual, chevron-mounted microchannel plate detectors with 50 ohm impedance matched signal output. A vacuum compatible, internal resistor/capacitor bridge provides detector biasing, DC isolation, and a clean, oscillation-free signal with gain of approximately $10^7$. This system was selected because it offers the greatest flexibility for future expandability. The mass range extends to 5,000 with 300-800 mass resolution. By rastering the surface of the sample with the laser, we anticipate the ability to produce mass spectrometric "images" of the sample's chemical content.

The above described components can be combined as a direct laser ablation/TOF-MS system in which laser ablation/pyrolysis products are swept directly into the mass analyzer without prior chromatographic separation. The ability to separate the products of the laser ablation/pyrolysis step by gas chromatography (GC) is desirable from a selectivity viewpoint. However, conventional GC suffers from an inability to transmit higher molecular weight components and from relatively long analysis times of 5-20 min for complex samples. We have initiated discussions with Thermedics Detection, Inc. (Chelmsford, MA) regarding a new approach to rapid GC analysis. Thermedics has recently contracted with Comstock to provide the Department of Energy with a portable instrument for analysis of PCBs and other environmental contaminants. The instrument uses a low power laser to volatilize material from contaminated surfaces, followed by a rapid GC separation on a Thermedics Flash™ GC instrument and subsequent analysis by TOF-MS. Flash™ GC uses special column heaters enclosing short fused silica capillary columns that can be rapidly programmed from ambient to 400 °C at 20 °C/sec. Flash™ GC can perform GC separations approx. 10 times faster than conventional GC instruments. Figure 1 shows a separation we obtained recently of a 17-component mixture. The chromatogram resulted in nearly baseline separation of all components in less than 90 s. This run time is dramatically faster than the 15-20 min required on a conventional capillary GC system. In the next few months, we will be conducting further investigations of the potential of Flash™ GC for coupling to laser ablation and TOF-MS. Of concern in these studies is the transmission of high molecular weight components through short capillary columns. Dr. Morgan is travelling to visit the Thermedics Detection site in Chelmsford, MA, in mid-May to continue discussions concerning these applications.

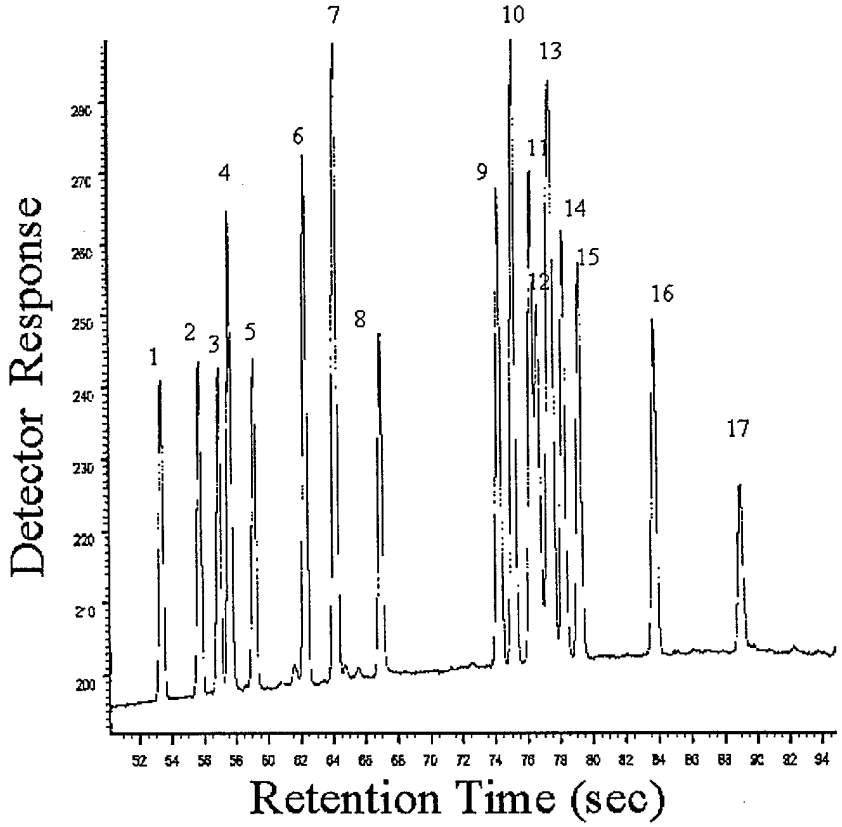


Figure 1. Flash™ GC separation of a sample containing a mixture of volatile and semi-volatile components with a wide-boiling range

Two significant upgrades of equipment in our laboratory, using funds from sources other than DoD, have expanded our capability for significant progress in applications of pyrolysis and mass spectrometry. An existing Hewlett-Packard (Palo Alto, CA) Model 5988 quadrupole GC/MS system will be upgraded with a new Microsoft Windows-based Hewlett-Packard ChemStation data system. This system has been extensively used in previous Py-GC/MS studies. A CDS Analytical (Oxford, PA) Model 2000 Pyroprobe is attached to its inlet. The second upgrade is the acquisition of a Hewlett-Packard GCD quadrupole mass spectrometer detector interfaced to a HP Model 6890 capillary GC instrument. This instrument is configured with a CDS model 2000 Pyroprobe with autosampler interface that holds a carousel of 20 quartz tubes for automated Py-GC/MS analysis.

Systematic differences between bacteria can be related to the presence or prominence of distinctive chemical markers in bacterial cells.[1-10] Examples of unique microbial pyrolysis products from microorganisms include identification of dianhydroglucitol from glucitol phosphate residues in the group-specific polysaccharide of group B streptococci[8] and differentiation of *B. anthracis* strains by a pyrolysis product from its cell wall galactose-N-acetylglucosamine polysaccharide.[11] A review of current literature in time-of-flight mass spectrometry with emphasis on analysis of biological samples (and more specifically, bacteria) has been performed. This compilation of research literature has focused our attention on capabilities available in competing technologies as well as state-of-the-art methods for analysis of biologically relevant polymers.

The initial focus is on chemical markers generated from carbohydrate and amino acid/peptide cellular sources. We have completed preliminary studies involving qualitative and quantitative analysis of monomeric carbohydrate content in bacterial polysaccharides by Py-GC/MS. Upon pyrolysis, carbohydrates produce anhydrosugar pyrolysis fragments that retain the stereochemistry of the parent sugar. We have identified unique anhydrosugars from all aldohexoses including glucose, mannose, galactose, talose, and allose. Pyrograms and mass spectra of di-, tri-, and other oligomers (including bacterial polysaccharides) can be interpreted by matching to these chemical markers. Differentiation of the aldohexose monosaccharides or determination of simple carbohydrate composition in polysaccharides can be achieved with little to no sample preparation by Py-GC/MS. As seen in Figure 2, the presence of a 1,6-anhydro-glucopyranose peak and a 1,6-anhydro-glucofuranose peak in pyrograms of purified LPS from *E. coli* confirm the presence of glucose. The *E. coli* strain 0127:B8 additionally contains galactose, as indicated by a 1,6-anhydro-galactopyranose peak and a 1,6-anhydrogalactofuranose peak. The *K. pneumoniae* LPS contains a complex heptasaccharide of three glucopyranosyl units, and one each of galactopyranosyl, galactofuranosyl, rhamnopyranosyl, and glucouronosyl units[12]. We have confirmed the aldohexose content of this LPS by Py-GC/MS: 1,6-anhydroglucopyranose peak and 1,6-anhydroglucofuranose products are indicative of the glucose monomer, while 1,6-anhydrogalactopyranose is indicative of galactose. A manuscript describing these results is in preparation.

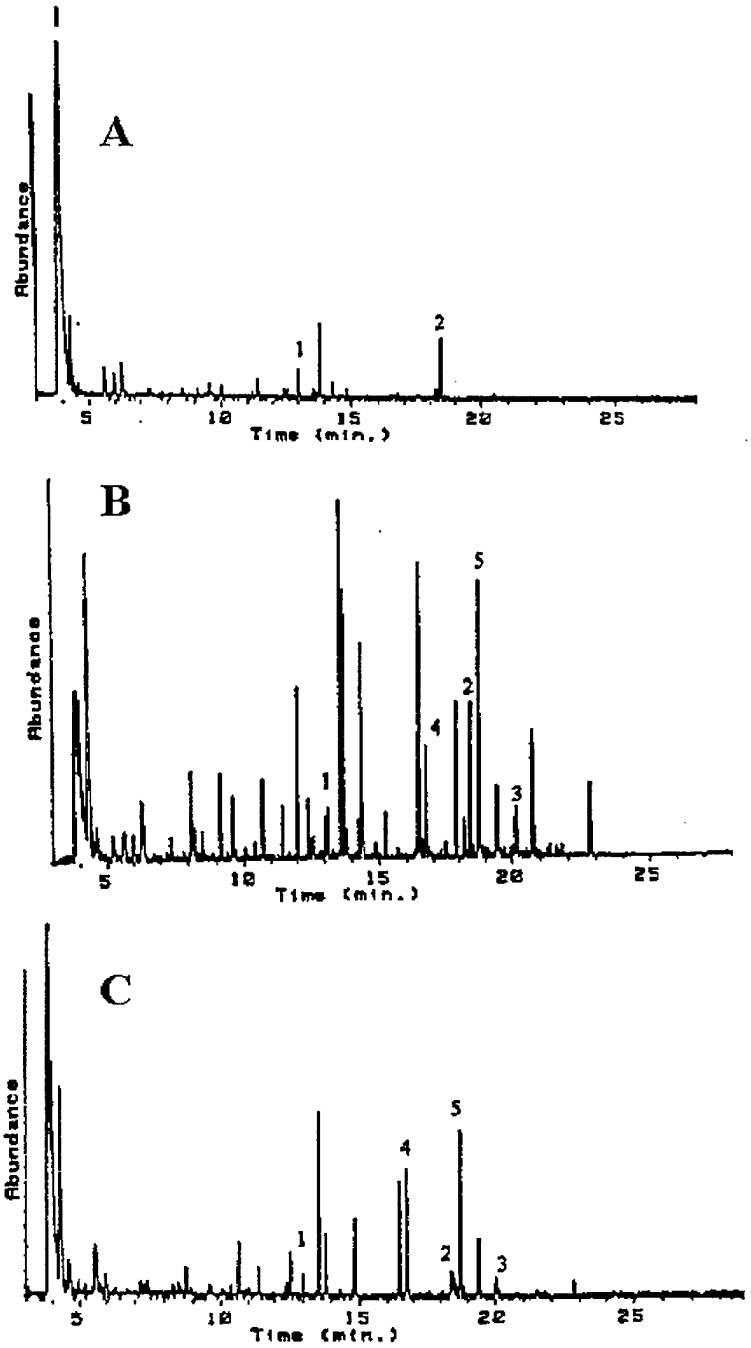


Figure 2. Total ion pyrograms of bacterial lipopolysaccharides. (A) *E. coli.* Strain 026:B6 (B) *E. coli.* Strain 0127:B8; (C) *K. pneumoniae.* Peak identities: (1) 1,4:3,6-dianhydro-α-D-glucopyranose; (2) 1,6-anhydroglucopyranose; (3) 1,6-anhydroglucofuranose; (4) 1,6-anhydrogalactopyranose; (5) 1,6-anhydrogalactofuranose.

We are also making further progress in defining approaches for multivariate pattern recognition applied to multidimensional MS or GC/MS data. As a test multidimensional data set we have used Py-GC/MS to analyze three monomers (glucose, fructose, and galactose), four dimers (melibiose, lactose, turanose, and sucrose), and one trimer (raffinose). The samples comprised a "molecular mixture design" of monomers, dimers, and trimers. Three dimensional data,

consisting of intensities of mass spectral ions from selected peaks, were generated by Py-GC/MS of these compounds. Because traditional two-dimensional (2-D) principal component analysis (PCA) can not be used on this cubic data matrix, we applied 3-mode PCA to analyze the relationships among these oligosaccharides and their monomeric constituents. We have written software to translate from proprietary data formats and to process the GC/MS data into a vector representation suitable for pattern recognition. Using a MatLab program, projections of data points into the space spanned by the first two factors revealed expected correlations between the monomers, the dimers, and the trimer from the molecular mixture design. A manuscript describing these results is in preparation. Comparisons of 3-mode PCA to results obtained by 2-D analysis of a stacked data matrix are also in progress.

***Participating scientific personnel:***

1. Kristen Sellers, Ph. D. candidate, Department of Chemistry & Biochemistry, The University of South Carolina, Columbia, SC 29208.

2. Mary Peyton Davis, Ph. D. candidate, Department of Chemistry & Biochemistry, The University of South Carolina, Columbia, SC 29208.

## BIBLIOGRAPHY

1. S. L. Morgan, A. Fox and J. Gilbart, *J. Microbiol. Methods*, 9 (1989) 57.
2. S. L. Morgan, B. E. Watt, K. Ueda and A. Fox, in A. Fox, S. L. Morgan, L. Larsson and G. Odham (Editors), *Analytical Microbiology: Chromatography and Mass Spectrometry*, Plenum Press, New York, 1990, Ch. 12, p. 179.
3. M. D. Walla, P. Y. Lau, S. L. Morgan, and A. Fox, *J. Chromatogr.* **1984**, 288, 399-413.
4. R. S. Whiton, S. L. Morgan, J. Gilbart, and A. Fox, *J. Chromatogr.* **1985**, *347*, 109-120.
5. J. Gilbart, A. Fox, R. S. Whiton, and S. L. Morgan, *J. Microbiol. Methods* **1986**, *5*, 271-282.
6. J. Gilbart, A. Fox, and S. L. Morgan, *European J. Clin. Microbiol.* **1987**, 6(6), 715-723.
7. A. Fox, S. L. Morgan, and J. Gilbart, in *Analysis of carbohydrates by GLC and MS*, C. J. Bierman and G. McGinnis, eds., CRC Press, FL., 1989; Chapter 5.
8. C. S. Smith, S. L. Morgan, C. D. Parks, A. Fox and D. G. Pritchard, *Anal. Chem.,* 59(1987) 1410.
9. C. S. Smith, S. L. Morgan and A. Fox, *J. Anal. Appl. Pyrol.*, 18 (1990) 97.
10. B. E. Watt, S. L. Morgan, and A. Fox, *J. Anal. Appl. Pyrol.*, 19 (1991) 237.
11. S. L. Morgan, B. E. Watt, and R. C. Galipo, "Characterization of microorganisms by pyrolysis GC, pyrolysis GC/MS, and pyrolysis MS", in: *Applied Pyrolysis Handbook*, T. Wampler, Ed., Plenum Press, NY, 1995.
12. J. W. Ezzell, Jr., T. G. Abshire, S. F. Little, B. G. Lidgerding, and C. Brown, *J. Clin. Microbiol.*, 28 (1990) 223.

# REPORT DOCUMENTATION PAGE

Form Approved
OMB No. 0704-0188



| 1. AGENCY USE ONLY *(Leave blank)* | 2. REPORT DATE | 3. REPORT TYPE AND DATES COVERED |
|---|---|---|
| | 1 June 1998 | Annual |

4. TITLE AND SUBTITLE

Rapid Biodetection of Bacterial Cells by Laser Pyrolysis/Mass Spectrometry

5. FUNDING NUMBERS

Grant Number N00014-97-1-0806
PR Number 97PR06312-00
PO Code 353
Disbursing Code N68892
AGO Code N66020
Cage Code 4B489

6. AUTHOR(S)

Stephen L. Morgan (PI), Scott R. Goode, S. Michael Angel

7. PERFORMING ORGANIZATION NAME(S) AND ADDRESS(ES)

The University of South Carolina

8. PERFORMING ORGANIZATION REPORT NUMBER

N00014-97-1-0806-1

9. SPONSORING / MONITORING AGENCY NAME(S) AND ADDRESS(ES)

ONR

10. SPONSORING / MONITORING AGENCY REPORT NUMBER

ONR

11. SUPPLEMENTARY NOTES

Prepared in coordination with University Research Initiative Program for Combat Readiness

12a. DISTRIBUTION / AVAILABILITY STATEMENT

APPROVED FOR PUBLIC RELEASE

12b. DISTRIBUTION CODE

13. ABSTRACT *(Maximum 200 words)*

This research project involves a systematic investigation of novel methods for biodetection of bacterial agents based on a combination of laser ablation/pyrolysis, fast gas chromatography (GC), and time-of-flight mass spectrometry. The new instrument to be developed combines a 266 nm Nd-Yag UV laser for micro sample ablation with time-of-flight mass spectrometry (TOF-MS) for rapid bacterial characterization. Microlaser ablation will be employed to pyrolyze single cells or small populations of cells. Time-of-flight mass spectrometry (TOF-MS) will then be used to identify chemical markers in the mixture of cellular fragments. By rastering the surface of the sample with the laser, mass spectrometric "images" of the sample's chemical content can be produced. Goals include targeting specific cellular structures (cell wall, lipopolysaccharides, cytoplasm, intercellular content, *etc.*), reducing sample size requirements, and achieving high selectivity. Another focus of these studies is to couple extremely fast (< min) gas chromatographic separations to TOF-MS for bacterial characterization. Chemometric data analysis using principal component analysis, multivariate discriminant analysis, and cluster analysis will permit statistical validation of the significance of differences observed between different samples.

14. SUBJECT TERMS

Chemical and Biological Warfare, Target Acquisition, Anti-Submarine, Combat Medicine, Biodeterioration, and Command Control and Communication

15. NUMBER OF PAGES

16. PRICE CODE

| 17. SECURITY CLASSIFICATION OF REPORT | 18. SECURITY CLASSIFICATION OF THIS PAGE | 19. SECURITY CLASSIFICATION OF ABSTRACT | 20. LIMITATION OF ABSTRACT |
|---|---|---|---|
| UNCLASSIFIED | UNCLASSIFIED | UNCLASSIFIED | 200 words |

# SECTION 3: COMMAND, CONTROL, AND COMMUNICATIONS

# Dynamic Decision Support for Command, Control, and Communications in the Context of Tactical Defense

John R. Rose

Department of Computer Science
University of South Carolina
Columbia, South Carolina 29208

Tel: (803) 777-2405
Fax: (803) 777-3767
Email: rose@cs.sc.edu

# Section 3-1: Dynamic Decision Support for Command, Control, and Communications in the Context of Tactical Defense

J. Rose

## ABSTRACT

Advances in communication and sensor technologies have brought about huge increases in the types and amounts of information available for battle management. Shortcomings in the ability to integrate and arbitrate missing and conflicting information and the current inability to correlate and reason about vast amounts of information in real-time are an impediment to providing a coherent overview of unfolding events. Integrating disparate information, such as voice, video images, and tactical displays, that has varying degrees of reliability is a first step towards battle management. Such integration can be accomplished through the application and further development of Bayesian network and intelligent agent methods. Bayesian networks provide a sound basis for a robust and potentially very efficient solution to the problems posed by incomplete or unreliable data and have proven suitable to the problem of integrating disparate types of data. Other aspects of managing different types of data can be addressed through intelligent agents.

Specific features of the decision support system that we are developing include:

- Dynamic Goal Reassessment
- Anytime Evaluation of Reliability and Value of Information
- Agent-Encapsulated Bayesian Models
- Local and Meta-level Agent Modeling
- Hierarchy of Collaborating Intelligent Agents
- Intelligent Routing to Reconfigure Interagent Information Flow

The overarching conceptual framework for the work in data fusion and battle management is Bayesian decision theory. The ability of commanders and warriors to perform risk assessment and make effective tactical decisions will be improved by a dynamic normative system that supports real-time integration and augmentation of disparate data.

## FORWARD

This project has been funded at the amount of $410,399 with a starting date of 6/01/97 and an ending date of 6/29/00. Work did not actually begin on this project until 7/01/97 due to administration processing delays.

In the original proposal, it was suggested that Bayesian networks form the basis for dealing with uncertainty and potentially unreliable data. During the first year of development, greater consideration of the problem area has motivated us to select decision networks rather than Bayesian networks as the fundamental paradigm for dealing with uncertainty. Since decision networks (also known as influence diagrams) are in a sense an augmentation of Bayesian networks, this is not major change but a rather a minor adjustment. In addition to providing the

probabilistic reasoning that Bayesian networks are capable of, decision networks also provide a formalism for action and utilities, and they support more directly the selection of optimal actions based on the expected utility of the competing actions.
During this first six months we have achieved completion of both six-month deliverables:

- Produced a comprehensive state of the art survey (Technical report DAG97-1).
- Compiled a set of evaluation scenarios (Technical report DAG97-2).

Both of these technical reports are available on request. To request a technical report contact:
John R. Rose
University of South Carolina
Department of Computer Science
Columbia, South Carolina 29208
(803) 777-2405 Phone
(803) 777-3767 Fax
rose@cs.sc.edu

We are on track to have completed the development of the following deliverables by the end of the first actual 12 months (6/30/98):

- General intelligent agent local model (Decision network)
- General intelligent agent meta-model (Decision network)
- Decision theoretic algorithm to evaluate information reliability
- Decision theoretic algorithm to assess the importance of missing information

## REPORT

### *Problem Studied*

The approach to dynamic decision support that we taking involves research and development in areas of data fusion, multi-agent collaboration, dynamic goal reassessment, and decision theory.

### Data Fusion

A real-time decision support system for tactical defense must provide an overall picture of the military significance of the information collected by different platforms. This information is represented in different levels of abstraction varying from raw sensor data to commander level data. Examples of raw sensor data include imaging data, position, velocity, acceleration, and identities. Some instances of commander level data are degree and imminence of threat, likely future actions of hostile platforms, and recommendations concerning appropriate friendly-force action. Difficulties in the ability to combine, analyze, and integrate enormous volumes and varieties of data have encouraged attempts to facilitate data fusion processes.

### Multi-agent Collaboration

Situation assessment of any significant spatial dimensions demands a distributed solution. Centralized systems provide better coherency to the problem solving, but at a cost of scalability and flexibility. When the problem is solved in a decentralized way, inter-agent collaboration is required to produce a coherent solution. Collaboration can be simple and efficient if agents have little autonomy in that every agent's role and capabilities are fixed and each agent does not need

to have an extensive model of another agent in order to collaborate. The more flexibility an agent has to act independently, the greater the need to either communicate frequently or model other agents extensively. On the other hand, a flexible solution will enable the system to handle both new situations and faults, but adds overhead as collaboration becomes complicated.

The important distinctions among various multi-agent designs boils down to the organization (organization type and predefined roles), flexibility (role switching, handling of uncertainty, incompleteness, and faults), and collaboration (semantic content of messages, level of modeling of other agents and environment, level of consistency enforced).

**Dynamic Goal Reassessment**

In order to work in a dynamic hostile environment, an agent must be able to consider different courses of action, and take one that will produce optimal results. To this end an agent must consider multiple goals which are often in competition. A goal is some structure that indicates either a state the agent must achieve or a set of actions the agent must perform. In order for an agent to consider multiple goals, the agent must be able to assess the relative importance of the goals. Some goals are more urgent than others; the agent should pursue these goals first. Also, it is likely that some goals will conflict with others. For example, an agent might have a directive that requires it to process data from its subordinates and send the resulting analysis to its superior. Another directive may be instantiated that requires the agent to avoid detection. An enemy might detect such communication and determine its source so that it might not be possible for both goals to be achieved simultaneously. Finally, some goals can overlap such that satisfying a part of one goal may also satisfy a part of another. Goal reassessment consists of dynamically reordering items on the agenda. Priorities of goals can change in response to changes in the agent or in the agent's environment.

**Decision Making and Time Criticality**

Decision theory provides an appropriate framework for dynamic decision support. An agent's preferences can be captured by utilities - the real numbers representing the desirability of a state. Utilities are combined with the outcome probabilities for actions to provide an expected utility (EU) for each action. In order to maintain sound decision making in the real world, an intelligent agent must follow the maximum expected utility (MEU) principle. In other words, an intelligent agent's mission, from a decision making perspective, is to find the best action, that is, the action that achieves the maximum expected utility for a given situation, based on the information available to the agent.

In many cases, utilities are dependent on time. The nature and timing of actions by a decision maker is often influenced by pressures generated by time-dependent processes. Normally, in the case of time-critical situations, the expected utility of an outcome decreases as a result of delaying action. Thus the utility of the possible outcomes of an action is a function of the action and the time at which the action is taken. The cost of delayed action for a particular delay can be characterized as the difference in the expected value of taking immediate action and delaying ideal corrective action until some specific later time.

**Reliability of Information**

A mission of an intelligent agent is to find the best action from given evidence. In the real world, however, an agent may receive incorrect information for various reasons: faulty sensors produce incorrect information; misleading information can be created intentionally by adversaries; human users can make mistakes as a result of confusion. Incorrect information that is not recognized as such will not only diminish the reliability of an agent's decision making system, but will cause the propagation of incorrect information through the entire network if it is connected with neighbors. Therefore, the degree of belief in given information should be decided before making any decisions on the basis of that information.

**A Probabilistic Approach to Prediction**

The dynamic aspect of the military decision assessment requires a framework that captures the beliefs of the agent before the current events and predicts the evolution of different scenarios. This framework should contain the following actions:

- Combine knowledge, probability, and time
- Optimize the decision process
- Predict the effect of each action in both the environment and the internal state of the agent

There are other temporal issues to consider in a military decision assessment, for example:

- The possibility that a reading from a sensor at a later time may become unreliable.
- A situation assessment during certain interval of time can recur in the future or be completely different from all previous situations.

All of these issues may require dynamic extensions of Bayesian networks or decision networks, and/or time-varying dynamic models.

***Summary of Important Results***

During the first year we have collected test scenarios and have abstracted salient features that must be considered in the development of the dynamic decision support system. We have also produced a state of the art survey of the areas of research that form the basis for the system that we are developing. Algorithms for evaluating reliability of information and assessing the value of missing information have been developed or adapted. Development of abstract intelligent agent decision theoretic local and meta models is progressing and should be complete by the actual end of the first year (6/30/98). Development of the specification of the interface between agents is nearing completion.

***Publications and Technical Reports***

1. Mark Bloemeke and Marco Valtorta. "A Hybrid Algorithm to Compute Marginal and Joint Beliefs in Bayesian Networks and Its Complexity". Accepted for presentation at the Fourteenth Annual Conference on Uncertainty in Artificial Intelligence (UAI-98), University of Wisconsin Business School, Madison, Wisconsin, July 24-26, 1998.
2. State of the Art Survey for Dynamic Decision Support: Data Fusion, Multi-Agent Collaboration, Dynamic Goal Reassessment, and Decision Theory. Technical report DAG97-1.
3. Evaluation Scenarios for Dynamic Decision Support. Technical report DAG97-2.

***Scientific Personnel***
Dr. John R. Rose
Dr. Marco Valtorta
Dr. Abhijit Sengupta
Dr. Suresh Singh
Miguel Barrientos
Mark Bloemeke
Young-Gyun Kim
Clif Presser
Wayne Smith

## LIST OF INVENTIONS

A Hybrid Algorithm to Compute Marginal and Joint Beliefs in Bayesian Networks.
As we investigated the organization of agent-encapsulated Bayesian networks, it became apparent that fast computation of marginal posterior probabilities involving more than one variable is necessary. Such marginals need to be propagated from agent to agent in order to prevent double-counting of evidence in the presence of undirected cycles in the agent communication graph. Existing algorithms for the computation of marginals are designed to compute either all marginals involving one variable or the marginal on an arbitrary but fixed subset of the variables. We invented a hybrid algorithm that carries out the computation of both all single-variable marginals and of the marginal on an arbitrary fixed subset of variables in essentially the same time as existing algorithms take to do one of the computations. We observe that this is, in worst case, an exponential speed-up, because each of the two problems requires, when addressed individually, the solution of an NP-hard problem. The algorithm is described in a paper accepted for presentation at UAI-98 and was developed by Mark Bloemeke, who is extending it as part of his doctoral research.
Reference: Mark Bloemeke and Marco Valtorta. "A Hybrid Algorithm to Compute Marginal and Joint Beliefs in Bayesian Networks and Its Complexity". To be presented at UAI-98.

## BIBLIOGRAPHY

1. Bloemeke, Mark and M. Valtorta. "A Hybrid Algorithm to Compute Marginal and Joint Beliefs in Bayesian Networks and Its Complexity". Accepted for presentation at the Fourteenth Annual Conference on Uncertainty in Artificial Intelligence (UAI-98), University of Wisconsin Business School, Madison, Wisconsin, July 24-26, 1998.
2. Durham, Stephen D., Jeffrey S. Smolka, and M. Valtorta. "Statistical Consistency with Dempster's Rule on Diagnostic Trees Having Uncertain Performance Parameters." International Journal of Approximate Reasoning , 6 (1992), 1, 67-81.
3. Escudero, Sonia (thesis advisor J. R. Rose). "A Bayesian Model for Reaction Classification." M.S. Thesis, University of South Carolina, 1995.
4. Gage, D. K. (thesis advisor J. R. Rose). "A Comparative Analysis of Bayesian Belief Networks and Classical Statistical Approaches." M.S. Thesis, University of South Carolina, 1995.

5. Graham, M. B. (thesis advisor J. R. Rose). "An Architecture for Implementing Rules in a Second Generation Database Management System." M.S. Thesis, University of South Carolina, 1996.
6. Kim, Young-Gyun and M. Valtorta. "On the Detection of Conflicts in Diagnostic Bayesian Networks Using Abstraction." In: Ph. Besnard and S. Hanks (eds.), Uncertainty in Artificial Intelligence: Proceedings of the Eleventh Conference. San Francisco, CA: Morgan-Kaufmann, 1995, 362-367.
7. Mani, Subramani, M. Valtorta, Suzanne McDermott. "MENTOR: A Bayesian Model for Prediction and Intervention in Mental Retardation." Working Notes of the Fifth International Workshop on Artificial Intelligence and Statistics (AIS-95), 366-371, Ft. Lauderdale, FL, January 1995.
8. Mani, Subramani, Suzanne McDermott, and Marco Valtorta. "MENTOR: A Bayesian Model for Prediction of Mental Retardation in Newborns." Research in Developmental Disabilities, 18 (1997), 5, 303-318.
9. Mechling, Randy and M. Valtorta. "A Parallel Constructor of Markov Networks." In: P. Cheeseman and R.W. Oldford (eds.). Selecting Models from Data: Artificial Intelligence and Statistics IV. New York: Springer-Verlag, 1994, pp. 255-261.
10. Piatkiewicz, Leszek (thesis advisor M. Valtorta). "On the Construction of a Bayesian Network for Agricultural Loan Assessment." M.S. Thesis, University of South Carolina, 1996.
11. Singh, Moninder and M. Valtorta. "An Algorithm for the Construction of Bayesian Network Structures from Data." In: D. Heckerman and E.H. Mamdani (eds.), Uncertainty in Artificial Intelligence: Proceedings of the Eighth Conference. San Mateo, CA: Morgan-Kaufmann, 1993, ISBN 1-55860-258-5, 259-265 (Winner of best student paper award).
12. Singh, Moninder and M. Valtorta. "Construction of Bayesian Belief Networks from Data: a Brief Survey and an Efficient Algorithm." International Journal of Approximate Reasoning, 12 (1995), 2, 111-131.
13. Wang, Shijie and M. Valtorta. "On The Exponential Growth Rate of Dempster-Shafer Belief Functions." Proceedings of the SPIE Conference on Applications of Artificial Intelligence X: Knowledge-Based Systems, Orlando, FL, 15-24, 1992.

# REPORT DOCUMENTATION PAGE

Form Approved
OMB No. 0704-0188



| 1. AGENCY USE ONLY *(Leave blank)* | 2. REPORT DATE | 3. REPORT TYPE AND DATES COVERED |
|---|---|---|
| | June 1, 1998 | Annual |

4. TITLE AND SUBTITLE

Dynamic Decision Support for Command, Control, and Communication in the Context of Tactical Defense

5. FUNDING NUMBERS

Grant Number N00014-97-1-0806
PR Number 97PR06312-00
PO Code 353
Disbursing Code N68892
AGO Code N66020
Cage Code 4B489

6. AUTHOR(S)

John R. Rose

7. PERFORMING ORGANIZATION NAME(S) AND ADDRESS(ES)

University of South Carolina

8. PERFORMING ORGANIZATION REPORT NUMBER

N00014-97-1-0806-1

9. SPONSORING / MONITORING AGENCY NAME(S) AND ADDRESS(ES)

ONR

10. SPONSORING / MONITORING AGENCY REPORT NUMBER

ONR

11. SUPPLEMENTARY NOTES

Prepared in coordination with University Research Initiative Program for Combat Readiness

12a. DISTRIBUTION / AVAILABILITY STATEMENT

APPROVED FOR PUBLIC RELEASE

12b. DISTRIBUTION CODE

13. ABSTRACT *(Maximum 200 words)*

This first annual report describes progress made in the development of a system designed to provide dynamic decision support for command, control, and communication in the context of tactical defense. The document provides a synopsis of the key research areas that are being investigated to provide a solution to dynamic decision support in a distributed environment. Current results and projected near-term results are summarized. Included is a brief description of an original algorithm for the computation of marginal and joint beliefs in a Bayesian network. In addition, one publication and two technical reports, which have come out of this research, are listed.

14. SUBJECT TERMS

Command Control and Communication

15. NUMBER OF PAGES

9 pages including this page

16. PRICE CODE

| 17. SECURITY CLASSIFICATION OF REPORT | 18. SECURITY CLASSIFICATION OF THIS PAGE | 19. SECURITY CLASSIFICATION OF ABSTRACT | 20. LIMITATION OF ABSTRACT |
|---|---|---|---|
| UNCLASSIFIED | UNCLASSIFIED | UNCLASSIFIED | 200 words |

# Survivable and Reconfigurable Optical/Wireless Tactical Networks

Suresh Singh

Department of Computer Science
University of South Carolina
Columbia, SC 29208

Tel: (803)777-2596
Fax: (803)777-3767
Email: singh@cs.sc.edu

# Section 3-2: Survivable and Reconfigurable Optical/Wireless Tactical Networks

Suresh Singh

## ABSTRACT

High-speed, real-time access and reliable dissemination of intelligence and reconnaissance information are key components of combat readiness. In order to maximize the effectiveness and timeliness of this information, it is necessary to flow the information quickly from the sensor(s) to the shooter and warfighter in addition to flowing it backwards to C2. In this project we are developing solutions to networking problems that will enhance the capability and battle readiness of heterogenous tactical networks. Specifically:

- Make wireless battlesite networks more reliable, adaptable, reconfigurable, and secure by using dynamic agent-based network management.
- Develop information processing and transmission systems for the seamless integration of wireless battlesite networks with high-bandwidth optical C2 networks.
- Enhance the reliability of on-board and on-shore optical networks by novel failure detection and fault avoidance schemes.
- Exploit multi-tiered network structures to perform local information filtering to reduce message overhead.
- Provide Quality of Service (QoS) guarantees for multimedia data traffic in mobile networks that are subject to jamming.

## FORWARD

This project was funded at the amount of $409,000for the period 6/01/97 – 6/29/00.

In the original proposal, we had suggested that modified versions of TCP and UDP protocols would be appropriate for the mobile network component of the system. However, our investigations revealed that the frequent mobility of users will cause a huge drop in TCP throughput (because round-trip delays very dramatically) and will result in poor applications performance. As a solution we have developed a protocol that allows an application to specify the degree of reliability desired for each packet and provides feedback that indicates whether the goal was met or not. Recovery is left up to the application.

We also evaluated the feasibility of using agent-based network management and determined that such a protocol would require an inordinate amount of computation at mobile end-points. Since battery power is a very precious resource in mobile networks, we decided to adopt simpler strategies that would be energy-efficient.

We evaluated the simulation tools available to study the performance of our techniques for large networks. As these tools were designed for electronic networks, they perform in

an unacceptably poor fashion for all-optical networks with large numbers of nodes. In order that our methods can be appropriately evaluated, we decided to implement a simulation system of our own. This is an object-oriented system based on the MODSIM language where objects can be added as directed by our research. The rationale for this software system was discussed with Dr. Nagle when he made a site visit in November 1997.

The results from our work thus far is available as technical reports:

- Network management protocol for mobile wireless networks (Technical Report TR-9802).
- Data transport protocol for multihop multimedia wireless networks (Technical Report TR-9803).

During the last 9 months, we have achieved the following deliverables. The last column indicates the percentage of the deliverable completed.

| Deliverables | Year 1 | Year 2 | Year 3 | Status |
|---|---|---|---|---|
| **Mobile UDP and TCP protocols for multihop wireless networks; demonstrate in a 6-node network** | X | | | DONE |
| **Automatic network configuration and management** | | X | | DONE |
| **Extended Mobile RTP for multihop wireless networks; Demonstrate MBONE applications.** | | X | | 75% DONE |
| **Implementation of QoS guarantees for multimedia data; demonstrate by simultaneous transmission of video/audio data** | | X | | 50% DONE |
| **Analyze performance of mobile gateways** | | | X | 25% DONE |
| **Topology design methodologies for static/dynamic wavelength routing** | X | | | DONE |
| **Online failure detection methods** | X | | | DONE |
| **Automatic network reconfiguration algorithms to avoid faults** | | X | | |
| **Analysis of performance degradation following failures** | | | X | |

## REPORT

### *Problem Studied*

We examine the problem of developing network management and data transport protocols for multihop wireless networks operating in hostile environments. Further, we study the problem of building reliable optical backbone networks for on-shore and on-ship applications. Finally, we study the problem of integrating these two types of networks via gateways.

### Data Transfer Protocol in Multihop Wireless Networks

In order to allow seamless integration of data networks between different agencies, the TCP/IP protocol suite has been adopted as a de facto standard for the Tactical Internet. A problem with using unmodified TCP and UDP protocols in multihop wireless networks is

that node mobility causes severe performance degradation in TCP's throughput and UDP's error-rate. Thus, newer protocols are desired that allow efficient data transfer while ensuring integration with TCP/IP protocols. Additional constraints imposed by the environment include a need to conserve battery power to extend battery life, a need to include security as an integral part of data transfer and a need to implement QoS guarantees to support different types of data traffic.

**Network Management Protocol for Multihop Wireless Networks**

Network management is a very important task in modern-day warfare. A good network management tool provides the warfighter with a global view of his resources thus allowing him to deploy them in strategic ways. We evaluated evaluated several existing network management protocols from the point of view of relevance to mobile networks and found them wanting. Specifically, protocols such as SNMP (Simple Network Management Protocol) that are widely used in the internet do not scale well to a mobile network where topology changes occur frequently. Furthermore, we observed that the security features built in these protocols were inadequate for mobile networks operating in a hostile environment.

**Implementing QoS guarantees for Multimedia Traffic**

We expect multihop wireless networks to be used in environments where there will be a need for transmitting multimedia data. To transmit such data, we need to be able to reserve bandwidth and buffer at each intermediate hop from the source (say a sensor in the field) to the gateway or network manager. Furthermore, these routes need to be discovered dynamically because the network topology changes continually. An added constraint is the need to ensure that the routes selected are the most energy efficient. In other words, it is probably a bad idea to forward data through nodes that have very depleted energy reserves because this will only expedite their demise. Some approaches that have beed developed for cellular networks, such as loss profiles, can be adapted for use in multihop networks.

**All-Optical Backbone Network**

High-speed communication via a multihop optical backbone network is feasible with current technology. However, a multihop implementation suffers from a bottleneck because of electro-optical wavelength conversion. Using optical devices such as wavelength converters, routers and amplifiers will allow us to achieve data rates in excess of 80Gbps. The avoidance of electro-optical conversions and usage of wavelength division multiplexing (WDM) techniques makes this achievement of high bandwidth possible. Further, methodologies need to be developed that will enable us to design complex topology all-optical networks with low blocking probability and high throughput.

**Routing with Dynamic Wavelength Assignment**

Static wavelength routing uses the knowledge of average-case traffic distribution to allocate wavelengths. Unfortunately, using average-case information leads to poor overall throughput because resources are not utilized efficiently. A better solution is to develop

dynamic strategies for wavelength allocation that adapts to varying network load. Tunable transmitters and receivers make the implementation of these schemes feasible.

**Fault Detection and Fault Management Schemes**
Failures of networking components can result in catastrophic system failure. There is thus a need to be able to detect link or node failures quickly and reroute traffic appropriately. A dynamic wavelength assignment scheme has an edge over static wavelength assignments because we can dynamically assign wavelengths and routes to connections. For failure detection, each node in the network needs to detect the local faults in nodes, links, and channels. Knowledge of these faults needs to be reliably disseminated to other nodes that can then cooperatively repair the network. One issue that needs to be examined is the degree of performance degradation due to specific types of failures (e.g., if a ship is hit on its starboard side, what are the possible effects on the network?).

***Summary of the most important results***
**Data transfer protocol for wireless multihop networks**:
We have developed a new protocol (implemented in UNIX) that is very well suited to the multihop environment. This protocol leaves recovery from lost packets to the application. However, it provides an indication of packets that were presumed lost. The protocol also supports multiple types of traffic allowing user to transmit multimedia data in a reliable fashion. We are currently documenting the performance of this protocol in a real 6-node wireless network. We will compare its throughput and loss behavior against TCP and UDP.

**Network management protocol for multihop wireless networks:**
We have developed a new network management protocol for multihop wireless networks. This protocol is loosely based on SNMPv3. However, unlike SNMP it is based on a 3-layer hierarchy. Mobiles automatically configure themselves into clusters each of which is managed by a clusterhead. All clusterheads are managed by a overall manager. In addition to this, we have incorporated a complete security model based on the model used in the military (i.e., each node has a security clearance, each data type has a security level and data can be organized into compartments which nodes either have access to or not). Finally, we have implement a Java-based GUI to allow the warfighter to manage this network.

**Extended Mobile RTP:**
RTP (Real-Time Protocol) is used for transmitting real-time multicast session data over the Internet's MBONE. We have extended RTP to support sessions where one or more participant is mobile. This extension is fully integrated with TCP/IP protocols and has been demonstrated in actual networks. We are now implementing RTP to work on top of our new data transfer protocol (discussed above). The implementation that remains will be completed shortly.

**Simulation Tool for All-Optical Networks:**
The design of the simulation system is now complete and implementation is in progress. We anticipate completion of the package by 6/30/98. We believe that our techniques might need parameter tuning after we have evaluated the performance of our algorithms.

**Design of All-Optical Networks and Routing Algorithms:**
We have designed methodologies to construct all-optical network topologies that optimize network cost in terms of router costs, switch costs and that optimize throughput assuming static wavelength routing. We have also designed dynamic routing algorithms:

- Using distributed lightpath formation algorithms
- Using virtual wavelength translation schemes (using multiple fibers in a bundle).

Our schemes have been tested for small size networks where wavelength utilization has been found to improve by an order of magnitude.

***Publications and Technical Reports***

1. Network management protocol for mobile wireless networks (Technical Report TR-9802).
2. Data transport protocol for multihop wireless networks (Technical Report TR-9803).
3. Power-Aware Routing in Mobile Ad Hoc Networks (submitted to Proceedings ACM MOBICOM'98 Conference).

***Participating Scientific Personnel***

1. Nitin Jain, M.S. August 1998.
2. Wenli Chen, M.S. August 1998.
3. Mike Woo, PhD candidate.
4. A. Ron Garber, M.S. Student
5. P. Chandrasekhar, M.S. Student.
6. Dr. Suresh Singh
7. Dr. Abhijit Sengupta
8. Dr. John Rose
9. Dr. Marco Valtorta

## LIST OF INVENTIONS

1. A new network management protocol (specification and implementation) for wireless multihop networks.
2. A new data transfer protocol for multihop wireless networks.
3. An implementation of RTP for mobile networks. Support for the MBONE.
4. A software simulation tool for all-optical network's that allows us to evaluate the performance of topology design methodologies and different routing schemes.

## BIBLIOGRAPHY

1. Nitin Jain, "Clustering-based management protocol for ad hoc networks", MS Thesis, May 1998, Department of Computer Science, University of South Carolina.
2. Wenli Chen, "Geographical-based management protocol for ad hoc networks", MS Thesis, May 1998, Department of Computer Science, University of South Carolina.
3. Suresh Singh, Mike Woo and C.S. Raghavendra, "Power-Aware routing in mobile ad hoc networks", Submitted to ACM MOBICOM'98 Conference.
4. Wenli Chen, Nitin Jain and Suresh Singh, "ANMP: Ad hoc Network Management Protocol", Submitted to IEEE Journal on Selected Areas in Communications.

# REPORT DOCUMENTATION PAGE

Form Approved
OMB No. 0704-0188



| 1. AGENCY USE ONLY *(Leave blank)* | 2. REPORT DATE | 3. REPORT TYPE AND DATES COVERED |
|---|---|---|
| | June 1, 1998 | Annual |

| 4. TITLE AND SUBTITLE | 5. FUNDING NUMBERS |
|---|---|
| Survivable and Reconfigurable Optical/Wireless Tactical Networks | Grant Number N00014-97-1-0806<br>PR Number 97PR06312-00<br>PO Code 353<br>Disbursing Code N68892<br>AGO Code N66020<br>Cage Code 4B489 |
| 6. AUTHOR(S)<br>Suresh Singh | |
| 7. PERFORMING ORGANIZATION NAME(S) AND ADDRESS(ES)<br>University of South Carolina | 8. PERFORMING ORGANIZATION REPORT NUMBER<br>N00014-97-1-0806-1 |
| 9. SPONSORING / MONITORING AGENCY NAME(S) AND ADDRESS(ES)<br>ONR | 10. SPONSORING / MONITORING AGENCY REPORT NUMBER<br>ONR |

11. SUPPLEMENTARY NOTES

"Prepared in coordination with University Research Initiative Program for Combat Readiness"

| 12a. DISTRIBUTION / AVAILABILITY STATEMENT | 12b. DISTRIBUTION CODE |
|---|---|
| APPROVED FOR PUBLIC RELEASE | |

13. ABSTRACT *(Maximum 200 words)*

High-speed real-time access and reliable dissemination of intelligence and reconnaissance information are key components of combat readiness. In order to maximize the effectiveness and timeliness of this information, it is necessary to flow the information quickly from the sensor(s) to the shooter and warfighter in addition to flowing it backward to C2. In this project we are developing solutions to networking problems that will enhance the capability and battle readiness of heterogenous tactical networks. Specifically,

- Make battlesite wireless networks more reliable, adaptable, reconfigurable and secure.
- Gateways to seamlessly integrate optical backbone networks with wireless networks.
- Provide Quality of Service (QoS) guarantees for multimedia traffic sent over wireless networks.
- Enhance the reliability of on-board and on-shore optical backbone networks.
- Develop dynamic wavelength assignment and routing strategies for improved throughput.

| 14. SUBJECT TERMS | 15. NUMBER OF PAGES |
|---|---|
| Chemical and Biological Warfare,Target Acquisition,Anti-submarine,Combat Medicine,Biodeterioration and Command Control and Communication. | Seven (7)<br>16. PRICE CODE |

| 17. SECURITY CLASSIFICATION OF REPORT | 18. SECURITY CLASSIFICATION OF THIS PAGE | 19. SECURITY CLASSIFICATION OF ABSTRACT | 20. LIMITATION OF ABSTRACT |
|---|---|---|---|
| UNCLASSIFIED | UNCLASSIFIED | UNCLASSIFIED | 200 Words |

# Massively Parallel Optical Image Compression Using Optical Rank Annihilation

M.L. Myrick

Department of Chemistry and Biochemistry
University of South Carolina
Columbia, SC 29208

Tel: (803) 777-6018
Fax: (803) 777-9521
Email: myrick@psc.sc.edu

# Section 3.3: Massively Parallel Optical Image Compression Using Optical Rank Annihilation

M.L. Myrick

## ABSTRACT

We have studied Lattice Boltzmann models for anisotropic diffusion of images, line processing systems, and Lattice Bolzmann simulation of flow by mean curvature. In addition we have modelled two distinct modes of operation for an optical data compression system using offset transmission masks. Development of corrected transmission masks is underway at present, with proof of principle of an optical data compression system scheduled for early summer, 1998 based on 2-dimensional Fourier series.

## FORWARD

This project was initially funded in June, 1997 at the level of $400,000 over three years.

## REPORT

### *Statement of the Problem Studied*

**Background**

As early as 1964, optical processing was proposed as a means of avoiding the costly/time-consuming task of computational transformations for real-time operations.[1] As a result of recent interest in optical transformations for the purpose of pattern recognition and image compression, a number of researchers have explored Fourier-optical approaches to achieving a usable transform. [2-9]

A host of problems plague Fourier-optical methods, not least of which are (a) complexity, (b) need for a laser, and (c) inflexibility. To date, no optical method for compressing images or interpreting them has found wide application, nor does it seem likely that any methods based on current optical technologies will find real application in the next decade. In addition, Fourier decomposition of an image is not by any means the most compact representation of image data that is possible. Wavelet-based decompositions allow for a large number of different decompositions, allowing mathematical functions to be represented in a compact manner which yields quality approximations using very few free parameters. For example, wavelets are well suited for image compression and surface modeling, and for solving certain partial differential equations.

The Discrete Wavelet Transform (DWT) allows us to implement many multi-resolution schemes very efficiently with an $O(N)$ transform. Still, there are many applications where this does not provide sufficient speed even when implemented on a state of the art computer. There are also

many operations based on standard wavelets that lead to time consuming operations. In addition, there are many wavelet type representations which cannot be implemented with an $O(N)$ transform and there is a need to find more efficient methods for implementing these representations. Optical DWTs could potentially meet this need.

Funding for basic imaging spectroscopy work in our laboratory by the ARO has resulted in significant advances over the past three years in the conceptual processes underlying the recording of optical data. The fundamental new concept we have developed is that of optical rank annihilation (ORA). A succinct statement of ORA might be: *the number of channels used to record light should be no larger than the underlying degrees of freedom in the source*. For example, if an image can be adequately compressed by a factor of 10 with a DWT after a CCD has recorded it, then one way of thinking about this is to consider 90% of the original recording process by the CCD to be redundant, requiring a computational step to repair. The Third Law of Thermodynamics can be applied directly to this conventional process: if work is required to compress the data after it was recorded, then the recording step was non-optimized, or irreversible in the thermodynamic sense.

The question remains how to achieve the recording of optimized data. Fortunately, work already performed has provided the answer. Most of the work performed at USC has been in the area of spectroscopic compression, rather than spatial compression, but the concepts are the same. Conventional spectrometers function by converting a spectroscopic degree of freedom in wavelength space into a spatial degree of freedom. Consequently, the following discussion deals with our development of ORA for the prediction of physical and chemical properties of materials using optical spectroscopy.

The paradigm of today for predictive spectroscopy, just as for data compression, is computational: a complete spectrum is acquired and a computer performs the calculations of equation 1. ORA provides a more efficient alternative.

Mathematically, equation one is a recipe for a series of simple multiplication and addition steps. Such simple multiplications (e.g., multiplying an intensity measurement by 0.5) can be performed by a simple optical filtering method, as shown in Figure 4, whereby an optical filter with a transmission of 0.5 performs the "calculation" prior to the data being recorded. The detector now records only half the original intensity of light, and its output, once digitized, reflects this value. Likewise, addition can be carried out all-optically: two beams of light both striking the same detector produce a detector output which sums the two individual beams (assuming incoherent light). ORA relies only on these simple forms of optical computing.

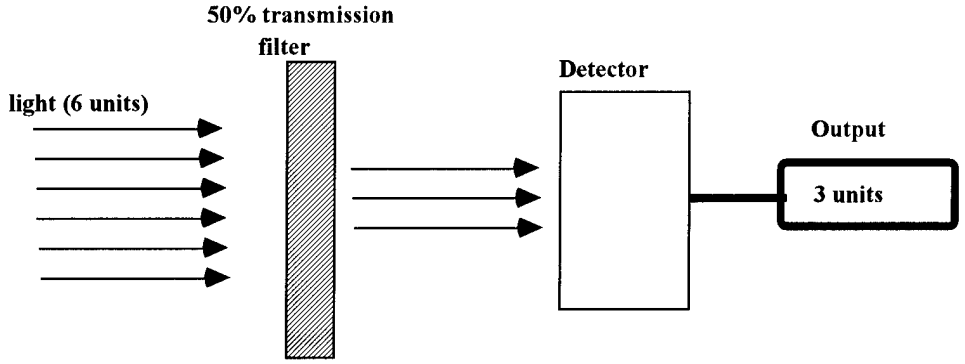


**Figure 4. 6 units of light passes through a 50%-transmitting partially-transparent filter.**

It is this reliance on simple forms of optical calculation that is the key to the successful implementation of ORA: no complex lasers or optics are necessary to produce a transformation. To achieve the full effect of equation 1 for the prediction of physical and chemical properties ORA, light passes through a partially-transparent filter whose transmission is dictated by the magnitude of the regression vector for each wavelength of light, designed by one of a number of methods (e.g., needle insertion method, modified inverse fourier transform method, etc.). The analog output of a single detector is then proportional to the magnitude of the predicted quantity, and can be digitized or passed directly to a readout.

In the example above, the important information contained in an optical signal could be derived from the direct product of a single vector (the regression vector) with the main signal. For image compression, the number of basis vectors is much larger. A separate mask is required for each basis function. There are a handful of ways that this can be done, including fiber optic networks and networks of holograms. However, each of these methods suffers from the disadvantage of requiring a large technological step beyond current technology to be implemented.

On the other hand, graduated (as opposed to binary) spatial filtering provides a facile method for each calculation. Figure 2 shows the experimental setup for a single calculation via spatial filtering to obtain the magnitude of a particular 2-D basis function in an image using a graded mask. As this figure illustrates, a single transformation is not difficult.

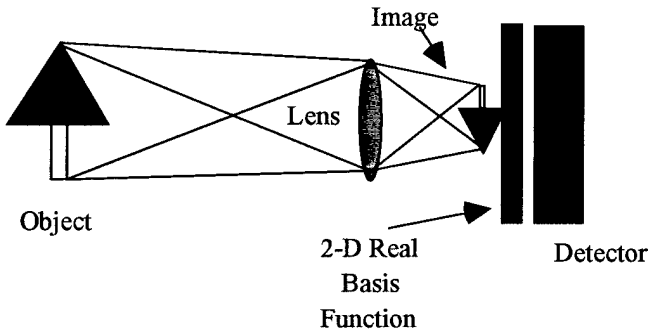


Figure 2 - Schematic of a simple tranformation. The 2-D Real Basis Function is a graduated mask with a density proportional to the magnitude of the basis function at each location (x,y) in the image.

The problem arises when many thousands of transforms are necessary, as in image compression.

Microlens arrays offer the most versatile apparatus for actually achieving data compression via ORA. A microlens array can be made by a simple process known as resist melting. In resist melting, lithography is used to expose a resist in a particular

pattern, the exposed portions of which are then chemically removed. The remaining dots of resist are heating to melting, and surface tension causes the dots to form lens-like shapes. Reports indicate that lens arrays with lenses ranging from 5 μm diameter to 5 mm diameter can be prepared, containing many thousands of lenses. The performance of these lenses is nearly diffraction limited, i.e., as good as a lens can be. Combining microlens arrays with photographically produced graded masks, and depositing the sandwich of these arrays and masks onto a CCD array can permit thousands of calculations simultaneously.

***Summary of Most Important Results***

This project consists of the following tasks: a) Derive equations for Fourier transformation using optical transmission masks in theory, b) Demonstrate single-frequency Fourier transformations using transmission masks, c) develop skills at manufacturing microlens arrays, d) demonstrate multi-frequency (parallel) Fourier transformations in off-line mode, e) Study more compact real wavelet representations for image transformations, f) demonstrate wavelet transformations for images, and g) make a highly-multiplexed (massively parallel) compression system.

The first goal has been met. In two dimensions,

$$F(\omega_x, \omega_y) = \iint f(x,y)\, e^{i(\omega_x x + \omega_y y)}\, dx\, dy,$$

where $F(\omega_x, \omega_y)$ is the two-dimensional Fourier transform into spatial frequency of f(x,y), a spatial function. Using Euler's relationship, this can be expressed as:

$$F(\omega_x, \omega_y) = \iint f(x,y)\, [\cos(\omega_x x + \omega_y y) + i \sin(\omega_x x + \omega_y y)]\, dx\, dy.$$

This relationship, in turn, can be decomposed into the following form:

$$F(\omega_x, \omega_y) = \iint f(x,y) \cos(\omega_x x + \omega_y y)\, dxdy + i \iint f(x,y) \sin(\omega_x x + \omega_y y)\, dxdy$$

In this form, the Fourier transformation is well-suited to parallel optical processing, since the integrations have been expressed in real forms, i.e., the calculations make use of real sine and cosine functions. Even though the function F is complex, the real and imaginary components have been separated out and the coefficients dealt with in a purely real sense.

The functions described in this equation are illustrated in Figure 1 below, in which a sine function with a spatial frequency of $\omega_x = 1$, $\omega_y = 2$ is shown.

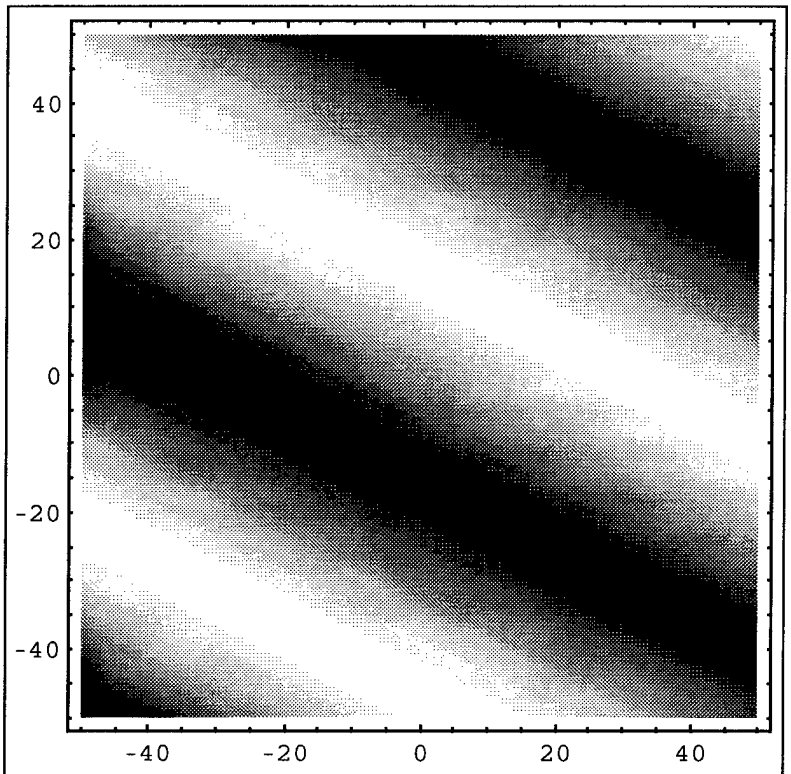


Figure 1 - 2-D sine function with $\omega_x = 1$, $\omega_y = 2$.

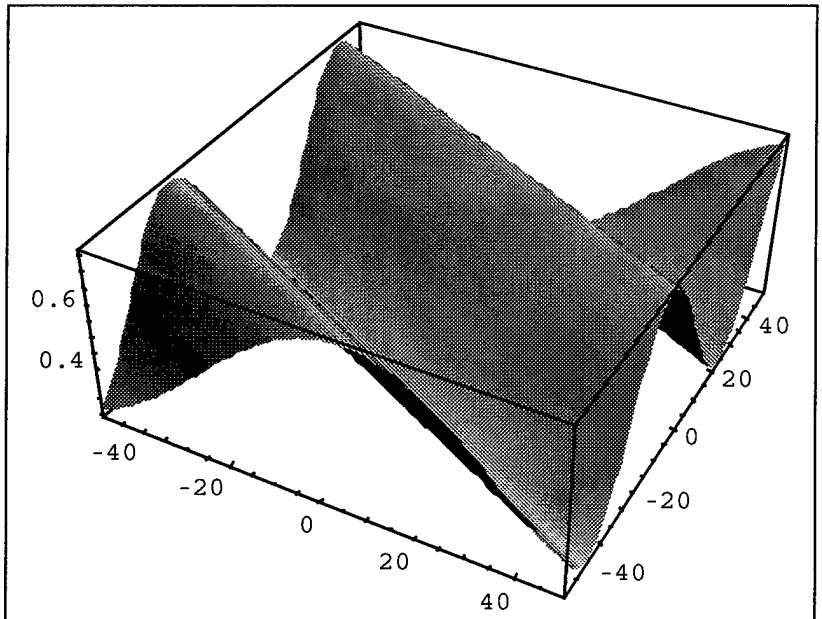


Figure 2 -Offset and scaled transmission for a sine function (transmission between 0 and 1, rather than between -2 and +2).

For comparison, a cosine function with the same spatial frequency would have its repeating wave pattern offset so that its extrema would occur at the points of zero-crossing for the form in Figure 1. In the optical computation, this form would be generated as a density (transmission) mask in the image plane above a detector element. The light detected by the detector element would then sum (integrate) the point-by-point product of the image function (f(x,y)) and the transmission mask (the Fourier basis function).

The form in Figure 1 has both positive and negative components while no transmission mask can have a negative transmission, and this can be treated in one of two different ways. In the first approach, the entire sine or cosine structure is offset to become positive. A second measurement using a uniform gray scale transmission mask (DC Fourier component) can then be subtracted from the signal obtained through the cosine/sine transmission mask. This has the effect of subtracting the DC offset from the sine or cosine measurement, giving the effect of a transmission mask with both positive and negative transmissions. Figure 2 shows a perspective plot of the offset sine function. If the average value of this function is subtracted from it, the result is an actual 2-dimensional sine function.

The second way of dealing with the non-negativity constraint for real masks is to bisect the sine or cosine function at the zero-crossings, inverting the negative and making two positive masks. Again, the difference of the two gives the effect of performing the integral of an image with a cosine or sine function.

To test these ideas, we constructed a model image composed of 8 pure frequencies scaled with intensities 0.5-4 in half-integral steps which was then offset to be purely positive; we then generated the mathematical Fourier transform of the image in Matlab. This was compared to the result of a model conversion using each of the two methods described above. The result of the mathematical transform was a DC magnitude of 36 units (arbitrary scaling), with 0.5-4 units of amplitude on each of the composing frequencies in half-integral steps. The result for the offset-to-positive/subtract average method was 36 for the DC frequency, but 36.5 to 40 for the amplitudes of the main frequencies without subtracting the DC component. Although this model gives the correct answer for each frequency, we can quickly see that a signal-to-noise limitation may be reached quickly because the DC component in a FT is frequency so much larger than that of any single harmonic. The split-at-zero-crossing method gave exactly the correct answers, without having the large DC offsets that needed subtracting. The only disadvantage of this second method is that twice as many masks are needed.

The second task is nearly complete. A post-doc (Dr. Pramod Khulbe) was hired in the fall of 1997 primarily for this project, but he left in early 1998 after accepting a position elsewhere. Dr. Xuexin Fang was hired in the mid-spring of 1998 to replace Dr. Khulbe, but he has applied for a change in Visa status which has invalidated his J-1 Visa, terminating his employment in April, 1998. Even though neither of these post-doctoral associates was present long enough to gain good understanding of the project, some progress was made. We set up a test system with single lens and masks, and made several masks to test their linearity. It is, of course, vitally important that the masks be made properly, and since our masks are being constructed photographically it was necessary to determine how to make masks that closely approximated the desired transmission qualities. Our first attempt was with color slide films as the basis of the masks. This lead to two main problems. The first is that the color slide films use dyes that do not have the same absorbance at each wavelength. Consequently we could expect a limited range of densities available to us. The second problem with color slide films is that their linearity is poor. We determined these quantities experimentally by recording visible and near-infrared absorbance measurements on uniformly-exposed film samples made by film-printing from Matlab. Using black-and-white negative films gave significantly better results because the film spectroscopy was uniform over a much wider spectral window. The range of densities available in this medium is also considerably greater, with optical densities of 3 or so possible. Using B&W film, we produced a series of uniformly-exposed "slides", and measured their transmission spectra. After this, a correlation between the Matlab gray scale value and optical transmittance of the film was made. The result was relatively non-linear (as expected). However, this leads us directly to a relationship between gray level and transmission that is necessary for making correct masks.

At this point we are without a post-doc for the experimental measurements, having gone through two already. However, we have hopes of adding another post-doc during the middle summer of

1998 to continue the experimental work. The experimental program will then procede to refining the correlation between gray-scale and transmission, film-printing corrected masks, and testing the system.

Tasks c and d are yet to be begun. However, task e has been the subject of extensive effort. The Jawerth group has been investigating a variety of mathematical transformas and models for image compression. Among these is an investigation of Lattice Boltzmann models for anisotropic diffusion of images (with Bjorn Jawerth and Eric Sinzinger). In recent years, the Lattice Boltzmann method has attracted more and more attention as an alternative numerical scheme to traditional numerical methods for solving partial differential equations and modeling physical systems. The idea of the Lattice Boltzmann method is to construct a simplified discrete microscopic dynamics to simulate the macroscopic model described by the partial differential equations. The use of the Lattice Boltzmann method has allowed the study of a broad class of systems that would have been difficult by other means. The advantage of the Lattice Boltzmann method is that it provides easily implemented fully parallel algorithms and the capability of handling complicated boundaries. Aniotropic diffusion has been extensively used as an efficient nonlinear filtering technique in image processing. In this project, we developed a Lattice Boltzmann model for nonlinear aniotropic diffusion of images. We showed that image feature selective diffusion can be achieved by making the relaxation parameter in the Lattice Boltzmann equation be image feature dependent. The numerical algorithms are efficient and easy to implement. We used our method to "clean" infrared airborne radar images. The results are promising. We also used our method to smooth sonar images for further processing.

A second area being investigated by the Jawerth group is an efficient line processing system. Optimization of energy-functionals provides a clear cut and very attractive framework for image segmentation. Based on the Mumford and Shah model for image segmentation, Shah proposed a set of minimizing functionals which incorporate an auxiliary function to determine edges. By minimizing the functionals, Shah's line processing model can be rewritten as coupled reaction-diffusion equations. The principal advantage of this system, which makes it especially attractive, is that the evolution equations are proceed to their stationary limit without the need for a difficult and time-consuming global search to stop the system. In this project we try to use the Lattice Boltzmann model to simulate the improved Shah's line processing model based on the Lattice Boltzmann computation of the reaction-diffusion systems. Since the Lattice Boltzmann model is fully parallelizable, we expect a very fast line processing system. We have worked out an algorithm, which still need to be refined. Eventually we will implement this system on SHARK.

Parallel to this work, a study of Lattice Boltzmann Simulation of Flow by Mean Curvature has been done. Geometric flow of fronts plays a significant role in various applications, such as fluid mechanics of multiphase flows, crystal growth, chemical kinetics, flame propagation, image processing, and surface modeling. The contemporary computer technology gives priorities to highly parallelizable numerical methods. Parallel computer hardware scientists see the Lattice Boltzmann Method as the simplest and fastest totally parallel algorithm with broad applications. In this project we try to use a Lattice Boltzmann Model to simulate the mean curvature flow. We have been trying to use a simple geometric feature dependent relaxation parameter in the Lattice

Boltzmann equation to recover the mean curvature evolution equation. We probably need use a linear collision operator instead of the single-time-relaxation approximation.

***Publications and Technical Reports***

There have been no reports of this work yet.

***Personnel***

In addition to the investigators, the following personnel have worked on this subproject.
Dr. Pramod Khulbe, post-doctoral associate with Dr. Myrick
Dr. Xuexin Fang, post-doctoral associate with Dr. Myrick
Dr. Peng Lin, post-doctoral associate with Dr. Jawerth

## BIBLIOGRAPHY

1. A. Vander Lugt "Signal Detection by Complex Spatial Filtering", *IEEE Trans. Informat. Theory* **10**(1964), 139-45.
2. F.T.S. Yu and Guowen Lu "Short-time Fourier transform and wavelet transform with Fourier-domain processing" *Appl. Opt.* **33**(1994), 5262-9.
3. H. John Caulfield and H.H. Szu "Parallel Discrete and Continuous Wavelet Transforms" *Opt. Eng.* **31**(1992), 1835-9.
4. H.H. Szu, B. Telfer and A. Lohmann "Causal Analytical Wavelet Transform" *Opt. Eng.* **31**(1992), 1825-9.
5. T.J. Burns, K.H. Fielding, S.K. Rogers, S.D. Pinski and D.W. Ruck "Optical Haar Wavelet Transform" *Opt. Eng.* **31**(1992), 1852-9.
6. Y. Sheng, D. Roberge and H.H. Szu "Optical Wavelet Transform" *Opt. Eng.* **31**(1992), 1840-5.
7. H. Szu, Y. Sheng and J. Chen "Wavelet Transform as a Bank of the Matched Filters" *Appl. Opt.* 31(1992), 3267-77.
8. Y. Sheng, T. Lu, D. Roberge and H.J. Caulfield, "Optical $N^4$ implementation of a two-dimensional wavelet transform", *Opt. Eng.* **31**(1992), 1859-1864.
9. B. Jawerth, Y. Liu, and W. Sweldens, "Signal Compression with Smooth Local Trigonometric Bases", *Opt. Eng.* **33**(1994), 2125-35.

# REPORT DOCUMENTATION PAGE

Form Approved
OMB No. 0704-0188



| 1. AGENCY USE ONLY *(Leave blank)* | 2. REPORT DATE | 3. REPORT TYPE AND DATES COVERED |
|---|---|---|
| | June 1, 1998 | Annual |

4. TITLE AND SUBTITLE

Massively Parallel Optical Image Compression Using Optical Rank Annihilation

5. FUNDING NUMBERS

Grant Number N00014-97-1-0806
PR Number 97PR06312-00
PO Code 353
Disbursing Code N68892
AGO Code N66020
Cage Code 4B489

6. AUTHOR(S)

M.L. Myrick

7. PERFORMING ORGANIZATION NAME(S) AND ADDRESS(ES)

University of South Carolina

8. PERFORMING ORGANIZATION REPORT NUMBER

N00014-97-0806-1

9. SPONSORING / MONITORING AGENCY NAME(S) AND ADDRESS(ES)

ONR

10. SPONSORING / MONITORING AGENCY REPORT NUMBER

ONR

11. SUPPLEMENTARY NOTES

Prepared in coordination with University Research Initative Program for Combat Readiness

12a. DISTRIBUTION / AVAILABILITY STATEMENT

APPROVED FOR PUBLIC RELEASE

12b. DISTRIBUTION CODE

13. ABSTRACT *(Maximum 200 words)*

We have studied Lattice Boltzmann models for anisotropic diffusion of images, line processing systems, and Lattice Bolzmann simulation of flow by mean curvature. In addition we have modelled two distinct modes of operation for an optical data compression system using offset transmission masks. Development of corrected transmission masks is underway at present, with proof of principle of an optical data compression system scheduled for early summer, 1998 based on 2-dimensional Fourier series.

| 14. SUBJECT TERMS | 15. NUMBER OF PAGES |
|---|---|
| Chemical and Biological Warfare, Target Acquisition, Snti-Submarine, Combat Medicine, Biodeterioration, Command Control and Communication | 13 |
| | 16. PRICE CODE |

| 17. SECURITY CLASSIFICATION OF REPORT | 18. SECURITY CLASSIFICATION OF THIS PAGE | 19. SECURITY CLASSIFICATION OF ABSTRACT | 20. LIMITATION OF ABSTRACT |
|---|---|---|---|
| UNCLASSIFIED | UNCLASSIFIED | UNCLASSIFIED | 200 WDS |

# Molecular Scale Electronic Arrays for the Design of Ultra-Dense and Ultra-Fast Computational Systems

**James M. Tour, PI**

Department of Chemistry and Biochemistry
University of South Carolina
Columbia, SC 29208

Tel: 803-777-9517
Fax: 803-777-9521
E-mail: tour@psc.sc.edu

# Section 3-4: Molecular Scale Electronic Arrays for the Design of Ultra-Dense and Ultra-Fast Computational Systems

James M. Tour

## ABSTRACT

In order to maintain technological superiority in command, control, and communications, new ultradense and ultrafast computation must continue to be developed. Conventional pattering techniques will not be suitable below the theoretical limit of 0.08 μm resolution, a mere three-fold decrease in present commercial technology. We are therefore compelled to push the limits of densely-packed computational systems by striving for molecular-sized architectures. The study here descibes (1) methods to model the electronic transport interactions in single molecules using density functional theory and quantum mechanics to provide a predictive tool for guiding the chemical syntheses of molecular wires and devices. This is the first computational approach of its kind to outline specific target molecules. And (2), outlined is a method to write arrays of single molecules on a surface and to address each one of those molecules. This will permit the addressing of molecular scale systems in the 10-50 Å regime. These studies will help to insure that the US maintains a technological edge in the race toward the ultimate in rapid computational systems for superiority of command and control issues. Excellent progress has already been acheived toward both of these proposed goals.

## FORWARD

Total award amount = $293,000 for three years. No approach changes have been made from the original proposal. Two main acheivments have been realized in the past year:

- Method of computational analysis for molecular logic gates, alligator clips, and controllers.
- Writing of molecular patterns with an STM tip in a self-assembled monolayer.

## REPORT

### *Statement of the problem*

The molecular CPU would be formed by small molecular units making the CPU itself a supramolecular unit. These units, which can be studied and designed exactly, will require parallel developments in synthetic efforts. New areas of technology would have to be created and developed like molecular control theory, molecular circuit theory, and molecular digital theory based on present ab initio theories of quantum chemistry. Given the tremendous computational power that can be obtained with molecular CPUs, a super high-level programming can be developed.

A molecular CPU would have to operate by electrostatic interactions rather than using electron currents as in present systems. Electron currents at the molecular level would produce energies

per unit of area that are impossible to be dissipated. On the other hand, the use of the electrostatic potentials around the atoms of the molecules is a perfect choice because it can be controllable (as the current in a transistor) just by the rearrangement of a small amount of the charge density equivalent to a charge several orders of magnitude smaller than the charge of one electron, and also because these small changes in electrostatic potential are easily detected by the neighboring molecules.

Molecular-based systems can offer distinct advantages in uniformity and potential fabrication costs. If devices were to be based upon single molecules, using routine chemical syntheses, one could prepare $6 \times 10^{23}$ (Avogadro's number) devices in a single reaction flask, hence, more devices than are presently in use by all the computational systems combined, world-wide [1,2]. However, the real problem facing synthetic chemists is how to arrange such a vast amount of molecular units. This process must be guided by precise laws of nature using quantum mechanics. Additionally, the properties of quantum systems can be used in a favorable manner at the molecular level. Thus molecular-based systems can offer distinct advantages in the density of structures that can be prepared and in their stability. Hence, molecular scale electronics would likely shift the software/hardware equilibrium in the direction of hardware, namely massively wired logic or CPU dominant. Molecular circuits offer the possibility of constructing large and fast CPUs with complicated functions. Using large molecular arrays, problems could be calculated within the CPU with minimal need for main or auxiliary memories. Wired-logic would supplant programmed-logic computing, thereby affording several additional orders of magnitude increase in performance [3-15].

### *Summary of the most important Results*

### Molecular Devices

Several molecular devices has been synthesize and theoretically tested to perform as digital logical gates, these gates are the basic units of a molecular central-processor-unit (CPU). Fig 1A shows a molecule working as a digital transistor and Fig. 2B shows a molecule working as a logical OR.

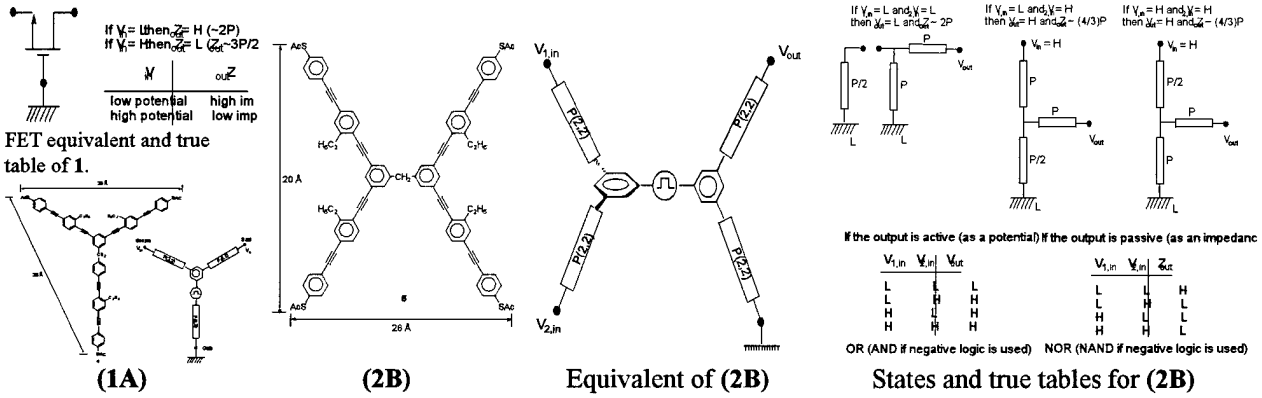


**Fig. 1.** Compounds (**A**) and (**B**) could be viewed as a molecular logic devices. The output is the electrostatic potential and the levels of the electrostatic potential represent the binary information. Corresponding true tables are given.

## MEP

The use of molecular electrostatic potentials (MEP) have been introduced as a possible and powerful alternative for molecular computation. Several candidate molecules have been successfully tested with MEPs to be suitable logical gates.

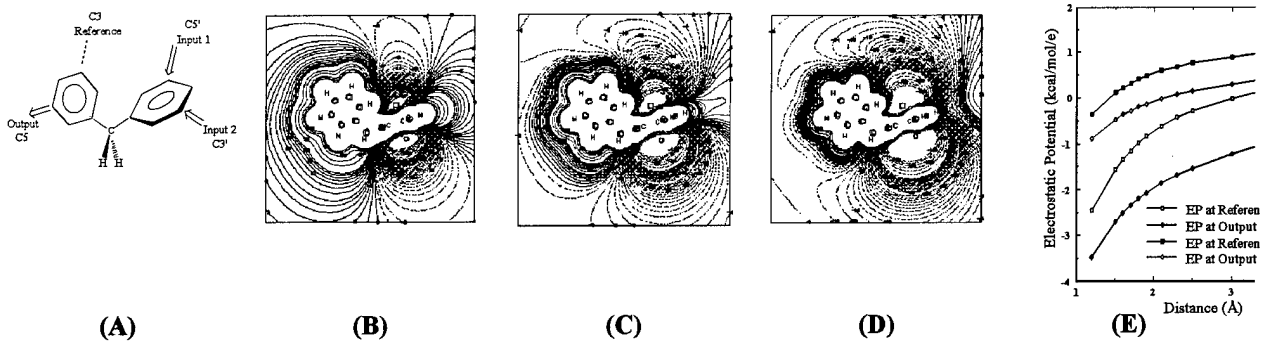


(A) (B) (C) (D) (E)

**Fig. 2.** (**A**) Diphenylmethane served as the model system for the *ab initio* calculations of logic device-like properties on (**B-D**) indicate the changes of electrostatic potential for an input signal. (**E**) shows results for all cases.

## Nanopore

Combined approaches, classical mechanics and quantum mechanics, have been use to explain successfully the behavior of molecules under electrical currents and several conditions of pressure and temperature.

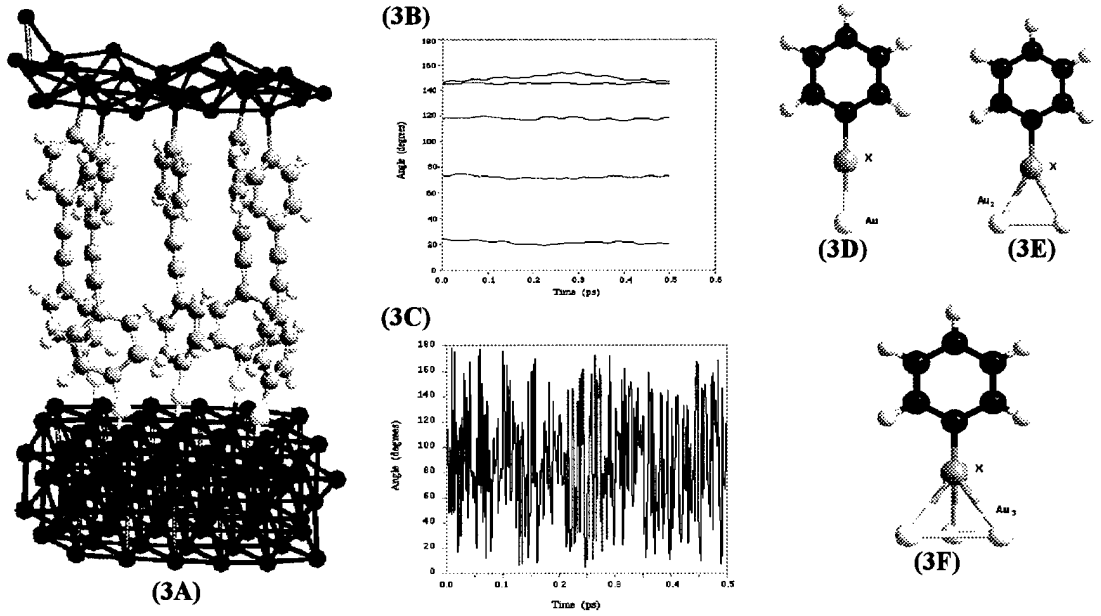


**Fig 3.** (**A**) The Thiotolane Sandwich (**B**) Variations of the angles between the two phenyl planes of each tolane molecule at 10 K. (**C**) Variations of the angle between the two phenyl planes for one of the tolane molecules at 30 K. Calculations on (**D-F**) systems imply that in order to have a decrease in the conductivity when using selenium instead of sulfur, the connection to the alligator clip has to be done to two or three gold atoms.

**Break Junction**

Chemically precise first principles ab initio methods, including density functional theory (DFT) have been introduced for the study of conductivity in single molecules.

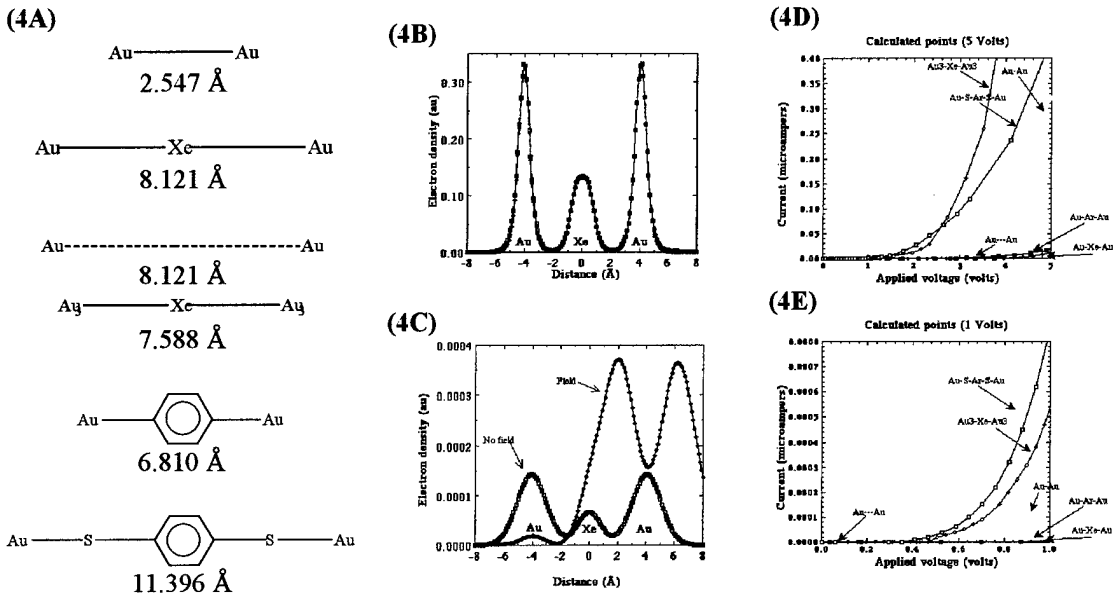


**Fig. 4.** (**A**) Few of the systems that have been studied. The electron densities along axes parallel to the Au-Xe-Au axis showing the effect of the external applied field when one electron is transferred from the Au atom on the right side of the junction to the Au on the left side. (**B**)at 0.8 Å, (**C**) at 3 Å from the Au-Xe-Au axis. Molecular I(V) characteristics for the systems Au-Au, Au-Xe-Au, $Au_3$-Xe-$Au_3$, Au-($p$-$C_6H_4$)-Au, and Au-S-($p$-$C_6H_4$)-S-Au. (**D**) 0-5 volts, and (**E**) 0-1 volt.

Specifically, we have used DFT techniques since these are the most powerful tools to deal with a relatively large number of atoms [16]. The use of DFT is fully justified due to the fact that it is an *ab initio* technique able to deal with a broad variety of systems. Several successful applications of DFT have been reported using the hybrid functionals where a portion of the exchange functional is calculated as a fully nonlocal functional of the wave function of an auxiliary noninteracting system of electrons. Since this resembles the exchange in the HF procedure (actually in any wave-function procedure), it is common to refer to this functional, or procedure, as a DFT-HF hybrid. However, we have to consider that the exchange is being calculated using a noninteractive wave function whose density, but not its wave function, corresponds to the real system. A detailed analysis and its theoretical rigor was recently reviewed [17]. The functional that we used is the B3PW91 with the triple split-valence basis set 6-311G** which includes polarization functions for all atoms [18-20].

We have presented several convergent synthetic routes to conjugated molecules with various potential digital device applications [21] including a 2-terminal molecular wire with a tunnel barrier, a molecular wire with a quantum well to serve as a resonant-tunneling diode (RTD), three terminal systems with switch-like possibilities, and four terminal systems that could serve as logical gates without the use of multiple transistor arrays. In each case, the conducting segments are based on p-conjugated oligo(phenylene ethynylene)s [22]. The transport barriers

are based on methylene ($CH_2$) units since SPM studies showed us that alkyl units pose larger electronic transport barriers (higher resistance) than the p-conjugated moieties in single molecular systems [23]. The ethyl groups impart solubility to the larger molecules so that synthetic manipulations and depositions can be freely executed in solution [22]. All of the final compounds described have termini bearing self-assembling moieties, namely protected thiols to serve as protected "alligator clips" [24]. The precise termini needed for the ultimate arrangement in a molecular-based CPU is, of course, not known, however, the capability of modern synthetic methods to construct precise molecular frameworks was exemplified.

Preliminary studies have permitted us to analyze, using DFT, the effects on real experimental situations performed at our own and other's laboratories. For instance, the modeling of gold [25] or palladium tips [26] to be used as contacts for molecular devices, the study of the effects on conductivity of single molecules [27] and the rationale for molecular scales systems [21] have all been investigated as well a related studies for the determination of optical bandgaps [28]. These works are the first of their kind. Several ab initio methods including density functional theory [16] and combined DFT/MD [29] will be used to determined the viability of several target molecules to be used as logical devices. In addition, these studies will aid in directing us to more viable target molecules for synthesis. This studies are the initial step toward the design of a molecular-CPU.

The second phase of this work dealt with writing of patterns of molecular systems in SAMs using a STM. With the current interest in molecular electronics, there is a need for a method of nanolithography for the precise positioning of components like molecular wires, into functional devices. Early work by Myrick's group [30] at the University of South Carolina showed the selective insertion of molecules into a self-assembled monolayer (SAM) of an alkanethiol on gold. It is hoped that the a method of nanolithography can be developed for the insertion of single wires into a SAM, giving smaller circuit sizes than are currently realized.

Gold on glass samples were annealed at high temperatures before exposure to 1 μM solutions of dodecanethiol for the formation of SAMs. After exposure to the alkanethiol solutions, the glass samples were rinsed with ethanol and dried under a stream of nitrogen. They were mounted onto aluminum stubs using a conductive silver paint, and immediately used in the Park Scientific Instruments STM.

A variety of imaging conditions were investigated in order to find a set applicable to both imaging under air and under dioxane solutions. Two sets of conditions (Table 1) were found that gave reproducible images of SAMs on gold, comparable to those images reported by other groups [31]. High resolution images were possible that showed the holes in the SAMs, the natural steps of the gold surface, and the relatively large flat areas of the annealed gold Au(111) surface. Simple imaging of SAMs on gold could use either of the two sets of optimal conditions, whereas lithographic pulsing experiments gave more reproducible results using the second set of conditions.

| Variable | Functional Range | Optimal Conditions | |
|---|---|---|---|
| | | *Normal Imaging* | *Lithography* |
| Tip Bias Current | 300 mV to 1000 mV | 1000 mV | 300 mV |
| Tip Current | 20 pA to 150 pA | 20 pA | 100 pA |
| Scan Rate | 4.07 Hz | 4.07 Hz | 4.07 Hz |
| Pulsing Voltage | - 4 V to + 5.4 V | N/A | + 2.5 V |
| Pulse Duration | 5 ms to 1000 ms | N/A | 500 ms |

**Table 1.** Optimal imaging conditions for the Park Scientific Instruments STM found in Professor Mark Reed's lab during a visit to Yale University. Two sets of conditions were found to give optimal images. Simple imaging of the SAMs on gold could use either set. Lithographic attempts were more reproducible using the second set.

Sequential deposition of the gold on glass in dodecanethiol and the monofunctionalized molecular wire (Figure 1), **1**, produced images complementary to those produced by Tour and co-workers [32]. Along natural boundaries and defects within the SAM, bright spots appeared where molecular wires had inserted into the SAM. It is unclear if these are single molecule insertions or multiple molecule insertions. Performing these sequential insertions when the molecular wires were dissolved in dioxane appeared to give the same images as those deposition done in THF [32].

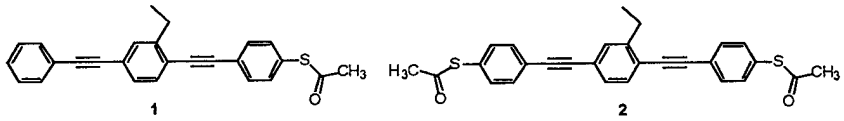


**Figure 1.** The monofunctionalized molecular wire **1** and difunctionalized molecular wire **2** [33].

Determination of the optimal conditions for imaging under dioxane was readily achieved. The addition of ammonium hydroxide and molecular wire **1** or **2** did not appear to change those conditions or the images obtained. It was noticed that after prolonged imaging times under dioxane, a precipitate would appear on the surface. The nature of this precipitate is unknown, though two possibilities have been proposed. It is possible that the epoxy coating on the STM Pt/Ir tip dissolves slowly over time in the dioxane, and is deposited on the surface. The second possibility is that the thiols form disulfides in dioxane, which precipitate out after ligomerization.

Conditions were examined to determine the best pulsing voltage and duration to selectively give pit formation. Pulsing voltages were examined ranging from -4 V to +5.4 V with respect to the sample. Reproducible pits were formed at +2.5 V. The duration of the pulse was varied from 5 ms to 1000 ms, with the most reproducible results coming around 500 ms. The pit size was dependent on how many times the surface was pulsed consecutively. The first pulse would give a pit between 50 and 100 Å wide and 20 Å deep. A second pulse would generate a pit 20 to 30 Å wide and 7 to 10 Å deep. Subsequent pulses generated no surface modification.

Insertion of the monofunctionalized molecular wire **1** and the difunctionalized molecular wire **2** were attempted. Imaging of the samples and pulsing experiments were performed under dioxane solutions containing the respective molecular wire in concentrations ranging from 1 pM to 1 μM.

Inserted wire **1** (Figure 2) can be seen readily after two consecutive pulses of +2.5 V for 500 ms to an area of the sample already containing a large pit as a reference feature. The first pulse gave a pit on the surface, and the second pulse generated an inserted molecular wire as is seen by the bright spot on the figure. Insertion of molecular wire **2** was not as conclusive (Figure 3). A white mound was seen in the second image, but its intensity is considerably less than that seen in Figure 2. Two explanations are possible to explain the difference in intensity. Multiple wires could have been inserted in the case of **1** whereas only one or two molecules were inserted in the case of **2**. A second possibility is that the wire is merely physisorbed to the surface of the SAM in the case of **2** and therefore not conductive enough to give the intensity seen with **1**.

While insertions of molecular wires into SAMs of alkanethiols on gold has been demonstrated, it is inconclusive whether these insertions were induced by the pulsing experiment or by a natural insertion into the holes inherent to the SAMs. While certain times, as with Figure 2, the wire is certainly inserted into a hole generated by the pulsing experiment, other times the white spots could be seen migrating across the surface over time.

Many questions remain unanswered and much work remains to be done in order to make nanolithography of single molecules feasible. Solvents other than dioxane may lead to a higher success of insertion during pulsing experiments and to less precipitate on the sample surface. The problem of being unable to obtain pits from more than two consecutive pulses must be addressed. Determination of whether single or multiple molecular wires have been inserted by a single pulse will be critical in evaluating the capacity of these molecules to function in defined circuits. The groundwork has been laid out but further research is necessary for this technique to see practical application.

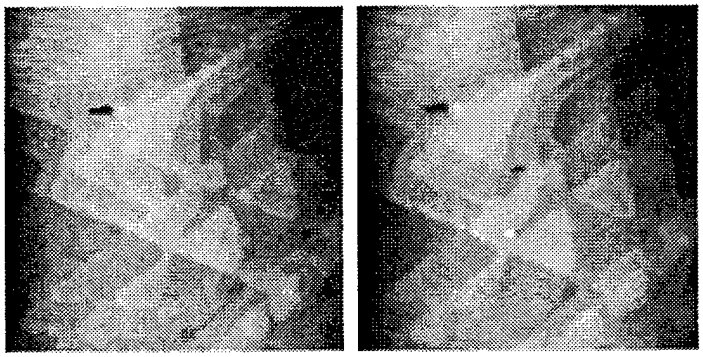

**Figure 2.** After pulsing with a +2.5 V pulse for 500 ms, a second put is formed on the SAM covered Au(111) surface. A second pulse led to insertion of **1**. These images (R97061780 and R97061781) have overall heights of 20 Å and dimensions of 250 × 250 nm (300 mV, 100 pA).

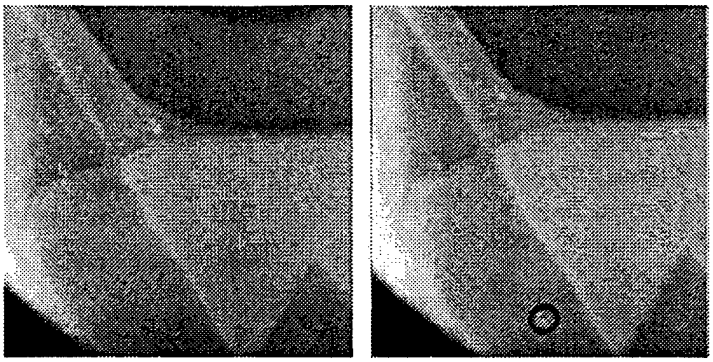

**Figure 3.** After pulsing for 500 ms with a +2.5 V pulse, a bright spot is seen to the left of the image, indicating the insertion of **2**. These images (R970617105 and R970617106) have overall heights of 20Å and dimensions of 250 250 nm (300 mV, 100 pA).

### *Publications and Technical Reports*

- J. M. Seminario and J. M. Tour, "Systematic Study of the Lowest Energy States of $Au_n$ (n=1-4) Using DFT", *Int. J. Quantum Chem.* **1997**, *65*, 749.
- J. M. Seminario, *A Combined DFT/MD Procedure for the Study and Design of Materials* in *Computational Chemistry and Chemical Engineering*, edited by G. Cisneros, J. A. Cogordan, M. Castro and C. Wang (World Scientific, Singapore, 1997), p. 255-267.
- J. M. Seminario, A. G. Zacarias, and J. M. Tour, "Theoretical Interpretation of Conductivity Measurements of a Thiotolane Sandwich. A Molecular Scale Electronic Controller," *J. Am. Chem. Soc.*, **1998**, in press.
- J. M. Seminario and J. M. Tour, *Ab Initio Methods for the Study of Molecular Systems for Nanometer Technology* in *Molecular Electronics-Science and Technology*, edited by A. Aviran and M. Ratner (New York Academy of Science, New York, 1998), submitted.
- J. M. Tour, M. Kozaki, and J. M. Seminario, "Molecular Scale Electronics: Approaches to Nanoscale Digital Computing," *J. Am. Chem. Soc.*, submitted.
- J. M. Seminario, A. G. Zacarias, and J. M. Tour, "Calculating Current(Voltage) Characteristics in Molecular Junctions," *J. Am. Chem. Soc.*, submitted.

### *Participating Scientific Personnel*

List of all participating scientific personnel showing advanced degrees earned by them while employed: James M. Tour, Lipscomb Professor of Chemistry; Jorge M. Seminario, Research Associate Professor; Angelica Garcia-Zacarias, Postdoctoral Research Associate; Charlotte Lee Asplund, Master's of Science; Alan Cassell, Ph.D.

## BIBLIOGRAPHY

[1] M. S. Montemerlo, J. C. Love, G. J.Opiteck, D. Goldhaber-Gordon, and J. C.Ellenbogen, in *Technologies and Designs for Electronic Nanocomputers* (MITRE, McLean., Virginia, 1996).

[2] J. M. Tour, *Conjugated Macromolecules of Precise length and Constitution: Organic Synthesis for the Construction of Nanoarchitectures*, Chem. Rev. 96, 537-553 **1996**.

[3] M. Bockrath, D. H. Cobden, P. L. McEuen, N. G. Chopra, A. Zettl, A. Thess, and R. Emalley, *Single-Electron Transport in Ropes of Carbon Nanotubes*, Science 275, 1922-1925 **1977**.

[4] A. Credi, V. Balzani, S. J. Langford, and J. F. Stoddart, *Logic Operations at the Molecular Level. An XOR Gate Based on a Molecular Machine*, J. Am. Chem. Soc 119, 2679-2681 **1997**.

[5] M. Dorogi, J. Gomez, R. Osifchin, R. P. Andres, and R. Reifenberger, *Room-temperature Coulomb blockade from a Self-assembled Molecular Nanostructure*, Phys. Rev. B 52, 9071-9077 **1995**.

[6] R. P. Andres, T. Bein, M. Dorogi, S. Feng, J. I. Henderson, C. P. Kubiak, W. Mahoney, R. G. Osifchin, and R. Reifenberger, *"Coulomb Staircase" at Room Temperature in a Self-Assembled MolecularNanostructure*, Science 272, 1323-1325 **1996**.

[7] A. J. Aviram, *Molecules for Memory, Logic, and Amplification*, J. Am. Chem. Soc. 110, 5687-5692 **1988**.

[8] C. Joachim, J. K. Gimzewski, R. R. Schlittler, and C. Chavy, *Electronic Transparence of a Single $C_{60}$ Molecule*, Phys. Rev. Lett. 74, 2102-2105 **1995**.

[9] A. Yazdani, D. M. Eigler, and N. D. Lang, *Off-Resonance Conduction Through Atomic Wires*, Science 272, 1921-1924 **1996**.

[10] C. M. Fischer, M. Burghard, S. Roth, and K. v. Klitzing, *Microstructured Gold/Langmuir-Blodgett Film/Gold Tunneling Junctions*, Appl. Phys. Lett. 66, 3331-3333 **1995**.

[11] H. Grabert, *Single Charge Tunneling: A Brief Introduction*, Z. Phys. B 85, 319-325 **1991**.

[12] C. Joachim and J. K. Gimzewski, *Electromechanic amplifier single molecule*, Chem. Phys. Lett. 256, 353-357 **1997**.

[13] V. Mujica, M. Kemp, and M. A. Ratner, *Electron Conduction in Molecular Wires. II. Application to Scanning Tunneling Microscopy*, J. Chem. Phys. 101, 6856-6864 **1994**.

[14] S. J. Tans, M. H. Devoret, H. Dai, A. Thess, S. Richard E, L. J. Geerligs, and C. Dekker, *Individual Single-wall Carbon Nanotubes*, Nature 386, 474-477 **1997**.

[15] R. M. Metzger, B. Chen, U. Höpfner, M. V. Lakshmikantham, D. Vuillaume, T. Kawai, X. Wu, H. Tachibana, T. V. Hughes, H. Sakurai, J. W. Baldwin, C. Hosch, M. P. Cava, L. Brehmer, and G. J. Ashwell, *Unimolecular Electrical Rectification in Hexadecylquinolinium Tricyanoquinodimethanide*, J. Am. Chem. Soc. 119, 10455-10466 **1997**.

[16] J. M. Seminario, *Recent Developments and Applications of Modern Density Functional Theory* (Elsevier, Amsterdam, 1996).

[17] A. Görling and M. Levy, *Hybrid schemes combining the Hartree-Fock method and density-functional theory: Underlying formalism and properties of correlation functionals*, J. Chem. Phys. 106, 2675-2680 **1997**.

[18] A. D. Becke, *A new mixing of Hartree-Fock and local density-functional theories*, J. Chem. Phys. 98, 1372-1377 **1993**.

[19] J. P. Perdew, J. A. Chevary, S. H. Vosko, K. A. Jackson, M. R. Pederson, D. J. Singh, and C. Fiolhais, *Atoms, Molecules, Solids, and Surfaces: Applications of the Generalized Gradient Approximation for Exchange and Correlation*, Phys. Rev. B 46, 6671-6687 **1992**.

[20] J. P. Perdew and Y. Wang, *Accurate and Simple Analytic Representation of the Electron-Gas Correlation Energy*, Phys. Rev. B 45, 13244-13249 **1992**.

[21] J. M. Tour, M. Kosaki, and J. M. Seminario, *Molecular Scale Electronics: Approaches to Nanoscale Digital Computing*, , (to be submitted) **1998**.

[22] L. Jones II, S. Schumm, and J. M. Tour, *Rapid Solution and Solid Phase Syntheses of Oligo(1,4-phenylene-ethylene)s with Thioester Termini: Molecular Scale Wires with Alligator Clips Derivation of Iterative Reaction Efficiencies on a Polymer Support*, J. Org. Chem. 62, 1388-1410 **1997**.

[23] L. A. Bumm, J. J. Arnold, M. T. Cygan, T. D. Dunbar, T. P. Burgin, L. Jones, II, , D. L. Allara, J. M. Tour, and P. S. Weiss, *Are Single Molecular Wires Conducting?*, Science 271, 1705-1707 **1996**.

[24] J. M. Tour, L. Jones, II, D. L. Pearson, J. S. Lamba, T. Burgin, G. W Whitesides, D. L. Allara, A. N. Parikh, and S. Atre, *Self-Assembled Monolayers and Multilayers of Conjugated Thiols, a,w-Dithiols, and Thioacetyl-*

*Containing Adsorbates. Understanding Attachments Between Potential Molecular Wires and Gold Surfaces*, J. Am. Chem. Soc. 117, 9529-9534. **1995**.

[25] J. M. Seminario and J. M. Tour, *Systematic Study of the Lowest Energy States of $Au_n$ (n=1-4) Using DFT*, Int. J. Quantum Chem. 65, 749-758 **1997**.

[26] A. G. Zacarias, M. Castro, J. M.Seminario, and J. M. Tour,*Lowest Energy States of $Pd_4$ Using DFT:Nanotips for Single Molecule Electronics*, Int. J. Quantum Chem. , (to be submitted) **1998**.

[27] J. M. Seminario, A. G. Zacarias, and J. M. Tour,*Theoretical Interpretation of Conductivity Measurements of Thiotolane Sandwich. A Molecular Scale Electronic Controller*, J. Am. Chem. Soc. In press **1998**.

[28] D.-S. C. Kim, S. Huang, M. Huang, T. S. Barnard, R. D. Adams, J. MSeminario, and J. M. Tour,*Revised Structures of N-Substituted Dibrominated Pyrrole Derivatives and their Polymeric Products.Termaleimide Models with Low Optical Bandgaps*, J. Org. Chem. in press **1998**.

[29] J. M. Seminario, *A Combined DFT/MD Procedure for the Study and Design of Materials* in*Computational Chemistry and Chemical Engineering*, edited by G.Cisneros, J. A. Cogordan, M. Castro and C. Wang (World Scientific, Singapore, 1997), p. 255-267.

[30] Patten, P. G. *Scanning Tunneling Microscopy Innovations for Chemical Synthesis and Analysis on the Nanometer Scale*. Doctoral Dissertation: University of South Carolina, 1996.

[31] (a) Kim, Y.-T.; McCarley, R. L.; Bard, A. J*Langmuir* **1993**, *9(8)*, 1941. (b) Nuzzo, R. G. Allara, D. L.*J. Am. Chem. Soc.* **1983**, *105*, 4481. (c) Chang, S.-C.;Chao, I.; Tao, Y.-T.*J. Am. Chem. Soc.* **1994**, *116*, 6792. (d) Nuzzo, R. G.; Fusco, F. A.; Allara, D.*J. Am. Chem. Soc.* **1987**, *109*, 2358. (e) Nuzzo, R. G.; Dubois, L. H.; Allara, D.*J. Am. Chem. Soc.* **1990**, *112*, 558. (f) Schoeneberger, C.; Sondag-Huethorst, J. A. M; Jorritsma, J.; Fokkink, L. G. J. *Langmuir* **1994**, *10(3)*, 611. (g) Sondag-Huethorst, J. A. M.; Schoeneberger, C.; Fokkink, L. G. J. *J. Phys. Chem.* **1994**, *98*, 6826.

[32] Bumm, L. A.; Arnold, J. J.;Cygan, M. T.; Dunbar, T. D.; Burgin, T. P.; Jones II, L.;Allara, D.L.; Tour, J. M.; Weiss, P. S. *Science* **1996**, *271*, 1705.

[33] Molecular wires **1** and **2** were prepared by Adam Rawlett, in Dr. Tour's group.

# REPORT DOCUMENTATION PAGE

Form Approved
OMB No. 0704-0188



| 1. AGENCY USE ONLY *(Leave blank)* | 2. REPORT DATE | 3. REPORT TYPE AND DATES COVERED |
|---|---|---|
| | June 1, 1998 | "Annual" |

4. TITLE AND SUBTITLE

Molecular Scale Electronic Arrays for the Design of Ultra-Dense and Ultra-Fast Computational Systems

5. FUNDING NUMBERS

Grant Number N00014-97-1-0806
PR Number 97PR06312-00
PO Code 353
Disbursing Code N68892
AGO Code N66020
Cage Code 4B489

6. AUTHOR(S)

James M. Tour

7. PERFORMING ORGANIZATION NAME(S) AND ADDRESS(ES)

University of South Carolina

8. PERFORMING ORGANIZATION REPORT NUMBER

N00014-97-1-0806-1

9. SPONSORING / MONITORING AGENCY NAME(S) AND ADDRESS(ES)

ONR

10. SPONSORING / MONITORING AGENCY REPORT NUMBER

ONR

11. SUPPLEMENTARY NOTES

Prepared in coordination with University Research Initiative Program for Combat Readiness

12a. DISTRIBUTION / AVAILABILITY STATEMENT

APPROVED FOR PUBLIC RELEASE

12b. DISTRIBUTION CODE

13. ABSTRACT *(Maximum 200 words)*

In order to maintain technological superiority in command, control, and communications, new ultradense and ultrafast computation must continue to be developed. Conventional pattering techniques will not be suitable below the theoretical limit of 0.08 μm resolution, a mere three-fold decrease in present commercial technology. We are therefore compelled to push the limits of densely-packed computational systems by striving for molecular-sized architectures. The study here descibes (1) methods to model the electronic transport interactions in single molecules using density functional theory and quantum mechanics to provide a predictive tool for guiding the chemical syntheses of molecular wires and devices. This is the first computational approach of its kind to outline specific target molecules. And (2), outlined is a method to write arrays of single molecules on a surface and to address each one of those molecules. This will permit the addressing of molecular scale systems in the 10-50 Å regime. These studies will help to insure that the US maintains a technological edge in the race toward the ultimate in rapid computational systems for superiority of command and control issues. Excellent progress has already been acheived toward both of these proposed goals.

14. SUBJECT TERMS

Command Control and Communication, Molecular Scale Electronics

15. NUMBER OF PAGES

10

16. PRICE CODE

| 17. SECURITY CLASSIFICATION OF REPORT | 18. SECURITY CLASSIFICATION OF THIS PAGE | 19. SECURITY CLASSIFICATION OF ABSTRACT | 20. LIMITATION OF ABSTRACT |
|---|---|---|---|
| UNCLASSIFIED | UNCLASSIFIED | UNCLASSIFIED | 200 words |

# SECTION 4: COMBAT MEDICINE

# Laboratory for Genetic Diagnosis and Control of Mosquitoes

Richard G. Vogt

Dept. of Biological Sciences
University of South Carolina
Columbia, SC 29208

Tel: 803-777-8101
Fax: 803-777-4002
Email: vogt@biol.sc.edu

# Section 4-1: Laboratory for Genetic Diagnosis and Control of Mosquitoes

R. Vogt

## ABSTRACT

Mosquitoes are annoying and potentially dangerous pests for US military personnel. Mosquito bites can be irritating, become infected, or be the source of debilitating diseases including malaria, yellow fever, dengue fever, and encephalitis. Although most of these pathogens can be controlled with medication and/or vaccination, the cost, side-effects, and development of insecticide-resistant strains diminishes the long-term viability of these treatments. Current chemical control methods of mosquitoes are of questionable compatibility with human health. A biorational integrated approach to control mosquitoes is desired. This project focuses on two specific aspects: (1) developing molecular genetic approaches for the rapid and efficient identification of species with high risk as pathogenic vectors; and (2) developing biorational control strategies for the repulsion of mosquitoes in areas of risk. Aim I is being met by identifying specific DNA sequences that discriminate South American *Anopheles* species. A virtual field kit will be designed employing these sequences for the rapid identification of potential decease vectors. Aim II is being met by identifying olfactory specific proteins (receptors) responsible for host odor recognition. These proteins will be used as probes to elucidate behaviorally specific olfactory pathways and as molecular tools for designing olfactory repellents and attractants.

## FORWARD

This project is funded at $500,000 for the period 6/01/97 to 5/31/99.

The project aim is twofold: (1) development of a genetically based diagnostic approach to distinguish and identify specific mosquito species in the field and (2) identification of odor recognition molecules in mosquito responsible for host odor discrimination.

During the first 9 months of this project, we have successfully:

- developed a protocol for collecting approximately 40 South American *Anopheles* species and initiated that collection process,
- developed a protocol and initial focus on four closely related *Anopheles* species, determining genetic criteria discriminating between these four species and two out group species,
- developed a protocol for identifying the full range of initial odor recognition proteins in one model species of mosquito.

## REPORT

### Background

Mosquitoes and the pathogens that they transmit are a worldwide problem for human health. Mosquitoes spread malaria, yellow fever, dengue fever, and several forms of encephalitis. Malaria alone infects nearly 500 million people worldwide and causes more than 2 million deaths annually (Goddard 1993). Malaria is endemic to much of the world, particularly developing nations where the U.S. military may be called on for regional conflict resolution and relief missions. Almost 99% of the malaria cases in the U.S. are due to infections acquired in other countries (Goddard 1993). Thus, the prevention and control of mosquito borne diseases is of particular concern to the U.S. military because significant numbers of U.S. military personnel may spend time where they will be exposed to mosquito species that transmit dangerous pathogens.

### Vector Identification

There are more than 3,000 species of mosquito. Nearly 10% of these species are dangerous vectors of human parasites; many vector species include differentiated populations (subspecies) with varying parasitic risks. Rapid identification of specific mosquito species and populations at a given location is critical for determining what parasites and diseases military personnel will be exposed to, and what control strategies should be employed.

Although almost all-female mosquitoes must feed on blood to acquire adequate nutrition to lay eggs, a relatively few mosquito species carry the most dangerous pathogens. The relative abundance of these mosquitoes varies over geographic regions and time, as does the frequency of pathogens within individuals of the species. Unnecessary vaccination and/or medication of personnel is expensive and not without potentially harmful side effects. Thus, two questions must be addressed before deploying personnel: 1) are particular pathogens present (e.g., Armstrong et al. 1995) and 2) are species present which are known to transmit particular pathogens (e.g., Wilkerson et al. 1995). Answers to the first question are directly relevant for human health concerns. However, it is very difficult to be certain that pathogens are absent even when they are not detected. Answering the second question concentrates on the disease vectors. Disease vectors are generally much easier to detect. Additionally, detection of potential disease vectors is more likely to suggest precautions - even against pathogens that are not detected directly. Concentrating on disease vectors emphasizes planning for, and solving, a broader range of potential health problems than may be suggested by direct sampling for pathogens.

Mosquito species are traditionally identified by anatomical differences (i.e. by looking at physical characters such as wing shape or bar patterns on the abdomen); this can be extremely difficult. Some species can be anatomically identified only through laboratory rearing and examination of multiple life stages (e.g. larval, pupal, and adult). Some anatomical groups actually include several "cryptic" species that are not discernible by morphology.

Mosquito species and differentiated populations can be readily distinguished by using DNA analysis (Wilkerson et al., 1993). We will, therefore, characterize DNA differences within and among anatomical groups (taxa) to identify mosquito species. We will focus on mosquito

species that are known malaria vectors. We will collect and use DNA sequence data from these species to develop easy to use assays for mosquito identification. Using these assays will allow military personnel to assess the presence of malaria vectors at previously uncharacterized sites without calling in mosquito experts or waiting for analysis of specimens shipped to experts.

**Vector disruption**

Mosquitoes are actively attracted to humans through a number of sensory modalities, including body odors, heat, and $CO_2$ (Bowen 1991). While this is generalizable to all problematic mosquito species and varieties, a detailed study has primarily focused on one species, *Aedes aegypti*, and work has been superficial at best. Sensory neurobiology has developed dramatically in the last 15 years, elucidating fundamental mechanisms at the molecular genetic level that allow insects to detect specific signals. Applying these developments to mosquito species will identify the specific molecular/neural pathways employed in host attraction, and thus define molecular targets against which to design biorational control strategies for the disruption of host attraction behavior.

While many species of mosquito act as vectors of pathogens dangerous to human health, only a subset of these species are attracted to humans (anthophilic); the remaining species are attracted to non-human hosts (zoophilic) for blood meals. The basis of these differential attractions is not understood, but likely involves host specific sensory cues. Of the sensory cues available, host specific body odors are the most likely discriminating signal.

The initial biomolecular step in odor recognition in insects, including mosquitoes, is the interaction between the odor molecule and an Odorant Binding Protein (OBP) (Vogt et al., 1991a,b; Vogt, 1995). Odorant Binding Proteins (OBPs) are small (15 kd), abundant water soluble proteins uniquely expressed in the olfactory sensilla of insect antenna. OBPs solubilize and transport volatile odorants in a specific manner, transporting odorants to neuronal receptor proteins. Each insect species has multiple OBP types which are differentially expressed among the functional classes of olfactory neurons/sensilla; the specific complement of OBPs has been proposed to reflect the odor types of interest to the insect (Vogt, 1995).

OBPs will be identified and sequenced from mosquito antennae. These proteins will provide molecular templates that can be used to design host odor attractants and repellents specifically tailored to the species of interest. Comparisons of OBP sequences among an assemblage of mosquito species will elucidate the olfactory genetic differences controlling anthophilic vs. zoophilic attractions and establish genetic markers, which can predict these attractions for untested mosquito species.

**Outcome**

An integrated approach to the control of mosquitoes will emerge from these studies. Rapid and efficient identification of problematic species or varieties will specify a need of action. The employment of targeted control strategies will maximize the impact on the mosquito vector while minimizing the impact on human health. Molecular systematic and molecular physiological approaches integrate to yield new and biorational approaches to mosquito management in areas of need.

**Experimental Approach**

Mosquito species vector a multitude of pathogens of significant human health risk; however, only a subset of these species are actually attracted to human hosts. The purpose of this project is to develop new strategies for the prevention of mosquito vector borne disease in humans. To that end, two approaches are being taken.

- **Approach I.** A virtual diagnostic kit is being developed, based on genetic markers, for the rapid in-field identification of mosquito host species to discriminate species which pose human health risks from species which do not.
- **Approach II.** The initial molecular step in host odor recognition by mosquitoes is being characterized by the identification and sequencing of mosquito Odorant Binding Proteins (OBP); it is expected that OBP phylogenies will discriminate anthophilic (human seeking) from zoophilic (non-human seeking) species of mosquito independent of mosquito-pathogen associations. Both approaches are being developed in model species, and will subsequently be expanded and tested on a larger set of South American *Anopheles* species.

***Summary of Important Results***

This project has three components indicated below: (1) Species Collection (Dr. Richard WIlkerson), (2) Genetic Analysis (Drs. Joseph Quattro, Travis Glenn), and (3) Olfactory Analysis (Dr. Richard Vogt).

**1. Species Collection**

Dr. Richard Wilkerson (Department of Entomology, Walter Reed Army Institute of Research) is responsible for collecting and supplying complete assemblages of two South American *Anopheles* groups belonging to two subgenera (*Nyssorhynchus* and *Kerteszia*). The complete species list is shown below (Table 1). Numbers in bold italics indicate species that must be obtained through collecting trips; non-bold numbers indicate species already available in Dr. Wilkerson's collection. Species numbered 9, 10, and 11 were successfully obtained during Dr. Wilkerson's 1/98 collecting trip to Brazil, supported by this project.

The rational for these assemblages is that they represent complete genera of *Anopheles* species which include members which are human relevant vectors of the malaria parasite. Not all of the species seek out human hosts, and therefore they offer an opportunity to test the resolving power of Odorant Binding Proteins in the discrimination between anthophilic and zoophilic species.

Dr. Wilkerson's proposed collection schedule is indicated below (Table 2), species names and numbers referencing the above table. During Dr. Wilkerson's 1/98 collecting trip, only 3 of the 5 indicated species were successfully obtained; the remainder will be obtained through later efforts. We stress that the bulk of our progress (and expenditures) to date has been associated with specimen acquisition. We have only recently begun steps II and III.

**2. Genetic Analysis**

Dr. Joseph Quattro (Department of Biological Sciences, University of South Carolina) is responsible for developing the methodology of genetic identification of *Anopheles* species. We began the development of DNA-based diagnostic assays by focusing on a small, closely-related

group of Brazilian malaria vectors. The group comprises four cryptic taxa within the *Anopheles albitarsis* species complex: *A. albitarsis*, *A. marajoara*, *A. deaneorum*, and *A. albitarsis* "Sp. B". Two closely related congeners (*A. darlingi* and *A. braziliensis*) are included as outgroup taxa. RAPD DNA and to some degree morphological analyses are the only suitable techniques for discriminating species within the *albitarsis* complex, and these methods are cumbersome and not entirely suitable for a rapid, field-based assay.

**TABLE 1.**

| | **Subgenus *Nyssorhynchus*** | 40 | ***darlingi (3/98)*** |
|---|---|---|---|
| *21* | *albimanus* | 41 | ***albitarsis (4 cryptic sp.)(3/98)*** |
| 22 | *oswaldoi* | 42 | ***braziliensis (3/98)*** |
| 23 | *konderi* | 43 | *parvus* |
| *24* | *galvaoi* | 44 | *nigritarsis* |
| 25 | *evansae* | 45 | *antunesi* |
| 26 | *aquasalis* | 46 | *lutzii* |
| *27* | *ininii* | | **Subgenus *Kerteszia*** |
| *28* | *anomolophylus* | *1* | *rollai* |
| 29 | *rangeli* | *2* | *gonzalezrinconesi* |
| 30 | *trinkae* | *3* | *auyantepuiensis* |
| 31 | *nuneztovari* | *4* | *neivai* |
| *32* | *strodei* | 5 | *pholidotus* |
| 33 | *rondoni* | *6* | *lepidotus* |
| *34* | *benarrochi* | *7* | *bambusicolus* |
| *35* | *triannulatus* | *8* | *homunculus* |
| 36 | *argyritaris* | *9* | *cruzii (3/98)* |
| *37* | *sawyeri* | *10* | *bellator (3/98)* |
| 38 | *lanei* | *11* | *laneanus (3/98)* |
| *39* | *pictipennis* | *12* | *boliviensis* |

**TABLE 2.**

| | date | site | species | species |
|---|---|---|---|---|
| 1 | 1/98 | Sao Paulo | ***cruzii***, homunculus, ***bellator***, ***laneanus***, galvaoi | **9**, 8, **10**, **11**, 24 |
| 2 | 4/98 | Nicaragua. | anomolophyllus, albimanus, strodei | 28, 21, 32 |
| 3 | 9/98 | Venezuela | First 3 Kerteszia species | 1, 2, 3 |
| 4 | 1998 | Cochabamba, Bolivia | boliviensis, lepidotus -- Collection by Army collaborator in Rio de Janeiro (maybe) | 12, 6 |
| 5 | 1998 | Meta, Colombia | boliviensis, bambusicolus -- Collection and rearing by Colombian collaborator | 12, 7 |
| 6 | 1/99 | Trinidad, Guyana | neivai, homunculus, bellator (return to US for rearings) | 4, 8, 10 |
| 7 | 4/99 | Para and Ceara, Brazil | ininii, sawyeri (rearings by collaborators in Belem) | 27, 37 |
| 8 | 9/99 | Ecuador or Colombia | sp. nr. triannulatus | 35 |
| 9 | 1/00 | Peru, Iquitos and vic. | benarrochi. | 34 |
| 10 | 7/00 | Panama | pholidotus. I still need a Panamanian collaborator | 5 |
| 11 | 12/00 | Chile | pictipennis. | 39 |

Our initial work involved methods for the preservation of field samples for subsequent DNA isolation. Ethyl-alcohol (70%) has proven to be an inexpensive, yet effective means for transporting field material. Nucleic acid isolation from alcohol preserved samples has yielded DNA samples of sufficient quality and quantity to be suitable template in Polymerase Chain Reaction (PCR) amplification.

Once we were confident that suitable nucleic acids could be routinely isolated from field specimens, we designed PCR amplification assays that would amplify a sufficiently variable region of the mitochondrial DNA (mtDNA) genome. To date, several assays have been designed, but we have settled on the cytochrome-b (*Cytb*) locus within the mtDNA genome for several reasons:

- the *Cytb* locus is suitable for studies at or below the species level in a variety of invertebrate and vertebrate taxa;
- we have designed primers that amplify *Cytb* from a wide variety of invertebrate taxa including mosquitoes;
- our initial amplifications with this primer set have been very promising in trials with all members of the *albitarsis* species complex including outgroups.

We are continuing these assays by sequencing products from several individuals representing each cryptic species within the *albitarsis* species complex. Samples have been chosen to represent the geographical extremes of each species' range. We will perform phylogenetic analyses on these sequences to test the hypothesis that each group represents a valid monophyletic taxon. These phylogenetic analyses will allow us to identify synapomorphic DNA substitutions within the *Cytb* locus that define each clade (species). These positions will form

the basis of our method for field identification. We plan to initially test and refine this identification test kit using members of the *albitarsis* species complex as an 'acid test'. Once we are confident that such assays are feasible, we will transfer the technology developed to include all other potential vectors described in Tables 1 and 2.

**3. Olfactory Analysis**

Dr. Richard Vogt (Department of Biological Sciences, University of South Carolina) is responsible for developing the olfactory analysis of mosquitoes. We have constructed a phylogenic analysis of 34 full length OBPs characterized from 10 species representing 4 insect orders (Lepidoptera, Diptera, Coleoptera, and Hemiptera) that reveal that OBPs are a multigene family represented by as many as 7 members (to date) in a single species. One feature all have in common is their abundance, representing major proportions of the total mRNA expressed in an antenna (olfactory organ). While it is feasible to use existing *Drosophila* clones either for hybridization probes for screening of a mosquito antennal cDNA library or for the design of degenerate PCR primers for the amplification of homologues from mosquito derived antennal cDNA, it has become clear that these approaches will not come near identifying a "full complement" of the OBP or OBP-like mRNAs expressed within the antenna.

We have therefore settled on a brute force approach to this problem. Complementary cDNA libraries will be constructed from male and female antennal mRNAs, and a randomly selected population of 300-400 cDNAs will be sequenced and analyzed by Blast homology search. This is actually a surprisingly reasonable approach because OBP mRNAs so far reported are small (800-1600 bp) and, as stated above, represent the major mRNAs within the population. This approach may be modified following the sequencing of the first 100 clones by performing a high stringency screening of the library with the clones identified as abundant (10-20%) and proceeding to sequence clones that were negative.

The chief hurdle to this approach is the development of a method of antennal isolation that does not lead to degradation of mRNA by endogenous nucleases. Our solution to this problem is to rapidly freeze recently emerged adults, freeze dry them to eliminate the hydrated state that permits nuclease activity, isolate male or female antennae in this nuclease inactive state, and then proceed with mRNA isolation. We have begun this effort using *Aedes aegypti*; this animal is an excellent initial test subject as it is readily available as eggs and quite easy to rear. Our basic conditions are being established in *Aedes aegypti*.

To date, we have:

- constructed a phylogeny of known OBP sequences to determine the expected size, diversity and depth of this multigene family;
- developed a method of antennal isolation and mRNA purification that does not allow for degradation of antennal mRNAs; and
- established a protocol for isolating a broad complement of OBPs from multiple mosquito species.

We are proceeding with the full characterization of OBPs from A. aegypti antennae as a model system, and also as a point of comparison with the *Anopheles* genus. Coincident with the *Aedes aegypti* studies, we will isolate mRNAs and construct antennal cDNA libraries to *Anopheles quadrimaculatus*, the prominent North American malaria vector. Having identified sequences from these species, we will construct PCR primers that can isolate and identify homologous DNA sequences from the *albitarsis* complex being characterized in component II above. Our strategy is to initiate this study using brute force methodology with species we can obtain in abundance through lab rearing, and then refine our strategy to an approach that can accommodate species that are available only in limited numbers.

***Participating Personnel***

| **Name** | **Degree** | **Year** |
|---|---|---|
| Richard G. Vogt | Ph.D. | 1984 |
| Joseph M. Quattro | Ph.D. | 1991 |
| Travis Glenn | Ph.D. | 1997 |
| Richard Wilkerson | Ph.D. | 1995 |
| Ge Xin | Ph.D. | 1990 |
| Zhaoyuan Hou | M.S. | 1996 |

## BIBLIOGRAPHY

Armstrong, P., D. Borovsky, R. E. Shope, C. D. Morris, C. J. Mitchell, N. Karabatsos, N. Komar, and A. Spielman. 1995. Sensitive and specific colorimetric dot assay to detect Eastern Equine Encephalomyelitis viral RNA in mosquitoes (Diptera: Culicidae) after polymerase chain reaction amplification. J. Med. Entomol. 32(1): 42-52.

Audtho M, Tassanakajon A, Boonsaeng V, Tpiankijagum S., and Panyim S (1995) Simple nonradioactive DNA hybridization method for identification of sibling species of Anopheles dirus (Diptera: Culicidae) complex. *Journal of Medical Entomology* 32(2): 107-111.

Bowen MF (1991) The sensory physiology of host-seeking behavior in mosquitoes. *Annual Review of Entomology* 36, 139-158.

Bruce-Chwatt LJ (1985) Mosquitoes, malaria, and war: Then and now. *J. R. Army Medical Corps* 131: 85-99.

Gershon D. (1995) DNA diagnostic tools for the 21st century: Technologies in DNA diagnostics on the horizon. *Nature Medicine* 1(2): 102-103.

Goddard J (1993) *Physian's guide to arthropods of medical importance.* CRC Press, Inc., Boca Raton, FL.

Pelosi P (1996) Perireceptor events in olfaction. *Journal of Neurobiology* 30, 3-19.

Steinbrecht RA (1996) Are odorant-binding proteins involved in odorant discrimination? *Chemical Senses* 21, 719-727.

Vogt RG (1995) Molecular genetics of moth olfaction: a model for cellular identitiy and temporal assembly of the nervous system. In *Molecular Model Systems in the Lepidoptera.* MR Goldsmith, AS Wilkins Eds. Cambridge University Press, Cambridge, pp. 341-367.

Vogt RG, Riddiford LM (1981) Pheromone binding and inactiviation by moth antennae. *Nature* 293, 161-163.

Vogt RG, Koehne AC, Dubnau JT, Prestwich GD. (1989) Expression of pheromone binding proteins during antennal development in the gypsy moth *Lymantria dispar. Journal of Neuroscience* 9, 3332-3346.

Vogt RG, Preswich GD, Lerner MR (1991a) Odorant-Binding-Protein subfamilies associate with distinct classes of olfactory receptor neurons in insects. *Journal of Neurobiology* 22, 74-84.

Vogt RG, Rybczynski R, Cruz M, Lerner MR (1993) Ecdysteroid regulation of olfactory protein expression in the developing antenna of the tobacco hawk moth, *Manduca sexta. Journal of Neurobiology* 24, 581-597.

Vogt RG, Rybczynski R, Lerner MR. (1991b) Molecular cloning and sequencing of General-Odorant Binding Proteins GOBP1 and GOBP2 from the Tobacco Hawk Moth *Manduca sexta*: Comparisons with other insect OBPs and their signal peptides. *Journal of Neuroscience.* 11, 2972-2984.

Wilkerson RC, Parsons TJ, Albright DG, Klein TA, Braun MJ. (1993) Random amplified polymorphic DNA (RAPD) markers readily distinguish cryptic mosquito species (Diptera: Culicidae: *Anopheles*). *Insect Molecular Biology* 1, 205-211.

Wilkerson RC, Parsons TJ, Klein TA, Gaffigan TV, Bergo E, Consolim J. (1995) Diagnosis by random amplifed polymorphic DNA polymerase chain reaction of four cryptic species related to *Anopheles* (*Nyssorhynchus*) *albitaris* (Diptera: Culicidae) from Paraguay, Argentina, and Brazil. *Journal of Medical Entomology* 32, 697-704.

# REPORT DOCUMENTATION PAGE

Form Approved
OMB No. 0704-0188



| 1. AGENCY USE ONLY *(Leave blank)* | 2. REPORT DATE | 3. REPORT TYPE AND DATES COVERED |
|---|---|---|
| | June 1, 1998 | ANNUAL |

**4. TITLE AND SUBTITLE**

Laboratory for Genetic Diagnosis and Control of Mosquitoes

**5. FUNDING NUMBERS**

Grant Number N00014-97-1-0806
PR Number 97PR06312-00
PO Code 353
Disbursing Code N68892
AGO Code N66020
Cage Code 4B489

**6. AUTHOR(S)**

Richard G. Vogt

**7. PERFORMING ORGANIZATION NAME(S) AND ADDRESS(ES)**

University of South Carolina, Columbia, SC 29208

**8. PERFORMING ORGANIZATION REPORT NUMBER**

N00014-97-1-0806-1

**9. SPONSORING / MONITORING AGENCY NAME(S) AND ADDRESS(ES)**

ONR

**10. SPONSORING / MONITORING AGENCY REPORT NUMBER**

ONR

**11. SUPPLEMENTARY NOTES**

Prepared in coordination with University Research Initiative Program for Combat Readiness

**12a. DISTRIBUTION / AVAILABILITY STATEMENT**

APPROVED FOR PUBLIC RELEASE

**12b. DISTRIBUTION CODE**

**13. ABSTRACT** *(Maximum 200 words)*

Mosquitoes are annoying and potentially dangerous pests for US military personnel. Mosquito bites can be irritating, become infected, or be the source of debilitating diseases including malaria, yellow fever, dengue fever, and encephalitis. Although most of these pathogens can be controlled with medication and/or vaccination, the cost, side-effects, and development of insecticide-resistant strains diminishes the long-term viability of these treatments. Current chemical control methods of mosquitoes are of questionable compatibility with human health. A biorational integrated approach to control mosquitoes is desired. This project focuses on two specific aspects: (1) developing molecular genetic approaches for the rapid and efficient identification of species with high risk as pathogenic vectors; and (2) developing biorational control strategies for the repulsion of mosquitoes in areas of risk. Aim I is being met by identifying specific DNA sequences that discriminate South American *Anopheles* species. A virtual field kit will be designed employing these sequences for the rapid identification of potential decease vectors. Aim II is being met by identifying olfactory specific proteins (receptors) responsible for host odor recognition. These proteins will be used as probes to elucidate behaviorally specific olfactory pathways and as molecular tools for designing olfactory repellents and attractants.

| 14. SUBJECT TERMS | 15. NUMBER OF PAGES |
|---|---|
| Chemical and Biological Warfare, Target Acquisition, Anti-Submarine, Combat Medicine, Biodeterioration, and Command Control and Communication | 16. PRICE CODE |

| 17. SECURITY CLASSIFICATION OF REPORT | 18. SECURITY CLASSIFICATION OF THIS PAGE | 19. SECURITY CLASSIFICATION OF ABSTRACT | 20. LIMITATION OF ABSTRACT |
|---|---|---|---|
| UNCLASSIFIED | UNCLASSIFIED | UNCLASSIFIED | 200 WORDS |

# Insure Access to Allogeneic Bone Marrow Transplantation for Correction of Marrow Failure and Hematologic Malignancies

P. Jean Henslee-Downey, M.D.

Center for Cancer Treatment and Research
7 Richland Medical Park
Columbia, SC 29036

Tel: 803-434-3550
Fax: 803-434-3949
E-mail: jean.hensleedowney@rmh.edu

# Section 4-2: Insure Access to Allogeneic Bone Marrow Transplantation For Correction of Marrow Failure and Hematologic Malignancies

P.J. Henslee-Downey

## ABSTRACT

Although an identical sibling is the ideal donor for a recipient requiring a transplant of hematopoietic cells after being exposed to radioactive, chemical or biological weapons resulting in hematological aplasia or cancer, only 25% of the patients would have the opportunity of receiving a transplant from their HLA-identical sibling. On the other hand, more than 95% of the patients could receive a transplant if a partially mismatched related donor (PMRD) was used. However, this type of transplant must be accompanied not only by pre-transplant high dose chemotherapy and consolidation, but also by post-transplant immunosuppression geared to finding a balance between suppressing graft versus host disease and allowing for a graft versus leukemia effect to occur.

In this program, we have identified four areas of research, which are required for the further development and success of this type of transplant protocol. These areas were described in our research proposal as the following:

1. Identify and positively select primitive hematopoietic stem cells that will provide the greatest long-term repopulating potential to ensure an established stable chimera.
2. Identify and remove lymphocyte subsets that result in the development of acute and chronic graft versus host disease.
3. Identify and enrich for lymphocyte subsets that ensure rapid immune reconstitution and thus, reduction in the risk of fatal infectious disease post-transplant.
4. Identify and manipulate lymphocyte subsets that can provide an anti-leukemic effect when required.

Each of these areas has been addressed during the first year of funding, and the following is a synopsis of our research efforts.

## FORWARD

During the first year of a three year grant award in the amount of $360,138 to support this project, $49,472 in funding was received as of February 1998. Work has progressed in all areas described in the proposal and is highlighted by advancements in understanding the cellular components and process of hematopoiesis and achievements in establishing engraftment across major-HLA barriers to allogeneic transplant. We have utilized a new human stem cell marker called AC133 to further delineate a subset of $CD34^+$ cells that may represent a highly primitive stem cell progenitor. In addition, we have made observations regarding the lapse of time from stimulation of hematopoietic progenitors in the marrow cavity through to migration to the peripheral blood compartment. In clinical studies using haploidentical HLA-mismatched related donors, we have made transplant immediately available to patients who did not have matched sibling or unrelated donor options. Methods used for manipulated of the marrow graft and therapeutics to modulate the immune system prior to and following transplant has resulted in a

100% engraftment rate and a 15% risk of moderate to severe acute graft-versus-host disease. All patients transplanted in early disease status continue to survive. Still most patients underwent transplant for advanced disease, despite readily available donors. Nonetheless, the overall survival for the patient cohort studied during this grant period was 56.7%, which appears better than published results using HLA-matched donors for similar types of patients. The major cause for failure included relapse and infection. Thus, work during the next year will focus on cellular immunotherapy specifically targeted against both tumor and antimicrobial antigens.

## DESCRIPTION OF ATTACHMENTS

Attachment 1: Analysis of the proportion of peripheral blood lymphocytes in patients who received haploidentical HLA-mismatched allogeneic marrow grafts comparing those who did or did not receive additional donor lymphocytes post-transplant.

Attachment 2: Analysis of the absolute number of peripheral blood lymphocytes in patients who received haploidentical HLA-mismatched allogeneic marrow grafts comparing those who did or did not receive additional donor lymphocytes post-transplant.

## REPORT

A description of work performed, in progress and planned is summarized below.

### 1. Identify and positively select primitive hematopoietic stem cells that will provide the greatest long-term repopulating potential to ensure an established stable chimera.

*Umbilical cord blood provides a source of very primitive hematopoietic stem cells.*
The hematopoietic system is one of a handful of continuously proliferating biological systems in the body. This means that any agent capable of interfering with the normal proliferative and differentiation process can potentially be harmful to the system and result in its temporary or even permanent dysfunction. Nevertheless, from the use of agents such as 5-fluorouracil, hydroxyurea, methotrexate, cyclophosphamide, as well as radiation, it has been possible to show that the cells that give rise to differentiated and mature blood cells, the hematopoietic stem cells, are organized in a hierarchical manner, such that the most mature stem cells are mono-, or at the most bipotential with the lowest capacity for hematopoietic repopulation, while the most primitive stem cells are capable of producing multilineage engraftment and possess the greatest long-term repopulating potential. Obviously, it is the latter population that is required for any type of human hematopoietic transplantation, regardless of whether bone marrow, peripheral blood or umbilical cord blood is used for the graft. Theoretically, fewer primitive, long-term repopulating cells should be required to reconstitute the hematopoietic system than more mature, short-term repopulating cells. However, considering that the whole stem cell compartment represents less than 0.1% of the total bone marrow cellularity, it is not surprising that the most primitive hematopoietic stem cells represent a minute population and are therefore extremely difficult to separate in quantity. To date, the two most important factors correlating with engraftment are either the total cell dose of the graft or the number of $CD34^+$ cells present in the

graft. The CD34 antigen is present not only on most of the stem cell populations, but also on early progenitor cell populations, i.e. those that have become determined and have entered a specific hematopoietic lineage. Therefore, a great deal of effort has been applied to identifying $CD34^+$ subpopulations capable of providing long-term engraftment. From work performed in the mouse and extrapolated to the human, such populations have been identified. Probably, the most important of these is designated the long-term culture-initiating cell (LTC-IC), and has been consider to be, for many years, the most primitive hematopoietic stem cell. The cell is identified by the presence of both CD34 and the CD90 (Thy-1) antigens on its surface. Indeed, the detection of this cell population, using in vitro culture techniques, is considered to be the "gold standard". Recently, however, a more primitive population than the LTC-IC has been detected using the non-obese diabetic severe combined immunodeficient (NOD-SCID) mouse, which can accept a graft of human cells without the associated graft versus host disease, by virtue of the fact that the animals do not possess an intact immune system. The cell population detected has been called the SCID-repopulating cells (SRC) and the methodology provides the only in vivo assay for human hematopoietic stem cells.

In order to identify other primitive hematopoietic stem cell populations, we have made use of information obtained from murine embryogenisis. One of us (INR) has previously demonstrated that the most primitive embryonic stem cell population, the so-called primordial germ cell (PGC), which is a non-hematopoietic stem cell, can be induced to differentiate, in culture, into multilineage hematopoietic cells. It was postulated that PGCs were not only capable of giving rise to the germ cells in the gonads, but also to hematopoiesis during ontogeny. One of the few identifying markers of PGCs, is the presence of the stage-specific embryonic antigen 1 (SSEA-1). The latter not only cross-reacts with human cells, but the human homologue of SSEA-1 is CD15, also called the Lewis X antigen, whose ligand is E-selectin. The CD15 antigen is present primarily on monocytes and granulocytes. However, we have found that it is also present on a subpopulation of human hematopoietic stem cells. If a non-hematopoietic totipotent stem cell subpopulation were to give rise to the hematopoietic stem cell population, then it would be expected that during human ontogeny, the greatest number would perhaps occur in the fetal liver. Since human fetal liver cannot be obtained, and it has been known for several years that the umbilical cord blood contains a higher percentage per unit volume of stem cells than the bone marrow or peripheral blood, we decided to investigate whether a similar stem cell population to that found in the mouse was present in human umbilical cord blood. In addition to CD34, we also used a new human stem cell marker called AC133, which further delineates a subset of $CD34^+$ cells.

Using flow cytometry and multiparameter analysis, different antibodies to surface antigens labeled with FITC were combined with AC133 conjugated to phycoerythrin (PE) and CD34 conjugated to allophycocyanine (APC) and all analyses were performed using CD45-PerCP (peridinin-chlorophyll conjugate). A mean of 3,550 ± 1,600 (SEM)/$10^6$ cord blood $CD34^+$ cells, representing between 0.12% and 0.80% of the $CD45^+$ population was obtained from 8 experiments. For $CD34^+CD90^+$ cells, 920 ± 537/$10^6$ cells, while 425 ± 388/106 cells were $CD34^+/AC133^+$. There were 90 ± 60 /$10^6$, $CD34^+AC133^+CD90^+$ cells and 35 ± 19/$10^6$ $CD34^+AC133^+CD15^+$ cells. It therefore appears that both the $CD90^+$ and $CD15^+$ populations represent a very minute and primitive stem cell component of cord blood. During the second year of this proposal, both in vitro and in vivo assays will be performed in order to determine the

functional characteristics of these populations. In order to obtain these populations, the cells will be separated using a new high-speed cell sorter that will be at our disposal in the second half of 1998. Although, in reality, insufficient numbers of these very primitive stem cell populations can be obtained, techniques are available to concentrate these cells. In addition, with new cytokine and culture techniques available, it may also be possible to expand these populations in vitro.

*Mobilized bone marrow may provide an extra source of stem cells to mobilized peripheral blood.* Another aspect of our work involving stem cells for use in transplantation has concentrated on the mechanisms involved in the mobilization of stem cells from the bone marrow to the peripheral blood by administration of the cytokine, granulocyte colony-stimulating factor (G-CSF). It has been known for some years that multiple doses of G-CSF can cause an outpouring of hematopoietic stem cells into the circulation. During the time period required for mobilization (about 5-6 days), the patient undergoes apheresis to collect the stem cells, which are initially frozen after each collection. At the time of transplant, all the collections are thawed, pooled together and infused into the patient. This is now a very common procedure for autologous transplantation, although the conditions for allogeneic transplantation using mobilized peripheral blood cells are far more complicated due to the high potential for graft versus host disease. Recently, significant strides have been taken in order to understand the mechanism by which the stem cells are mobilized from the bone marrow. However, in contrast to other investigations, which have compared mobilized peripheral blood with that under normal condition, we have compared both peripheral blood and bone marrow in parallel after G-CSF mobilization. Five normal donors were administered G-CSF on days 1 to 5. On days 0, 3, 6, 9, and 15, PB and BM were collected. Total $CD34^+$ cells decreased to the lowest values in the BM between days 6 and 9 and then returned to base line, while PB $CD34^+$ cells were maximum on day 6 and then decreased. Since mobilization has been shown to be dependent on adhesion molecules, we also studied the role of integrins in this process. Integrin subunit $\alpha_4$ (VLA-4, CD49d) and $\alpha_5$ (VLA-5, CD49e) expression on mobilized PB and BM was also evaluated. Whereas, both $\alpha_4$ and $\alpha_5$ remained constant for mobilized BM during the observation period, an indirect correlation between $\alpha_4$ and $\alpha_5$ was noted. By day 6 in PB, $\alpha_4$ expression had reached its maximum whereas $\alpha_5$ attained its minimum at the same time. Coupled with this, was the observation that CD44 (H-CAM) expression, known to be involved in homing, also reached a maximum on day 6 in PB, at the same time as $\alpha_4$ integrin subunit expression, and gradually increased in BM during the study period. This suggests that $\alpha_5$ down-regulation is required for BM cells to enter the circulation, while both $\alpha_4$ and CD44 are required for mobilized PB cells to home back into the BM. Since CD95 (Fas) expression, which is involved in the apoptotic mechanism, remained stable in BM cells, but increased from day 3 onward in PB cells, we suggest that those cells that do not home back into the BM, undergo apoptosis. By comparing both PB and BM, the data provide a new insight into the mobilization and homing mechanism, by which infused stem cells have to find and enter the bone marrow in order to seed and proliferate to reconstitute the hematopoietic system.

**2. Identify and remove lymphocyte subsets that result in the development of acute and chronic graft versus host disease (GvHD).**

The most efficient and cost-effective manner to identify allogeneic stem cell donors for every individual in need is through the use of haploidentical family members. This donor genetically

shares one full HLA haplotype, including all other antigenic determinants within the major histocompatibility complex. However there is a potential for complete mismatching of the unshared MHC complex. These antigenic differences create barriers to successful engraftment, though once accomplished, the reverse results in the potential for rapid allogeneic stimulation of a GvHD response. Using unmodified haploidentical marrow grafts, early clinical results suggested that the risk of graft failure might be approximately 15% and the risk of moderate to severe (Grade II to IV) acute GvHD might exceed 80%. Unfortunately, the implementation of extensive T-cell depletion (between 4 to 5 log depletion), as a promising modality to control acute GvHD, was found to increase the risk of graft failure to as high as 50%. Thus, it appears that some donor T-cells in the graft are necessary to overcome recipient barriers to engraftment. We have previously evaluated two anti-CD3 monoclonal antibodies (T10B9 and OKT3), activated by compliment, to produce subset T-cell depletion but of a more moderate degree. Our published results indicate that an approximate 2.5 log T-cell depletion can result in > 90% successful engraftment using haploidentical donors. However, usually these donor T-cells ultimately result in the development of acute GvHD that is unacceptable. More recently, we have shown that combining partial T-cell depletion with post-transplant immunosuppression, results in better control of both donor and recipient reactions. Despite achieving clinical success, a definition of the cellular components of the graft that governs these immunologic interactions remains poorly understood.

In the first year of this grant, clinical and laboratory studies have been conducted in an effort to better define the graft characteristics of partially T-depleted haploidentical marrow grafts. We have examined results from consecutive transplants, which have a minimum of 3 months follow-up. Between 4/9/97 to 1/7/98, 37 haploidentical transplants were performed using OKT3 and compliment incubation to prepare the marrow grafts. The median harvest volume was 1,253 ml (range 477 – 1,896) and pre-manipulation characteristics were as follows:

| | |
|---|---|
| Harvest Nucleated Cell Dose/Kg | $4.75 \times 10^8$ ($1.78 \times 10^8 - 15.46 \times 10^8$) |
| Harvest CD34 Dose /Kg | $2.8 \times 10^6$ ($0.3 \times 10^6 - 12.2 \times 10^6$) |
| Harvest CD5 (T-cell) Dose/Kg | $45.2 \times 10^6$ ($23.4 \times 10^6 - 155.7 \times 10^6$) |
| Harvest CFU-GM Dose/Kg | $115.6 \times 10^4$ ($30.4 \times 10^4 - 389.7 \times 10^4$). |

After initial buffy coat recovery, a median of 92% (range 66.1 – 121) of cells were recovered however, only approximately 31.6% (range 21 – 48) remained after ficoll separation. This fraction was incubated with monoclonal antibody to coat mature donor cells followed with complement to activate T-cell lysis. These studies were performed with complement taken from a single lot and antibody obtained from 5 lots of clinically FDA-approved material. One graft required 2 cycles of complement incubation to achieve the desired T-cell depletion. At completion of T-cell depletion, approximately 20% (range 9.9 – 35) of cells were present in the graft. Limiting dilution analysis indicated that a median 3 log (range 1.5 – 3.8) depletion was achieved. The final characteristics of the grafts used for clinical transplant were as follows:

| | |
|---|---|
| Infused Volume (ml) | 112 ml (50 ml – 329 ml) |
| Infused Cell Dose/Kg | $0.93 \times 10^8$ ($0.31 \times 10^8 - 4.53 \times 10^8$) |
| Infused CD34 Dose/Kg | $1.9 \times 10^6$ ($0.1 \times 10^6 - 2.68 \times 10^6$) |
| Infused CD5 (T-cell) Dose/Kg * | $3.8 \times 10^4$ ($0.6 \times 10^4 - 30.2 \times 10^4$) |

Infused CFU-GM Dose/Kg $44.8 \times 10^4$ ($19.4 \times 10^4 - 248 \times 10^4$).

The study sought to deliver a T-cell dose that was below the threshold of $4.5 \times 10^5$/kg and this was achieved in all grafts.

In an effort to define the manipulation process and graft characteristics further, flow cytometric studies were performed prior to and following T-cell depletion. The studies were designed to quantitate the proportion of cells with CD34, CD2, CD3, CD5, CD16/56, and CD19 antigenic expression. The process was shown to enrich for $CD34^+$ cells, deplete T and NK cells and not alter B cell content.

Most (92%) patients entered on the clinical trial suffered from advanced leukemia. Adverse risk was further compounded by an advanced (median 30 years) recipient age. Clinical results demonstrated that all eligible patients (n=34) engrafted. There were 3 early deaths that precluded engraftment. The 3rd day with a white count >1000 was considered the time to successful engraftment, which occurred at a median of 16 days (13 – 25) following graft infusion. All engrafted patients were considered eligible for evaluation of acute GvHD. Moderate to severe disease occurred in 5 patients (14.7%); severe in only 2 patients (5.8%). The 100-day mortality risk was 35%, consistent with published results in high-risk recipients of matched sibling donor transplant. Twenty-one (56.7%) patients were surviving with follow-up ranging between 111 to 370 days. Additional patient accrual is required to permit statistically meaningful analysis. Future analysis will seek to determine correlations between graft characteristics and clinical outcomes. We anticipate that an additional 40 patients will be entered on this study during the next year of funding.

New studies are planned to evaluate a more refined and controlled method of graft engineering. In preparation for a pilot clinical study, we plan to perform pre-clinical studies using samples from donor-recipient pairs that consent to participate. We would seek to determine whether there were demonstrable differences in graft composition when utilizing a positive-selection enrichment method versus a negative-selection depletion method. Therefore we would use marrow samples not to exceed 100 ml to compare $CD\text{-}34^+$ selection with $CD\text{-}2^+$ depletion. To do this using a minimum of materials, we will attempt to utilize the CellPro combination system. Ultimately, we will compare the characteristics of OKT3-depleted marrow grafts with the enriched or depleted graft products described above using the following analysis: 1.) flow cytometry to determine CD-2, CD-3, CD-5, CD-10, CD-19, CD-34, CD-45, CD-16, CD-56, CD-TCR $\alpha\beta$ and CD-TCR $\gamma\delta$ content, 2.) hematopoietic assays to determine CFU-GM, BFU-E, CFU-GEMM content, 3.) viability assessment by trypan blue exclusion and flow cytometric analysis of 7AAD, 4.) calculation of total recovery and dose of nucleated cells, $CD\text{-}34^+$ cells, $CD\text{-}3^+$ cells, $CD\text{-}5^+$ cells, 5.) calculation of log T-cell depletion, and 6.) assessment of procedure process to include time expenditure, complication rate and cost.

In addition, a pilot clinical trial is proposed to examine reduction of pre-transplant conditioning therapy in an effort to reduce toxicity. Although leukemic eradication is a primary goal of high-dose chemo-radiotherapy, successful donor engraftment is more dependent on recipient immunoablation. Therefore, we intend to explore the use of a highly potent polyclonal antibody

preparation to destroy recipient immune barriers. This product may also be studied for post-transplant in vivo depletion to enhance control of GvHD.

**3. Identify and enrich for lymphocyte subsets that ensure rapid immune reconstitution and thus, reduction in the risk of fatal infectious disease post-transplant.**

Amongst the patients entered into the above described clinical trial using haploidentical donors, nine patients were given additional donor lymphocytes at approximately 100 days post-transplant as an effort to expand a graft-versus-leukemia effect that might reduce a considerable risk for post-transplant relapse. One patient received cyropreserved donor cells while all others were given fresh, unmanipulated donor cells. Most patients received a T-cell dose of approximately $5x10^4$/kg and a few received a larger single dose or repeated doses. We sought to determine whether these patients might have experienced quicker immune recovery as a secondary benefit.

To evaluate immune reconstitution, we examined the absolute numbers and relative proportions of lymphocyte subsets in patients surviving at various time points after transplant. Due to the small number of data points, only preliminary comparisons can be made between patients who received donor lymphocytes in their graft and those who received a similar number of donor lymphyocytes in the marrow graft and additional donor lymphocytes approximately 3 months post-transplant. Currently, there are no obvious differences in lymphocyte recovery, as indicated in the graphs displayed on attachments 1 & 2. Additional patient accrual and longer follow-up is required to allow meaningful analysis and conclusion. As accrual continues in the next year of the grant, we hope to expand the observations and will include additional functional assays.

During the upcoming year, we also plan to explore methods to produce lymphocyte clones that are specifically targeted against viral antigens. Since invasive cytomegalovirus infection is associated with a > 80% fatality rate in bone marrow transplant recipients, we plan to use this virus as a model to develop virus-specific cytotoxic lymphocytes. We will take advantage of the fact that most CMV-specific cytotoxic lymphocytes recognize a single, structural CMV protein named pp65. We will isolate the pp65 protein from CMV and feed this protein to dendritic cells, which can stimulate the growth of CMV specific cytotoxic lymphocytes using donor peripheral blood cells. In due course, we hope to expand this technique to grow cytotoxic lymphocytes to other viral or other microbial antigens.

**4. Identify and manipulate lymphocyte subsets that can provide an anti-leukemic effect when required.**

We have followed two pathways in order to identify and manipulate cell populations which may either be directly involved in a graft versus leukemia (GvL) effect or participate in this reaction. We have identified a subpopulation of lymphocytes, the γδ T cells, which may be clinically relevant in the GvL effect. In addition, we have also grown and expanded dendritic cells from both $CD34^+$ normal bone marrow and from primary leukemic patient samples in order to use these to prime T cell populations to be cytotoxic T cells (CTL).

*γδ T cells demonstrate leukemic cell cytotoxicity in vitro and may be involved in the GvL response.*

Our group has previously reported observations suggesting that γδ T-cells might play a role in mediating a graft versus leukemia (GvL) effect after partially mismatched bone marrow transplantation when the donor cells were partially T-cell depleted using a monoclonal antibody, designated $T_{10}B_9$. This antibody appears to deplete T cells possessing the αβ T cell receptor (TCR). Another antibody called OKT3 is an anti-CD3 antibody which has also been used for pan-depleting T cells before grafting into the patient. Using either of these antibodies to achieve partial T cell depletion of the bone marrow graft, those patients who developed greater than 10% γδ T cells post-transplant after 100-150 days appear to demonstrate a longer disease-free survival than those who produce smaller numbers or no members of this T cell subset. These data implied that the γδ T cell subset might, in some way, be involved in the GvL response. However, studying the interactions between T cells and leukemic targets has proven difficult since γδ T-cells comprise a very small percentage of circulating T cells and are not easily expanded in vitro. We therefore developed a culture system whereby γδ T-cells, derived from bone marrow transplant donors, could be expanded in vitro under conditions simulating those found in partially mismatched transplant recipients. The rationale being that once sufficient numbers of cells can be generated in this way, their phenotypic and functional capacity could be studied and perhaps used for adoptive immunotherapy. To this end, donor mononuclear cells obtained from peripheral blood were depleted of αβ T-cells using anti-CD4 and anti-CD8 immunomagnetic microspheres. Peripheral blood leukemic blasts were obtained using a Ficoll gradient followed by Percoll separation to remove other hematopoietic cells and were irradiated immediately prior to plating. Donor and recipient blast cells were then co-cultured both in the presence and absence of immobilized δ1 monoclonal antibody, previously shown to stimulate the limited expansion of $\gamma\delta^+$ T-cells in vitro. Donor cells co-cultured with recipient blasts alone failed to undergo expansion. However, in the presence of immobilized antibody and blast cells, donor cells underwent an expansion characterized by a 1000-2000 fold increase in the number of $V\delta1^+$, γδ T-cells. By contrast, donor cells exposed only to monoclonal antibody, underwent similar expansion, but were found to be almost entirely $V\delta2^+$. These results suggest that populations of cells very similar to those observed clinically can be generated in vitro and used to study potential GvL responses. Preliminary cytotoxicity assays, have indicated that addition of γδ T cells from the donor to the respective patient leukemic cells, result in the killing of the leukemic cells. Present and future experiments will concentrate on obtaining similar results from more donor-patient pairs followed by in vivo assays to determine whether γδ T cells can kill patient leukemic cells in a pre-clinical NOD-SCID mouse model.

*Use of dendritic cells to expand γδ T cells*

In a second, but related avenue of research, we have investigated the possibility of using dendritic cells as antigen-presenting cells to expand γδ T cells for possible use in order to take advantage of the GvL effect and therefore reduce minimal residual disease. As mentioned in the previous section, T cells expressing the γδ TCR comprise a small subpopulation of lymphocytes. In contrast to the method described above for expanding γδ T cells, we have also explored the possibility of using dendritic cells (DC) and autologous $CD4^+$ T helper cells to expand the γδ T cell population. $CD4^+$ T-cells and γδ T-cells were purified from normal donor peripheral blood using cell sorting. Dendritic cells were generated with cytokines from autologous marrow $CD34^+$

cells or allogeneic $CD34^+$ leukemic cells from a patient with AML. Dendritic cells were purified using the CD11c-mediated Miltenyi immunomagnetic separation system. Sorted γδ T-cells were co-cultured with DC ± $CD4^+$ T-cells in medium containing 20 U/ml rhIL-2. Expansion (~150 fold) of γδ T-cells occurred after weekly stimulation with autologous DC alone or $CD4^+$ T-cells alone. A significantly larger expansion (~1500 fold) of γδ T-cells was achieved in cultures with weekly stimulation of both DC and $CD4^+$ cells. The proportion of γδ T-cells was 86% ± 10% in cultures harvested at day 21. Phenotypic analysis showed that expanded γδ T-cells were predominantly (>80%) oligoclonal for TCR v1 or v2 chain expression, but with little v9 chain co-expression. γδ T-cells could also be expanded by stimulation of allogeneic AML-derived DC and autologous $CD4^+$ T-cells. The γδ T-cells were cytotoxic against leukemic cell lines: K562, Molt-4, Raji, but not normal PHA-induced lymphoid blasts. Cytotoxicity of γδ T-cells against multiple myeloid leukemic cell lines (e.g. K562, KBM5 and KG1a), and primary leukemia was significantly up-regulated by incubation with anti-TCR antibody. Human γδ T-cells can, therefore, be successfully expanded and functionally activated using this type approach. Again, the next major stage of the research will concentrate on investigating whether the γδ T cell population can actually kill patient primary leukemic cells in vivo.

To this end, we have established a human-murine model utilizing the NOD-SCID mouse strain (mentioned above) to grow and expand primary patient leukemic cells. It is envisaged that the next year will bring significant information indicating, whether in fact, the γδ T cells can kill leukemic cells and under what conditions this reaction occurs.

## BIBLIOGRAPHY

1. Henslee-Downey PJ, Abhyankar SH, Parrish RS, Pati AR, Godder K, Neglia WJ, Goon-Johnson KS, Lee CG, and Gee AP: Use of partially mismatched related donors extends access to allogeneic marrow transplant. Blood 1997; 89(10):3864-3872.

2. Szydlo R, Goldman JM, Klein JP, Gale RP, Ash RC, Bach FH, Bradley BA, Caster JT, Flomenberg N, Gajewski JL, Gluckman E, Henslee-Downey PJ, Hows JM, Jacobsen N, Kolb H-J, Lowenberg B, Masaoka T, Rowlings PA, Sondel PM, van Bekkum DW, van Rood JJ, Vowels MR, Zhang MJ, and Horowitz MM. Results of allogeneic bone marrow transplants for leukemia using donors other than HLA-identical siblings. J Clin Oncol 1997; 15 (5): 1767-77.

3. Lamb LS, Robbins NF, Abhyankar SA, Joyce M, Stetler-Stevenson MA, Henslee-Downey PJ, Gee AP. Flow cytometric cell sorting combined with molecular chimerism analysis to detect minimal recurrent leukemia: good news and bad news. Bone Marrow Transplantation 1997 June; 19(11): pp1157 - 61.

4. Henslee-Downey PJ: Allogeneic Related Partially Mismatched Transplantation. *In* The Clinical Practice of Stem Cell Transplantation,, 2nd Edition. John Barrett and Jennifer Treleaven (eds);In press.

5. Cytomegalovirus in Bone Marrow Transplantation: Management of the High-Risk Patient. Eds: LeMaistre CF, Carabasi M, Henslee-Downey PJ, Trigg ME, mL MEDCOM Inc., Mount Vernon, New York.

6. Lamb LS, O'Hanlon TP, Henslee-Downey PJ, Hazlett L, Parrish RS, King SM, Washington L, and Gee AP: Comparative effects of T-cell depletion (TCD) with T10B9 or OKT3 on the recovery of peripheral blood lymphocytes (PBL) during the first year following bone marrow transplantation (BMT) from a partially mismatched related donor (PMRD). *Presented* in June 1997 at the International Society of Hematopoiesis and Graft Engineering, Bordeaux, France.

7. Henslee-Downey PJ, Lee CG, Hazlett LJ, Pati AR, Godder KT, Abhyankar SH, McGuirk JP, Christiansen NP, Parrish RS, Lamb LS, and Gee AP: Rare failure to engraft following haploidentical T-cell depleted marrow transplantation using enhanced host immunoablation and OKT3 graft purging. *Presented* in August 1997 at the International Society for Experimental Hematology, Cannes, France.

8. Ye Z, Gee AP, Lamb L, Harris G, Lee C, Reiser BY, Henslee-Downey PJ, Rich IN. Generation and purification of a large number of CD-11C+ dentritic cells from human marrow CD34+ cells for immunotherapy. Blood, 90 (10 Suppl 1) p 367a. *Presented* in December 1997 at the American Society of Hematology, San Diego, USA.

9. Lee C, Henslee-Downey PJ, Christiansen N, Godder K, Abhyankar S, Chiang KY, Brouillette MB, Turner M, Hazlett L, Gee A: Consistent prompt engraftment and low risk of acute graft-versus-host disease following haploidentical transplant. Accepted for presentation in June 1998 at the International Society of Hematopoiesis and Graft Engineering, Baltimore, Maryland, June 1998.

10. Godder, K, Abhyankar SA, Chiang KY, Christiansen NP, Hazlett LJ, Parrish RS, Bridges K, Goon-Johnson K, Henslee-Downey PJ, Absence of Peripheral Blasts and Younger Donor are Associated with Improved Outcome of Acute Leukemia Following Partially Mismatched Related Donor Bone Marrow Transplantation. Accepted for presentation in June 1998 at the 4th Meeting of the Transplantation in Children: Current Results and Controversies, Palm Beach, USA.

11. Musk P, Harris WG, Rich IN, Lee C, Henslee-Downey PJ, Lamb LS. Co-culture of T cell depleted donor cells and leukemic blast cells in the presence of anti-$\gamma\Delta$ antibody stimulates the invitro proliferation of $\gamma\Delta^{+}$T cells. *Submitted* 1998 to the International Society of Experimental Hematology, Vancouver, Canada.

12. Ye Z, Rich IN, Lamb LS, Harris WG, Lee C, Gee AP, Henslee-Downey PJ. Use of dendritic cells and CD4+ T cells to expand $\gamma\Delta^{+}$T cells for immunotherapy. *Submitted* 1998 to the International Society of Experimental Hematology, Vancouver, Canada.

13. Chiang KY, Ye Z, Rich IN, Henslee-Downey PJ. Parallel comparison of generation of dendritic cells from granulocyte colony-stimulating factor-mobilized bone marrow and

peripheral blood. *Submitted* 1998 to the International Society of Experimental Hematology, Vancouver, Canada.

14. Chiang KY, Lamb L, Harris G, Henslee-Downey PJ, Rich IN. Characteristics of hematopoietic cells in the bone marrow and peripheral blood during mobilization by granulocyte colony-stimulating factor. *Submitted* 1998 to the International Society of Experimental Hematology, Vancouver, Canada.

**Attachment 1.**

**Analysis of the proportion of peripheral blood lymphocytes in patients who received haploidentical HLA-mismatched allogeneic marrow grafts comparing those who did or did not receive additional donor lymphocytes post-transplant**

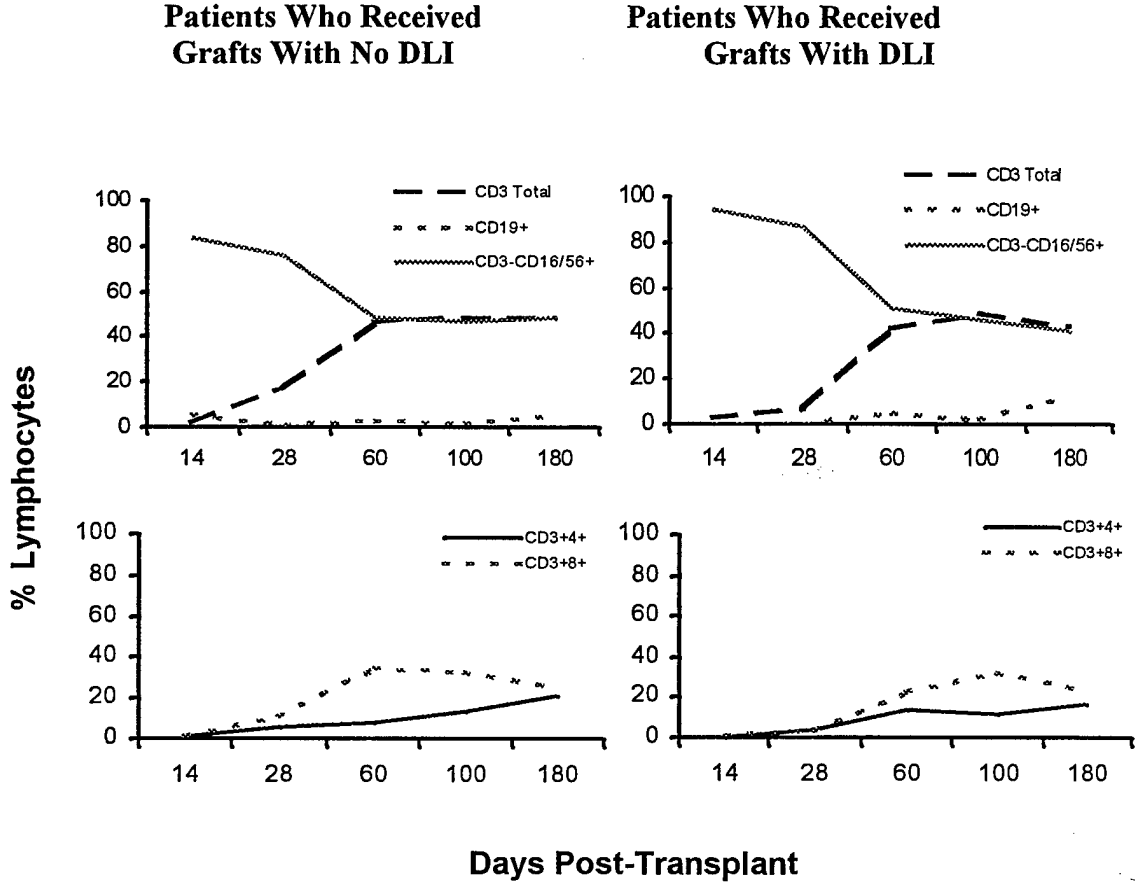

**Attachment 2.**

**Analysis of the absolute number of peripheral blood lymphocytes in patients who received haploidentical HLA-mismatched allogeneic marrow grafts comparing those who did or did not receive additional donor lymphocytes post-transplant**

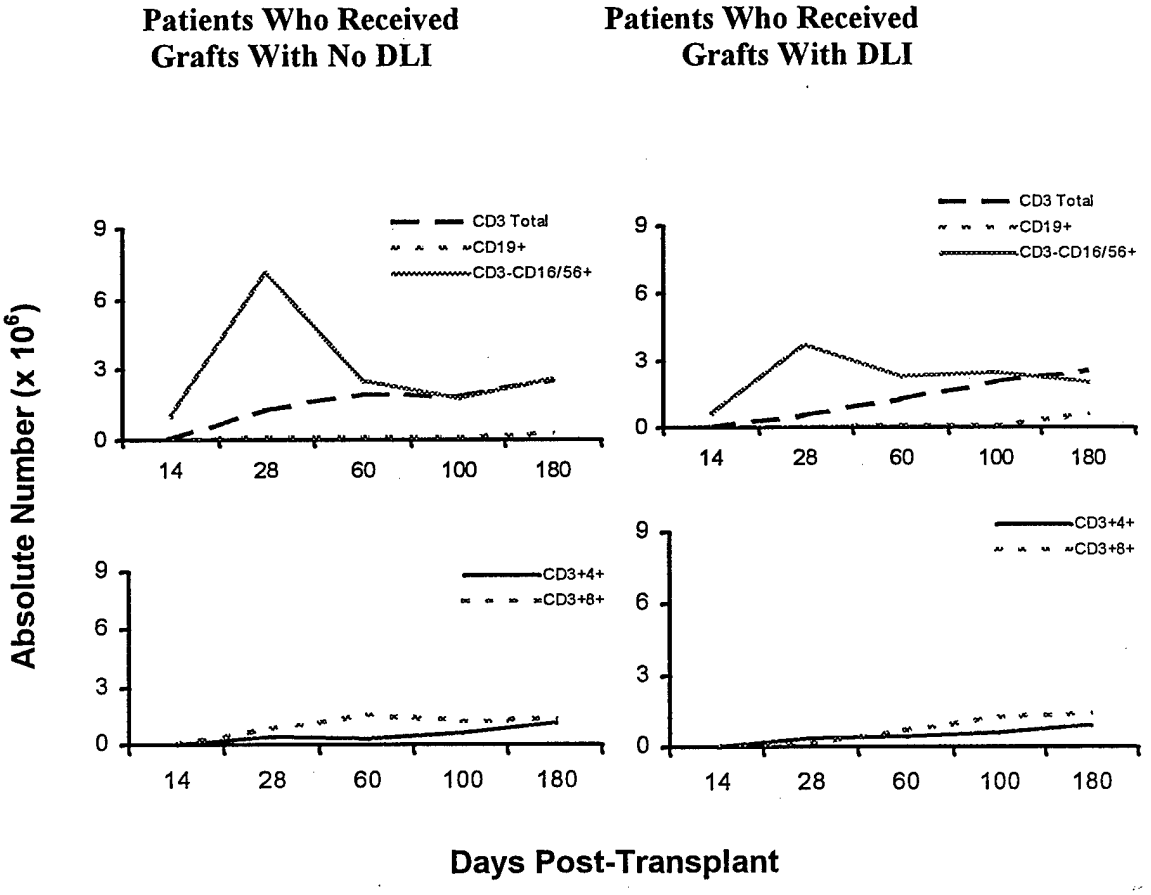

PART 53-FORMS 53.301-298

| REPORT DOCUMENTATION PAGE | Form Approved OMB No. 0704-0188 |
|---|---|



| 1. AGENCY USE ONLY *(Leave blank)* | 2. REPORT DATE | 3. REPORT TYPE AND DATES COVERED |
|---|---|---|
| | June 1, 1998 | Annual; April 1997 – April 1998 |

| 4. TITLE AND SUBTITLE | 5. FUNDING NUMBERS |
|---|---|
| Insure Access to Allogeneic Bone Marrow Transplantation | Grant # N00014-97-1-0806<br>PR # 97PRO632-00<br>PO Code 353<br>Disbusing Code N68892<br>AGO Code N66020<br>Cage Code 4B489 |
| 6. AUTHOR(S)<br>P. Jean Henslee-Downey, M.D. | |
| 7. PERFORMING ORGANIZATION NAME(S) AND ADDRESS(ES)<br>University of South Carolina, Columbia, SC<br>Palmetto Richland Memorial Hospital, Columbia, SC | 8. PERFORMING ORGANIZATION REPORT NUMBER<br>N00014-97-1-0806-1 |
| 9. SPONSORING / MONITORING AGENCY NAME(S) AND ADDRESS(ES)<br>ONR | 10. SPONSORING / MONITORING AGENCY REPORT NUMBER<br>ONR |

11. SUPPLEMENTARY NOTES
Prepared in coordination with University Research Initiative Program for Combat Readiness

| 12a. DISTRIBUTION / AVAILABILITY STATEMENT | 12b. DISTRIBUTION CODE |
|---|---|
| APPROVED FOR PUBLIC RELEASE | |

13. ABSTRACT *(Maximum 200 words)*

Work in this project is highlighted by advancements in understanding the cellular components and process of hematopoiesis and achievements in establishing engraftment across major-HLA barriers to allogeneic transplant. We have utilized a new human stem cell marker called AC133 to further delineate a subset of CD34+ cells that may represent a highly primitive stem cell progenitor. In addition, we have made observations regarding the lapse of time from stimulation of hematopoietic progenitors in the marrow cavity through to migration to the peripheral blood compartment. In clinical studies using haploidentical HLA-mismatched related donors, we have made transplant immediately available to patients who did not have matched sibling or unrelated donor options. Methods used for manipulated of the marrow graft and therapeutics to modulate the immune system prior to and following transplant has resulted in a 100% engraftment rate and a 15% risk of moderate to severe acute graft-versus-host disease. All patients transplanted in early disease status continue to survive. Still most patients underwent transplant for advanced disease, despite readily available donors. Nonetheless, the overall survival for the patient cohort studied during this grant period was 56.7%, which appears better than published results using HLA-matched donors for similar types of patients.

| 14. SUBJECT TERMS | 15. NUMBER OF PAGES |
|---|---|
| Chemical and Biological Warfare, Target Acquisition, Anti-Submarine, Combat Medicine, Biodeterioration, Command Control and Communication | 14 |
| | 16. PRICE CODE |

| 17. SECURITY CLASSIFICATION OF REPORT | 18. SECURITY CLASSIFICATION OF THIS PAGE | 19. SECURITY CLASSIFICATION OF ABSTRACT | 20. LIMITATION OF ABSTRACT |
|---|---|---|---|
| UNCLASSIFIED | UNCLASSIFIED | UNCLASSIFIED | 200 words |

# Tissue Engineered Cartilage and Advanced Bioadhesives for the Rapid Healing of Combat and Training Injuries to Bone

Brian Genge

Department of Chemistry and Biochemistry
University of South Carolina
Columbia, SC 29208

Tel: (803) 777-6470
Fax: (803) 777-9521
Email: genge@psc.sc.edu

## Section 4-3: Tissue-Engineered Cartilage and Advanced Bioadhesives for the Accelerated Healing of Combat and Training Injuries to Bone

Brian Genge, Licia Wu, Glenn Sauer, and Roy Wuthier

## 1. ABSTRACT

Chondrocytes in fracture callous play a critical role in the process of repairing broken bones. Acceleration of growth, differentiation and mineralization of chondrocytes is key to developing effective therapies for more rapid healing and fracture repair of battlefield injuries to bone. It is known that expression of local growth factors plays a pivotal role in normal development and calcification of fracture-callous cartilage. Our ability to grow mineralizing chondrocyte cultures provides an outstanding opportunity to create a biomaterial that enables the expedited healing and repair of bone injuries. Using formulations of specific cytokines and growth factors, our chondrocyte cultures can be tissue-engineered to produce a matrix-mineral composite that may be implanted into the injury sites. We also propose to develop an advanced synthetic bioadhesive for immediate, in the field repair of fractured bone. We have discovered several distinct biochemical components crucial to bone mineral formation and have developed a proprietary process enabling a unique recombination of the purified components. This material can be formulated to harden with 2 hours and may be used to provide a bone-like weld in fractured bone to stabilize the injury. We anticipate that these novel biomaterials could tremendously speed the bone healing process.

## 2. FORWARD

The total amount of this award is $900,000 for the period 6-1-97 to 5-31-99.

The long-term design goals of this grant is to provide rapid stabilization of bone fractures, even to weight bearing bones, and to aid and accelerate the normal cell-mediated healing process. During this past grant period, we have succeeded in developing formulations of self-hardening biocompatible bone pastes that may be useful for first aid to combat bone injuries. Accomplishments for this past year, as described in the body of the report, include the following:

- Development of a thermomechanical process for the solid state preparation of a highly reactive form of α-tricalcium phosphate powders.
- Synthesis and analysis of various formulations of bone cement powders using highly reactive α-tricalcium phosphate.
- Devised a regimen for converting the bone cement powder into a formable, self-setting paste.
- Development of a biocompatible catalyst that stimulates the hardening reaction of the bone paste in serum.
- Design and implementation of a system for testing the mechanical and physico-chemical properties of the bone cement.
- Discovery of a series of polymers that augment the compressive strength of our bone cement.
- Achieved a formulation that has the highest compressive strength of any calcium phosphate based biomaterial reported in the scientific or patent literature.
- Demonstrated that the chemical composition and architecture of the bone cement is compatible with living cells.

## 3. DESCRIPTION OF ATTACHMENTS and APPENDICES

None.

# 4. INTRODUCTION AND PROGRESS REPORT

## A. Mechanism of Chondrocyte-Mediated Bone Fracture Repair

Bone is a composite material made up of organic and inorganic components. The inorganic component of bone consists mostly of calcium and phosphate. This mineral phase of bone is a poorly crystalline analogue of carbonated hydroxyapatite [$Ca_{10}(PO_4)_6(OH)_2$]. Calcifying chondrocytes function in the repair of bone fractures by elaborating an extracellular matrix and subsequently depositing calcium ($Ca^{2+}$) and inorganic phosphate (Pi) during mineral formation. Cells are central to the calcification process that occurs during the healing of fractured bones. Callus chondrocytes pass through a sequence of developmental stages that parallels that found in the epiphyseal growth plate of growing long bones with distinct proliferative and hypertrophic phenotypes being expressed. It is within the hypertrophic region of the growth plate or callus that matrix mineralization ensues.

During the calcification process, chondrocytes accumulate large amounts of $Ca^{2+}$ and Pi prior to the onset of extracellular mineralization. As the cytosolic $Ca^{2+}$ levels increase in the chondrocyte, a cascade of events ensue, leading to the formation of cell-derived membrane-enclosed microstructures termed matrix vesicles (MV). Matrix vesicles are critical to the bone healing process because they are the initial site of mineral deposition in the extracellular matrix. The nascent matrix vesicles are preloaded with large amounts of $Ca^{2+}$ and Pi, and a complex consisting of $Ca^{2+}$, Pi, and several key proteins and lipids. Upon incubation of isolated MV in synthetic cartilage lymph, there is an initial rapid increase in the amount of amorphous calcium phosphate, and a decline in the proportion of the complex. With further incubation, the amorphous calcium phosphate phase is converted into poorly crystalline hydroxyapatite. The interaction of these key components in MV appears to provide the critical driving force for biomineralization that occurs during normal bone growth and healing fracture repair.

## B. Using a Biomimetic Approach to Synthesize Advanced Materials For Bone Repair

Biomimetics is the science of copying complex natural structures such as silk or bone for the purpose of producing useful synthetic analogues. In order to successfully apply biomimetics, a good understanding of the structure to be copied and the mechanism of its *de novo* formation is necessary. Biostructures such as bone have a mineral composition, an organic matrix composition, and a higher order organization of the mineral ions ($Ca^{2+}$ and Pi) on the matrix. Since the early discovery of the similarity between the mineral phase of bone and hydroxyapatite there has been increasing interest in using calcium phosphates as biomaterials. Since isolated matrix vesicles initiate biomineralization in healing fracture callus by acquiring large amounts of using $Ca^{2+}$ and Pi, they make an excellent model on which to base the fabrication of clinically useful biomaterials for stimulating bone healing. The development of our biocements for bone repair is based on our collective knowledge and understanding of the mechanism of matrix vesicle mediated calcification.

## C. Development of a Biomaterial For the Rapid Repair of Battlefield Injuries to Bone

We are developing a biomaterial that may be used in the field to repair bone fractures. Our goal is to produce a biocomposite with the following characteristics (1): 1.) Ability to be surgically implanted into the injury site by injection. 2.) Once implanted, it will stabilize the fracture within a short period of time. 3.) The composite material will cure to form a mineral phase similar to bone. 4.) After the biomaterial has stabilized the fracture, it will be soluble enough to be resorbed and replaced by the normal activity of osteoclasts in living bone. 5.) The biomaterial may be formulated to contain agents that promote and accelerate the normal cell mediated healing process.

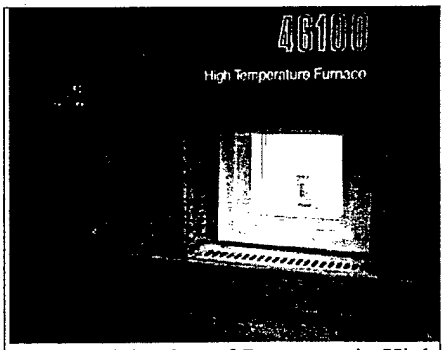


**Fig 1.** Calcination of Reactants in High Temperature Furnace Heated by Super Kanthal Elements.

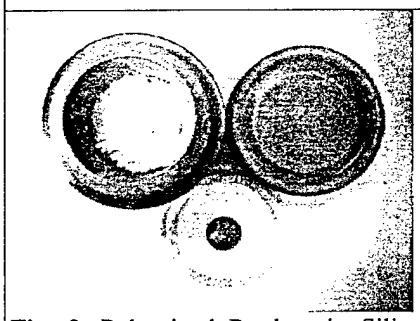

**Fig. 2.** Pulverized Product in Silicon Nitride Ball and Jar.

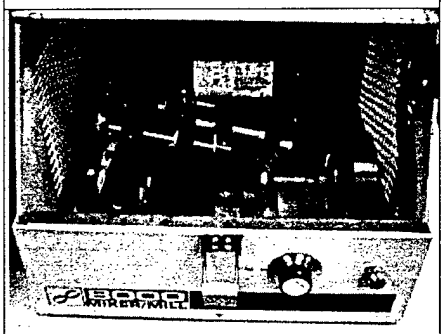

**Fig. 3.** Communition and Blending of the Cement Powder Using a SPEX 8000 Mixer/Mill.

**Fig. 4.** Finely Ground Cement Product in Polished Agate Mortar

## PREPARATION OF REACTIVE POWDERS FOR USE IN BIOMIMETIC BONE CEMENT

Since bone is mostly calcium and phosphate, biomaterials based on these mineral ions have attracted much attention for potential use in dental and orthopedic applications. In fact, experience with calcium and phosphate-based implants for the replacement of skeletal tissue has existed for many years. However, most of the implants have been in the form of prefabricated thermally processed hydroxyapatite blocks or granules. These preformed materials have several drawbacks (2); the sintered blocks have a limited ability or conform to skeletal defects, while the granules lack structural integrity and stability because the particles do not bond together. Since these products are produced by high temperature calcination, they lack carbonate and their resultant ceramic properties make them generally nonresorbable in biological systems. Hence, there exists a need to develop a calcium and phosphate-based cement that is resorbable, biocompatible, and can transform over time to the carbonated, poorly crystalline hydroxyapatite-like mineral phase of bone.

Early studies by Monma (3) showed that α-tricalcium phosphate (α-TCP) can be hydrolyzed in water at 60-100 °C to form a calcium deficient hydroxyapatite. On the other hand, the low temperature form of tricalcium phosphate, (β-TCP) is almost inert under the same conditions. Recently, it has become possible to develop resorbable calcium phosphate hydraulic cements based on α-TCP (1). However, the consistent preparation of highly pure α-TCP is difficult. We, and others have found that the synthesis conditions of the quantitative preparation of α-TCP is affected by the nature of the starting material, the Ca/P atomic ratio of the mixture, the calcination temperature, the sintering time, the cooling rate, the particle size of the reactants, and the grinding medium used to prepare the reactants (4). This past funding period, we have developed a proprietary solid-state process (Figs. 1-4) that enables the consistent preparation of doped, highly reactive, α-TCP powders (Fig. 4). These powders comprise the major chemical ingredient in our biomimetic bone cement. Using this α-TCP, we have developed a formulation that produces a putty-like paste that remains formable at room temperature then sets quickly at body temperature. After hardening, the material appears to have a stable chemical structure that may be similar to the poorly crystalline mineral phase of bone (Fig. 13).

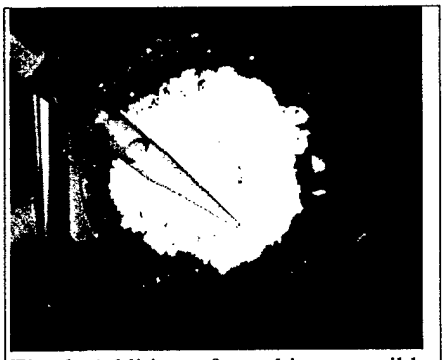

**Fig 6.** Addition of our biocompatible, aqueous-based buffer to our bone cement formulation.

**Fig. 7.** Mixing of the bone cement powder and liquid rapidly forms a sticky paste.


**Fig. 8.** Rapid hardening and curing of the bone cement continues even when it is immersed in serum.

**Fig. 9.** Compression strength testing of our serum-cured bone cement

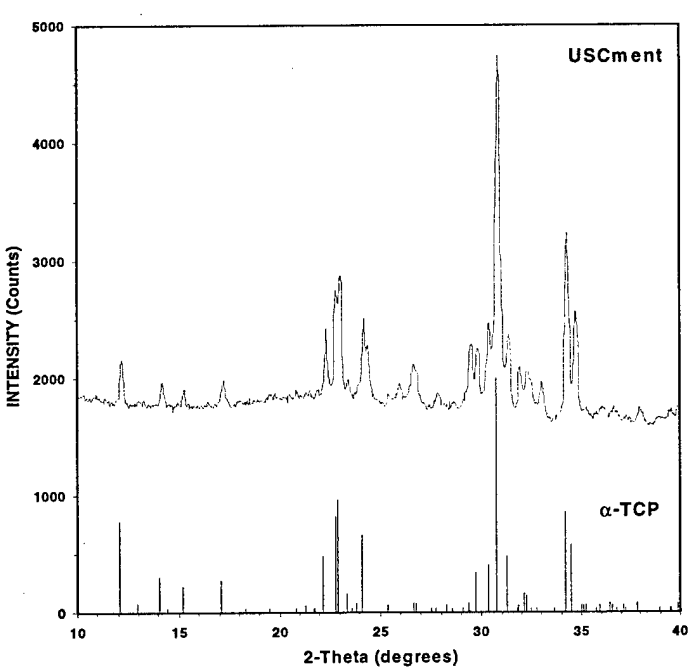


**Figure 5. Powder X-ray Diffaction of USCment.** X-ray diffraction pattern of USCment was obtained in the Department of Chemistry and Biochemistry, University of South Carolina by Drs. Claridge and Zur Loye using a Rigaku X-Ray Diffractometer. Note the similarity in the diffraction peaks of USCment and standardized α-TCP.

## FORMULATION AND TESTING OF OUR BIOMIMETIC BONE CEMENT

The basic composition of our biomimetic bone cement is prepared by combining the reactive α-TCP powder with other calcium, phosphate and carbonate compounds. An organic polymer is also added later to impart a thixotropic property to the cement paste. We have termed this bone cement mixture "USCment". The X-ray diffraction pattern of USCment shows its similarity to the calculated diffractogram of standardized α-TCP (Fig. 5).

The powdered formulation (Fig. 6) is mixed with a biocompatible buffer in an agate mortar to make a sticky paste (Fig. 7). The paste is spatulated into nylon molds to fill 9.8 mm cylindrical holes. To simulate physiological conditions that may exist in the microenvironment of the broken bone, the molded paste is allowed to briefly set in a 37°C, 100% humid atmosphere. After 15 minutes, the hardened pellets are removed from the molds and immediately immersed in serum at 37°C (Fig. 8). At various times, the bone cement pellets are removed from the serum and tested for compressive strength (Fig. 9).

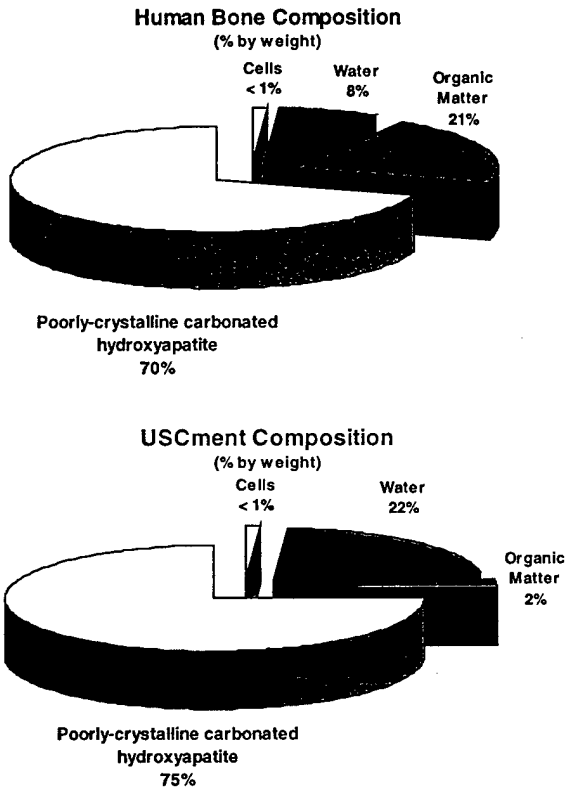


**Fig. 10.** Comparison of the composition of human bone and USCment.

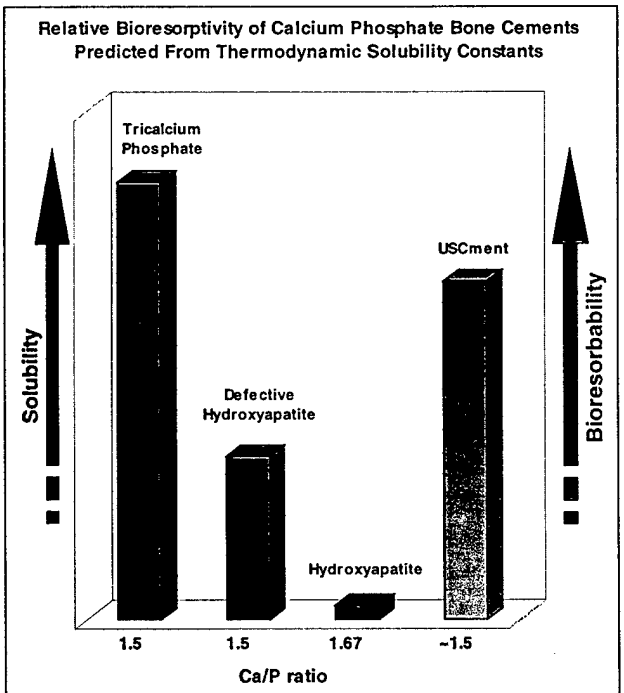


**Fig. 11.** Predicted relative bioresorptivity of USCment.

As previously stated, we are using a biomimetic approach to help guide the development of our biomaterials to enhance fracture healing. To successfully parlay the potential of biomimetics, it is important to know and understand the structure to be copied; i.e. bone. The composition of human bone has long been known to consist mostly of calcium and phosphate. Our cement formulation is chemically similar to bone. Compared to human bone, our current cement formulation matures in serum to a more hydrated composite (Fig. 10). We predict that formulations that mature to a highly hydrated biomaterial will be more rapidly resorbed in the body by osteoclastic activity. More rapid bioresorption of the bone cement should expedite its rate of replacement by native bone. A synthetic bone substitute that is fully resorbed and replaced by host bone is desirable in order to restore original load bearing and structural properties specific to the particular damaged bone. To date, calcium phosphate materials have demonstrated only partial resorbability *in vivo* with significant amounts of the starting material being found at the implant site even after time periods of longer than one year (5). Our bone cement can harden and cure in an aqueous system (serum), yet its carefully designed chemical formulation predicts that it will be a fully resorbable bone cement (Fig. 11). Our long-term design goal of the formulation is to emulate the composition of human bone by increasing the amount of bioorganic material in the cement.

## CHARACTERIZATION OF OUR BIOMIMETIC BONE CEMENT

Our calcium phosphate bone cement has self-hardening capability. This setting reaction of calcium phosphate cements appears to occur through dissolution of the calcium phosphate particles and reprecipitation as a poorly crystalline hydroxyapatite (8). Recent scanning electron microscopy (SEM) pictures of fracture surfaces of our cement at different times show

**Fig. 12.** SEM pictures showing the evolution of the microstructure of the activated bone cement after various immersion times in serum.

**Time = 0 hour**

**Time = 0.25 hour**

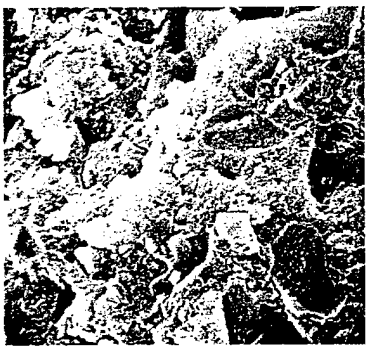

**Time = 4 hours**

**Time = 24 hours**

the progress of the reaction and the evolution of the microstructure (Fig. 12). Samples were fixed with glutaraldehyde, dehydrated in ethanol, and critical point dried. Specimens were then coated with gold and SEM observations were performed using a Hitachi S-2500 Delta SEM at an accelerating voltage of 15 kV. Magnifications are 5000X. The cement powder initially exhibits a loose granular form (Fig. 12). After just 15 minutes, the smaller cement particles appear to have dissolved and reprecipitated, filling in the gaps with a semi-porous material. By 24 hours, the larger particles have become surrounded by a more compact calcium deficient hydroxyapatite.

The chemical reaction that occurs during the setting of our biomimetic bone cement in serum was also monitored using infrared spectroscopy. Fourier transform infrared spectroscopy was performed using dried USCment (1 mg) incorporated into KBr (300 mg) pellets under vacuum at 12,000 psi. The pellets were examined by averaging 32 scans over a range of 4000-400 $cm^{-1}$ using a Perkin Elmer 1600 spectrometer operated at 4 $cm^{-1}$ resolution. These spectra indicate the changes that occur during the hardening reaction (Fig. 13). After 24 hours, the absorptions bands at 1035 $cm^{-1}$ and 605 $cm^{-1}$ become sharper and more pronounced, indicating the formation of calcium deficient hydroxyapatite (8). A large band appearing at ~3415 $cm^{-1}$ suggests that water is absorbed during the hardening reaction.

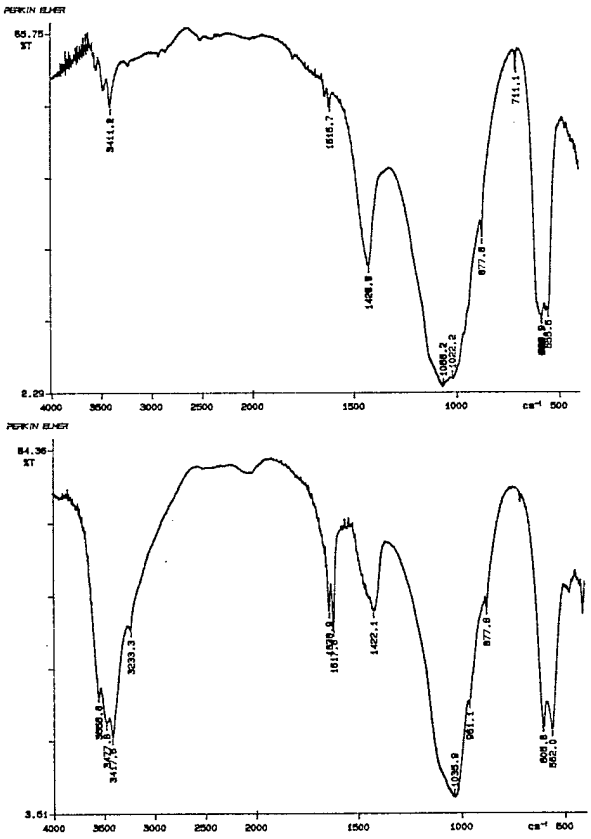


**Fig. 13** FTIR spectra of USCment.

**Time = 0 h**

**Time = 24 h (in serum)**

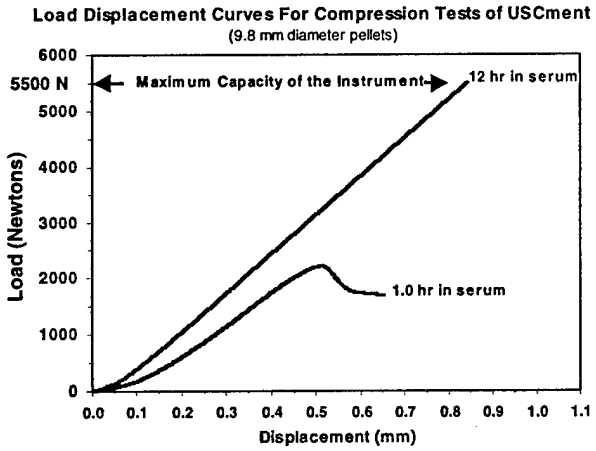


**Fig. 14.** Load displacement curves for compression tests of USCment hardened in serum at 37°C.

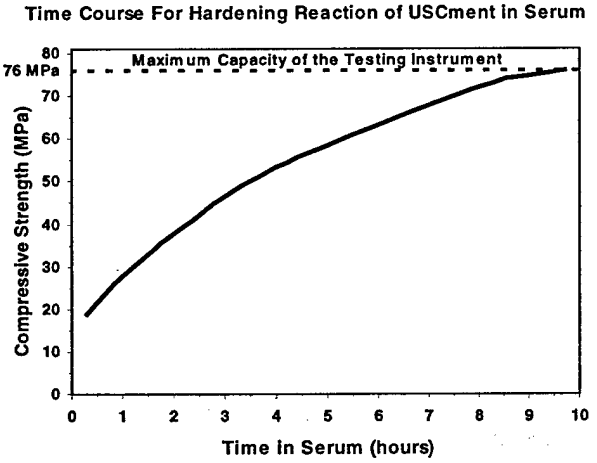


**Fig. 15.** Time course study shows compressive strength of USCment increases when incubated in serum.

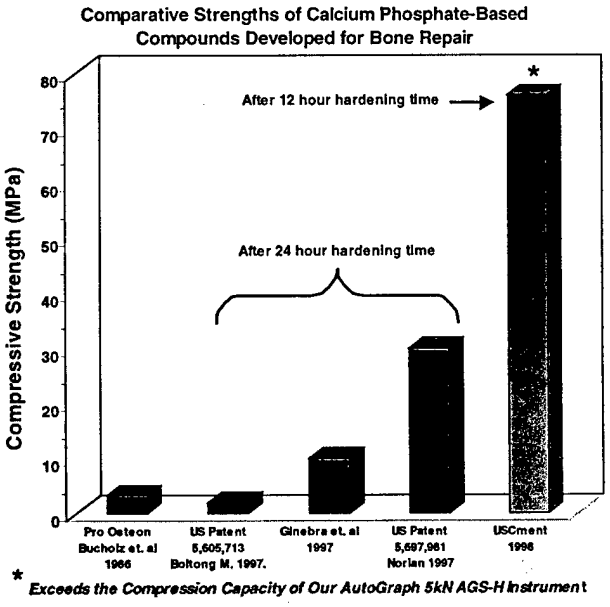


**Fig. 16.** Compressive strength comparison of USCment to other calcium phosphate biomaterials used in bone repair.

To date, calcium and phosphate based biomaterials have been used only to aid in the repair of non-weight bearing fractures and boney defects. This is primarily because of their relatively low compressive strength compared to cortical bone. We have conducted studies of the reaction responsible for the setting of our bone cement using X-ray diffraction, FTIR, and SEM. These studies have lead to improved biochemical and physical properties compared to other cement formulations. **For example, this past grant period, we have developed a biomimetic bone cement that can attain a compressive strength of over 76 megapascals (Mpa) in just 12 hours, even when it is immersed in serum.** (Figs. 14-16). In fact, after 12 hours of serum curing, the strength of our bone cement pellets exceeds the force capacity of our compression testing instrument (Figs. 14-16). Other calcium phosphate biomaterials (6-10) have been shown to have only about 10-60% of this strength, even after 24 hours (Fig. 16).

One feature of an ideal bone cement is to have a surface with the necessary physical and chemical composition to support the attachment, spreading, division and differentiation of osteoprogenitor cells so that remodeling of bone can take place (5). Our cement appears to have the requisite chemical composition and architecture to support living osteoprogenitor cells such as a calcifying chondrocytes as shown in Fig. 17.

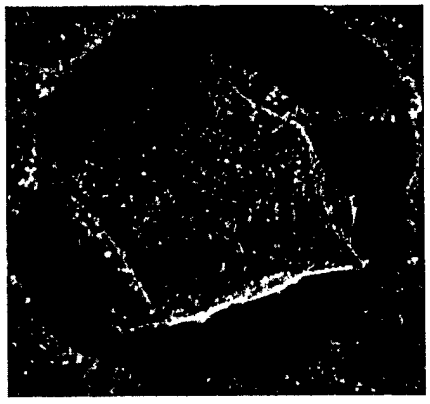

**Fig. 17.** SEM of a living chondrocyte residing in a micropore and attached through cell processes to our bone cement.

## RESEARCH PERSONEL ON THE PROJECT

| Name | Degree | Year |
|---|---|---|
| Genge, Brian | Ph.D. | 1989 |
| Wu, Licia N.Y. | Ph.D. | 1973 |
| Sauer, Glenn | Ph.D. | 1986 |
| Wuthier, Roy | Ph.D. | 1960 |
| Lu., Min | M.S. | 1997 |

## 5. LIST OF INVENTIONS None

## 6. BIBLIOGRAPHY

1. Constanz, B., Ison, I., Fulmer, M., Poser, R., Smith, S., VanWagoner, M., Ross, J., Goldstein, S., Jupiter, J., Rosenthal, D. Skeletal repair by in situ formation of the mineral phase of bone. *Science* **264:**1796-1799, 1995.

2. American Dental Association Health Foundation, Chow, L. and Takagi, S. Self-setting calcium phosphate cements and methods for preparing and using them. *United States Patent* **# 5525148**, Issued 1996.

3. Monma, H., Kanazawa, T. The hydration of α-tricalcium phosphate. *Yogyo-Kyokai-Shi* **84:** 209-213, 1976.

4. Bohner, M., Lemaitre, J., Legrand, A., d'Espinose, J., Caillerie, d., Belgrand, P. Synthesis, X-ray diffraction and solid-state $^{31}P$ magic angle spinning NMR study of α-tricalcium othophosphate. *J. Materials Science: Materials in Medicine* **7:** 457-463, 1996

5. Einhorn, T. Current concepts review: Enhancement of fracture-healing. *J. Bone and Joint Surgery* **77:** 940-956, 1995.

6. Bucholz, R., Carlton, R., Holmes, R. Interporous hydroxyapatite as a bone graft substituted in tibial plateau fractures. *Clinical Orthopedics* **240:** 53-62, 1989.

7. Boltong, M. Process for the preparation of calcium phosphate cements and its application as bio-materials. *United States Patent* **# 5605713,** Issued 1997.

8. Ginebra MP, Fernandez E, Maeyer EP, Verbeeck, RH, Boltong MG, Ginebra FM, Driessens FC, Planell JA: Setting Reaction and Hardening of an Apatitic Calcium Phosphate Cement. *J. Dental Research* **76:** 905-912, 1997.

9. Norian Corporation, Constanz et al. Method for repairing bone. *United States Patent* # **5697981**, Issued 1997.

10. Cherng A., Takagi S., Chow L. Effects of hydroxypropyl methylcellulose and other gelling agents on the handling properties of calcium phosphate cement. *J. Biomedical Material Research* **35**(3):273-277,1997.

PART 53-FORMS 53.301-298

# REPORT DOCUMENTATION PAGE

Form Approved
OMB No. 0704-0188



| 1. AGENCY USE ONLY *(Leave blank)* | 2. REPORT DATE | 3. REPORT TYPE AND DATES COVERED |
|---|---|---|
| | June 1, 1998 | ANNUAL |

| 4. TITLE AND SUBTITLE | 5. FUNDING NUMBERS |
|---|---|
| Tissue-Engineered Cartilage and Advanced Bioadhesives for the Rapid Healing of Combat and Training Injuries to Bone | Grant Number N00014-97-1-0806<br>PR Number 97PR06312-00<br>PO Code 353<br>Disbursing Code N68892<br>AGO Code N66020<br>Cage Code 4B489 |
| 6. AUTHOR(S)<br>Genge, Brian | |
| 7. PERFORMING ORGANIZATION NAME(S) AND ADDRESS(ES)<br>University of South Carolina | 8. PERFORMING ORGANIZATION REPORT NUMBER<br>N00014-97-1-0806-1 |
| 9. SPONSORING / MONITORING AGENCY NAME(S) AND ADDRESS(ES)<br>ONR | 10. SPONSORING / MONITORING AGENCY REPORT NUMBER ONR |

11. SUPPLEMENTARY NOTES
Prepared in coordination with University Research Initiative Program for Combat Readiness

| 12a. DISTRIBUTION / AVAILABILITY STATEMENT | 12b. DISTRIBUTION CODE |
|---|---|
| APPROVED FOR PUBLIC RELEASE | |

13. ABSTRACT *(Maximum 200 words)*

Chondrocytes in fracture callous play a critical role in the process of repairing broken bones. Acceleration of growth, differentiation and mineralization of chondrocytes is key to developing effective therapies for more rapid healing and fracture repair of battlefield injuries to bone. It is known that expression of local growth factors plays a pivotal role in normal development and calcification of fracture-callous cartilage. Our ability to grow mineralizing chondrocyte cultures provides an outstanding opportunity to create a biomaterial that enables the expedited healing and repair of bone injuries. Using formulations of specific cytokines and growth factors, our chondrocyte cultures can be tissue-engineered to produce a matrix-mineral composite that may be implanted into the injury sites. We also propose to develop an advanced synthetic bioadhesive for immediate, in the field repair of fractured bone. We have discovered several distinct biochemical components crucial to bone mineral formation and have developed a proprietary process enabling a unique recombination of the purified components. This material can be formulated to harden with 2 hours and may be used to provide a bone-like weld in fractured bone to stabilize the injury. We anticipate that these novel biomaterials could tremendously speed the bone healing process.

| 14. SUBJECT TERMS | 15. NUMBER OF PAGES |
|---|---|
| Chemical and Biological Warfare, Target Acquisition, Anti-Submarine, Combat Medicine, Biodeterioration, and Command Control and Communication. | |
| | 16. PRICE CODE |

| 17. SECURITY CLASSIFICATION OF REPORT | 18. SECURITY CLASSIFICATION OF THIS PAGE | 19. SECURITY CLASSIFICATION OF ABSTRACT | 20. LIMITATION OF ABSTRACT |
|---|---|---|---|
| UNCLASSIFIED | UNCLASSIFIED | UNCLASSIFIED | 200 words |

# SECTION 5: ANTI-SUBMARINE WARFARE

Office of Naval Research: N00014-97-1-0806
University Research Initiative Program for Combat Readiness

# Wavelet-Based Algorithms for Acoustic and Non-Acoustic Antisubmarine Warfare

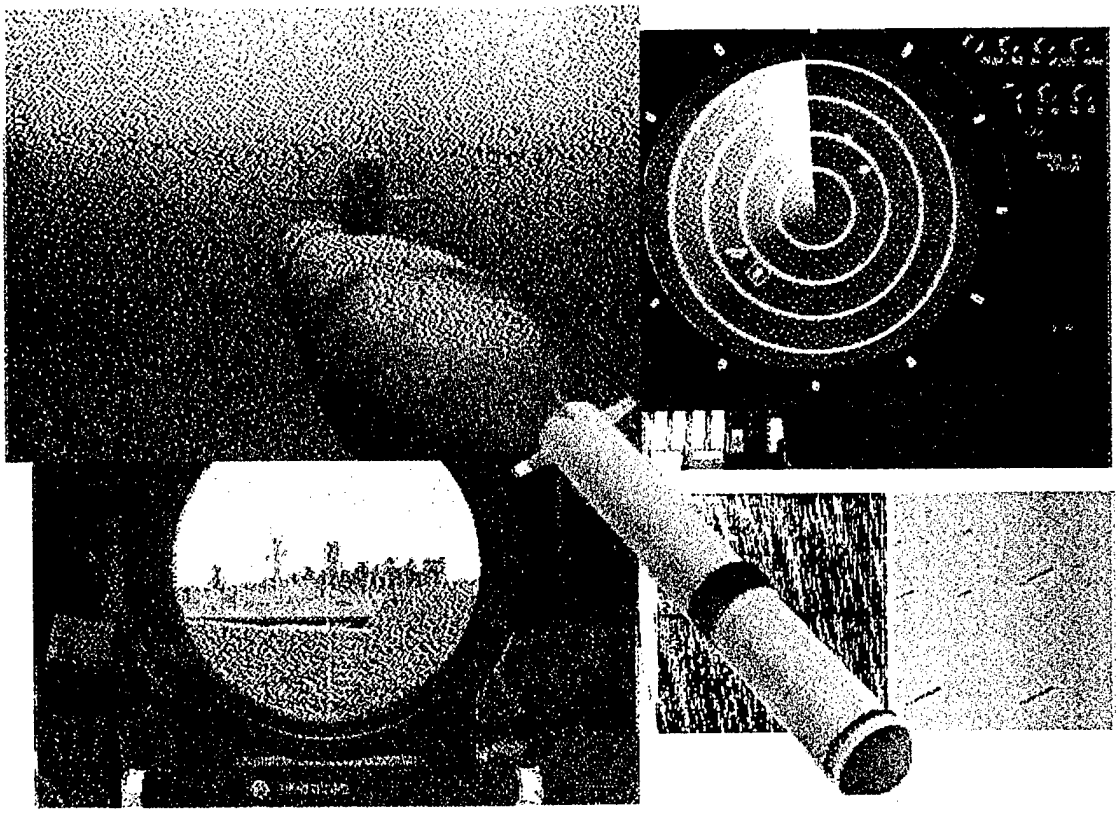

**PI: Terry Huntsberger, PhD**
**Intelligent Systems Laboratory**
**Department of Computer Science**
**University of South Carolina**
**Columbia, SC 29208**
**Ph: (803) 777-2404**
**FAX: (803) 777-3767**
**terry@cs.sc.edu**

**co-PI: Björn Jawerth, PhD**
**Industrial Mathematics Initiative**
**Department of Mathematics**
**University of South Carolina**
**Columbia, SC 29208**
**Ph: (803) 777-6218**
**FAX: (803) 777-3783**
**bj@math.sc.edu**

# Section 5-1: Wavelet-Based Algorithms for Acoustic/Nonacoustic Antisubmarine Warfare

Terry Huntsberger, Björn Jawerth

## 1. ABSTRACT

The two main detection methods used in tactical antisubmarine warfare (ASW) are acoustic (sound) and nonacoustic. For the acoustic studies we are exploiting the similarity between the Helmholtz equation and Laplace's equation for the development of fast solver techniques for multi-line towed sonar array systems currently fielded by the Navy. Our work in non-acoustic ASW methods has concentrated on the study of boundary value problems for Maxwell's equations on arbitrary nonsmooth domains, in arbitrary dimensions and on the detection and analysis of submarine wakes from low grazing angle (LOGAN) radar data.

## 2. FORWARD

This project was funded for $525,000 for the period June 1, 1997 to May 31, 2000. We have decided to use the SKY Computer system with 4 PowerPCs/36 SHARC DSP chips for the implementation of the algorithms. This decision was made after consideration of Navy needs and examination of the algorithms. The system has been ordered and is to be shipped May 1, 1998. The original Year 1 Milestone was the port of our algorithms to the Intel Paragon system, which was postponed due to system downtime. Accomplishments for the past year, as described in the body of the report, include:

- Developed efficient versions of the integral operators present in PDEs associated with EM scattering.
- Developed recognition techniques for detection of submarine wakes in the wavelet coefficients from LOGAN radar data.
- Developed efficient algorithms for Lattice Boltzmann analysis of flow for surface extraction.
- Developed a hybrid LDB/wavelet packet method for analysis of large format sonar images.
- Developed an algorithm for recovery of surface using multiple sonar sensor returns.
- Developed an affine, morphological Gallilean invariant algorithm for recovery of scale and acceleration of objects.

## 3. DESCRIPTION of ATTACHMENTS and APPENDICES

None

## 4. BODY

### 4a. Statement of Problem

The Navy has recently developed a new lightweight directional hydrophone suitable for deployment in large numbers from aircraft. This is coupled with the multi--line towed sonar array system which has long-range capabilities and much wider field coverage. The images that are assembled from the towed sonar arrays can be efficiently processed and analyzed in the wavelet domain. In addition, operations such as image enhancement can be performed very efficiently in the wavelet coefficient space.

The results of preliminary studies demonstrate that appropriate layer potential singular integral operators can be used to obtain solutions to the time independent, or reduced, Maxwell's equations in three dimensions. Techniques centered around the second generation wavelets seem to be

flexible enough to adapt to the efficient numerical treatment of full time dependent scattering problems even on nonsmooth domains. During the first phase of the project we have concentrated on the characterization of acoustic and electromagnetic scattering from surfaces and objects.

## 4b. Summary of Results

### Electromagnetic Scattering from Non-Smooth Domains

Our group has concentrated on the study of boundary value problems for Maxwell's equations on arbitrary nonsmooth domains, in arbitrary dimensions. The results of preliminary studies demonstrate that appropriate layer potential singular integral operators can be used to obtain solutions to the time independent, or reduced, Maxwell's equations in three dimensions. Techniques centered around the second generation wavelets seem to be flexible enough to adapt to the efficient numerical treatment of full time dependent scattering problems even on nonsmooth domains.

### Wavelet Analysis of LOGAN Radar Data

We have been investigating the wavelet analysis of low grazing angle (LOGAN) radar data. The range-time-intensity (RTI) plots can be treated as a surface and deformations of the surface from the sea clutter state could indicate the presence of a submarine in littoral waters. An example of the analysis is shown in Figure 1, where the anomaly corresponding to a submarine wake in the RTI plot of VV polarization LOGAN data is directly detected in all resolutions of the wavelet coefficient space. In effect, this means that a coarse-to-fine strategy can be used to quickly detect and then localize and track a submarine.

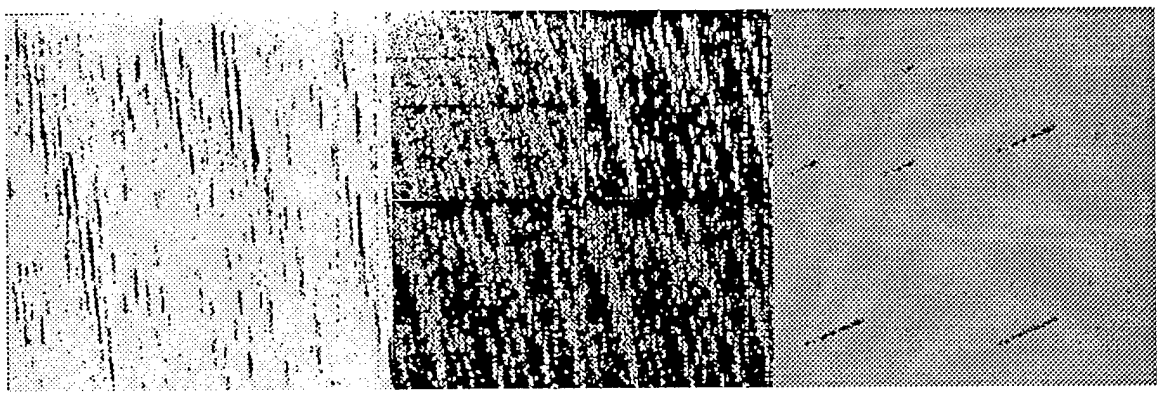

**Figure 1**: Detection of submarine wake in wavelet coefficient space of RTI plot (left image courtesy of NAWC).}

### Lattice Boltzmann Simulation of Flow by Mean Curvature

Geometric flow of front plays a significant role in various applications, such as fluid mechanics of multiphase flows, crystal growth, chemical kinetics, flame propagation, image processing, and surface modeling. The contemporary computer technology gives priorities to highly parallelizable numerical methods. Parallel computer hardware scientists see the Lattice Boltzmann Method as the simplest and fastest totally parallel algorithm with broad applications. In this project we try to use a Lattice Boltzmann Model to Simulate the mean curvature flow. We have been trying to use a simple geometric feature dependent relaxation parameter in the Lattice Boltzmann equation to recover the mean curvature evolution equation. We probably need use a linear collision operator instead of the single-time-relaxation approximation.

## Target Detection with Local Discriminant Bases and Wavelets

One classification method suitable for digital images or sampled speech, is Local Discriminant Bases (LDB), (see SAIT96). We have developed an algorithm that uses the LDB together with a library of wavelet bases, the wavelet packets, for automatic target detection. There are some problems with the lack of translation invariance of the wavelet transform which must be solved for this application area.

One solution (SAIT96) of the problem is to extend the input data to include a number of translates of the training data. However, for the analysis of images the calculation of a large amount of translated transforms is costly, and should be avoided in order to keep the time complexity down. We have developed a multistage algorithm for the target detection process that avoids the translated transform calculations. It consists of first training the algorithm on fixed position (time/space synchronized) data, then determining the position/localization of the interesting signal, repositioning the signal in the original (training) position and classifying in the normal way, and finally translating the signal back. Now we have knowledge of both the class and the synchronization of the signal. An example of the algorithm performance is shown in Figure 2. The large sonar image contains 98 sub-images, which are separately processed. Our false detection rate of 3.9%/sub-image gives a maximum of 4 false target detections per large image.

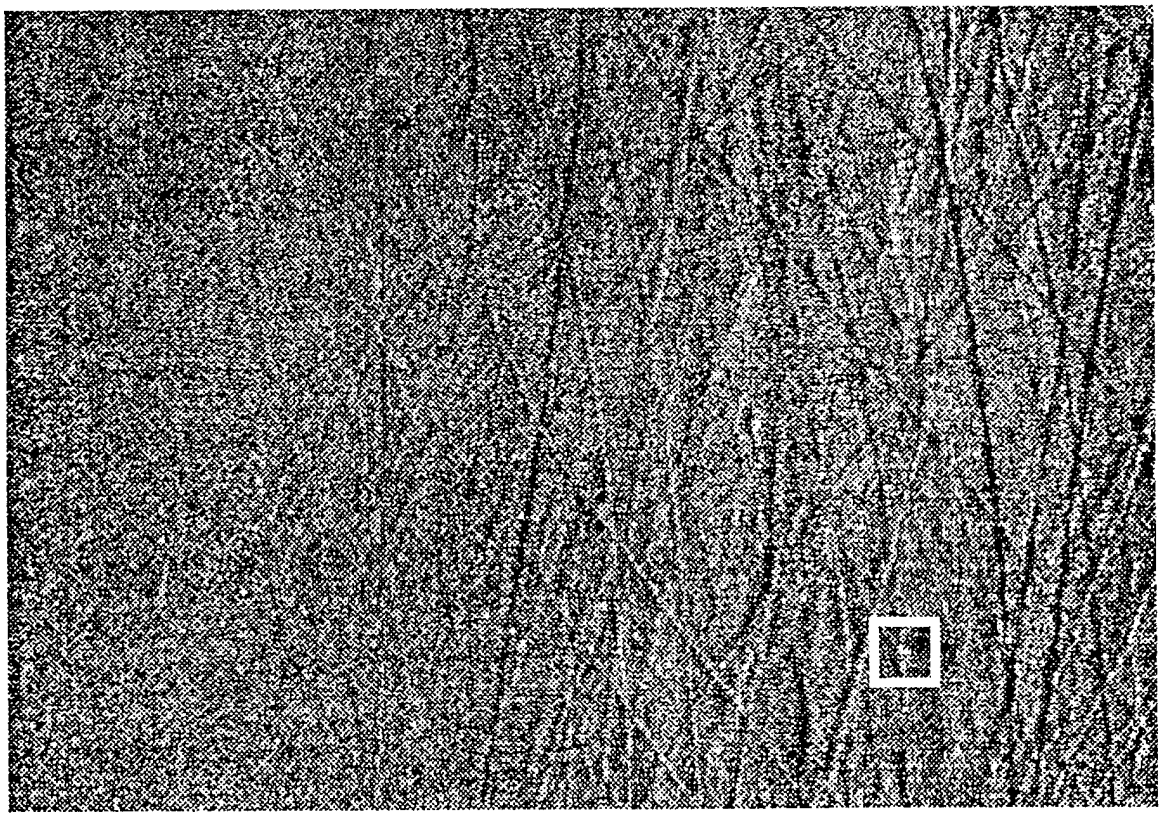

**Figure 2:** A typical large format sonar image. Detected target position is boxed.

## Surface Reconstruction from Two Photometric Images

Determining surface orientation and characteristics is one of the fundamental problems in computer vision. One approach is to use photometric stereo (WOOD80). In this system, the viewing position is held fixed while the lighting conditions are changed. Other approaches include

shape-from-shading (HORN77), stereo vision (MARR79) and shape-from-motion (ULLM79). The work done here is focused on reducing the number of photometric images required and on improving the surface integration from the normals.

A novel method for surface integration has been developed. It is different then traditional methods, in that it lets the geometry drive the integration path. This method divides the surface into small regions. The surface is integrated over each small path. Small patches are joined in order of their likelihood to be correct. The joining is accomplished by raising or lowering the smaller patch to smoothly connect to the larger patch on their common boundaries. A result of the integration is shown in Figure 3. The surface normals had a singularity around the tear duct of the eye as well as a steep decline in the middle of the nose due to an error. The integration routine worked around these errors and joined them at the end so that they would not affect the global shape.

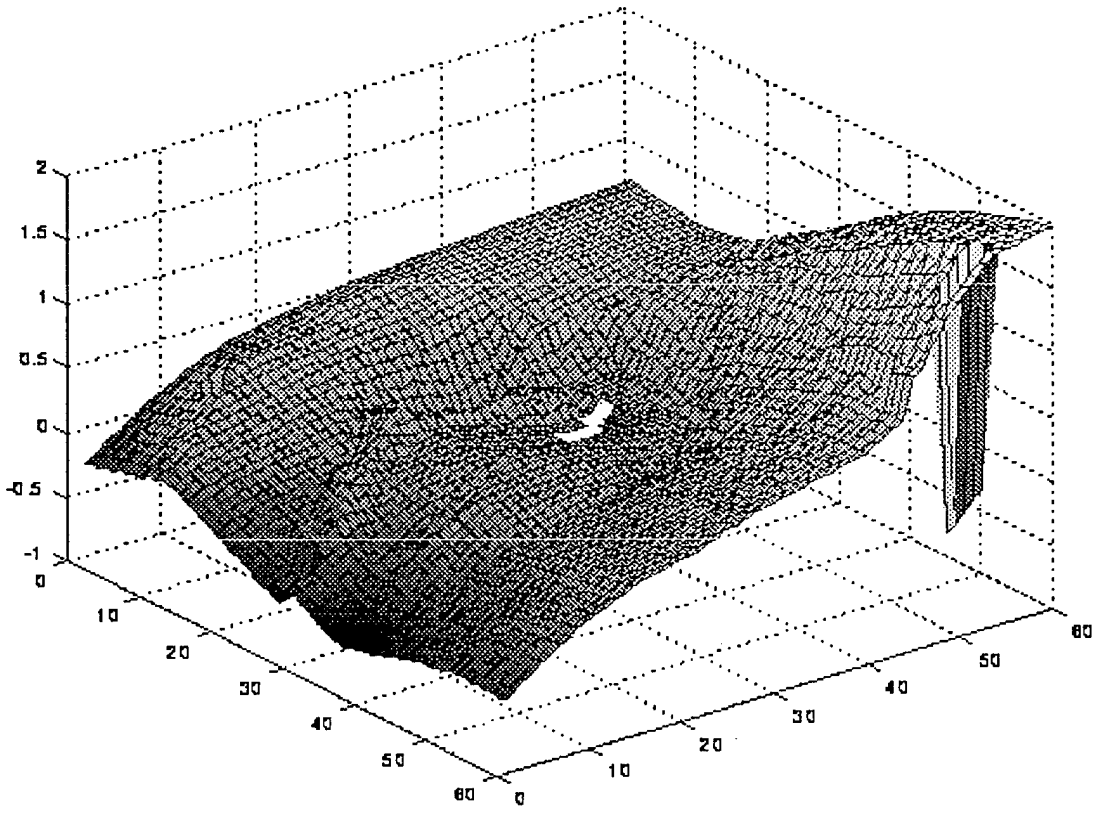


**Figure 3:** Reconstructed quadrant of a face.

## AMG Analysis of Time Dependent Sensor Returns

It has been proved that there exists a unique affine, morphological Gallilean invariant (AMG) scale-space for time dependent sequences. This defines a multi-scale analysis given by the solution to an elliptic partial differential equation. The successive removal of objects is made in the sequence such that certain invariants exist. This makes it possible to extract an object in a sequence based on its scale and acceleration.

A multi-scale analysis operator smooths the sequence, creating another sequence. The way the smoothing is done defines the invariants. The elliptic PDE AMG equation uses level sets perpendicular to the flow of time to characterize the image flow field. An example of the application

of this process to a 3 frame sequence is shown in Figure 4, where the accelerating object is shown enclosed in a box in the 2nd and 3rd frames.

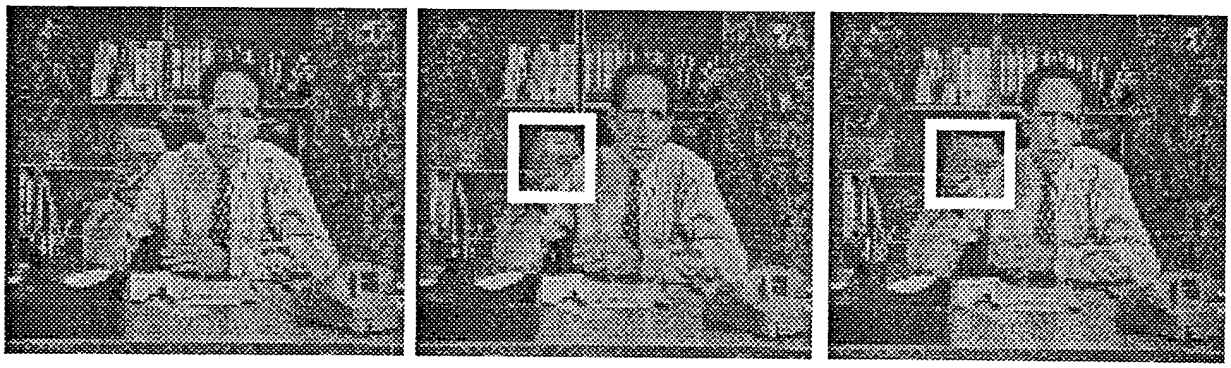

**Figure 4:** Accelerated object recovery using AMG analysis applied to 3 frame sequence.

## 4c. Publications

1. E.D. Sinzinger and B.D. Jawerth, "Surface representation from photometric stereo with wavelets", in *Proc. SPIE Conf. on Wavelet Applications*, Vol. 3169, San Diego, CA, 1997.
2. E.D. Sinzinger, "Numerical Methods for Ill-Posed Problems in Image Processing and Computer Vision", M.S. Thesis, Department of Computer Science, University of South Carolina, Columbia, SC, 1998.
3. T. Kubota and T. L. Huntsberger, "Edge dipole and edge field for boundary detection," in *Proc. SPIE Conf. Hybrid Image and Signal Processing VI*, Vol. 3389, Orlando, FL, Apr 1998.
4. F. Espinal and R. Chandran, "Wavelet-based fractal signature for texture classification," in *Proc. SPIE Conf. on Wavelet Applications V*, Vol. 3391, Orlando, FL, Apr 1998.
5. T. Kubota and T. L. Huntsberger, "Adaptive pattern recognition system for scene segmentation," *Optical Engineering, Special Section on Advances in Pattern Recognition*, Vol. 37, No. 3, pp. 829-835, 1998.
6. F. Espinal, T. L. Huntsberger, B. Jawerth, and T. Kubota, "Wavelet-based fractal signature analysis for automatic target recognition," *Optical Engineering, Special Section on Advances in Pattern Recognition*, Vol. 37, No. 1, pp. 166-174, 1998.
7. G. Fernandez and T. L. Huntsberger, "Wavelet-based system for recognition and labeling of polyhedral junctions," *Optical Engineering, Special Section on Advances in Pattern Recognition*, Vol. 37, No. 1, pp. 158-165, 1998.
8. T. Kubota, T. L. Huntsberger and C. O. Alford, "A vision system with real-time feature extractor and relaxation network," to appear in *Int. Journal Pattern Recognition and Artificial Intelligence*, May 1998.
9. B.D. Jawerth, P. Lin, and E.D. Sinzinger, "Lattice Boltzmann methods for anisotropic diffusion of images", *Mathematical Imaging*, in review.

## 4d. Personnel

| | |
|---|---|
| PI: | Dr. Terry Huntsberger |
| co-PI: | Dr. Björn Jawerth |
| Research Associates: | Dr. Toshiro Kubota |
| | Dr. Weimin Zheng |
| | Dr. Peng Lin |
| | Eric Sinzinger, M.S., Computer Science |
| | Henrik Storm |
| | Goran Kronquist |
| | Marcus Kozica, M.S., Mathematics |
| | Michael Cox |

## 5. LIST of INVENTIONS

None

## 6. BIBLIOGRAPHY

[HORN77] B. K. P. Horn, "Understanding image intensities", *Artificial Intelligence*, Vol. 8, pp. 201-231, 1977.
[MARR79] D. Marr and T. Poggio, "A computational theory of human stereo vision", *Proceedings of the Royal Society of London*, Vol. 204, pp. 301-308, 1979.
[SAIT96] N. Saito and R. R. Coifman, "Improved Local Discriminant Bases using empirical probability density estimation, in *Proc. Conf. on Statistical Computing*, American Statistical Assoc., 1996.
[ULLM79] S. Ullman, The Interpretation of Visual Motion, MIT Press, Cambridge, MA, 1979.
[WOOD80] R. J. Woodham, "Photometric method for determining surface orientation from multiple images", *Optical Engineering*, Vol. 19, pp. 139-144, 1980.

| REPORT DOCUMENTATION PAGE | Form Approved OMB No. 0704-0188 |
|---|---|



| 1. AGENCY USE ONLY *(Leave blank)* | 2. REPORT DATE | 3. REPORT TYPE AND DATES COVERED |
|---|---|---|
| | 1 June 1998 | Annual |

| 4. TITLE AND SUBTITLE | 5. FUNDING NUMBERS |
|---|---|
| Wavelet-Based Acoustic/Non-Acoustic AntiSubmarine Warfare | Grant: N00014-97-1-0806<br>PR: 97PR06312-00 |
| 6. AUTHOR(S)<br>PI: Terry Huntsberger, co-PI: Björn Jawerth | |
| 7. PERFORMING ORGANIZATION NAME(S) AND ADDRESS(ES)<br>University of South Carolina | 8. PERFORMING ORGANIZATION REPORT NUMBER<br>N00014-97-1-0806-1 |
| 9. SPONSORING / MONITORING AGENCY NAME(S) AND ADDRESS(ES)<br>ONR | 10. SPONSORING / MONITORING AGENCY REPORT NUMBER<br>ONR |

11. SUPPLEMENTARY NOTES
Prepared in coordination with University Research Initiative Program for Combat Readiness

| 12a. DISTRIBUTION / AVAILABILITY STATEMENT | 12b. DISTRIBUTION CODE |
|---|---|
| APPROVED FOR PUBLIC RELEASE | |

13. ABSTRACT *(Maximum 200 words)*

The two main detection methods used in tactical antisubmarine warfare (ASW) are acoustic (sound) and nonacoustic. For the acoustic studies we are exploiting the similarity between the Helmholtz equation and Laplace's equation for the development of fast solver techniques for multi-line towed sonar array systems currently fielded by the Navy. Our work in non-acoustic ASW methods has concentrated on the study of boundary value problems for Maxwell's equations on arbitrary nonsmooth domains, in arbitrary dimensions and on the detection and analysis of submarine wakes from low grazing angle (LOGAN) radar data.

| 14. SUBJECT TERMS | 15. NUMBER OF PAGES |
|---|---|
| Antisubmarine Warfare, Wavelets | 7 |
| | 16. PRICE CODE |

| 17. SECURITY CLASSIFICATION OF REPORT | 18. SECURITY CLASSIFICATION OF THIS PAGE | 19. SECURITY CLASSIFICATION OF ABSTRACT | 20. LIMITATION OF ABSTRACT |
|---|---|---|---|
| UNCLASSIFIED | UNCLASSIFIED | UNCLASSIFIED | 200 words |

# Real-Time UV Fluorescence for Dissolved Hydrocarbon Tracking

M.L. Myrick, P.I.

Department of Chemistry and Biochemistry
University of South Carolina
Columbia, SC 29208

Tel: (803) 777-6018
Fax: (803) 777-9521
Email: myrick@psc.sc.edu

# Section 5-2: Real-Time UV Fluorescence for Dissolved Hydrocarbon Tracking

M.L. Myrick

## ABSTRACT

A post-doc (Dr. Yuan Yan) was hired for this project beginning in January, 1998. We have begun and nearly completed the design phase of a 2nd-generation two-dimensional excitation-emission fluorimeter. Excitation sources, detectors, spectrometers, and integrated programming languages have been extensively reviewed and selected, and a site-visit to Oregon State University and WETlabs, Inc. (Corvallis, Oregon) has been conducted to study pressure-case design and construction for underwater optical instrumentation. Communications hardware is currently under review, and should be defined by May, 1998. Funding for this project has resulted in collaborations with Vanguard Research, Inc. for proposals in very-shallow-water/surf zone (VSW/SZ) mine detection using C-130-deployed instruments.

## FORWARD

This project was initially funded in June, 1997 at the level of $293,000 over three years.

## REPORT

### Statement of the Problem Studied

Our project is to design and construct a 2nd-generation two-dimensional fluorimeter for rapid detection and speciation of organic compounds in seawater. The purpose of this detection is to recognize the presence of anthropogenic hydrocarbons associated with submarine activity and to use this hydrocarbon signature for tracking purposes.

### Background

Aromatic hydrocarbons are pervasive environmental contaminants of waters, originating from both natural and man-made sources. Examples are humic and fulvic acids, which are naturally-occurring mixtures of aromatic organic acids leached from decaying plant matter, and petroleum refinates containing heavier polyaromatic compounds such as naphthalene ($C_{10}H_8$), anthracene ($C_{14}H_{10}$), and pesticides. Complex residues of many compounds are found as contaminants in water that originate from fuels and dissolution of plasticizers from polymers. Examples of these residues might include marine greases leaching into seawater or the dissolution of diesel fuel from the leaking seals of an engine into water.

Conventional methods for detecting aromatic hydrocarbons (e.g., GC-MS) in water rely on sampling the water and transporting the sample to a laboratory for analysis, often requiring a week or more. While extremely sensitive and accurate, such cumbersome and expensive procedures prevent extensive study of transport phenomena for aromatic compounds in aqueous

media and frustrate the continuous monitoring that would be necessary to control discharges and/or provide real-time location of sources.

Fluorescence is an extremely sensitive method for detecting compounds which fluoresce, typically yielding detection limits approaching or exceeding 1 ppb. Using appropriate instrumentation, fluorescence spectra can be acquired on the 1-second to 10-second time scale, enabling measurements in near-real-time. Conventional fluorescence measurements are performed by selecting a particular wavelength for sample excitation (typically in the UV spectral region for small organic compounds), and then monitoring the emission intensity of the sample as a function of wavelength. The primary limitation in the use of these conventional measurements is that spectra of mixtures tend to be highly overlapped, so that clear distinction of the contributions made by individual components is difficult. As a result of this spectroscopic overlap, fluorescence is rarely used in cases where the concentrations of a single or few components are desired from a complex or unknown matrix.

One way around this problem is to record emission spectra using a series of different excitation wavelengths - the resulting excitation-emission-matrix (EEM) spectrum has the format of an "image" rather than a "spectrum", and contains sufficient information to differentiate contributions from distinct species in the mixture. The statistical basis for "higher-order" data analysis is currently being refined. The Investigator (M.L. Myrick) and his laboratory have been involved in the development of optical methods for the detection of organic residues in water for 3+ years, and have recently published reports of extremely rapid (e.g., <10 second total analysis) 2-D detection of contaminants.**[1,2]**

***Summary of the Most Important Results***

The project can be divided into the following tasks:

*Year 1 tasks*: (a) hire a post-doctoral associate with experience in two-dimensional spectroscopic analysis, (b) train the post-doc in higher-order data analysis, programming and instrument design/construction as needed, (c) review available light sources, spectrometers and detectors, (d) determine whether commercial components are compatible with the design goals of the instrumentation we are to construct and evaluate, (e) in cases where commercial components are inadequate to meet the goals of the system, design adequate components, (f) evaluate computational and communication needs and review available technology, resolving any problems that will be unique to the new instrumentation.

*Year 2 tasks*: (g) acquire components and begin construction and assembly, (h) write dedicated software to implement the selected three-mode data analytical methodology selected above and to control all aspects of the instrument operation and data interpretation, (i) complete instrument construction in pressure vessel, (j) integrate software and hardware and test on prepared standard samples, and

*Year 3 tasks*: (k) deploy instrument in Lake Murray, S.C. and at the USC Marine Field Station.

Task (a) was completed with the arrival of Dr. Yuan Yan in January, 1998. Dr. Yan is one of the few analytical spectroscopists trained in the use of two-dimensional fluorescence spectroscopy. His experience to date has been with commercial laboratory-based scanning instruments of conventional design, and he has required training in the design and construction of optical

instrumentation, programming and multivariate analysis. The second task, (b), has now been successfully completed. Dr. Yan has now been trained to program in the LabVIEW 5.0 (National Instruments, Inc.) programming environment, which has become the language of choice in the Myrick Laboratory and which is reaching common usage in scientific instrumentation, with the assistance of Professor Myrick and Matthew P. Nelson (graduate assistant), both of whom are experienced programmers in this environment and who have previously programmed several complex optical instruments. Dr. Yan is now familiar with the MATLAB (Math Works, Inc.) and Mathematica (Wolfram Research, Inc.) environments as well, which permits him to quickly program and evaluate multivariate data analysis schemes offline before incorporating them into a LabVIEW VI.

Task (c) has now been completed. To take the matter of lamps first, the first generation instrument utilizes a 1000 W Hg/Xe arc lamp. This powerful UV lamp has four main disadvantages. First, it has very high power consumption. Second, it requires very efficient cooling. Third, the arc is far larger than can possibly be used. Finally, in the UV region the output is dominated by Hg emission lines (most notably the 254 nm emission line), making the initial instrument only fully two-dimensional in concept. In fact, the spectrometer could reasonably be considered a 7-band excitation system, rather than a continuous-excitation spectrometer, because of the dominance of the Hg lines (Figure 1). To get around these problems, we have elected to use a high-pressure Xenon arc lamp, which has a pseudocontinuous emission profile in the UV region of interest to us (Figure 2). The large size of the 1000 W arc means that a lower power lamp could give improved optical performance in the arc size scales with power. Dr. Yan evaluated a large number of different lamps, comparing their arc sizes, reflector configurations, power requirements, and optical spectra in the UV region.

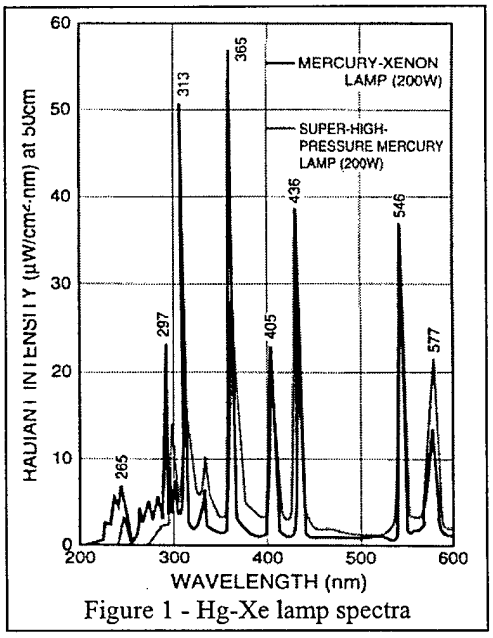

Figure 1 - Hg-Xe lamp spectra

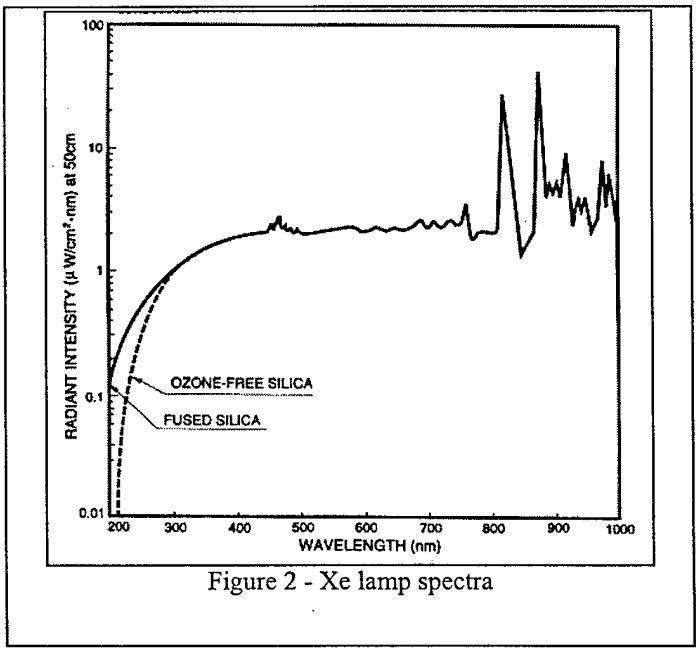

Figure 2 - Xe lamp spectra

After comparing the lamp specifications of different companies quantitatively, Oriel and Hamamatsu were found to be the manufacturers of lamps with the highest average power in the

UV region to 200 nm, with broad-band spectra. Of these two companies, data for a 1000 W lamp, two typical 150 W lamps and a 75 W lamp are shown in Table 1.

Table 1 typical Specification comparison for Oriel and Hamamatsu Xenon arc lamps

| Company | Effective Arc size (mm) | Spectral Distribution (nm) | lamp Voltage (Vdc) | lamp current (dc amps) | Power Consumed (W) | operating life(h) | radiance @ 280nm/ arc $mm^2$ |
|---|---|---|---|---|---|---|---|
| Oriel | 1 × 3.0 | 200-900 | 23 | 43.5 | 1000 | 1000 | 0.094 W |
| Oriel | 0.5 × 2.2 | 200~900 | 20 | 7.5 | 150 | 1200 | 0.029 W |
| Oriel | 0.25 × 0.5 | 200-900 | 14 | 5.4 | 75 | 400 | 0.101 W |
| Hamamatsu | ? × 2.0 | 185~2000 | 18 | 8.5±0.5 | 150 | 3000 | 0.030 W |

On the basis of numerical comparison and correcting for the arc size, we find that a 75 W xenon arc lamp should perform approximately as well as the present Hg/Xe lamp because of the very small size and high brightness of the arc. This should reduce the power consumption of the light source by a factor of 13 and dramatically reduce cooling requirements, while simultaneously giving full spectral coverage in the UV down to approximately 250 nm. Some consideration to pulsed Xe flashlamps was given, but even the brightest of these lamps have arcs of large size and hence low power density. Run at their highest possible duty cycle, we could not expect a performace within an order of magnitude of the 75 W CW Xenon lamp.

Spectrometer selection from the available commercial systems proved essentially impossible. The design goals for spectrometer selection were to obtain a system with moderate to good imaging characteristics capable of 2-5 nm spectral resolution in the UV region, with apertures of f/3 or better, and with an optical train optimized for the spectral region (200-400 nm for excitation, 300-600 nm for emission), while at the same time maintaining a nearly linear geometry so that the instrument could be introduced into a cylindrical pressure vessel of compact design. A summary of a number of the commercially available systems that were considered for the application are given in Table 2.

Table 2 Typical monochromator specifications

| Model | Focal Length | best Aperture | resoln | Dimension(mm) | dispersion (nm/mm) |
|---|---|---|---|---|---|
| ST 9060 | 200 mm | f/2.7 | 0.15nm | 129×251×387 | 3.3 |
| ISA H10 | 100 mm | f/3.5 | 1 nm | 128×114×84 | |
| ISA CP200 | 200 mm | f/3 | | | 24 |
| ISA 270M | 270 mm | f/4 | 0.1 nm | 394×413×190 | |
| Oriel Fics | 135 mm | f/2.1 | 2 nm | | |
| 77250 | 250 mm | f/3.7 | 1 nm | 127×102×184 | |
| MS10 | 96 mm | f/2.5 | 1 nm | 132X77X53 | |

Of the available spectrometers, all had some serious disadvantage for this project. The most common being that they could not be incorporated into a linear geometry for the pressure vessel. Of the examined systems, fewer than 10 were found that improved the aperture (f #) of the instrument compared to the first generation instrument.

To resolve this problem, we have opted for a prism-based instrument. Using data from reference 3 for fused silica, we fit the observed refractive index of silica to the polynomial shown below in the wavelength range between 200 nm and 700 nm.

$$n_{fs}(\lambda) = 1.4385 + \frac{764653}{\lambda^3} - \frac{1995}{\lambda^2} + \frac{12.8436}{\lambda}$$

From this point, we used angular dispersion equations for prism to obtain a formula for the linear dispersion for a prism spectrometer as a function of the center wavelength of the spectrometer, focal length and wavelength of interest, using fused silica as the prism material. This equation is given below, where f is focal length, λc is the center

$$y(\lambda) = -f \tan A \frac{1}{3} pJ - \frac{764653}{\lambda c^3} + \frac{1995}{\lambda c^2} - \frac{12.843}{\lambda c} + \frac{764653}{\lambda^3} - \frac{1995}{\lambda^2} + \frac{12.843}{\lambda} \text{ NE}$$

wavelength, λ is wavelength in the region of interest, and y is the position (in millimeters) of the focal point of wavelength λ in the output focal plane of the spectrometer. If we plot this function for a center wavelength of 300 nm and a focal length of 150 mm (for a proposed f/3 system with 50 mm silica optics), we see (Figure 3) that dispersion is greatest in the UV region (as expected), which will result in higher resolution in the UV region.

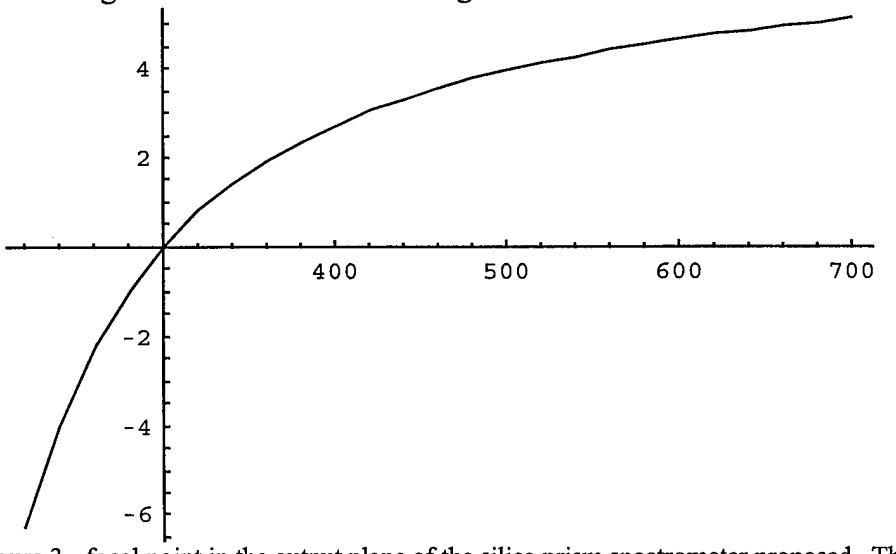


Figure 3 - focal point in the output plane of the silica prism spectrometer proposed. The vertical axis is position in millimeters, while the horizontal is wavelength in nanometers.

We can determine the dispersion directly by differentiating y(λ) as a function of λ (Figure 4, for the same parameters as Figure 3).

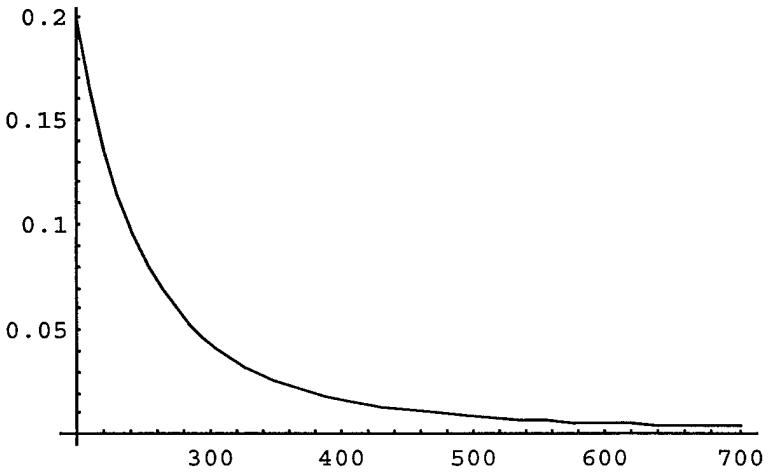


Figure 4 - linear dispersion as a function of wavelength for a silica prism spectrometer.
The vertical axis is dispersion in mm/nm, the horizontal axis is wavelength in nanometers.

If we wish to determine the effective resolution achievable with this spectrometer (neglecting aberrations, which is reasonable in the low-resolution limit), we can take the reciprocal of the dispersion and multiply it by the slit width, giving the resolution in nanometers at each wavelength. If we assume a 200 micrometer slit, the result is shown in Figure 5.

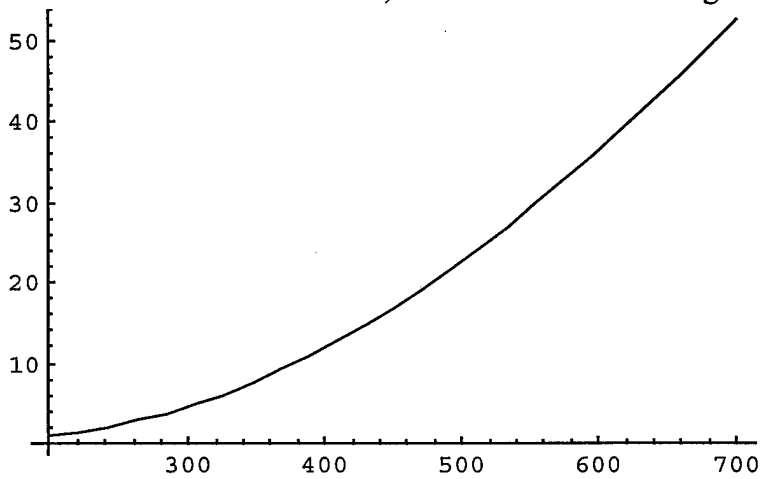


Figure 5 - Resolution of a prism spectrometer as a function of wavelength.
Vertical axis is resolution in nanometers, Horizontal axis is wavelength in nanometers.

Figure 5 shows that for a silica prism spectrometer, the resolution in the nanometer basis can be quite good (approaching 2 nm) in the UV spectral region (of greatest importance to this work), but beyond approximately 400 nm becomes relatively poor (increasing to 50 nm at 700 nm). This is somewhat misleading, however, for fluorescence spectroscopy. In the case of fluorescence, the resolution necessary to record features varies with wavelength because electronic spectroscopy is fundamentally related to energy units such as optical frequency or wavenumbers ($cm^{-1}$) rather than wavelength. Since the relationship between energy and wavelength is a reciprocal one, we can convert the resolution shown in nanometer units in Figure 5 into energy units of wavenumbers by application of the chain rule and calculation of the appropriate quantities. If we do so, we get the result shown in Figure 6 below.

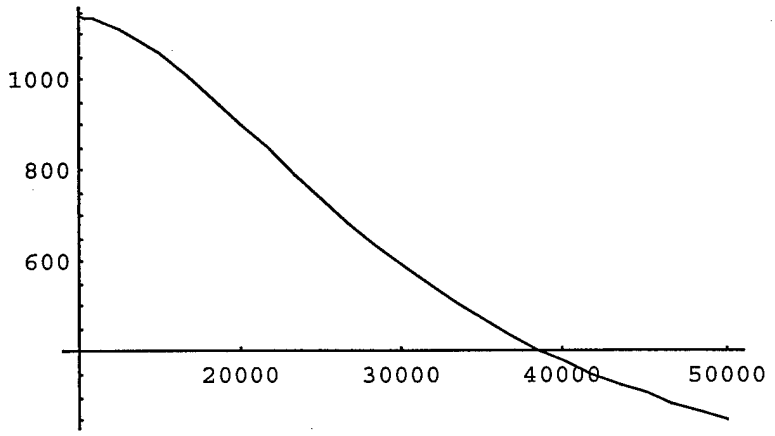


Figure 6 - Resolution of a prism spectrometer as a function of wavelength.
Vertical axis is resolution in wavenumbers, Horizontal axis is light frequency in wavenumbers.

Figure 6 is in different units from Figure 5, but they cover the same wavelength region (although the axes are reversed relative to one another). The 50000 $cm^{-1}$ position in Figure 6 corresponds to 200 nm, while the 20000 $cm^{-1}$ position corresponds to 500 nm. What we observe in Figure 6 is that, rather than resolution decreasing by a factor of 25 over the spectral region shown, it decreases by a factor of less than 4. Even at the worst, the resolution is no worse than 1100 cm-1 for the experimental parameters used; this should still be sufficient to record relatively high-fidelity fluorescence spectra, while retaining the highest resolution for the UV region in which excitation occurs. Consequently, we find that a modest-resolution instrument using a prism design is practical for this problem. The inherently "bent" rather than 90-degree geometry of prism systems is ideal for our application, and throughput of a prism spectrometer can be a factor of 2-10 better than for a grating spectrometer while having reduced stray light, depending on how well the grating spectrometer has been optimized. Given these considerations, we have decided to base our underwater system around spectrometers of this type.

Detection systems proposed for the underwater instrument are all based on CCD technology. Tables 3a and 3b list some a variety of the possible choices for commercial and non-commercial CCD-based systems. The SBIG ST-5C camera, for example, has a quantum efficiency in the UV of less than 0.1, uses a lower-grade Texas Instruments chip with relatively small pixel dimensions. This makes it problematic for applications in 2-D UV fluorescence because the pixel size restricts the range of wavelengths that can be covered. It also has a relatively high readout noise and dark current. However, it has a relatively low power consumption because its cooling requirements are not demanding. On the other end, the Hamamatsu EB-CCD is an intensified CCD with greater sensitivity but lower quantum efficiency, larger dark current, and read noise. The array is large in size, but requires an 8000 V supply to function properly.

Table 3a Partial selection and specifications of some CCD cameras

| Specification | SBIG ST-5C | Oriel Instaspec IV | Cooke SensiCam | Hamamatsu EB-CCD |
|---|---|---|---|---|
| Resolution | 320×240 pixels | 1024×256 | 640×480 VGA | 512×512 |
| Pixel Size | 10μm square | 27 μm square | 9.9 μm square | 24 μm square |
| Full Well Capac. | 50,000 e- | 65536 e- | 35,000 e- | 300,000 e- |
| Array Area | 3.2mmx2.4mm | 26.6×6.6mm | 6.3×4.8mm | 12.3×12.3 |
| Frame Buffer | full buffer | none | none | none |
| Readout Noise | ≥25e- | 10 e- | 14e- | 50e- |
| Dark Current | 5e-/pix-s @-5C | 0.1e-/pix/s - 55C | 0.1e-/pix/s | 300e/pixel/s, at0C |
| A/D resolution | 16 bits | 16bits | 12bits | N/A |
| Pixel Rate | 25kHz, 3 sec FF | 150Hz | 30fps FF | up to 1MHz |
| Spectral window | UV-Vis | Vis (UV avail.) | 290 to 1000nm | 200 to 1000nm |

Based on extensive review of the available camera systems, we have opted to purchase a Hamamatsu camera head with 1 stage thermoelectric cooling, drive hardware, and a back-illuminated CCD chip, for which we will write our own software drive routines in LabVIEW. The quantum efficiency curve for this camera is shown in Figure 7 below compared to a typical front-side-illuminated UV-capable camera. As shown, the efficiency of a back-side illuminated chip above the direct bandgap energy of silicon is 5-6 times greater than a front-illuminated device. This translates directly into improved speed and/or lower detection limits, which are already at the ppb level.

Table3b (continued)

| Specification | SI-003A CCD imager | 600 series CCD (Spectral Instr.) | Kodak 768×512 CCD(Princeton) |
|---|---|---|---|
| Resolution | 1024×1024 | | 768×512 |
| Pixel Size | 24microns | | 9.0microns |
| Full Well Capac. | | | 85,000 electrons |
| Array Area | | | 6.91×4.6mm |
| Frame Buffer | none | none | 0.407 s / 1MHz |
| Readout Noise | | | 10e- @ 500kHz |
| Dark Current | | | <0.006e-/pix-s |
| A/D resolution | | 16bit (Labview) | 12bits |
| Pixel Rate | | 20-200kHz | up to 1MHz |
| Spectral window | UV to NIR | | 190 to 1080nm |

Our fourth and fifth task results have already been alluded to above: We will purchase commercially available lamps and detector heads, but will modify the electronics of the lamp and the cooling system for the lamp to be compatible with a pressure vessel. The spectrometer will be completely constructed in-house as a prism spectrometer.

The sixth task is in progress at the moment. To obtain a reasonable overview of the communication/computation systems in current use, we are traveling to Oregon State University during the last week of April, 1998 to meet with faculty in the College of Oceanography and with staff at WETLabs, Incorporated. The currently-available instrumentation that is most similar to that which we are constructing has been constructed and used by these scientists, as reported in reference 4. In that instrument, whose layout is reproduced in Figure 8 below, three excitation wavelengths are cycled and fluorescence spectra of plankton is measured using visible excitation. The principal investigator has worked with the OSU research team in the past on ocean optical instrumentation (see references 5 and 6). Although the design of the OSU instrument is quite different from that expected for the USC instrument and of more limited capability, many of the data communications and pressure-case issues are identical, and we believe the USC instrument will assume its final design shape shortly after the lessons learned at OSU are digested.

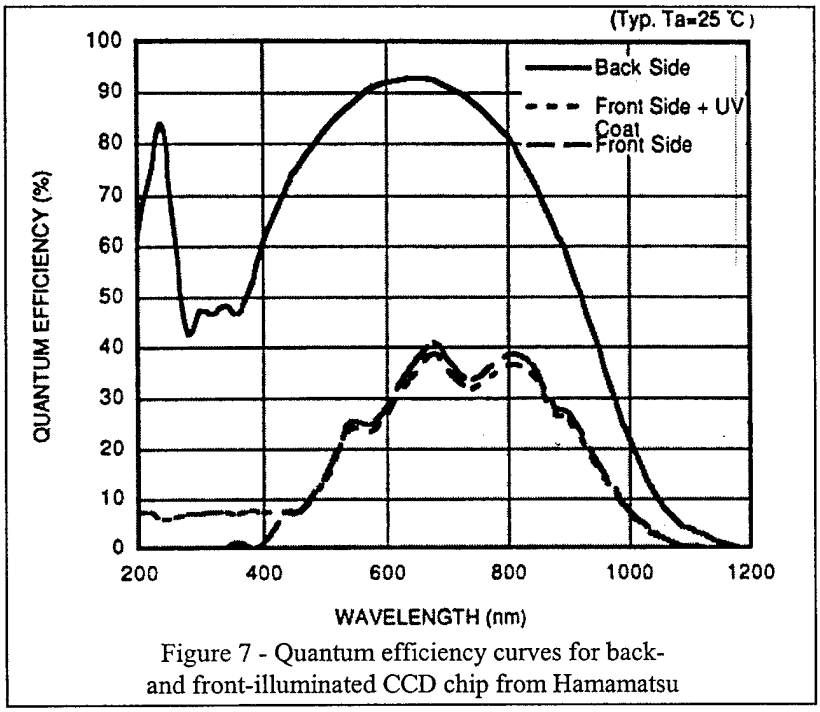


Figure 7 - Quantum efficiency curves for back- and front-illuminated CCD chip from Hamamatsu

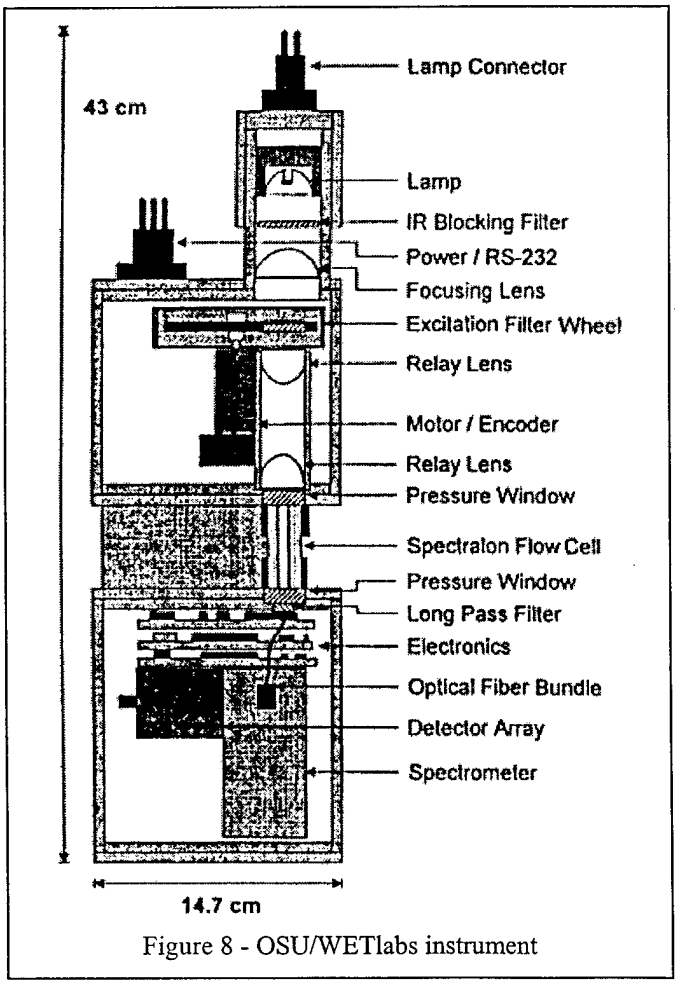


Figure 8 - OSU/WETlabs instrument

Data analysis methods used for the first-generation two-dimensional fluorimeter are not optimal for the analytical project being undertaken. Parallel Factor Analysis (PFA) and other three-way multivariate methods are computer-intensive and are designed to solve a slightly different problem from the one this instrument is aimed to solve. In the case of PFA, the method determines the number of species present in a 2-D data matrix and what the "excitation" and "emission" spectra for each are when all else is unknown. The instrument we are designing and building will search for known sets of compounds in an unknown matrix, where it is not of first importance to achieve a complete understanding of the sample. To meet the design goal of more rapid measurement, we can obviate the need for time-consuming data inversions by using a technique known as generalized rank annihilation method (GRAM). This algorithm requires that a calibration matrix be supplied. The peaks in the calibration matrix must have the same peak parameter(s) and spectra as the desired chemical components in the unknown data matrix. Quantitation can be achieved in the form of the ratio of the concentrations of the components in the two matrices. The simplest case is where there is one component in the calibration data set and one additional (overlapped) compound in the unknown data set. In GRAM, the data matrix is quickly decomposed and its eigenvalues determined. From the eigenvalues, the effective rank of the data matrix can be determined; as

spectroscopists, we typically would identify the rank of the matrix with the number of spectroscopically dissimilar species in the mixture. The data matrix is then modified by the subtraction of a varying fraction of the calibration data (2-D spectrum for the desired analyte), and the eigenvalue spectrum determined. If the analyte appears in the 2-D spectrum then removing a portion of its contribution from the data should reduce the rank of the matrix somewhat. When a fraction of the known calibration data is subtracted that exactly equals the amount of that compound in the unknown mixture, the determined rank of the matrix should pass through a minimum and begin increasing again. This minimum rank position is used to determine the ratio of the desired compound in the unknown to that in the known. The main reason this process operates rapidly is that singular value decomposition (SVD) of a large data matrix can be done rapidly. Only when many different species are to be analyzed does PFA begin to become competitive for analytical purposes.

***Publications and Technical Reports***

So far no publication or technical reports have been made on our design work. However, we have one manuscript in progress, to be submitted before June 1, 1998.

"Detection of Water-Soluble Petrochemicals by UV-induced Fluorescence" A. Muroski, M. Groner, E.L. Raleigh and M.L. Myrick (manuscript in preparation)

***Personnel***

A post-doctoral associate, Dr. Yuan Yan, was hired in January, 1998. Mr. Matthew P. Nelson has also been supported partially by this subgrant

## BIBLIOGRAPHY

1) "Single-Measurement Excitation/Emission Matrix Spectrofluorometer for Determination of Hydrocarbons in Ocean Water 1. Instrumentation and Background Correction" A.R. Muroski, K.S. Booksh and M.L. Myrick Anal. Chem. 68(1996), 2524.
2) "Single-Measurement Excitation/Emission Matrix Spectrofluorometer for Determination of Hydrocarbons in Ocean Water 2. Calibration and Quantitation of Naphthalene and Styrene" K.S. Booksh, A.R. Muroski and M.L. Myrick Anal. Chem. 68(1996), 3539.
3) O.V. Mazurin, M.V. Streltsina and T.P. Shvaiko-Shvaikovskaya "Handbook of Glass Data: Part A", Elsevier (New York), 1983.
4) "Multiple Excitation Fluorometer for In Situ Oceanographic Applications" R.A. Desiderio, C. Moore, C. Lantz and T.J. Cowles Appl. Optics 36(1997), 1289.
5) "Microstructure Profiles of Laser Induced Chlorophyll Fluorescence Spectra: Evaluation of Backscatter and Forward Scatter Fiber Optic Sensors" R.A. Desiderio, T.J. Cowles, James N. Moum, Michael Myrick J.Atmos.Oceanic Tech. 10(1993),209.
6) "Fluorescence Microstructure using a laser/fiber optic profiler" T.J. Cowles, R.A. Desiderio, J.N. Moum, M.L. Myrick, D.G. Garvis, S.M. Angel Ocean Optics 10 R.W. Spinrad, Ed., SPIE Vol. 1302, p. 336 (1990).

# REPORT DOCUMENTATION PAGE

Form Approved
OMB No. 0704-0188



| 1. AGENCY USE ONLY *(Leave blank)* | 2. REPORT DATE | 3. REPORT TYPE AND DATES COVERED |
|---|---|---|
| | June 1, 1998 | Annual |

| 4. TITLE AND SUBTITLE | 5. FUNDING NUMBERS |
|---|---|
| Real-Time UV Fluorescence for Dissolved Hydrocarbon Tracking | Grant Number N00014-97-1-0806<br>PR Number 97PR06312-00<br>PO Code 353<br>Disbursing Code N68892<br>AGO Code N66020<br>Cage Code 4B489 |
| 6. AUTHOR(S)<br>M.L. Myrick | |
| 7. PERFORMING ORGANIZATION NAME(S) AND ADDRESS(ES)<br>University of South Carolina | 8. PERFORMING ORGANIZATION REPORT NUMBER<br>N00014-97-0806-1 |
| 9. SPONSORING / MONITORING AGENCY NAME(S) AND ADDRESS(ES)<br>ONR | 10. SPONSORING / MONITORING AGENCY REPORT NUMBER<br>ONR |

11. SUPPLEMENTARY NOTES

Prepared in coordination with University Research Initative Program for Combat Readiness

| 12a. DISTRIBUTION / AVAILABILITY STATEMENT | 12b. DISTRIBUTION CODE |
|---|---|
| APPROVED FOR PUBLIC RELEASE | |

13. ABSTRACT *(Maximum 200 words)*

A post-doc (Dr. Yuan Yan) was hired for this project beginning in January, 1998. We have begun and nearly completed the design phase of a 2nd-generation two-dimensional excitation-emission fluorimeter. Excitation sources, detectors, spectrometers and integrated programming languages have been extensively reviewed and selected, and a site-visit to Oregon State University and WETlabs, Inc. (Corvallis, Oregon) has been conducted to study pressure-case design and construction for underwater optical instrumentation. Communications hardware is currently under review, and should be defined by May, 1998. Funding for this project has resulted in collaborations with Vanguard Research, Inc. for proposals in very-shallow-water/surf zone (VSW/SZ) mine detection using C-130-deployed instruments. One publication is in preparation.

| 14. SUBJECT TERMS | 15. NUMBER OF PAGES |
|---|---|
| Chemical and Biological Warfare, Target Acquisition, Snti-Submarine, Combat Medicine, Biodeterioration, Command Control and Communication | 13 |
| | 16. PRICE CODE |

| 17. SECURITY CLASSIFICATION OF REPORT | 18. SECURITY CLASSIFICATION OF THIS PAGE | 19. SECURITY CLASSIFICATION OF ABSTRACT | 20. LIMITATION OF ABSTRACT |
|---|---|---|---|
| UNCLASSIFIED | UNCLASSIFIED | UNCLASSIFIED | 200 WDS |

# SECTION 6: BIODETERIORATION

# Section 6.0: Accelerated Research in Biofouling Control

M. Fletcher

## ABSTRACT

The formation of biofouling communities on deployment devices, sensors, and on ship and submarine hulls represents a significant limitation to the efficient operation of instrumentation and vessels. We propose to develop novel approaches for control of microbial biofouling by (1) developing fouling-resistant surfaces using disordered layers of polar organic structures, and (2) applying molecular methods and neural net analysis to characterize composition and succession in biofilms on different materials used in naval applications. SAMs constructed from oligo(ethylene glycol)-terminated units have been shown to result in decreased adhesion of proteins and bacteria, and we propose to enhance these antifouling properties by controlling the degree of disorder in the organic coatings and to validate methods for depositing polymers on metallic surfaces utilized in military applications. Microbial biofilms will be analyzed at different stages during their development on test surfaces and metal surfaces to determine community composition and biopolymer properties that are controlled by substratum properties. 16S rRNA analysis will target specific microbial species or groups. Total community profiles will be determined and compared by neural net analysis of low molecular weight RNA (5S and tRNA) polyacrylamide gels and cluster analysis. These studies as a whole offer both the development of new anti-fouling surfaces and knowledge of biofilm community composition that can be correlated with specific alterations in device/sensor failure or performance.

## FORWARD

The total award for this project is $383,251 for the budget period 6/01/97-6/29/2000.
In this initial stage of the project period, work has focused on (1) generation of a range of organic polymer surfaces with potential antifouling properties, (2) measurement of bacterial attachment to these test surfaces, and (3) characterization of microbial communities attached to a subset of the test surfaces. A significant change from the approach described in the original proposal is that we are now producing test surfaces by depositing coats of various organic polymers on epoxy-coated metal surfaces, rather than constructing test surfaces from self-assembled monolayers (SAMs). Our current approach still allows chemical manipulation of the surface and produces more durable coatings than those produced by the SAMs, which would be less able to withstand the stresses of field applications. Analysis of constituent species in microbial biofilms by 16S RNA sequencing and of biofilm polymers will be initiated as soon as a subset of test surfaces is identified for future study. Major achievements for this report period are:

- Methods have been developed for depositing novel organic polymer coatings on metal surfaces.
- Variations in the degree of bacterial fouling on initial test surfaces have been identified, as well as differences in community compositions (1) in biofilms *vs.* the adjacent water phase and (2) on selected polymer surfaces.

## REPORT

### *Statement of the Problem Studied*

The future of combat-readiness in ocean systems will involve the use of "tactical oceanography" to promote successful accomplishment of military missions. This will include sensor deployments, the use of sophisticated undersea coastal surveillance systems to detect, recognize, and track potential "unfriendly" objects (Incze, 1996). Such systems will reduce risks to U.S. forces while maximizing the probability of success on a mission (Parrish et al., 1996). The formation of biofouling communities on deployment devices, sensors, and on ship and submarine hulls represents a significant limitation to the efficient operation of vessels and sensors.

The formation of a biofouling community occurs through a sequence of specific, poorly understood chemical and biological processes. Biofouling begins with the formation of a conditioning layer of solutes which forms spontaneously on any submerged surface (Marshall, 1985). Once the conditioning film is in place, bacterial attachment to the surface and the formation of a biofilm microbial community begins. The climax biofilm microbial community then develops through a series of successional events (Lappin-Scott and Costerton, 1989; Wolfaardt et al., 1994), which are particularly poorly understood for surfaces in the marine environment. During and after the development of the biofilm microbial community, planktonic juveniles of sessile invertebrate species recruit onto the surface, ultimately resulting in a mature biofouling community with all its attendant problems.

The proposed research focuses on two aspects of the biofouling process: (1) initial attachment of bacteria to newly immersed surfaces and the development of attachment-resistant surfaces, and (2) colonization of surfaces by assemblages of microorganisms and microbial interactions that stabilize fouling communities. Preliminary studies (Wiencek and Fletcher, 1995; Ista et al., 1996) indicate that self-assembled monolayers (SAMs) offer a new approach for developing highly effective, fouling resistant surfaces. Researchers at the University of South Carolina (USC) are at the forefront in construction of SAMs of various types and evaluating bacterial adhesion on such substrata. Our objective is to create a specific organic polymer surface that is virtually fouling-resistant.

Antifouling surfaces that are exposed to severe mechanical disruption or abrasion may not remain completely intact and microbial fouling ensues. In such cases, the types of organisms attaching and the characteristics of their excreted polymers determine overall film strength, thickness, and chemical characteristics. Characterization of microbial biofilms is extremely difficult because of the complexity of microbial communities and the inability to culture most (>99%) in the laboratory. New molecular approaches combined with data analysis via neural networks are currently being utilized by researchers at USC and offer significant advances in profiling and characterizing complex microbial communities. We are well positioned to make clear progress in community analysis using modern molecular and computer approaches.

*Summary of Results*

**Development of polymer test surfaces**

The first task for this project has been the development of polymer-coated steel test surfaces. In general, the procedure for sample preparation is quite a lengthy process as the steel must be treated in the correct manner to yield a clean, rust-free coating. First, the steel is cut into 3" × 1" coupons and cleaned with a rag and hexane to remove any oil or grease. Any rust which exists is subsequently removed with sandpaper. Next, the cleaned steel is placed in the fume hood and spray-coated with a clear epoxy paint followed by an overlayer of polyurethane paint once the epoxy has cured (Fig. 1). The steel is coated in this manner to permit a good bond between the steel and the polymer coating as a whole. The polyurethane of choice is used by some of the large paint companies due to its weather and chemical resistance. It consists of a polyester polyol (Desmophen R-221-75) and the isocyanurate of hexamethylenediisocyanate (Desmodur N-3300), which react to form the polyurethane. Desmodur is used in a 10 % molar excess to leave some available isocyanate groups for reactions with the top-coat. The top-coat is then applied via paint-sprayer and the coating allowed to cure at room temperature in a glove bag with a constant flow of nitrogen. Each type of top-coat molecule was hydroxy-functionalized to ensure reaction with the isocyanate of the polyurethane. Although some of the top-coat polymers are water soluble they are not washed off the surface due to the chemical attachment with the polyurethane.

**Figure 1**

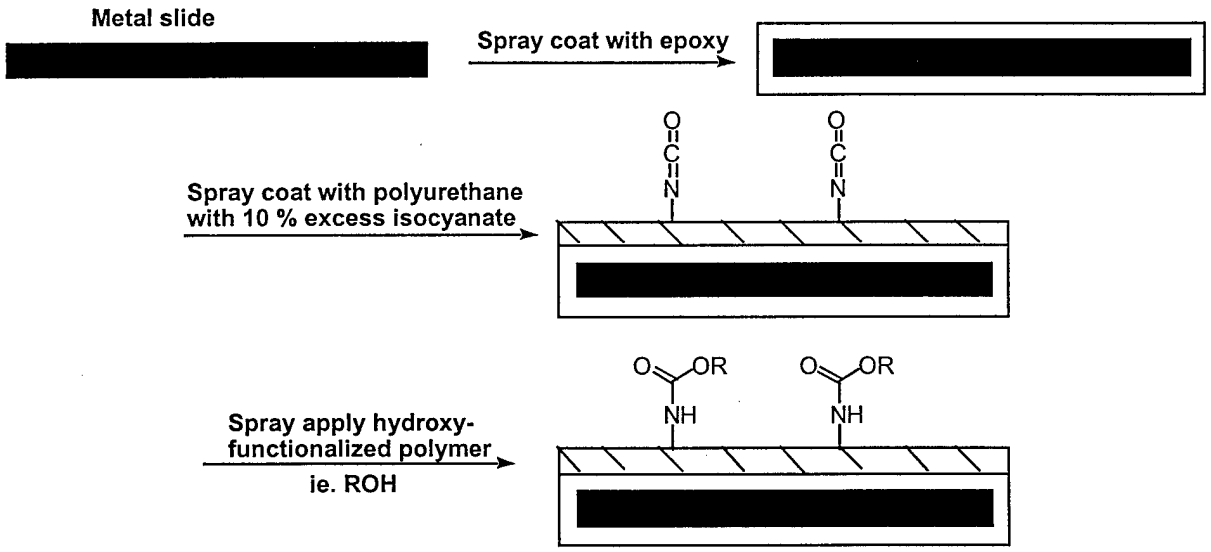


The surfaces which have been generated are: PEG-OH (hydroxy terminated PEG); MW 200, 300, 400, 600, 1,000, 35,000. PEG-OMe (methoxy terminated PEG); MW 350, 550, 750. PVA; MW 50,000. Poly(2,6-dibromophenylene oxide); MW ≈ 6,000.

Initially the surfaces were being prepared by allowing the polyurethane coat to cure for 48 h. The curing process is simply a time when the solvents employed to thin the paint are allowed to evaporate. The solvents used are methyl ethyl ketone (MEK) and propylene glycol methyl ether

acetate. After the 48 h had elapsed the PEG top-coat was applied. More recently, we have moved to a shorter cure time (≈ 10 min) for the polyurethane to ensure reaction with the applied PEG top-coat. This method resulted in better, smoother surfaces. The smoothest surfaces were those generated from the lower molecular weight PEG-OH (i.e. 200 - 1,000) and PEG-OMe (i.e. 350 - 750), probably due to their solubility and ease of application.

PEG of molecular weight 35,000 proved problematic for spray application. Initially a coating was prepared using water to dilute the PEG, but this proved unsuccessful due to the incompatibilities of the two components. The high molecular weight PEG proved to be soluble in MEK and propylene glycol methyl ether acetate only at elevated temperatures, and the solution solidified on cooling. This meant the coating must be applied when still warm. However as the spraying apparatus uses a flow of nitrogen to spray the solution, this cooled it down leading to blockage of the sprayer. A further attempt was made to prepare a surface with this PEG using a small paint brush, but again it cooled down and solidified during application.

Spraying a coating with the poly(2,6-dibromophenylene oxide) was also slightly difficult. The polymer was not soluble in MEK at room temperature, but was soluble in tetrahydrofuran (THF). The surface was therefore applied using THF as the solvent. However, as the polymer was applied, the solvent evaporated leaving only the solid polymer to coat the surface. To circumvent this problem, the polymer was dissolved in hot MEK and remained in solution on cooling. The polymer was then reapplied giving better results.

Rusting of the steel has proven to be a problem that has detrimentally affected the analysis of the coatings. Unfortunately as the rust caused the coatings to bubble and weaken, sometimes they peeled off when samples were rinsed and processed after exposures to seawater for bacterial attachment. This peeling was thought to be due to application of only one coat of both the epoxy and the polyurethane. However, on subsequent trials with multiple coats of both epoxy and polyurethane, it is apparent that rust is penetrating the edges of the steel coupons and spreading from there. We expect that this problem will be eliminated by the use of an epoxy primer provided by the Naval Research Laboratory. Another option is to move to coating small Plexiglas coupons, negating rust as an obstacle.

Initial results from the screening of test materials for bacterial attachment (see below) suggested that the poly(2,6-dibromophenylene oxide) coating inhibited fouling to some extent. This result prompted research into different brominated aromatic polymers. Since 2,2',6,6'-tetrabromo bisphenol-A (**1**) (Fig. 2) was readily available, it seemed logical to attempt to make its polycarbonate. The original conditions proved unsuccessful using dimethyl carbonate with an acid catalyst. However, the reaction between terabromobisphenol A and carbonyl diimidazole (**4**) (a phosgene substitute) proved to work to form low molecular weight polymer (Fig. 2). Another polycarbonate has also been made using the bis(hydroxyethyl ether) of tetrabromo bisphenol-A (**3**). Polyesters of **1** and **3** were also synthesized using terephthaloyl chloride (**2**). However, the tetrabromobisphenol-A based polyester turned out to be insoluble. More rigorous screening of bacterial attachment to poly(2,6-dibromophenylene oxide) and PEG has not demonstrated significant differences in numbers of attached cells, but the compositions of communities on these surfaces appear to be different (see below).

**Figure 2**

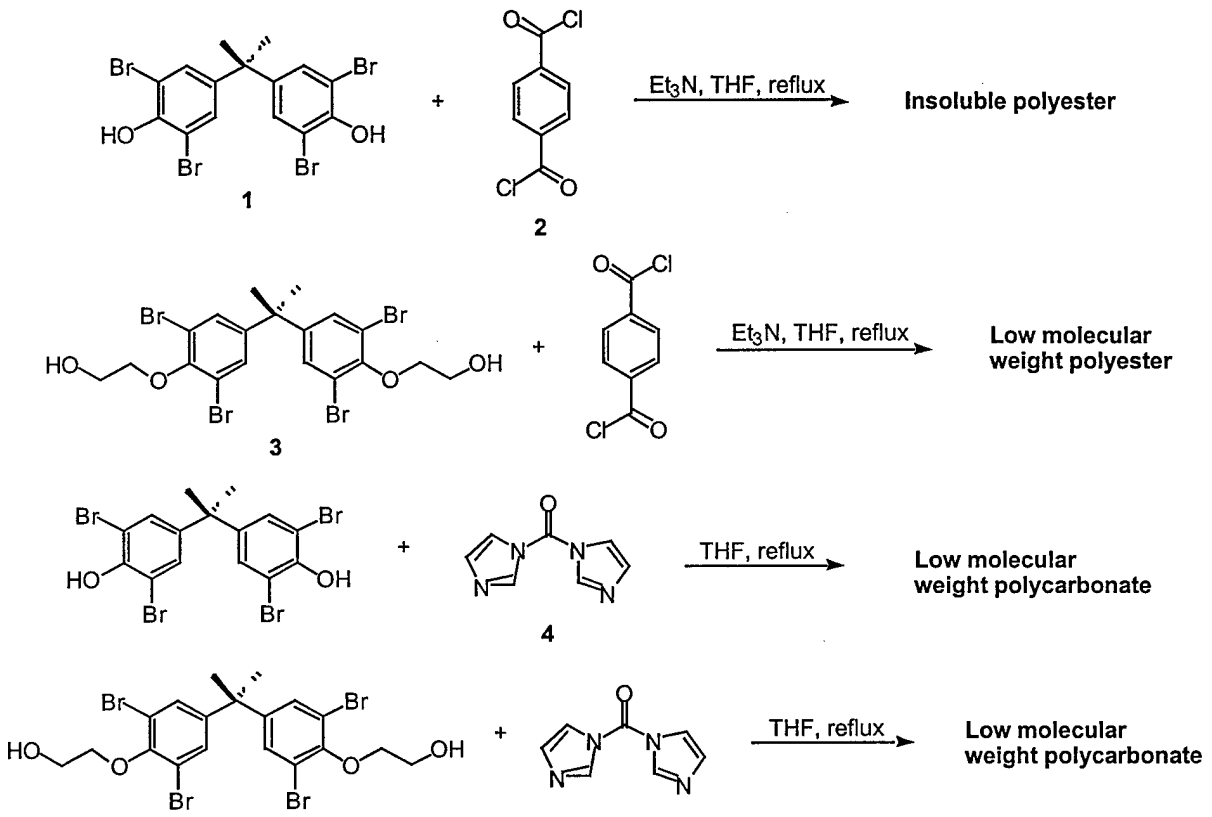


**Screening of test surfaces for resistance to bacterial attachment**

To screen the various test surfaces for their ability to resist bacterial colonization, much initial work has focused on establishing protocols. Considerable care has been taken to ensure quality control of data and consistency among the various data-collectors in the laboratory. As test surfaces become colonized, cells are distributed both as single cells and as larger aggregations and complex clusters of organisms. Moreover, as time of submersion of surfaces increases, there is generally an increase in the numbers and size of aggregates. This presents a challenge for numerically assessing both coverage and distribution of the surface. To accurately and reproducibly measure degree of bacterial attachment to our test surfaces, we have used image analysis combined with light microscopy. Image analysis programs have been adapted and statistical analysis macros have been constructed to rapidly determine (1) numbers of individually attached cells, (2) numbers of aggregates, and (3) percentage of the test surface covered by attached cells.

Preliminary screening of surfaces was performed on PEG-OMe 350, PEG 600, PEG 35,000, PVA, and poly(2,6-dibromophenylene oxide). These surfaces were immersed in circulating seawater tanks at the Baruch Institute culture facility for 24 h. Upon removal, half of the plates were rinsed to remove debris and loosely attached cells, and the surfaces were evaluated by microscopy. The remaining half were not rinsed. Microscopic fields were photographed, grids

superimposed on the photographs and the numbers of individual cells and colonies counted by eye. Statistical analysis of the unrinsed surfaces revealed that there were significantly fewer colonies and individual cells on PEG 35,000, poly(2,6-dibromophenylene oxide), and PVA surfaces than on PEG-OMe 350 and PEG 600 surfaces ($\alpha = 0.05$). Similar results were obtained for rinsed surfaces, with poly(2,6-dibromophenylene oxide) and PEG 35,000 having the least colonies and individual cells. The experimental protocols for these initial assessments have subsequently been fine-tuned to establish reproducible rinsing procedures.

To date, screening of additional test materials has demonstrated some significant differences in their abilities to be colonized by bacteria. However, these early experiments have not yet identified a strong candidate for anti-fouling control. Differences in degree of colonization appear within 72 hours of submersion, with consistently lower levels of attachment to PVA, while total coverage increases almost ten-fold on PEG-300 by 168 hours.

**Characterization of microbial biofilms by molecular analysis**

Molecular analysis of microbial communities is currently being carried out on test surfaces exposed to running seawater in the Baruch Institute culture facility in the College of Science and Mathematics. Communities are being "fingerprinted" by extraction and polyacrylamide gel electrophoresis of their low molecular weight RNA (5S ribosomal RNA and tRNA). The first step in this analysis has been to establish RNA extraction procedures from marine biofilm material and to determine whether biofilm communities differed from those bacteria remaining suspended in the aqueous phase. In other words, during the attachment and colonization process, particular components of the microbial community may be selected because of increased adhesiveness or adaptation to the surface environment, thus enriching for a particular type of microorganisms. Since there are no established protocols for extracting SLMW RNA from organic polymer-coated surfaces, we tested several procedures to determine which provided the highest quality and quantity of RNA. The optimum method has been to swab the attached microorganisms off the surface with sterile cotton gauze, followed by dispersal of cells in buffer using a vortex. Cells are pelleted by high-speed centrifugation and then extracted for RNA by previously described methods (Bidle and Fletcher, 1995; Noble et al., 1997). Repeated extractions of microorganisms from different test surfaces demonstrated that RNA purity is somewhat dependent on the surface chemistry, although the detailed nature of this dependence is not yet clear.

We compared free-living and biofilm bacteria by extracting RNA from the bulk water and from biofilms formed over 2 or 5 months on the glass culture tank walls (Tanks 1, 2 = 2 months; Tank 3 = 5 months) (Fig. 3). Results indicated that attached and free-living communities differ noticeably. 5S rRNA from attached communities were dominated by a single band in the 118 nt region, whereas the free-living community RNA was dominated by two bands: the more intense band is in the 120 nt region and a weaker band near 115 nt. These differences were consistent for both 2 and 5 month incubation periods (Fig. 4).

We have now begun characterization of communities that form on organic polymer test surfaces, i.e. PEG-OH 400 or PEG-OMe-550 and bis-(2-hydroxyethyl-ether) of tetrabromobisphenol A , as brominated surface similar to poly(2,6-dibromophenylene oxide) (Fig. 5). 5S rRNA profiles are similar for biofilms forming on the PEG and the glass tank walls. In contrast, biofilms formed on the brominated surface differ with one major band in the 116 nt region. These results demonstrate that different subpopulations of the total microbial communities may be selected on different types of surfaces, which in turn may result in differences in their comparative overall adhesiveness or in their suitability to be subsequently colonized by macroorganisms, such as invertebrate larvae.

**Deliverables**

Poster presentation at annual meeting of American Society for Microbiology, Atlanta, Georgia, May 1998. "The adhesion of marine microbial communities to surfaces coated with novel synthetic polymers."

***Participating Scientific Personnel***

Madilyn Fletcher, Professor
James M. Tour, Professor
Charles R. Lovell, Associate Professor
Alan W. Decho, Assistant Professor
Peter A. Noble, Research Assistant Professor
Graduate students: Hongyue Dang, Monica Hoffman, Wesley Johnson, Steven T. Lindsay, Alex Morgan, D. Brian Shortell, Adam Rawlett
Undergraduate students: Megan Danzler, Megan Kelley, Caroline Roper, Sara Thieben

## BIBLIOGRAPHY

Bidle, K. D.; Fletcher, M. *Appl. Environ. Microbiol.* **1995**, *61*, 944-952.

Incze, B.I. *Sea Technol.* **1996**, *37*, 43-49.

Ista, L. K.; Fan, H.; Baca, O.; Lopez, G. P. *FEMS Microbiol. Lett.* **1996**, *142*, 59.

Lappin-Scott, H.M; Costerton, J.W. *Biofouling* **1**, 323-342.

Marshall, K.C. Mechanisms of bacterial adhesion at solid-water interfaces, pp. 133-161. In D.C. Savage and M. Fletcher (eds.) *Bacterial Adhesion*, Plenum Press, New York, 1985.

Noble, P.A.; Bidle, K.; Fletcher, M. *Appl. Environ. Microbiol.* 1997, *63*, 1762.

Parrish, J.; Jensen, S.; Hollis, W.C. *Sea Technol.* **1996**, *37*, 51-60.

Wiencek, K.M.; Fletcher, M. *J. Bacteriol.* **1995**, *177*, 1959-1966.

Wolfaardt, G.M.; Lawrence, J.R.; Robarts, R.D.; Caldwell, S.J.; Caldwell, D.E. *Appl. Environ. Microbiol.* **1994** *60*, 434-446.

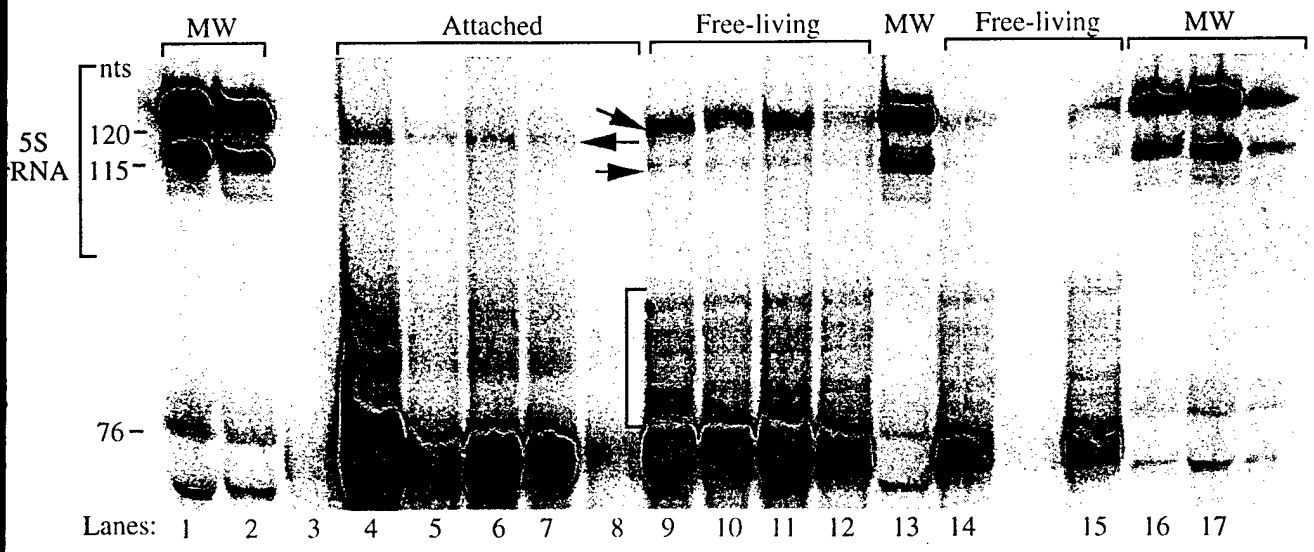


**Fig. 3.** Autoradiograph of SLMW RNA obtained from microbial communities from Tank-3. Results show that microbial communities attached to the walls are different from those in the free-living state as depicted by differences in the molecular weights of 5S rRNA bands (arrows). Also, note differences in tRNAs (red bracket). MW, molecular weight standards; nts, nucleotides.

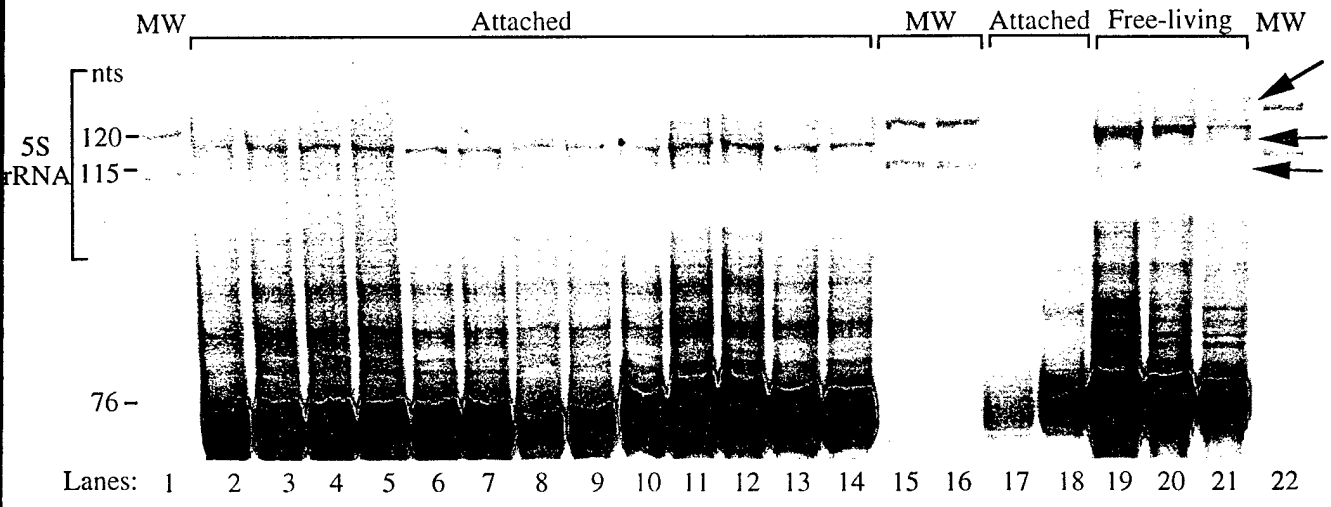


**Fig. 4.** Autoradiograph showing SLMW RNA banding patterns of attached and free-living microbial communities. Tank-1 samples are shown in lanes 2 to 7, and 19. Tank-2 samples are shown in lanes 8 to 11 and 20. Tank-3 samples are shown in lanes 12 to 14, 17, 18 and 21. Arrows depict regions of the 5S rRNA that are different among the free-living microbial communities. MW, molecular weight standards; nts, nucleotides.

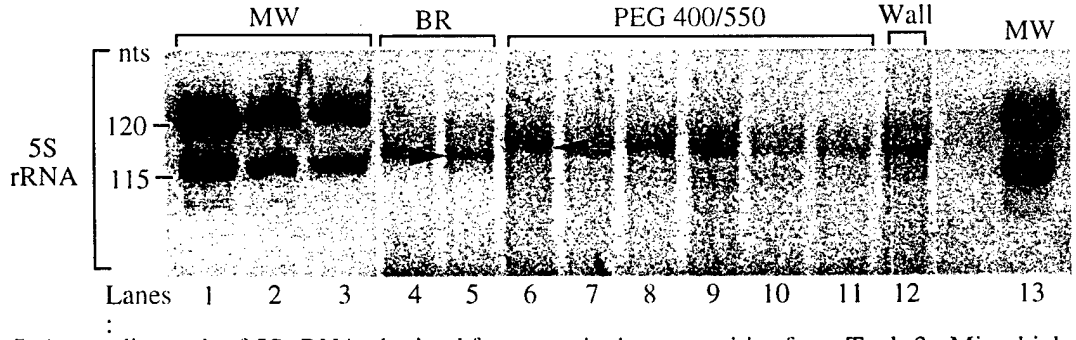


**Fig. 5.** Autoradiograph of 5S rRNA obtained from attached communities from Tank-3. Microbial communities attached to (Bis-(2-hydroxyethyl-ether) of tetrabromobisphenol A) are different than those attched to PEG (polyethylene glycol 400/550), or those attached to the walls of Tank-3. Arrows depict differences in molecular weight of 5S rRNA bands. MW, molecular weight standards; nts, nucleotides.

# REPORT DOCUMENTATION PAGE

Form Approved
OMB No. 0704-0188



| 1. AGENCY USE ONLY *(Leave blank)* | 2. REPORT DATE | 3. REPORT TYPE AND DATES COVERED |
|---|---|---|
| | June 1, 1998 | Annual |

| 4. TITLE AND SUBTITLE | 6. FUNDING NUMBERS: |
|---|---|
| Accelerated Research in Biofouling Control | Grant Number N00014-97-1-0806<br>PR Number 97PR06312-00<br>PO Code 353<br>Disbursing Code N68892<br>AGO Code N66020<br>Cage Code 4B489 |
| 5. AUTHOR(S)<br>Madilyn Fletcher | |
| 7. PERFORMING ORGANIZATION NAME(S) AND ADDRESS(ES)<br>University of South Carolina | 8. PERFORMING ORGANIZATION REPORT NUMBER<br>N00014-97-1-0806-1 |
| 9. 0SPONSORING / MONITORING AGENCY NAME(S) AND ADDRESS(ES)<br>ONR | 10. SPONSORING / MONITORING AGENCY REPORT NUMBER<br>ONR |

11. SUPPLEMENTARY NOTES

Prepared in coordination with University Research Initiative Program for Combat Readiness

| 12a. DISTRIBUTION / AVAILABILITY STATEMENT | 12b. DISTRIBUTION CODE |
|---|---|
| APPROVED FOR PUBLIC RELEASE | |

13. ABSTRACT *(Maximum 200 words)*

The formation of biofouling communities on deployment devices and sensors and on ship and submarine hulls represents a significant limitation to the efficient operation of instrumentation and vessels. We propose to develop novel approaches for control of microbial biofouling by (1) developing fouling-resistant surfaces using disordered layers of polar organic structures, and (2) applying molecular methods and neural net analysis to characterize composition and succession in biofilms on different materials used in naval applications. Test surfaces have been produced by depositing on steel coats of hydroxy terminated-poly ethylene glycol (PEG), methoxy terminated-PEG (of molecular weights ranging from 200 to 35,000), polyvinyl alcohol, and poly(2,6-dibromophenylene oxide). Test surfaces have been screened for their ability to be colonized by marine microorganisms, and the compositions of microbial communities becoming established on a subset of the test surfaces have been determined by analysis of their stable low molecular weight RNA (5S rRNA, tRNA). The major accomplishments of this project period are (a) the development of methods for depositing novel organic polymer coatings on metal surfaces, and (b) determination of differences in degree of fouling on different test surfaces, in biofilms vs. the liquid phase, and on different polymer surfaces.

| 14. SUBJECT TERMS | 15. NUMBER OF PAGES |
|---|---|
| Chemical and Biological Warfare, Target Acquisition, Anti-Submarine, Combat Medicine, Biodeterioration, and Command Control and Communication | 10 |
| | 16. PRICE CODE |

| 17. SECURITY CLASSIFICATION OF REPORT | 18. SECURITY CLASSIFICATION OF THIS PAGE | 19. SECURITY CLASSIFICATION OF ABSTRACT | 20. LIMITATION OF ABSTRACT |
|---|---|---|---|
| UNCLASSIFIED | UNCLASSIFIED | UNCLASSIFIED | 200 words |

# SECTION 7: SUPPORTING RESEARCH

# Development of a Field-Portable LIBS System for Elemental Analysis

Scott R. Goode

Department of Chemistry and Biochemistry
University of South Carolina
Columbia SC 29208

803-777-2601 (Voice)
803-777-9521 (Fax)
Goode@sc.edu

# Section 7: Development of a Field-Portable LIBS System for Elemental Analysis

Scott R. Goode

## ABSTRACT

The fabrication and testing of a laser induced breakdown spectroscopy (LIBS) system is complete. The LIBS spectrometer utilizes a high-resolution dispersion device (an echelle grating) in concert with a charge-induced device (CID) array detector and Nd-YAG laser. The LIBS system uses the laser to form plasma, and then uses fiber optics to bring the emission from the plasma to the spectrometer. The device provides quantitative chemical analysis of solid samples without any dissolution or pretreatment step. During the first year of the grant, the LIBS spectrometer, including laser, have been procured, modified to accept emission via fiber optic, and the system has been tested and certified by Laser Safety. The spectrometer, laser, data collection, and data treatment software has been integrated and tested. The first actual study of LIBS emission that utilizes high spectral resolution is in progress and preliminary results are extremely promising.

## FORWARD

The award if for the period 6/1/97 - 6/29/00 and in the amount of $434,700.

- During the first year the following objectives have been addressed
- Instrument fabrication completed
- Instrument certified by Laser Safety
- Interface to utilize fiber optic collection completed
- LIBS data have been collected
- Data interpretation has begun

## REPORT

### *Problem studied*

Laser-Induced Breakdown Spectroscopy (LIBS) shows great potential as a method for determining the composition of solid samples without preparation. The method can be adapted to field use, and is applicable to nearly all types of samples. The LIBS signal is proportional to analyte concentration, but the matrix influences this proportionality. If the technique is to be applied to a wide variety of samples, the factors that influence the signal must be studied, and methods that use LIBS must be validated. The proposed research examines two important samples: the determination of the lead content of dried paint and the determination of the composition of metallic alloys.

*Important Results*

**Instrumentation**

The research is progressing well, and the first phase, fabricating the instrument, is essentially complete. The LIBS instrument has been assembled, tested, and approved by the USC Health and Safety.

The heart of the instrument is a high-resolution (echelle) spectrometer that uses a charge-induced device (CID) detector in concert with sophisticated software to obtain the entire emission spectrum, from 200-800 nm, in a single exposure. We know of no other spectrometer systems that have been used to study the development of the signal in LIBS. We faced an important decision point soon after the delivery of the spectrometer. We could acquire preliminary spectra with the standard lens system, or we could adapt the instrument to accept the LIBS emission via fiber optic. Since the ultimate goal of the project is to supply a system capable of remote analysis, eventually, fiber optics will be employed to gather the light from the LIBS plasma. We chose to perform this important research task before obtaining any spectra because it would allow us to obtain artifact-free information, and it provided an exceptionally flexible optical entrance that we could exploit in several future stages of the research. The LIBS system required several months to align and test and to ensure that we were producing images of the highest possible spectral resolution. The use of the echelle spectrometer would be obviated by resolution losses due to inferior light coupling and defocusing, so we spent a great deal of time in perfecting the interface.

**Measurements of alloy composition**

Initial studies have revolved around the signals from binary alloys. We have chosen to use brass samples for our initial work, simply because their composition is simple; steel samples will be investigated at the next phase. Certified reference samples of brasses of different composition have been purchased. These brasses are primarily copper, with added zinc. Five certified reference materials with zinc concentrations ranging from 2 to 30% have been tested.

The initial studies are designed to develop a method for determining the amount of material ablated from the sample in a single, or a group, of laser pulses. Preliminary information in our lab and in the literature indicates that the amount ablated is not always a constant. For certain classes of materials, such as glasses and copper-based alloys, the LIBS signal from the first pulse is larger than that of the second, which is larger than that of the third, etc. For other materials, such as lead, the opposite effects are observed. These data are important to evaluate if the determination of carbon in steels is to be performed.

The first experiments measure the emission ratio of zinc (relatively volatile) to copper (relatively nonvolatile) as a function of laser spot size. Changing the sample-to-lens distance changes the spot size in this study. Two typical experiments are shown below.

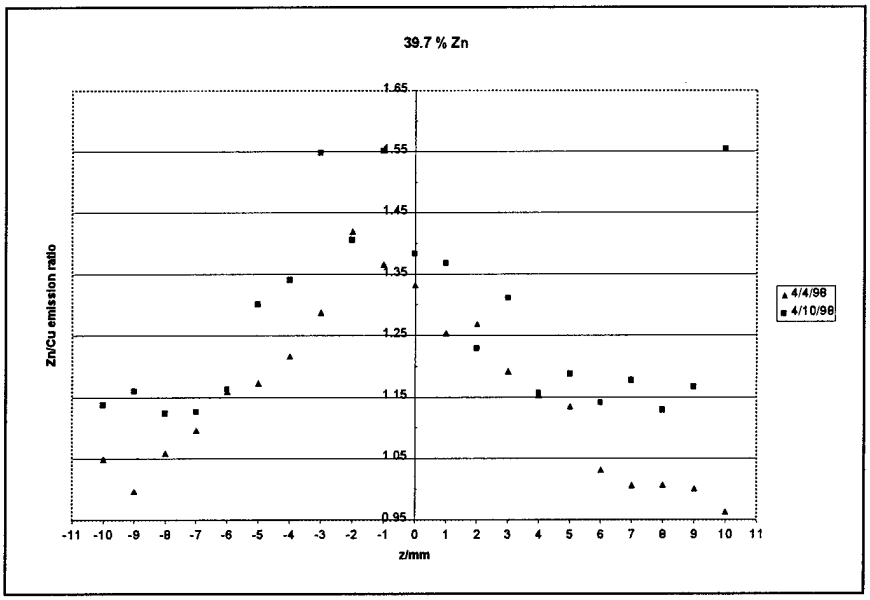


Figure 1. Zinc-to-copper emission ratios for a sample containing 39.7% Zn.

The figure shows data replicated approximately one week apart. The important point to note is that the graph shows bilateral symmetry; the maximum emission is seen when the focus is at the surface, and the emission ratio decreases as the focal point changes.

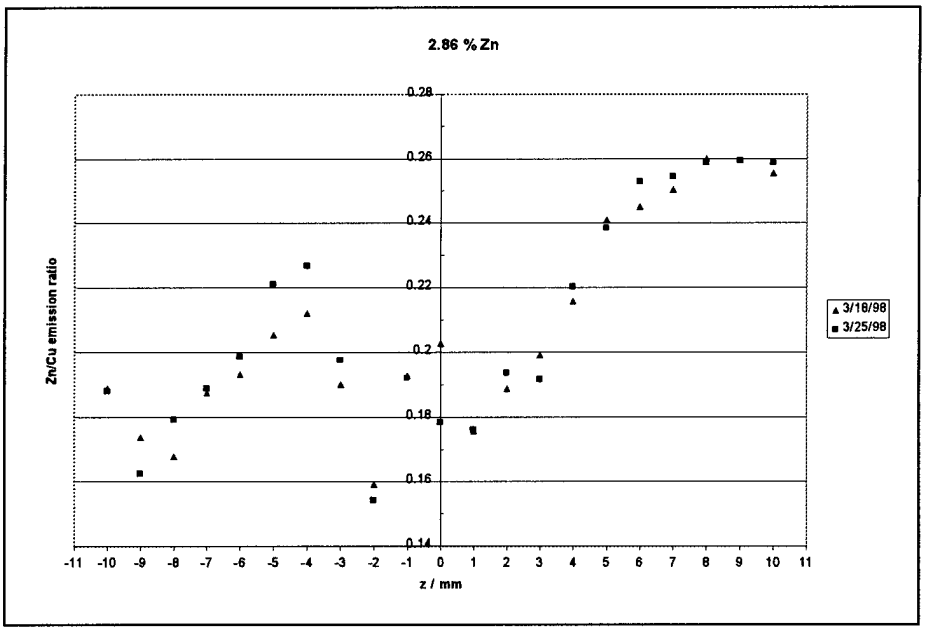


Figure 2. Zinc-to-copper emission ratios for a sample containing 2.86% Zn.

The effect of the matrix is clear. When the brass contains a substantial concentration of zinc, (Figure 1) defocusing the laser produces predictable results that can be explained by a simple theory --the emission increases with power density.

Figure 2 indicates that this theory fails for samples with low zinc, since the results show are asymmetric. These results are consistent with prior experience using LIBS with glass samples and with literature reports of similar behavior.

The results are reproducible, both with the same samples and with different samples. The identical asymmetric relationship is seen in all samples in which the zinc concentration is less than approximately 15%. As the concentration of zinc goes from high to low, the behavior smoothly changes from that shown in Figure 1 to that shown in Figure 2.

The next step is to determine the masses of materials that are vaporized, and such experiments are in progress.

**Determination of the lead content of paint**

Factors affecting the LIBS signal from lead are being investigated using a time-resolved imaging apparatus that consists of an acousto-optic tunable filter (AOTF) along with a gated intensified charge-coupled device (ICCD). This instrument allows us to obtain time-resolved images of the emission from a single atomic transition. Time-resolved plasma images obtained have shown lead emission intensity to increase as well as the overall shape of the plasma with increasing number of laser shots. For example, Figure 3 shows images of the plasma emission obtained under the same conditions with the exception of the number of times the same region was sampled. For these experiments the laser repetition rate and laser power were held constant at 2 Hz and 300 mJ per pulse (7ns) respectively. In addition, the plasmas were formed using the fundamental 1064 nm output of a Nd:YAG laser and the images were acquired 2.5 μs after the laser pulse over a 250 ns gate width. As can be seen, the height of the lead emission observed from the 100th sampling to the 2400th sampling of the same region increases significantly from 0.63 mm to 2.75 mm.

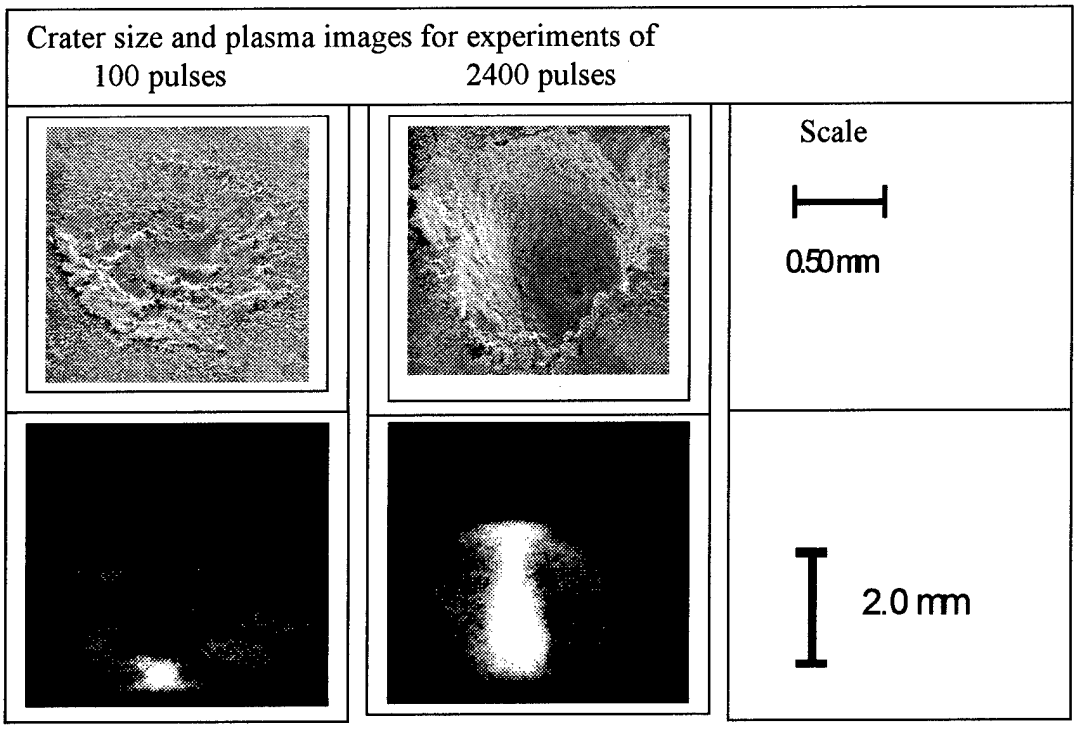


Figure 3. Top: Measurements of crater topology by scanning electron microscope. Bottom: Images of plasma emission at the lead atomic line

This effect is summarized in Figure 4 for two different delay times. The same general trend of increasing plasma emission height is observed at the 1.0 μs as well as the 2.5 μs delay times. In addition, the 2.5 μs delay time plasma images are overall higher than the 1.0 μs delay time since the plasma has expanded and grown up over time.

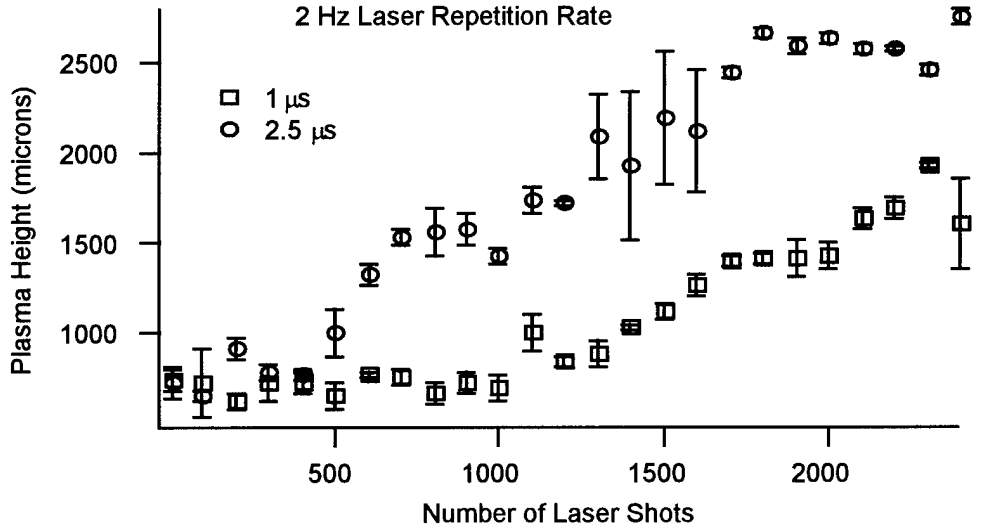


Figure 4. Height of plasma as a function of the number of laser pulses, measured at two different delay times.

The change of the plasma emission intensities seems to be related to the size and shape of the crater that is formed in the lead sample. Figure 3 shows SEM (scanning electron microscopy) images of the lead craters corresponding to the plasmas shown in Figure 1. A rough estimation of the crater depths that correspond to these images vary from approximately 0.1 mm for 100 laser shots to about 1mm for 2400 laser shots. One explanation for the signal enhancement is that increasing laser shots causes deeper craters with a defined shape that may act to funnel the ablated material preferentially in the direction of the incoming laser beam. This effect would increase the laser/particle interactions and thereby increase the excitation and emission observed.

***Publications and technical reports***

None at this time. The initial research results are so striking, that it is clear that they will be of wide interest to the scientific community and will be published within a year.

***Participating personnel***

Paul Harhay, first year Ph.D. candidate
Dimitra Stratis, second year Ph.D. candidate
Scott Goode (summer) Principal Investigator
S. Michael Angel (summer) Co-Principal Investigator

# REPORT DOCUMENTATION PAGE

Form Approved
OMB No. 0704-0188



| 1. AGENCY USE ONLY *(Leave blank)* | 2. REPORT DATE | 3. REPORT TYPE AND DATES COVERED |
|---|---|---|
| | June 1, 1998 | Annual |

| 4. TITLE AND SUBTITLE | 5. FUNDING NUMBERS |
|---|---|
| Development of a Field-Portable LIBS system for the Identification of Alloys | Grant No. N00014-97-1-0806<br>PR No. 97PR06312-00<br>PO Code 353<br>Disbursing Code N68892<br>AGO Code N66020<br>Cage Code 4B489 |
| 6. AUTHOR(S)<br>Scott R. Goode | |
| 7. PERFORMING ORGANIZATION NAME(S) AND ADDRESS(ES)<br>University of South Carolina | 8. PERFORMING ORGANIZATION REPORT NUMBER<br>N00014-97-1-0806-1 |
| 9. SPONSORING / MONITORING AGENCY NAME(S) AND ADDRESS(ES)<br>ONR | 10. SPONSORING / MONITORING AGENCY REPORT NUMBER<br>ONR |

11. SUPPLEMENTARY NOTES

Prepared in coordination with the University Research Initiative Program for Combat Readiness

| 12a. DISTRIBUTION / AVAILABILITY STATEMENT | 12b. DISTRIBUTION CODE |
|---|---|
| APPROVED FOR PUBLIC RELEASE | |

13. ABSTRACT *(Maximum 200 words)*

The fabrication and testing of a laser induced breakdown spectroscopy (LIBS) system is complete. The LIBS spectrometer utilizes a high-resolution dispersion device (an echelle grating) in concert with a charge-induced device (CID) array detector and Nd-YAG laser. The LIBS system uses the laser to form a plasma, and then uses fiber optics to bring the emission from the plasma to the spectrometer. The device provides quantitative chemical analysis of solid samples without any dissolution or pretreatment step. During the first year of the grant, the LIBS spectrometer, including laser, have been procured, modified to accept emission via fiber optic, and the system has been tested and certified by Laser Safety. The spectrometer, laser, data collection, and data treatment software has been integrated and tested. The first actual study of LIBS emission that utilizes high spectral resolution is in progress and preliminary results are extremely promising.

| 14. SUBJECT TERMS | 15. NUMBER OF PAGES |
|---|---|
| Chemical and Biological Warfare, Target Acquisition, Anti-Submarine, Combat Medicine, Biodeterioration, and Command Control and Communication | 16. PRICE CODE |

| 17. SECURITY CLASSIFICATION OF REPORT | 18. SECURITY CLASSIFICATION OF THIS PAGE | 19. SECURITY CLASSIFICATION OF ABSTRACT | 20. LIMITATION OF ABSTRACT |
|---|---|---|---|
| UNCLASSIFIED | UNCLASSIFIED | UNCLASSIFIED | 200 words |